BERNARD LAVALLÉE

MODÉLISATION DE COMPORTEMENTS TRANSITOIRES DE LA BIOMASSE DANS LES PROCÉDÉS DE BOUES ACTIVÉES À L'AIDE D'UN MODÈLE MÉTABOLIQUE

MODELLING OF TRANSIENT BEHAVIOR OF ACTIVE BIOMASS IN ACTIVATED SLUDGE PROCESSES USING A METABOLIC MODEL

Thèse présentée
à la Faculté des études supérieures de l'Université Laval
dans le cadre du programme de doctorat en génie civil
pour l'obtention du grade de philosophiae doctor (Ph. D.)

DÉPARTEMENT DE GÉNIE CIVIL
FACULTÉ DES SCIENCES ET GÉNIE
UNIVERSITÉ LAVAL
QUÉBEC

2009

Résumé

Les modèles de boues activées ASM 1, 2 et 3 de l'International Water Association (IWA) sont acceptés comme la norme dans l'industrie du traitement des eaux usées. Toutefois, plusieurs auteurs ont remarqué que les constantes cinétiques de ces modèles dépendent du type de substrat, de la configuration du procédé et de l'âge des boues. Dans ces modèles, la répartition des flux de substrat entre la croissance et le stockage est une fonction empirique.Certains auteurs ont indiqué que les constantes cinétiques des modèles de boues activées peuvent être influencés par la régulation de la production d'enzymes.

Ainsi, un ingénieur cherchant à modifier un système spécifique ne peut prédire la réponse du système réel une fois les modifications apportées, ni choisir la bonne configuration ou les bonnes modifications avec le même ensemble de constantes cinétiques.

Il y a 60 ans, Monod (1949) a proposé d'appliquer l'équation de Michaelis-Menten décrivant la cinétique enzymatique à une culture de microorganismes. Afin de simplifier la relation mathématique proposée, Monod (1949) réduit la cellule entière en un seul enzyme génétiquement exprimé à une seule intensité. Toutefois, le métabolisme de la cellule est basé sur un grand nombre de réactions biochimiques.

Le chapitre 2 de ce travail revoit la littérature afin d'identifier les facteurs contrôlant le métabolisme de la cellule et la régulation de l'activité spécifique de la cellule. La revue de la littérature a été rédigée de façon à souligner les mécanismes de régulation qui induisent une variation du taux de croissance afin de les exprimer mathématiquement ($d\mu/dt$). L'étude de ces mécanismes vise à modéliser la variation de l'activité spécifique. La revue est limitée aux organismes procaryotes hétérotrophes sous des conditions aérobies.

Dans la littérature, des modèles cybernétiques ont été proposés pour modéliser la croissance cellulaire et portent, entre autres, sur la régulation de la production d'enzymes, c'est-à-dire sur l'induction. L'objectif de ce travail est donc de présenter un modèle de boues activées qui imite l'induction enzymatique de la biomasse active dans le cadre des modèles de boues activées. Dans le modèle proposé au chapitre 3, les taux de réaction peuvent s'ajuster aux conditions environnementales et à l'historique cellulaire. Dans un premier temps, le

modèle théorique a été calé sur les données trouvées dans la littérature. Les données colligées lors d'expériences transitoires à court et à long terme ont toutes été modélisées avec le même ensemble de constantes cinétiques, ce qui n'était pas possible avec les autres modèles. Le modèle proposé offre ainsi un regard plus réaliste de l'activité spécifique de la biomasse active sous des conditions d'opération du procédé hautement variables.

Dans un deuxième temps, un protocole expérimental est proposé pour évaluer l'état métabolique des microorganismes présents dans la boue activée, et évaluer la performance du modèle proposé. Le protocole a été conçu pour caractériser l'évolution de plusieurs composants intracellulaires au cours de comportements transitoires de la biomasse.

Au chapitre 5, le modèle théorique proposé au chapitre 3 a été adapté au protocole expérimental et calé sur les données expérimentales obtenues. Au cours des expériences effectuées, une réduction temporaire de l'activité métabolique a été observée après que la capacité de stockage ait été comblée. Selon les simulations effectuées, et la concordance des résultats obtenus avec une revue de littérature approfondie, il semble que la régulation croisée du carbone et de l'azote puisse être utilisée pour modéliser certains comportements transitoires et la régulation des flux métaboliques vers la croissance et le stockage.

Au chapitre 6, les modèles à strucuture ARN-r sont proposés afin de donner une description de l'état métabolique des microorganismes à l'aide de nouvelles techniques moléculaires et prédire l'accélération de la croissance ($d\mu/dt$) de la boue activée. Dans ces modèles, la synthèse du système de synthèse des protéines (PSS) est décrite par un mécanisme autocatalytique. La cinétique du processus autocatalytique présente un fondement métabolique de l'accélération de la croissance et de la phase de latence. Les modèles ARN-r sont en mesure de décrire adéquatement l'accélération de la croissance pour différentes configurations de réacteurs. Ainsi, ce type de modèles fait appel à des constantes cinétiques à caractère «intrinsèque» et peut être utilisé de façon moins restrictive que les modèles à caractère plus empirique. Ceci constitue un avantage pour le développement de modèles de conception plus fiables.

Abstract

For wastewater treatment, the activated sludge models (ASMs) 1, 2, and 3 of the International Water Association (IWA) are accepted as industrial standard. However, many authors have observed that the kinetic parameters of these models depend on the type of substrate, process configuration, and sludge age. Some publications showed that the kinetic parameters of ASMs could be influenced by regulation of enzyme production. In the models currently used to describe the activated sludge process, the distribution of the substrate flux between growth and storage is an empirical function.

Therefore, an engineer aiming to make some modifications to a specific treatment system is not able to predict the response of the real system after the modifications and choose the right configuration or modifications with the same set of parameters.

Sixty years ago, Monod (1949) proposed the application of the Michaelis Menten relation describing enzyme kinetics to a culture of micro-organisms. For the purpose of simplification, the mathematical relation proposed by Monod (1949) reduced the entire cell to a single enzyme genetically expressed at a single level. However, cell metabolism is based on a large number of biochemical reactions.

Chapter 2 of this thesis reviews the literature to identify the controlling factors of cell metabolism and the regulation of the specific activity of the cell. The literature review was designed to highlight which regulation mechanisms induce a growth rate variation so that they can be expressed mathematically ($d\mu/dt$). The study of these processes will focus on modeling the specific activity variation. The review is limited to heterotrophic prokaryote organisms growing under aerobic conditions.

Cybernetic models are proposed for modeling cell growth and focus, among other things, on regulation of enzyme production, that is to say on induction. The objective of this work is to present an activated sludge model that mimics the enzymatic induction of active biomass within the framework of ASMs. In the proposed model presented in chapter 3, process rates are modulated according to the environmental conditions and cell history. In a first step, the model was fitted on the basis of data found in the literature. All data collected

from short and long transient experiments were fitted with the same set of parameters, which was not possible with various models. The proposed model gave a more realistic picture of active biomass and of its specific activity under highly varying process conditions.

In a second step, an experimental protocol is presented to perform the evaluation of the structured biomass model. The protocol was designed to induce transient behaviour and characterize the evolution of several internal biomass components. In chapter 5, the theoretical model proposed in chapter 3 is adapted to an experimental protocol and fitted to the collected data. In these experiments it was observed that filling the storage capacity of cells leads to special transient behaviour and a temporarily reduced metabolic activity. The model-based interpretation of the results showed that the observed transient behaviour can be explained by cross-regulation of carbon and nitrogen metabolism. Hence, according to an extensive literature review, the cross-regulation of carbon and nitrogen can be used to model some observed transient behavior and regulation of the storage process in activated sludge.

In chapter 6, rRNA-structured biomass models are proposed to describe the metabolic status of cells using new molecular techniques in view of predicting the growth response ($d\mu/dt$) of cells in the activated sludge process. The autocatalytic reaction rate of the synthesis of the PSS component (rRNA) can provide a mechanistic explanation for the growth response and the growth lag phase. The proposed models were able to properly describe and predict the growth response of the biomass in various types of reactor. Such models could be more widely applicable by using intrinsic model parameters, and this could be a key improvement as it could lead to improved models for design.

Avant-Propos

Tout d'abord, je désire remercier de tout cœur M. Paul Lessard qui m'a offert la possibilité d'effectuer une thèse en dépit de ma situation d'étudiant adulte peu commune. Sans son soutien et son ouverture d'esprit et sa patience ce travail n'aurait pas été possible. Avec la perspective du temps, je peux dire que l'achèvement de cette thèse est le résultat de son œuvre. En dehors du travail scientifique, je retiens surtout de son enseignement la stabilité et la persévérance, dans la vie comme dans la recherche.

Naturellement, je remercie chaleureusement M. Peter Varolleghem pour toute sa contribution scientifique, les opportunités offertes et le travail qu'il m'a aidé à accomplir. Son enthousiasme et sa passion ont été une source de motivation et d'inspiration. Ce que je retiens le plus de cette collaboration est sans contredit ce qui le caractérise le mieux, sa pensée positive.

Paul et Peter m'ont donné davantage que ce que leur travail exigeait. Les remerciements que je peux formuler me semblent bien peu. Je ne peux que m'engager envers mes devoirs à leur égard.

M. Mark van Loosdrecht s'est montré généreux par la disponibilité qu'il a démontrée et par les échanges constructifs que nous avons eus sans autre intérêt que la curiosité scientifique. Je lui en suis redevable. Sa rigueur et son honnêteté m'ont plut dès notre première rencontre et me sont toujours demeurés agréables. D'ailleurs je souhaite exprimer ma gratitude à M. Yves Comeau pour avoir favorisé cette rencontre.

J'ai beaucoup apprécié la gentillesse de M. Dominic Frigon, de l'université McGill avec qui j'ai eu l'occasion de collaborer. Espérant que d'autres travaux effectués en collaboration seront possibles dans le futur. Je n'oublie pas Alain Garnier, du département de génie chimique de l'université Laval, qui a montré beaucoup d'intérêt pour mon travail et qui m'a apporté son soutien en plusieurs occasions.

Je remercie également M. Michel Bisping pour sa collaboration au laboratoire. Toujours d'une agréable compagnie, il a toujours fait preuve d'une patience constante.

Enfin, j’exprime ma profonde gratitude à Manon pour sa patience sans fin et son appui indéfectible, à qui je voue toute mon affection. Je n’oublie pas Vincent et Léandre qui ont su comprendre le manque de disponibilité de leur père en plusieurs occasions.

Être ou ne pas être, telle est la question
(Shakespeare W., 1564-1616. Hamlet.)

Table des matières

Liste des tableaux

Liste des figures

Liste des symboles

b_C [d^{-1}] : Taux de dépérissement des constituants cellulaires structuraux.

b_{BP} [d^{-1}] : Taux de dégradation des matériaux constituants intracellulaires.

b_H^{max} [d^{-1}] : Taux de dépérissement maximal de la biomasse hétérotrophe.

b_{MF} [d^{-1}] : Taux de dépérissement de la micro-faune.

b_{PSS} [d^{-1}] : Taux de déprérissement du système de synthèse intracellulaire.

B_P [mg DCO L^{-1}] : Matériaux constituants intracellulaires (precursors ou building blocs).

B_{PSS} [mg L^{-1}] : Système de synthèse des protéines.

B_S [mg DCO L^{-1}] : Substrat intracellulaire.

B_{STO} [mg DCO L^{-1}] : Matériaux de stockage intracellulaires.

C [unité] : Capacité metabolique

dk_{STO} [mg DCO (mg DCO)$^{-1}$ L^{-1}] : Taux spécifique de dégradation des matériaux de stockage.

D [d] : Taux de dilution (Volume du réacteur/débit).

E_A [unité L^{-1}] : Antitoxine (protéine).

$E_{BS(\text{ha ou la})}$ [unité L^{-1}] : Enzymes de transport transmembranire du substrat soluble (ha= haute affinité; la faible affinité).

$E_{BS(\text{SMP})}$ [unité L^{-1}] : Enzymes de transport transmembranire du substrat SMP.

E_G [mg DCO L^{-1}] : Enzymes de croissance (protéines-ribosomales du sytème de synthèse intracellulaire).

E_h [unité L^{-1}] : Enzyme d'hydrolyse.

E_{STO} [unité L^{-1}] : Enzyme de production des produits de stockage.

E_T [unité L^{-1}] : Toxine (protéine).

f_{PSS} [mg (mg DCO)$^{-1}$] : Fraction du système de synthèse intracellulaire.

f_{PSS}^{max} [mg (mg DCO)$^{-1}$] : Fraction maximale du système de synthèse intracellulaire.

f_{STO}^{max} [mg DCO (mg DCO)$^{-1}$] : Fraction maximale des matériaux de stockage intracellulaires.

fu [mg DCO (mg DCO)$^{-1}$] : Fraction non-biodegradable de la biomasse.

I [unité] : Niveau d'induction

i_{nx} [mg N (mg DCO)$^{-1}$] : Fraction des microorganismes (X_H) et des enzymes de croissance (E_G), des matériaux constituants intracellulaires, des constituant cellulaires structuraux, consituée d'azote.

k_{BS}^{max} [mg DCO (unite)$^{-1}$ d^{-1}] : Activité maximale des enzymes de transport transmembranaire $E_{BS(ha \text{ ou } la)}$ du substrat soluble exogène.

k_{BSMP}^{max} [mg DCO (unite)$^{-1}$ d^{-1}] : Activité maximale des enzymes de transport transmembranaire du substrat SMP.

k_h^{max} [mg DCO (unite)$^{-1}$ d^{-1}] : Activité maximale des enzymes d'hydrolyse E_h.

k_P [mg DCO (mg DCO)$^{-1}$ d^{-1}]: Taux spécifique de production de matériaux constituants cellulaires.

k_{PSS} [mg (mg)$^{-1}$ d^{-1}]: Taux spécifique de production de du système de synthèse des protéines.

k_{RBS}^{max} [mg DCO (mg DCO)$^{-1}$ d^{-1}] : Taux spécifique de production de produits microbiens solubles.

k_S [mg DCO (mg DCO)$^{-1}$ d^{-1}]: Taux spécifique de production de susbtrat intracellulaires.

k_{STO} [mg DCO (mg DCO)$^{-1}$ d^{-1}]: Taux spécifique de production de matériaux de stockage.

k_{STO}^{max} [mg DCO (unite)$^{-1}$ d^{-1}] : Activité maximale des enzymes de production de matériaux de stockage.

K_{BP} [mg DCO L^{-1}] : Constante d'affinité pour les matériaux constituants intracellulaires.

K_{BS} [mg DCO L^{-1}] : Constante d'affinité pour le substrat intracellulaire.

K_{bsof} [mg DCO L^{-1}] : Constante de demi-saturation du processus de production des SMP par le substrat intracellulaire.

$K_{BS,STO}$ [mg DCO L^{-1}] : Constante d'affinité pour le substrat intracellulaire du processus de production des matériaux de stockage.

Ki_{BS} [mg DCO(mg DCO)$^{-1}$] : Constante d'inhibition du processus de transport du substrat exogène par le subtrat intracellulaire.

Ki_{STO} [mg DCO(mg DCO)$^{-1}$] : Constante d'inhibition du processus de production des matériaux de stockage intracellulaires par les matériaux de stockage.

K_{iT} [mg L^{-1}] : Constante d'inhibition de la toxine par l'antitoxine.

K_{MFO} [mg O_2 L^{-1}] : Constante d'affinité de la micro-faune pour l'oxygène dissous.

K_{mR} [mg L^{-1}] : Constante d'affinité pour la structure *mR*.

K_{NH} [mg N L^{-1}] : Constante d'affinité des microorganismes pour le NH_4^+.

K_O [mg O_2 L^{-1}] : Constante d'affinité des microorganismes pour l'oxyène dissous.

$K_{S(ha\ ou\ la)}$ [mg DCO L^{-1}] : Constante d'affinité du processus de transport transmembranaire pour le substrat exogène.

K_{SMP} [mg DCO (mg DCO)$^{-1}$] : Constante d'affinité du système de transport pour le substrat S_{MP}.

K_{STO} [mg DCO (mg DCO)$^{-1}$] : Constante d'affinité pour les produits de stockage.

$K_{X/MF}$ [mg DCO L^{-1}] : Constante de demi-saturation de la micro-faune par les bactéries hétérotrophes.

K_{XSS} [mg DCO L^{-1}] : Constante de demi-saturation par les particules en suspension lentement biodégradables.

N [unité] : nombre d'espèces d'organismes

mR [unité L^{-1}] : Structure à courte demi-vie du système de synthèse intracellulaire. Variable sans DCO.

S_{MP} [mg DCO L^{-1}] : Produits microbiens solubles.

S_{NH} [mg N L^{-1}] : NH_4^+ soluble.

S_0 [mg(-DCO)L^{-1}] : Oxygène dissous, O_2 en DCO négative.

S_S [mg DCO L^{-1}] : Substrat soluble exogène.

S_0 [mg DCO L^{-1}] : Concentration initiale du substrat.

t [unité] : Temps.

X [mg DCO L^{-1}] : Biomasse.

X_C [mg DCO L^{-1}] : Constituants cellulaires structuraux.

X_H [mg DCO L^{-1}] : Microorganismes hétérotrophe.

X_{ii} [mg DCO L^{-1}] : Particules inertes en suspension.

X_{MF} [mg DCO L^{-1}] : Micro-faune incluant les protozoaires et les metazoaires.

X_{SS} [mg DCO L^{-1}] : Particules en suspension lentement biodégradables.

X_0 [mg DCO L^{-1}] : Concentration initiale de la biomasse

Y_{BS} [mg DCO (mg DCO)$^{-1}$] : Coefficient de rendement du substrat intracellulaire sur le substrat exogène.

Y_{BSMP} [mg DCO (mg DCO)$^{-1}$] : Coefficient de rendement du substrat intracellulaire sur les produits microbiens solubles.

Y_H [mg DCO (mg DCO)$^{-1}$] : Coefficient de rendement des microorganismes hétérotrophes.

Y_{MF} [mg DCO (mg DCO)$^{-1}$] : Coefficient de rendement de la micro-faune sur les bactéries hétérotrophes.

Y_C [mg DCO (mg DCO)$^{-1}$] : Coefficient de rendement des matériaux constituants intracellulaires sur le substrat exogène.

α_{EA} [d^{-1}] : Taux de production de l'antitoxine E_A.

$\alpha_{EBS(ha\ ou\ la)}$ [d^{-1}] : Taux de production des enzymes de transport transmembranaire $E_{BS(ha}$ ou la).

α_{EG} [d^{-1}] : Taux de production des enzymes de croissance E_G du système de synthèse intracellulaire.

α_{Eh} [d^{-1}] : Taux de production des enzymes d'hydrolyse E_h.

α_{ESMP} [d^{-1}] : Taux de production des enzymes de transport $E_{BS(SMP)}$.

α_{ESTO} [d^{-1}] : Taux de production des enzymes de stockage E_{STO}.

α_{ET} [d^{-1}] : Taux de production de la toxine E_T.

α_{mR} [d^{-1}] : Taux de production du composant mR.

β_{BP} [d^{-1}] : Taux de dépérissement des matériaux constituants intracellulaires.

β_{EA} [d^{-1}] : Taux de dépérissement de la protéine antitoxine E_A.

β_{EBS} [d^{-1}] : Taux de dépérissement de l'enzyme de transport transmembranaire $E_{BS(ha\ ou\ la)}$.

β_{EBS} [d^{-1}] : Taux de dépérissement de l'enzyme de transport transmembranaire E_{BSMP}.

β_{EG} [d^{-1}] : Taux de dépérissement de l'enzyme de croissance E_G.

β_{Eh} [d^{-1}] : Taux de dépérissement de l'enzyme d'hydrolyse E_h.

β_{ESTO} [d^{-1}] : Taux de dépérissement de l'enzyme E_{STO}.

β_{ET} [d^{-1}] : Taux de dépérissement de la toxine E_T.

β_{mR} [d^{-1}] : Taux de dépérissement du composant mR.

δk_{STO}^{max} [d^{-1}] : Activité maximale des enzymes de dégradation des produits de stockage.

φ_{EG} [mg DCO (mg DCO)$^{-1}$] : Rapport du taux de production de l'enzyme E_G et du taux de croissance des microorrganismes.

μ_C^{int} [d^{-1}] : Taux de croissance des constituants cellulaires structuraux.

μ_H [d^{-1}] : Taux de croissance des microorganismes heterotrophes

μ_{obs} [d^{-1}] : Taux de croissance observé des microorganismes

$\mu_{H\max}^{int}$ [d^{-1}] : Taux de croissance maximal intrinsèque des microorganismes hétérotrophes.

$\mu_{MF\max}$ [d^{-1}] : Taux de croissance maximal de la micro-faune.

Introduction

Avec l'augmentation de la densité de la population dans le monde, la gestion de l'eau, et particulièrement la gestion des eaux usées, est devenue une préoccupation pour l'ensemble des citoyens des pays industrialisés. Si ces matières polluantes sont rejetées directement dans la nature, elles y sont dégradées par les microorganismes présents et cela entraîne une détérioration du milieu aquatique. Ainsi afin de maintenir une qualité acceptable de l'environnement, la plupart des pays industrialisés ont choisi de traiter leurs eaux usées avant de les rejeter dans le milieu naturel.

En principe, un système de traitement d'eau usée favorise la dégradation des matières polluantes par les microorganismes afin d'éviter que ce processus s'effectue dans le milieu récepteur. Lors du traitement des eaux usées, les matières polluantes biodégradables sont ingérées par un consortium de microorganismes, puis transformées en matière cellulaire. Cette transformation biologique est suivie d'une séparation de la masse cellulaire (ou biomasse) de la phase liquide, ce qui laisse l'eau ainsi traitée, libre de contaminants biodégradables.

Afin d'aider les ingénieurs à concevoir les systèmes de traitement d'eau usée, des modèles mathématiques ont été proposés pour prévoir la performance ou l'efficacité du traitement biologique (Tchobanoglous et al., 1991). Dans ces modèles, le consortium de microorganismes présents dans le système, de même que le métabolisme complexe des microorganismes qui effectuent le traitement sont caractérisés par une entité unitaire simple (X) qui est définie par sa masse. Le taux de croissance (μ) et le taux de dépérissement (b) de la biomasse X décrivent la cinétique d'assimilation des polluants. Le coefficient de rendement (Y) décrit le rapport stoechiométrique entre la production de biomasse et la consommation des matières polluantes représentées par le substrat (S). Ces modèles sont basés sur le modèle empirique proposé par Monod (1949).

Actuellement, les modèles ASM (Activated Sludge Models – Modèles de boues activées) proposés par l'International Water Association sont largement utilisés (Henze et al., 2000). Dans ces modèles, la représentation de la biomasse est plus structurée. Les populations de microorganismes qui effectuent ces transformations sont représentées par trois groupes, soit

les bactéries hétérotrophes (X_H), les bactéries nitrifiantes (X_A) et les bactéries déphosphatantes (X_{PAO}). Selon la représentation adoptée, le substrat ou le phosphore peuvent être emmagasinés sous forme de réserves intracellulaires (X_{STO} ou X_{PP}) par les bactéries hétérotrophes ou déphosphatantes. Quoique plus complexes, avec ces modèles plus structurés les ingénieurs et scientifiques arrivent à évaluer la concentration de divers composants tel que la demande chimique en oxygène (DCO), l'oxygène dissous, différentes formes azotées et de phosphore à l'effluent d'un système de traitement biologique.

Cependant, un système de traitement biologique des eaux usées est un procédé utilisant le vivant, et les modèles proposés incluent une représentation très simplifiée du métabolisme complexe des microorganismes. Il en résulte donc que ces modèles donnent une description imparfaite du comportement dynamique d'un système de traitement (Daigger et Grady, 1982a; 1982b; Grady et al., 1996).

Les constantes cinétiques utilisées dans ces modèles décrivent des réactions d'assimilation, de croissance cellulaire ou de certaines transformations énergétique, selon une cinétique invariable qui dans les faits, peut varier dans le temps ou suivant la configuration du procédé (Frigon et al., 2002a; Frigon et al., 2006; Grady et al., 1996; Hadana et al., 2001; Lavallée et al, 2002; Martinage, 1999; Templeton and Grady, 1988). D'ailleurs les auteurs des modèles ASM mentionnent que la valeur expérimentale des constantes cinétiques est dépendante des conditions d'opération et de la configuration du système à l'étude (Henze et al., 2000). Il en résulte qu'une calibration du modèle doit être effectuée afin d'obtenir une simulation précise de la réponse du système de traitement (Gernaey et al., 2004). Puisque la valeur de ces constantes cinétiques dépends de facteurs abiotiques, ceux-ci sont dits «extrinsèque» (terme proposé par Grady et al., 1996).

Cette problématique soulève donc une question fondamentale. Chacun des modèles ASM se veut une représentation mathématique des processus de transformation biologique impliqués dans le procédé de traitement biologique à l'étude. Or, puisque la valeur des constantes cinétiques est dépendante de l'histoire de la biomasse et de la configuration du procédé, ces modèles révèlent leur caractère empirique en donnant une image statique dépendante des conditions prévalant au moment de la calibration, et spécifique au procédé de traitement. La question est donc de déterminer si on désire modéliser le système de

traitement à l'aide d'un modèle empirique à constantes cinétiques «extrinsèques», ou si on désire modéliser la biomasse elle-même avec un modèle plus fondamental et des constantes cinétiques qui représentent la nature «intrinsèque» (terme proposé par Grady et al., 1996) du métabolisme des microorganismes, et ainsi éventuellement affranchir le modèle et les constantes cinétiques de l'histoire de la biomasse et de la configuration du procédé.

L'objectif visé par l'utilisation d'un modèle à constantes cinétiques «intrinsèques» serait d'augmenter la fiabilité des simulations, de réduire l'effort de calibration requis et d'élargir la plage d'utilisation des modèles à des comportements transitoires de la biomasse.

Afin d'atteindre cet objectif et obtenir une meilleure description des divers processus de transformation biologique, plusieurs auteurs (Daigger et Grady, 1982a; Marr, 1991; Ramkrishna, 1983; van den Berg, 1998) ont cherché à développer des modèles dont les équations et les constantes cinétiques détaillent de façon plus structurée le métabolisme des microorganismes.

Ces auteurs ont cherché entre autre, à intégrer aux modèles proposés une représentation du système de synthèse des protéines (PSS) afin de représenter l'état métabolique des microorganismes et simuler la modulation de leur taux de croissance ($d\mu/dt$). Il est reconnu que le taux de croissance des microorganismes augmente proportionnellement à la concentration relative de l'acide ribonucléique ribosomal (ARNr), un des principaux composants du PSS (Keener et Nomura, 1996a). Plusieurs auteurs proposent d'ailleurs de quantifier le rapport ARNr/ADN pour définir l'état métabolique des microorganismes (Dell'Anno et al., 1998; Kaplan, 2001; Kerkhof et Ward, 1993; Milner et al., 2001; Muttray et al., 2001).

Ainsi, dans ces modèles, les microorganismes ne sont plus représentés que par un composant unique (X_H pour la biomasse hétérotrophe) dont la croissance est décrite par un taux de croissance invariable (μ_H), mais plutôt par une représentation structurée de plusieurs composants, dont la cinétique de croissance dépends de leurs concentrations relatives et de leurs interactions.

Cependant, pour calibrer de tels modèles devient nécessaire de quantifier les composants et d'en définir les taux de transformation.

Or, à l'aide des nouvelles techniques moléculaires, il est devenu possible de quantifier l'ADN et l'ARNr dans la biomasse d'un procédé de boues activées, et donc de définir l'importance relative du PSS. Il devient donc possible de calibrer un modèle à biomasse structurée sur des données expérimentales.

Toutefois, avant d'en arriver à un modèle achevé, plusieurs problèmes demeurent à solutionner. Les microorganismes sont hautement adaptables, et la cinétique qui décrit leur comportement varie selon les voies métaboliques qui s'activent en fonction des conditions auxquelles ils sont exposés. Il est nécessaire de déterminer quelle structure sera appropriée pour décrire la biomasse lors de son adaptation, de déterminer quelles sont les voies métaboliques qui s'expriment, et dans quelles circonstances chacunes d'elles contrôlent la cinétique du procesus de traitement.

Ce travail constitue donc l'ébauche d'un modèle à biomasse structurée, proposé pour simuler les comportements d'adaptation de la biomasse aux conditions prévalant dans divers systèmes de traitement d'eau usée. Ces mécanismes d'adaptation entraînent divers comportements transitoires, dont quelques uns seront étudiés en vue de parfaire le modèle proposé.

Ces travaux s'inscrivent dans un courant scientifique généré par le développement de nouveaux outils, tel que les techniques de marquage génétique (Wilderer et al., 2002). Ces nouvelles techniques permettent de caractériser une population de microorganismes dans un système donné. Les nouvelles techniques de mesure moléculaires basées sur l'acide ribonucléique des ribosomes (ARNr) permettent d'obtenir une compréhension plus profonde du métabolisme des microorganismes présents dans les procédés de boues activées, et de mieux comprendre la réponse dynamique de ces systèmes.

Ces techniques moléculaires présentent de nouvelles informations sur les caractéristiques de la biomasse des procédés de boues activées. La gestion de cette nouvelle information requiert donc le développement de nouveaux modèles à biomasse structurée, puisqu'une

méthode directe de quantification de la population active de microorganismes dans la biomasse nécessitera la prise en compte de leur état métabolique.

Le principal objectif visé dans ce travail est d'obtenir une représentation plus réaliste des micro-organismes présents dans la biomasse, qui soit représentative de leur état métabolique. La représentation plus structurée des micro-organismes cherche à décrire des mécanismes de régulation de leur activité spécifique, et ainsi obtenir une information «intrinsèque» ou de meilleure qualité lors de l'évaluation des constantes cinétiques. Par voie de conséquence, cet objectif vise ainsi à obtenir un outil capable de prévoir la réponse dynamique d'un système exposé à de larges transitoires, ou de prévoir la réponse du système de traitement pour différentes configurations sans avoir recours à des pilotes pour calibrer la réponse du modèle pour chacune de diverses conditions d'opération ou pour chacune des différentes configurations étudiées.

Les modèles à biomasse structurée présentent un degré de complexité plus élevé que ceux utilisés actuellement. Toutefois, ce niveau de complexité, permet d'obtenir des constantes cinétiques moins spécifiques aux conditions d'évaluation. Ainsi, l'évaluation des constantes cinétiques devient une procédure indépendante de la configuration ou du mode d'opération du procédé, ce qui pourrait diminuer l'effort de calibration, augmenter la fiabilité des simulations et élargir la plage d'utilisation du modèle calibré.

N.B. Le travail qui suit est constitué d'une suite d'articles qui ont été publiés, ou qui sont en voie d'être publiés dans quelques revues scientifiques. Il en résulte que le texte de cette thèse passe du Français à l'anglais à plusieurs reprises puisque les articles publiés sont présentés intégralement.

De plus afin de limiter l'ampleur de cette thèse, de façon générale la discussion se limite à l'analyse du métabolisme et des cinétiques associés aux microorganismes hétérotrophes.

CHAPITRE 1 ÉNONCÉ DU PROBLÈME

À la base, le concept des modèles ASM assume que la biomasse active (X_H ou X_A) est homogène, et ne subit pas de changement de son état métabolique dans le temps. L'évaluation des constantes cinétiques se fait, dans la mesure du possible, sur la réponse d'une biomasse entretenue dans un état stable. Les postulats de base du modèle établissent donc que l'état métabolique de la biomasse est constant, et il en découle que la valeur des constantes cinétiques comme le taux de croissance maximal (μ_{max}), le coefficient de rendement de la biomasse sur le substrat (Y) et le taux de dépérissement de la biomasse (b) est constante (Henze et al., 2000). D'ailleurs, les auteurs de ce modèle considèrent que la valeur des constantes cinétiques est dépendante du type de substrat, de la configuration du procédé et de l'âge des boues. On peut donc assumer que la représentation de la biomasse est comme une image statique de son état métabolique. Selon le système d'équations proposé, la réponse cinétique de la biomasse active est du point de vue mathématique, invariable (Ramkrishna, 1983).

1.1 Respiration spécifique

Selon les hypothèses soutenant le modèle, la respiration spécifique maximale de la biomasse active peut être définie par l'équation suivante (adapté de Vanrolleghem et al., 1999) :

$$\frac{rO_{2\max}}{X_H} = \mu_{H\max} * \frac{(1-Y_H)}{Y_H} \qquad [\ 1\text{-}1]$$

Comme μ_{Hmax} et Y_H sont des constantes, le taux de respiration maximal spécifique est par définition constant.

Ainsi, pour quantifier les bactéries hétérotrophes dans la biomasse d'un système de traitement, une méthode proposée consiste à en mesurer le taux de respiration maximal lors d'un essai en cuvée et d'en déduire la population initiale (Vanrolleghem et al., 1999). Pour que cette méthode soit utilisable, le taux de croissance (μ_{Hmax}) et le coefficient de rendement (Y_H) doivent être connus. Cette méthode indirecte demeure applicable dans la mesure où le taux de respiration spécifique demeure constant.

Cependant, beaucoup de modèles biochimiques décrivent l'état métabolique des micro-organismes comme étant un processus inductible (Gallant, 1979; Jensen et Pedersen, 1990; Nyström, 1998), donc du point de vue mathématique comme un processus variable. Dans ces modèles, l'état du bagage enzymatique et des molécules d'ARN détermine la vitesse de production des macromolécules, et donc le taux de croissance des bactéries (Jensen et Pedersen, 1990).

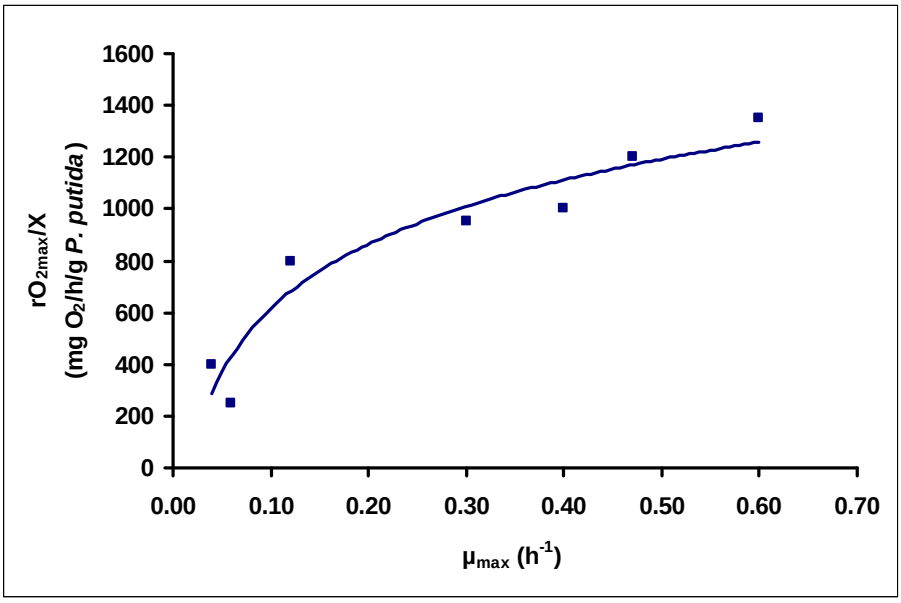

Figure 1-1 rO_2/X d'une culture de *Pseudomonas putida* (Adapté de Daigger et Grady, 1982b)

Daigger et Grady (1982b) démontrent aussi que la respiration spécifique de la biomasse active est dépendante du taux de croissance, c'est à dire de l'état métabolique des microorganismes présents dans une boue activée (Figure 1-1). Les observations de ces auteurs démontrent que μ_{Hmax} ou Y_H peuvent varier, et que la description mathématique du

modèle semble incomplète. On constate donc que l'hypothèse du modèle demeure valable pour un seul état métabolique, c'est à dire pour les conditions qui prévalaient lors de la caractérisation.

Il y a donc lieu d'étudier plus en détails la portée de ce constat sur l'évaluation du taux de croissance et du coefficient de rendement.

1.2 Taux de croissance

Grady et al. (1996) ont démontré que l'évaluation du taux de croissance maximal de la biomasse active (μ_{max}) est fortement influencé par son état métabolique initial, et par le rapport substrat microorganismes initial (S_0/X_0) utilisé.

Daigger et Grady (1982a) expliquent que le taux de croissance instantané dépend du taux de dilution imposé sur le chemostat d'où est tirée la biomasse. La valeur ainsi obtenue des constantes cinétiques a été qualifiée d'*extrinsèque* par Grady et al. (1996). Les constantes cinétiques *extrinsèques* seraient dépendantes des conditions expérimentales, contrairement aux constantes cinétiques *intrinsèques* qui seraient caractéristiques du métabolisme cellulaire. Aussi, plusieurs auteurs recommandent d'évaluer le taux maximal de croissance d'une biomasse à l'aide d'une méthode en cuvée, dont le rapport S_0/X_0 est inférieur à 2, de façon à ne pas modifier l'état métabolique des micro-organismes et influer sur le taux de croissance mesuré (Chudoba et al., 1992; Grady et al., 1996).

Ces recommandations sont en concordance avec les modèles biochimiques proposés dans la littérature. Kovárová-Kovar et Egli (1998) expliquent que les propriétés cinétiques montrées par une cellule pour un substrat donné, seraient intimement liées au niveau d'expression des enzymes impliqués dans la voie métabolique de ce substrat. Jensen et Pedersen (1990) indiquent de plus qu'une carence en substrat entraîne une diminution de la vitesse de la transcription génétique, ainsi implique une diminution de la quantité de ribosomes disponibles pour la construction anabolique, et par conséquent cause un ajustement de la vitesse de croissance de la cellule à la disponibilité du substrat.

Pour des cultures mixtes, il semble que le taux de croissance est une variable qui dépend de l'état métabolique des espèces responsables de la dégradation du substrat et aussi de la composition de la biocénose (Kovárová-Kovar et Egli, 1998).

Ces observations indiquent donc que le taux de croissance μ_{Hmax} et le taux de respiration spécifique peuvent varier suivant l'état métabolique de la biomasse et selon la méthode expérimentale utilisée. Ces ajustements métaboliques de la biomasse peuvent donc entraîner une déviation de la réponse du modèle par rapport à la réponse du système réel.

1.3 Coefficient de rendement

Le coefficient de rendement (Y) a été défini par Monod (1949) comme le rapport entre la quantité de bactéries formées et la quantité de substrat utilisé. Le rapport observé était constant pour les cultures en phase exponentielle. Plus tard, Herbert (1958) a constaté que Y diminue avec le taux de croissance et introduit la notion de métabolisme endogène. Herbert a traduit mathématiquement ce phénomène par une croissance négative.

Les auteurs des modèles ASM ont opté pour le concept proposé par Herbert (1958) et ont retenu le taux de dépérissement de la biomasse active (b_H) dans les modèles. Le dépérissement conduit à une réduction de la quantité de biomasse hétérotrophe (X_H).

Toutefois, à partir de résultats semblables à ceux obtenus par Herbert (1958), Pirt (1965) a présenté plutôt le concept de maintenance ou une partie du substrat est utilisé pour le maintien de la biomasse, alors que le dépérissement est nulle (aucune croissance négative). Le concept de maintenance regroupe différents phénomènes tels que les dépenses d'énergie pour la mobilité, les cycles énergétiques futiles, la régulation osmotique, le renouvellement des composants macromoléculaires, la diffusion extracellulaire de métabolites, etc. Par la suite, Pirt (1982) a démontré que la maintenance variait avec le taux de croissance.

Par conséquent, la variation de la maintenance aurait un effet sur l'évaluation du coefficient de rendement Y_H.

1.4 Taux de dépérissement

Certains auteurs s'interrogent sur la signification de la constante de dépérissement mesurée par respirométrie (van Loosdrecht et Henze, 1999 ; Grady et al., 1996). Selon ces auteurs, différents ajustements métaboliques se produisent au cours de la respiration endogène, et la constante de dépérissement mesurée inclut plusieurs phénomènes. Ces derniers ne constituent pas nécessairement une diminution de la quantité de biomasse active, mais incluent potentiellement une réduction du pouvoir respiratoire de la biomasse et différents processus de sporulation ou de dormance des bactéries.

Selon van Loosdrecht et Henze (1999) une partie du taux de dépérissement de la biomasse active mesuré par respirométrie serait associé à la régulation enzymatique (*internal decay*), et une autre partie pourrait être associée à la mortalité cellulaire et à la prédation (*external decay*).

Conformément aux hypothèses avancées par van Loosdrecht et Henze (1999), Lavallée et al. (2002) ont observé une variation de la respiration spécifique relativement à l'activité d'un système enzymatique de référence (le système de transport d'électron). Selon ces auteurs, cette observation laisse voir une erreur dans la procédure d'évaluation du taux de dépérissement de la biomasse active effectuée par respirométrie. Les observations de ces auteurs serait en contradiction avec certaines hypothèses du modèle ASM 1, puisqu'elles impliquent que la respiration maximale spécifique de la biomasse active (rO_{2max}/X) varie lors d'une carence, et par voie de conséquence, entraîneraient un biais dans l'estimation de la biomasse active.

1.5 Problématique de recherche

Ainsi, on constate que certaines constantes des modèles ASM, peuvent varier ou être influencées par l'état métabolique de la biomasse et par la disponibilité du substrat. La respiration spécifique maximale ainsi que le taux de croissance maximal de la biomasse active varieraient selon le rapport substrat/microorganismes appliqué sur la biomasse, ou selon la durée de la période de carence. De plus, selon le concept de maintenance, la portion de substrat utilisé pour l'anabolisme varie avec le taux de croissance.

La problématique de recherche consiste donc à trouver une représentation mathématique des caractéristiques «intrinsèques» du métabolisme des microorganismes, et ainsi éventuellement affranchir le modèle et les constantes cinétiques de l'histoire de la biomasse et de la configuration du procédé.

Pour atteindre cet objectif, ou du moins s'en approcher, il devient nécessaire d'intégrer au modèle des descriptions mathématiques plus détaillées du métabolisme des microorganismes. Au chapitre 2, la littérature présente divers modèles biochimiques qui peuvent détailler chacune des réactions biochimiques qui constituent les voies métaboliques impliquées dans les processus de transformation du substrat.

Le modèle proposé au chapitre 3 a été élaboré à partir des informations retenues dans la revue de littérature. Ce modèle métabolique est donc une représentation structurée des micro-organismes, tout en étant une représentation simplifiée des modèles biochimiques complexes.

Le chapitre 4 présente la méthode expérimentale qui a été élaborée dans le but de caractériser l'évolution dans le temps de chacun des composants proposés pour décrire la biomasse, afin d'en tirer une caractérisation des cinétiques métaboliques. Enfin, aux chapitres 5 et 6 les structures mathématiques proposées ont été validées par un processus expérimental.

Sommairement, le modèle métabolique proposé décrit la réponse «d'ajustement de la croissance» ($d\mu/dt$) de la biomasse observé dans la littérature. Le chapitre 7 place ainsi en perspective de nouveaux axes de recherche qui sont basé sur de nouvelles méthodes moléculaires en vue de déterminer des descripteurs de l'état métabolique des microorganismes présents dans la biomasse, comme le rapport ARN-r/ADN.

CHAPITRE 2 REVUE DE LITTÉRATURE

Le métabolisme de la cellule est décrit par un grand nombre de réactions biochimiques. Toutes ces réactions se produisent suivant certaines séquences, et sont régulées par différents inducteurs et inhibiteurs. Des milliers d'enzymes différentes sont impliquées dans toutes ces réactions. La description de seulement quelques chaînes enzymatiques peut devenir complexe.

Un modèle est une idéalisation d'une situation réelle, dans lequel uniquement les composants les plus importants sont identifiés, incluant une description de leurs interactions (Daigger et Grady, 1982a). Ainsi un modèle mathématique ne devrait retenir que les principales composantes des modèles biochimiques afin de conserver des dimensions acceptables pour les utilisateurs.

Afin d'élaborer un modèle à biomasse structurée, une revue de littérature a été effectuée afin d'identifier les principaux composants cellulaires, leurs interactions ainsi que leurs mécanismes de régulation pour les intégrer dans une représentation organisée et hiérarchisée. Cet exercice visait à définir et justifier du point de vue biochimique la signification des variables et des équations mathématiques proposées.

L'article qui suit a été publié en 2005 dans la revue Journal of Environmental Engineering and Science, volume 4: 517–532.

REVIEW OF PROCARYOTE METABOLISM IN VIEW OF MODELING MICROBIAL ADAPTATION FROM FAST GROWTH TO STARVATION CONDITIONS

Lavallée B.*, Lessard P.*, Vanrolleghem P. A. †.

*Département de Génie Civil, Faculté des Sciences et de Génie, Université Laval, Québec, Canada, G1K 7P4.

†Department of Applied Mathematics, Biometrics and Process Control, Ghent University, Coupure Links 653, B-9000 Gent, Belgium

Abstract: More than 50 years ago, Monod (1949) proposed the application of the Michaelis-Menten relation describing enzyme kinetics to a culture of micro-organisms. For the purpose of simplification, the mathematical relation proposed by Monod (1949) reduced the entire cell to a single enzyme genetically expressed in a single intensity. However, cell metabolism is based on a large number of biochemical reactions. This paper reviews the literature to identify the controlling factors of cell metabolism and the regulation of the specific activity of the cell. The literature review was designed to highlight which regulation mechanisms induce a growth rate variation so that they can be expressed mathematically. The study of these processes will focus on modeling the specific activity variation. The review is limited to heterotrophic procaryote organisms under aerobic conditions.

Key words: modeling, metabolism, regulation, growth rate, cell death, maintenance, activated sludge.

Résumé : Il y a plus de 50 ans, Monod (1949) a proposé d'appliquer l'équation de Michaelis-Menten décrivant la cinétique de l'enzyme à une culture de microorganismes. À des fins de simplification, la relation mathématique proposée par Monod (1949) réduit la cellule entière en un seul enzyme génétiquement exprimé à une seule intensité. Toutefois, le métabolisme de la cellule est basé sur un grand nombre de réactions biochimiques. Le présent article revoit la littérature afin d'identifier les facteurs contrôlant le métabolisme de

la cellule et la régulation de l'activité spécifique de la cellule. La revue de la littérature a été conçue pour souligner les mécanismes de régulation qui induisent une variation du taux de croissance afin de les exprimer mathématiquement. L'étude de ces procédés portera sur la modélisation de la variation de l'activité spécifique. La revue est limitée aux organismes procaryotes hétérotrophes sous des conditions aérobies.

Mots clés : modélisation, métabolisme, régulation, taux de croissance, mort cellulaire, maintenance, boues activées.

2.1 Introduction

Cell growth modeling is used mainly in wastewater treatment, more specifically for activated sludge processes. Several models, all of which are based on Monod kinetics, have been proposed to represent and predict the dynamic response of these processes (Lessard and Beck 1991; Henze et al. 2000). Current models assume that the cells, or the biomass, have a single level of expression or specific activity. The experimentally determined parameters are thus inherently dependent on the operating conditions and the configuration of the system under study (Henze et al. 2000).

However, cell metabolism is based on many biochemical reactions. All these reactions occur in ordered sequences and are regulated by different inducers and inhibitors. There are thousands of different enzymes and several hundreds of them may be involved in these reactions (Bailey and Ollis 1986).

As the cell has a variable specific activity level, any variation in process operating conditions or any modification to the system will cause a deviation in model response. For instance, it is well known that μ_{Hmax}, the maximal growth rate of heterotrophic biomass will change according to culture conditions (Daigger and Grady, 1982a). Also, k_{STO}, the rate of storage in activated sludge model (ASM) 3 is not universal, and the value of this constant changes with environmental conditions (Hanada et al. 2001).

An engineer striving to optimize a system configuration or wishing to modify a given system has therefore little chance to predict the system response to modifications, to define the optimal configuration, or to determine the corrective actions that would be best.

Actually, engineers use standard design rules and their knowledge to design wastewater treatment plants (Gernaey et al. 2004). Models are being used more and more often, but in such cases, ASMs can only be of some assistance in optimization of design and operation because they do not take into account the metabolic adjustment of the active biomass and subsequent variation of the parameters. Wild et al. (1994) showed the value of this problem for denitrification in the activated sludge process. Variation of the volume ratio or of the anaerobic:aerobic:anoxic time ratio changes the induction time of particular enzymatic chains. Thus, this changes the level of specific activity of the biomass and the dependant parameters. Schmid (2002) showed this phenomenon with resonance induction. Therefore, to perform the optimisation process with ASMs, several experiments must be conducted as done by Schmid (2002). Liu et al. (1999) proposed some modifications to ASM1 to optimize the aerobic-anoxic period in a denitrification process to minimize the experimental part. These authors proposed the inclusion in ASM1 of some cybernetic functions to model the diauxic growth on O_2 and NO_3. Similar analysis should be done to optimize the sequencing batch reactor (SBR) process. In this case, a number of possibilities should be analyzed. van Loosdrecht and co-workers (Smolders et al. 1994, 1995a, 1995b; Kuba et al. 1997) published several papers on SBR, but in most of these publiations a 2:4 anaerobic/oxic period ratio was used. Kuba et al. (1997) performed a validation of the "Technical University Delft Phosphorus" model on different cycle lengths but it was calibrated on experiments with similar "total induction time". Therefore, recalibration of the parameters was not required. This work aims to model the variations in rates under transient conditions or under different induction times. Thus, it would help an engineer to choose the optimal ratio of volumes or cycle lengths (induction time) and the optimal process configuration. A new or improved model would help in understanding the transient behaviour of the activated sludge process and in optimizing the design and operation of the process.

Also, nucleic acid probes are used more and more often in studies of wastewater treatment processes and microbial ecology (Amann and Ludwig, 2000; Wilderer et al. 2002). So, quantification of active cells with probes will require models with further refinement in the description of active biomass, as variation of specific activity is taken into account. Moreover, ribosomal ribonucleic acid (rRNA) theory does not explain all transient

behaviour of active cells (Daigger and Grady 1982b). According to biochemistry literature, the mechanisms describing the growth process seem to be well understood, but the dynamics of the whole process are not yet well defined (Cangelosi and Brabant 1997; Muttray et al. 2001). Therefore, the development of more realistic mathematical models is necessary and appropriate. Regulation of cell growth rate should thus be integrated in mathematical models to predict biomass behaviour after system modifications.

The objective of this paper is thus to review the literature and from it deduce a conceptual model that mimics the variation of the specific activity, or the regulation of growth of active biomass. With such a model, it should be possible to access the intrinsic value of parameters (parameters independent of the physiological state of the organism (Grady et al. 1996)) defining the growth rate of the biomass on a given substrate. Therefore, with the same set of parameters, it would then be possible to predict the response of continuous systems, or semi-continuous systems and batch processes which is not possible with ASM.

In this paper, the substrate metabolism will be studied following the main metabolic pathways information from the literature review will be used to probe the cell metabolism deeply. This study focuses on regulation of the processes at the transcription level, i.e. regulation of deoxyribonucleic acid (DNA) code expression and regulation of the cell's specific activity. In the first part of the paper, the substrate uptake and its use are studied. The review will first discuss the substrate uptake rate (Sect. 2.3) and then bifurcations in metabolism, such as the storage products and soluble microbial products (SMPs) or exopolymeric substances (EPSs) (Sect. 2.4). In the second part of the paper (Sect. 2.5), the central metabolism is summarized as a growth process and studied through the protein synthesis system (PSS), which is a major component in the regulation of the growth process (Zhang et al. 2002). A simplified representation of the PSS is presented to model the regulation of the growth process. In the third part of the literature review (Sect. 2.6), some phenomena that have an influence on the evaluation of yield or growth rate such as cell death and maintenance are studied. Finally, some extra-cellular mechanisms such as the evolution of the population of micro-organisms in activated sludge, or predation are discussed (Sect. 2.7). Therefore, several processes are studied to get an overview of what

occurs in activated sludge in terms of adaptations or transient phenomena. The chapter 3 presents the model mathematically with validation results.

2.2 A quick overview of the main metabolic pathways

The cell's ability to multiply depends mainly on its capacity to assimilate a given substrate and to metabolize it into cell constituents. The regulation of various metabolic pathways represents the ability of the cell to adapt to its environment. The regulatory mechanisms of these processes must be reviewed to model them properly. The literature review is limited to procaryote heterotrophic organisms exposed to aerobic conditions.

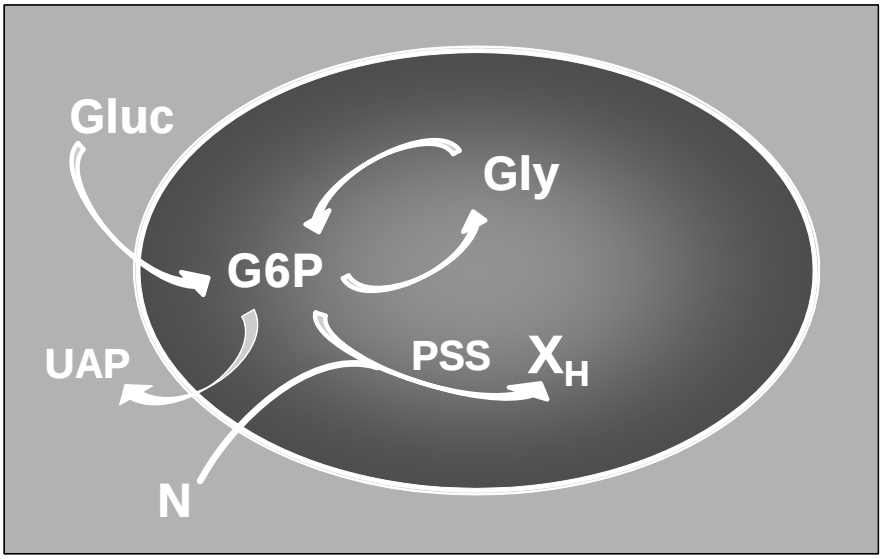

Figure 2-1 Schematic representation of main metabolic pathways

In short, it could be said that the substrate uptake rate is regulated by the substrate transporter density in the cell membrane, which increases with the substrate concentration (Ferenci 1999). It seems that this regulation process changes the affinity constant of the biomass for the substrate. Following its uptake, the substrate could be used for growth but several bifurcations exist in the cell metabolism. The two main bifurcations studied in carbon metabolism are the formation of storage products and the production of SMP. Storage products are mainly polyhydroxybutyrate (PHB) or glycogen (Dawes and Senior 1973). Their rate of formation and degradation is regulated by different metabolites as well as at the transcription level (Preiss 1996; Kessler and Witholt 2001). Production of SMPs is

not yet well understood and the following discussion attempts to give an overview of the state of the knowledge about SMP production.

Regulation of the growth process is associated mainly with regulation of the PSS (Zhang et al. 2002). The transcription and the translation are two key steps in protein synthesis that are regulated by the energy level of the cell (Zhang et al. 2002).

A simplified schematic of these mechanisms is presented in Figure 2-1. In this figure, glucose (Gluc) is taken up by the cell and used to form an intracellular substrate (glucose 6-phosphate (G6P)). The latter could be used for growth (X_H), or formation of utilization-associated products (UAP) or glycogen (Gly). A similar representation was adopted by Dircks et al. (2001). Beun et al. (2000) used a similar representation for cells growing on acetate. According to these authors, acetate is used to form pyruvate as endogenous substrate, and the latter forms PHB rather than glycogen as storage product. Also, as indicated in Figure 2-1, nutrients (N) are required for growth. The growth process is regulated by the state of the PSS. The PSS is discussed below.

The more detailed discussion that follows emphasizes regulation dynamics. The focus is on regulation at the transcriptional regulation level, i.e. the expression of enzymes associated with the particular process under discussion.

2.3 Substrate uptake

Because the cell prioritizes consumption over growth (van Loosdrecht et al. 1997) and this process is inducible (Ferenci 1999), modeling the substrate consumption rate becomes important. This impacts the storage processes and the SMP formation. Moreover, it is possible to observe in experiments with activated sludge, that the specific substrate consumption rate varies according to culture conditions (Beun et al. 2000; van Aalst-van Leeuwen et al. 1997; Sin 2004). Sin (2004) clearly showed that the substrate uptake rate increases with the initial substrate to biomass ratio (S_0/X_0).

Certain authors have demonstrated that cells adapt the transport enzyme density in the membrane according to environmental conditions (Ferenci 1999). Also according to Ferenci (1999), the level of expression of various transport enzymes of glucose is regulated

by the substrate concentration. Three types of porins are located on the external membrane and may affect its permeability. Three types of transport enzymes are located on the cytoplasmic membrane. Apparently, the substrate uptake rate is dependent on the induction intensity or, in other words, on the porin and enzyme concentration in the cell wall. At low substrate concentrations, a transport enzyme system with a high affinity would be induced at a higher intensity than a transport system with a low affinity, which is favoured at high glucose concentrations. Ferenci (1999) proposed mathematical equations to model the substrate uptake rate.

Therefore, when trying to model a transient culture one would perhaps have to model the regulation of the substrate uptake rate at the induction level. According to the Figure 2-1, the induction intensity of the transport enzyme(s) of the exogenous substrate is regulated by the concentration of this substrate.

2.3.1 Variation of the affinity constant

As already mentioned, according to Ferenci (1999), the intensity of expression of various transport enzymes varies with substrate concentration. It also seems that these enzymes show different affinity constants (K_S). Kovárová-Kovar and Egli (1998) established a relationship between the affinity constant and the growth rate of *Escherichia coli* on glucose. A high growth rate and low glucose concentration resulted in the derepression of a high-affinity transport system. High substrate concentrations favoured the induction of a low-affinity system (Ferenci 1999).

It seems that K_S is not a constant for mixed cultures, but rather a variable that depends on the species selected and their relative population size, the metabolic state of the species responsible for substrate degradation, and the growth rates (Kovárová-Kovar and Egli 1998). Moreover, based on the competition principle, we know that rapid-growth bacteria populations show a higher affinity constant than slow-growth species (Stumm-Zollinger and Harris 1971). Modifications in the population structure of the biomass may therefore cause variations in the observed affinity constant.

Moreover, some chemical phenomenon such as mass-transfer resistance in large flocs, may affect the assessment of the affinity constant (Characklis 1978; Shieh 1980; Lau et al. 1984; Chu et al. 2003). These phenomena must be taken into account in the calibration procedure of a model.

One can see that the cell itself adapts to the environment but at the same time, the population structure and floc size may affect the affinity constant value observed. Therefore, the formulation of a model to model affinity constant variation may be complex.

2.4 Bifurcations in the use of metabolites by the cells

"*Micro-organisms capable of rapidly storing and consuming substrate in a more balanced manner have a competitive advantage over organisms that cannot do it*" (van Loosdrecht et al. 1997). During a starvation period, cells with this competitive advantage increase their chance of survival. In fact, the storage of reserves becomes paramount during batch or semi-continuous feed system (RBS) cultures.

The substrate that is taken up could be used for growth as well as for storage. The storage process is well depicted in some metabolic models (Henze et al. 2000; Smolders et al. 1994), but these models do not take into account the regulation of the process at the transcription level. Sin (2004) showed that the rate of these processes could vary with the original substrate to biomass ratio (S_0/X_0) in batch experiments. Thus, the following discussion focuses on the induction mechanisms to highlight how transcriptional regulation could change the specific rates.

A similar discussion will be presented on other bifurcations of the cell's metabolism such as SMP formation and EPS productions.

2.4.1 Accumulation of storage products

Some of the models proposed in the literature tend to model the kinetics of biomass growth not on external substrate but rather on internal substrate or on endogenous reserves (Krishna and van Loosdrecht 1999; Henze et al. 2000). However, these models do not take into account the variation of the specific rate of reserve synthesis. Certain observations

showed that the specific polyhydroxyalkanoate (PHA) production rate varies with operating and environmental conditions (Hanada et al. 2001).

Metabolic pathways used by the cell to produce glycogens or PHB are relatively well known (Dawes and Senior 1973). Glycogens are formed from glucose 6-phosphate through a sequence operated by four enzymes (Dawes and Senior 1973; Preiss 1996). The formation of PHB starts with acetyl-CoA and follows a sequence operated by three enzymes (Dawes and Senior 1973; Kessler and Witholt 2001). According to the model presented by Dircks et al. (2001), it would be possible to model glycogen synthesis or degradation using a single reaction. According to Beun et al. (2000), this would also be true for PHB.

However, the regulatory mechanisms for PHB synthesis are not well known. Regulation is carried out at the genetic transcription level and at the enzymatic level (Kessler and Witholt 2001). Kessler and Witholt (2001) proposed a biochemical model in which genetic expression of PHB synthesis and degradation enzymes is inhibited by absence of substrate for PHB production. The nicotinamine adenine dinucleotide phosphate, reduced form to nicotinamine adenine dinucleotide phosphate, oxidized form ($NAD(P)H/NAD(P)^{+}$) ratio regulates the enzymes activity and thus the formation and degradation of PHB (Dawes and Senior 1973; Kessler and Witholt 2001). Also, depolymerization of PHB appears to be inhibited in the presence of a soluble substrate favouring rapid growth (Kessler and Witholt 2001). However, certain observations seem to indicate that degradation of PHB occurs at the same time as its synthesis (Kessler and Witholt 2001).

Glycogen production is regulated by genetic expression and enzyme activity (Preiss 1996). A high energy charge (the adenylate form ratio) removes the inhibition of the enzymes responsible for glycogen synthesis. The cell appears to regulate its metabolic capacity to convert the carbon substrate into glycogen in response to the substrate availability (Preiss 1996). This regulation occurs at the level of gene expression through cyclic adenosine monophosphate and guanosine tetraphosphate (ppGpp) (Preiss 1996). Also the expression of enzymes responsible for the synthesis and degradation of glycogen is regulated by the same operons (Preiss 1996). Therefore, one can assume that their expression is proportional.

One can also assume that the expression of enzymes involved in reserve synthesis and degradation would be proportional and regulated by the G6P concentration (the operons inductor) in the cell (Figure 2-1).

2.4.2 Production of soluble microbial products

In addition to storage phenomena, metabolite release processes have been observed by several authors (Grady et al. 1972; Huang and Cheng 1987; Hao and Lau 1988). It seems that most soluble organic matter in the effluent of a wastewater treatment plant is SMP (Barker and Stuckey 1999). Soluble microbial products included a large variety of products, such as humic and fulvic acids, polysaccharides, proteins, nucleic acids, various organic acids, antibiotics, steroids, cell structural components and metabolic products. The molecular weight of these products can vary from <500 to >50,000 Da (Barker and Stuckey 1999).

According to the literature review by Barker and Stuckey (1999), SMP are composed of all soluble products leaving the biological system that were not present in the influent. A part of these products seems to be biodegradable and of low molecular weight. These products are associated with growth (UAP) and accumulation of intermediate metabolites. These are generally defined as metabolic products derived from the substrate (Barker and Stuckey 1999).

Hao and Lau (1988) proposed an exponential relationship of the growth rate to describe the specific production rate of UAP, especially at high dilution rates. According to these authors, a limitation in nutrients or in oxygen tends to favour UAP production. Also according to them, biomass capable of producing PHB and extra-cellular polymer reserves produces less UAP.

Chang and Rittmann (1989) propose a Luedeking-Piret type of relationship to describe UAP production. Others (Furumai and Rittmann 1992; Lu et al. 2001) have used this relationship in several other ASMs to describe SMP production. Models presented by some of these authors correspond well to experimental results (Lu et al. 2001), but do not shed light on UAP or SMP metabolism.

Because the UAP production rate and the biomass growth rate are proportional to the intracellular metabolite concentration, we could represent this model graphically (Figure 2-1). The UAP production could thus follow an exponential relationship in relation to growth rate, as proposed by Hao and Lau (1988). Modeling UAP production during nutrient or oxygen shortages and assessing the effect of storage processes is possible with this representation.

Another part of the SMP consists of high molecular weight products and is associated with endogenous respiration or cellular lysis of the biomass (BAPs). These high molecular weight SMPs seem to be mainly humic and to have toxic effects on biomass (De Souza Melo 1984). Other BAPs seem to form at the end of the exponential growth period, such as certain EPSs (Davies 1999), or during toxic or thermal shocks (Barker and Stuckey 1999). Biomass associated products included several molecules, and additional research is required to identify all their production mechanisms (Barker and Stuckey 1999).

2.4.2.1 Aerobic fermentation

Several authors (Akesson et al. 1999; Aon and Cortassa 2001; Chang et al. 1999; Doelle et al. 1982; Han et al. 1992; Majewski and Domach 1990) have reported aerobic fermentation processes that can be associated with UAP. However, the inclusion of fermentation products in UAPs remains a topic of discussion (Barker and Stuckey 1999).

It seems that above a critical substrate uptake rate, aerobic respiration can limit growth rate (Han et al. 1992; Majewski and Domach 1990; Akesson et al. 1999). Moreover, in such circumstances the aerobic respiration should be downregulated and this can further limit the growth rate (Doelle et al. 1982). Different hypotheses have been proposed to explain this phenomenon. Han et al. (1992) propose a limited capacity in the tricarboxilic cycle (TCA). According to Chang et al. (1999), when the respiration chain is rate limiting, the $NADH/NAD^+$ ratio increases, and thus the TCA enzymes are inhibited. However, these authors also showed that aerobic fermentation is due to an oversupply of pyruvate, and a mutant capable of PHB storage could maintain a normal growth rate. Aon and Cortassa (2001) showed that nitrogen-related anabolic fluxes would determine when ethanol fermentation is triggered. Han et al. (2002), using the concentration of the intracellular

metabolites showed that there is no bottleneck and proposed that the decline in μ is associated with a specific soluble microbial product, which is induced by the population density. This specific microbial product is usually called a quorum sensing signal.

Aerobic fermentation seems to be an overflow of the metabolism, but no clear trend was found in the literature to explain the regulation mechanism of this process.

Thus, limitation of the growth rate by aerobic respiration could be introduced into the model at a later stage, when this process is better uderstood.

2.4.3 Production of exopolymers (EPS)

Exopolymeric substances, or exopolysaccharides are a particular type of SMPs. The literature focuses on them because they represent the main biofilm "glue" or matrix and their production kinetics seems different than that of other SMPs (Characklis 1990).

Alginate is an EPS-type substance produced by *Pseudomonas*, among others, and it is one of the main components of the glycocalyx, or bacterial biofilm (Davies, 1999). It does not seem that EPSs build food reserves, as most bacteria cannot degrade the EPSs they produce (De Vuyst et al. 2001). However, Sutherland (2001) states that several species have enzymes capable of depolymerising EPSs. These enzymes would be intracellular, but cell lysis could help them attack EPSs.

It appears that EPS production is encouraged by the same conditions favouring PHB or glycogen synthesis, and it seems to compete for glucose 6-phosphate or glucose 1-phosphate (De Vuyst et al. 2001; Sutherland 2001; Ramos et al. 2001).

There is relatively little information on factors triggering EPS production in the environment, as the production level is generally not detectable (Davies 1999).

Davies (1999) speculates that the triggering factor in EPS production is a communication signal of the "quorum detection" type. The signal comprising a homoserine lactone type of molecule seems to control several genes, including production of EPSs and a regulon triggering the stationary phase. This author's hypothesis seems to be in accordance with the fact that EPS production is inversely proportional to the growth rate.

In short, EPSs do not build food reserves but can be hydrolyzed by enzymes released during lysis. The production level is generally undetectable in the environment (Davies 1999). Production modeling EPS would thus be required only when modeling biofilm or floc formation.

2.4.4 Conclusion

A schematic representation of the main metabolic pathways in the proposed model is shown in Figure 2-1. A similar representation was initially proposed by Dircks et al. (2001). In Figure 2-1, exogenous substrate is taken up by the cell to form an intracellular substrate. The induction intensity of transport enzyme is regulated by the concentration of the exogenous substrate. The cell can grow on the endogenous substrate, make stored products or produce UAPs. The proposed model includes proportional expression of enzymes for synthesis and degradation of reserve products, and the expression level is regulated by the endogenous substrate concentration in the cell. The UAP production rate is proportional to the concentration of endogenous metabolites. With this view, the UAP production rate can be modeled during a nutrient or oxygen limitation and the effect of the storage processes can be assessed. Therefore, UAP formation would be associated to the level of endogenous substrate, which slightly modifies the definition of UAPs and BAPs. Usually it is assumed that UAP are produced at a rate proportional to the rate of substrate utilisation and BAP are produced at a rate proportional to the concentration of biomass. According to the new definition, the UAP production rate would be proportional to the concentration of intracellular substrate. Thus, it would be strongly dependent on the substrate consumption rate, but with this definition the UAPs could still be produced after the depletion of the exogenous substrate. With this new definition the Luedeking-Piret type equations will be less usefull for modeling UAP formation and the synthesis of some others SMP (produced at the end of the exponential growth) would be modeled with the process describe previously . Therefore, BAP formation (produced during the endogenous phase) would be associated only with decay or cell death processes.

2.5 Protein synthesis system

According to the literature, proteins represent the greatest part of cellular biomass (Bremer and Dennis 1996; Herbert 1976). The protein content of a suspension is sometimes used to define cellular biomass (Atlas and Bartha 1998). Some authors argue that "…exponential growth can be monitored as increase in proteins; this implies that growth regulation is closely coupled to control of ribosome synthesis…" (Zhang et al. 2002). Therefore, in this literature review, the PSS has been subjected to a comprehensive study to define the major determinants regulating growth rate.

Several observations indicate a correlation between the magnitude of the PSS (or the rRNA) and the cell growth rate (Bremer and Dennis 1996). Correlation between the rRNA/DNA ratio and growth rate has been clearly demonstrated for various continuous cultures with a high growth rate. This correlation is no longer valid when the growth rate decreases, which is characteristic of activated sludge (Bremer and Dennis 1996; Muttray et al. 2001; Cangelosi and Brabant 1997).

The rRNA molecule is quite stable and does not give a good indication of the growth rate under transient conditions (Cangelosi and Brabant 1997; Muttray et al. 2001). Like the rRNA molecule, the tRNA is stable (Björk 1996), and therefore it does not yield additional information on the variation in growth rate either (Bremer and Dennis 1996; Davis et al. 1986). Pre-rRNA (a product of transcription) is a better alternative than rRNA because it has a relatively short half-life and it seems to give a better indication of the cell metabolic state during short length transients (Cangelosi and Brabant 1997; Muttray et al. 2001; Oerther et al. 2002).

The messenger RNA (mRNA) molecule has a short time constant, and some authors argue that this component or transcription itself could play a role in regulating the growth rate (Roels 1982; Vanrolleghem et al. 1998; Zhang et al. 2002).

It is well known that transcription is a key step in the regulation of the ribosome concentration and transcription of the ribosome gene (rrn) has been studied widely (Zhang et al. 2002). Some authors (Shepherd et al. 2001; Zhang et al. 2002) observed that the transcription rate is limited by the RNA polymerase concentration in the cell. These authors

proposed that the transcription activity could be described by a classical Michaelis-Menten kinetic model of free RNA polymerase concentration. Moreover, adenosine triphosphate (ATP), guanosine triphosphate (GTP), and ppGpp regulate the initiation step of the transcription process of gene coding for ribosomal constituents (Jöres and Wagner 2003).

Simulation with mathematical models that include a component with a short half life could fit the variation of the growth rate during short transients (Baloo and Ramkrishna 1991). The time constant of this component is several times shorter than that of rRNA. However, such a model would not be able to describe the long transient behaviour without changing the time constant of this component. Thus, some additional components are needed to model the PSS and thus, short and long transients without changing the time constants and parameters of the model.

The literature review that follows gives an overview of the PSS and its regulation with a view to finding the best way to model short and long transient behaviour of the active biomass.

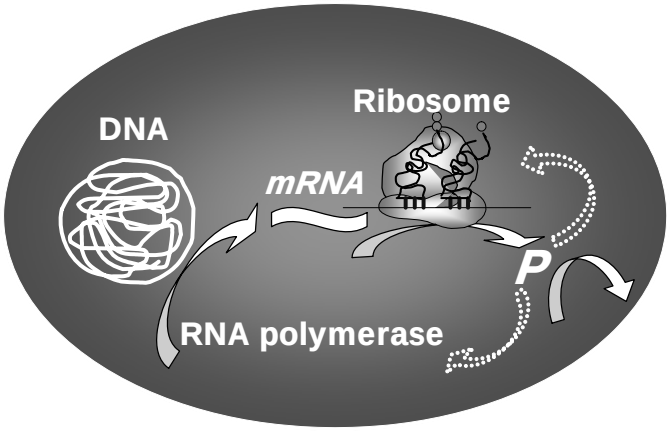

DNA, deoxyribonucleic acid; RNA, ribonucleic acid;
mRNA, messenger RNA; P, proteins.

Figure 2-2 The conceptual model of the protein synthesis system

2.5.1 The chosen conceptual model of the protein synthesis system

According to the preceding and following discussions, Figure 2-2 shows the conceptual model of the PSS. In this model, three components i.e. mRNA, rRNA and RNA polymerase make up the PSS. According to this view, protein is synthesized in two steps. During the first step, the RNA polymerase transcribes the DNA code to produce mRNA. In the second step, ribosomes translate the mRNA to produce proteins. The transcription and translation are mimicked by a classical Michaelis-Menten kinetic mechanism. Zhang et al. (2002) and Draper (1996) used similar equations for the kinetic description of transcription and translation initiation respectively. Obviously, the real process is much more complex than this representation, and several steps and components are not included in the model.

2.5.2 Regulation of the protein elongation process

The objective of this paper is to present a model that mimics the variation of the specific growth rate of an active biomass. Thus, in the following paragraphs, some important factors in the regulation of these processes are highlighted.

2.5.2.1 Transcription regulation

The search for the determinants of the rate of transcription initiation remains at the frontiers of research (Record et al. 1996). Subunits of RNA polymerase or various elongation factors can alter the transcription rate of specific genes according to the metabolic state of the cell (Richardson and Greenblatt 1996). Therefore, the adequate description of the transcription rate of a specific gene is a complex task.

However, from a more general point of view, some authors have tried to find some of the most important determinants of the overall transcription rate. For years, many authors (Gallant 1979; Jensen and Pedersen 1990; Östling et al. 1993; Nyström 1998) state that the stringent response regulates the transcription process. The stringent response is usually observed during shift down experiments through the regulation of some energy carriers, e.g., ATP, GTP, ppGpp in the cell. Thus, this mechanism was studied during shift-down

and shift-up experiments because it exerts an overall control on the protein synthesis process.

2.5.2.1.1 Shift down experiment and the stringent response

The stringent response seems to be an overall control mechanism of cell metabolism. The availability of carbon substrate and amino acids regulates this mechanism (Östling et al. 1993; Nyström 1998). When amino acids or carbon are deficient, the ppGpp synthease protein (RelA) fastens to the (vacant) active site of a ribosome and transfers phosphorus from ATP to GTP to form ppGpp (Cozzone 1981; Arbidge and Chesbro 1982; Gerdes 2000). Accumulation of ppGpp in the cell is related to the induction of the stringent response (Gallant 1979; Cozzone 1981; Stouthamer 1984; Östling et al. 1993; Nyström 1994; Gerdes 2000). According to Zhang et al. (2002), ppGpp decreases the activity of the initiation step, and thus the rate of transcription. Other studies (Nomura 1999; Schneider et al. 2002) showed that the RNA polymerase activity is regulated proportionally to GTP and ATP. More specificaly, some authors recently showed that GTP and ATP compete with ppGpp for the active site of RNA polymerase during the initiation step (Jöres and Wagner 2003). Several biochemical models are proposed in the literature, and for all of these initiation remains a key step in the transcription process (Jöres and Wagner 2003; Schneider et al. 2002; Zhang et al. 2002).

Thus, according to these authors, the transcription activity is limited by the RNA polymerase concentration, and the activity of this enzyme is regulated by the energy carriers (Jöres and Wagner 2003; Schneider et al. 2002; Zhang et al. 2002). So, the first effect of stringent response is to downregulate the RNA polymerase activity with the decrease of GTP and the increase of ppGpp levels.

Thus according to the previous discussion, with the stringent response the GTP level decreases (and the ppGpp level increases), the transcription and the translation slow down, and owing to its high turnover, the mRNA level decreases. As ribosomes are more stable than mRNA, the latter decreases faster and, under these conditions, ribosomes become in excess relative to the actual growth rate. The observations of Flärdh et al. (1992) showed that slow-growing cells could have more ribosome than required. In other words, in slow-

growing bacteria, ribosomes are undersaturated by mRNA, and according to the Michaelis-Menten kinetics, a larger part of ribosomes is in stand by. Effectively, the translation rate can be described by a kinetics that is dependent on the availability of mRNA and the ribosome subunits (Draper 1996). This phenomenon could explain the loss of linearity of the correlation between the rRNA/DNA ratio and the growth rate under slow-growth conditions, as in activated sludge.

2.5.2.1.2 Shift up experiment

Some observations have shown that one of the first effects of a nutritional enrichment of a slow-growing biomass is an increase in the RNA synthesis rate (Kjeldgaard et al. 1958; Koch and Deppe 1971; Cangelosi and Brabant 1997). A nutritional enrichment leads to an increase in the ATP level of starved cells (Atkinson 1977). After a shift up, because the GTP level is in tight equilibrium with the ATP level (Borel et al. 1997), the GTP will increase with the ATP, and the activity of RNA polymerase will increase quickly with ATP and GTP availability. The variation of the ppGpp level occurs within 1 or 2 min (Molin et al. 1977; Lagosky and Chang 1980) and Koch and Deppe (1971) clearly showed the start-up of the transcription process within 2 min after a shift up. So, after a shift up, the transcription rate increases and with the increase of mRNA level, the waiting ribosomes will translate the newly synthesized mRNA, and raise the growth rate. Accordingly, some experiments have shown that transcription and RNA availability limit the process over only a short period of time after induction (Sandén et al. 2002; Vanrolleghem et al. 1998). The limitation of protein elongation by transcription could explain the cell's ability to increase quickly the growth rate as discussed by Daigger and Grady (1982a). Thus, it is possible to make the hypothesis that in addition to rRNA, mRNA is a key component in the description of the growth rate (Vanrolleghem et al. 1998). Because mRNA has a short relaxation time, this component could explain some of the observed short transient behaviours of active biomass.

After the end of the limitation by transcription, other processes will limit the growth rate. As discussed previously, a correlation between the rRNA/DNA ratio and the growth rate has been clearly demonstrated for various continuous cultures that are cultivated at high growth rate (Bremer and Dennis 1996). Thus, the translation process is also a key step in

the description of the growth rate; this is known as the rRNA theory (Daigger and Grady 1982b). The following paragraph discusses the regulation of this process.

2.5.2.2 Translation regulation

As mentioned previously, the stringent response directly regulates the transcription through GTP. The GTP molecule is also required in several steps in the protein synthesis process (Prescott et al. 1990). According to Nomura (1999), the transformation of this nucleotide into ppGpp during the stringent response can limit the rate of the translation process. Schneider et al. (2002) showed the dependence of the translation rate on the ATP and GTP concentration. Thus, transcription and translation are tightly co-regulated, as suggested by Jensen and Pedersen (1990).

In fast growing cells, the fraction of ribosome subunits engaged in translation is constant, and with increasing growth rate, the mRNA becomes more crowded with ribosomes (Bremer and Dennis 1996). The fact that the fraction of unengaged ribosomes is constant under various growth rates, according to the saturation equation proposed by Draper (1996), indicates that the amount of ribosome subunits limits the protein synthesis rate. Elsewhere, Cole and Nomura (1986) stated that the translation process limits the growth rate.

According to Draper (1996), binding of the ribosome subunits to mRNA is a key step in the translation process. The observed translation rate depends on the binding constant, the concentration of ribosome subunits and mRNA availability (Draper 1996; de Smit and van Duin 1990). So, in some circumstances, a low level of mRNA could limit the translation rate. However, the relaxation time of mRNA synthesis is small, and transcription (and thus mRNA availability) limits the process over only a short period of time after induction (Sandén et al. 2002). During exponential growth, translation seems to be the limiting factor of protein synthesis (Cole and Nomura 1986; Sandén et al. 2002). Thus, in sequence, either mRNA or rRNA could limit the rate of protein elongation and the growth rate.

2.5.3 Regulation of the synthesis rate of the protein synthesis system

Beyond its direct regulation on transcription and translation, it seems that GTP can also indirectly affect the size of the PSS (Jensen and Pedersen 1990).

The decrease in GTP caused by the stringent response will decrease the rRNA and mRNA synthesis rates. The stringent response results in a drop in the production of the elements that constitute the ribosomes and thus in the concentration of ribosome in the cell. The quantity of ribosomes will thus be adjusted to the availability of precursors and the specific elongation rate of each remaining ribosome will increase. The ppGpp synthesis rate will thus decrease and the equilibrium state will be a compromise between the number of ribosomes and their specific synthesis rates (Jensen and Pedersen 1990).

The ribosome proteins (r-proteins) and RNA polymerase are ribosome products as well. Therefore, the regulation of their synthesis rate could also be controlled by transcription and translation. Because “the specific rate of protein synthesis changes much more slowly than the specific rate of RNA synthesis ” (Koch and Deppe 1971), it appears that the translation rate limits the rate of ribosome assembly. Cole and Nomura (1986) stated that a translational feedback regulation is in fact responsible for the apparent growth-rate dependency of the synthesis of r-proteins. The translation rate, and thus the ribosome level, could limit the rate of increase of ribosome level or the increase of growth rate (Cole and Nomura 1986). Accordingly, an increase in the ribosome concentration will show a larger relaxation time than that of RNA synthesis, as shown by Cangelosi and Brabant (1997). In this experiment, after a shift up, the level of mRNA increased quickly and reached a stable level after a few minutes, but the level of stable rRNA showed only a slow increase over 4 h. In these conditions, after a few minutes, the ribosome concentration becomes the bottleneck of the protein synthesis.

So, for modeling purposes, we could assume that translation limits the growth rate and the increase of the growth rate after a shift up. Thus, in the model, the ribosome synthesis rate will increase with the square of the growth rate, as observed by Keener and Nomura (1996b).

The rate of mRNA synthesis is dependent on the RNA polymerase level (Jöres and Wagner 2003; Schneider et al. 2002; Zhang et al. 2002), and the level of the latter is proportional to the ribosome level (Bremer and Dennis 1996). In *E. coli*, several genes of the RNA polymerase subunits are located directly downstream from the gene for ribosome subunit proteins (Berlyn et al. 1996). Some are co-expressed with the ribosome subunit proteins after attenuation (Steward and Linn 1991). Thus, the synthesis of RNA polymerase should be modeled in proportion to the ribosome synthesis.

2.5.4 Conclusions

For modeling purposes, it appears possible to model the regulation of the cell growth rate using a mathematical representation of the PSS. Modeling of ribosome, RNA polymerase and mRNA levels within the cell could be a first step in a proposed model. These components will describe the limitation by transcription under stringency, and the limitation by translation under fast growth conditions. Accordingly, after a shift up, the growth rate will increase quickly with mRNA and afterwards it will increase slowly with an increasing ribosome level, as observed by Kjeldgaard et al. (1958) and Cangelosi and Brabant (1997). Under slow growing conditions, because mRNA has a high turnover, it will reduce quickly, and according to the Michaelis-Menten kinetics, the ribosomes will be in excess when compared with the actual growth rate. This seems to be in agreement with the observations of Flärdh et al. (1992).

The regulation of transcription and translation is shown in Figure 2-3. In this figure, the processes are represented by bold arrows and the process regulation by dashed arrows. The components are represented by blocks. The substrate transport process is modeled by the uptake of the external substrate (S_S) and the endogenous substrate (B_S) formation. The transcription process is modeled by the increase of the short half life component, mR. The RNA polymerase and the ribosomes are modeled with the growth enzyme component, E_G. The component mR has a short relaxation time as does mRNA whereas E_G has a longer one similar to rRNA. The concentration of these components in the cell (mR/X_H or E_G/X_H) regulates the rate of the growth process (μ_H) as well as the rate of increase of their own concentrations. According to the previous discussion, the component mR limits the growth

rate under stringency, and the component E_G will be the bottleneck of the process during fast-growth conditions. As E_G regulates the growth rate as well as its own concentration, it increases with the square of the growth rate. After a down-shift, E_G is in excess compared with the actual growth rate.

The schematic representations shown in Figs. 2.2 and 2.3 are coherent with the current understanding presented in the literature. The ATP and the GTP are not modeled because these components have very short relaxation time. In the model, the energy level could be assumed to be proportional to the concentration of the intracellular substrates (Daigger and Grady 1982a). Moreover, the variation of the concentration of metabolites in the cells induces short transients (Chassagnole et al. 2002; Vanrolleghem et al. 2004) with a time constant of the same magnitude of ATP and GTP variations.

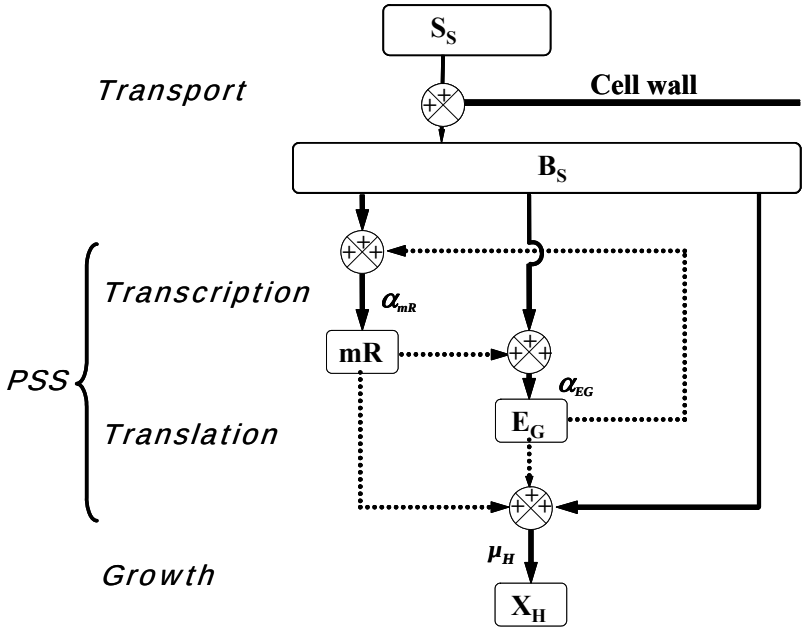

S_S, external substrate; B_S, endogenous substrate; mR, short half-life component of the PSS; α_{mR}, production rate of mR; α_{EG}, production rate of E_G; μ_H, growth rate of heterotrophic organisms; X_H, heterotrophic organisms.

Figure 2-3 Schematic of the protein synthesis system and growth rate regulation mechanisms.

2.6 The decay of biomass

Several factors may affect the assessment of the growth rate or more specifically, the decay of the biomass. Biomass maintenance and decay have a significant impact on the assessment of the growth rate (Herbert 1958, Pirt 1965). These two processes are two different interpretations of similar data and are usually described with a single parameter (Beeftink et al. 1990). However, some authors have modeled these two processes with distinct descriptions (Beeftink et al. 1990 Nicolaï et al, 1991). These were reviewed to propose a simplified metabolic representation that could lead to a mathematical definition.

2.6.1 Cellular death

The endogenous decay concept proposed by Herbert (1958) was used in most models and led to the concept of active and non-active biomass (Weddle and Jenkins 1971). "Discrimination between viable and dead microorganisms is a fundamental problem of microbiology" (Kaprelyants et al. 1993). So, first of all, one needs to specify the concept of cellular death and differentiate it from dormancy or a viable but nonculturable (VBNC) state. Indeed, according to some authors certain procaryote organisms may go into dormancy and survive long starvation periods (Huisman et al. 1996). Dormancy is characterized by a low specific activity (Kaprelyants et al. 1993). Other bacteria appear to maintain their normal metabolic activity but seem incapable of multiplying. Following specific protocols, some researchers have demonstrated that it may be possible to bring the cells back to a cultivable state. These observations are the basis of the VBNC cell concept (Kaprelyants et al. 1993). A debate on the exact definition of dormancy and the VBNC state is on-going. Nyström (2001) considers the VBNC cells as not yet dead. Nyström (2001) argues that the loss in activity of cells is the result of stochastic deterioration of proteins and DNA by attacks from reactive oxygen species. This author showed that loss of culturability can be counteracted by omitting oxygen in the starved culture, and argue that the apparent resuscitation of VBNC cells is the result of growth of a small fraction of already cultivable cells.

Alternatively, according to the concept proposed by Yarmolinsky (1995), toxin-antitoxin (TA) couples would be expressed continuously during growth. The toxin would have a

longer half-life than the antitoxin. Thus, in the absence of gene expression, a decrease in antitoxin concentration would leave the toxin free to act. Also, Aizenman et al. (1996) identified a TA couple called mazEF. Experimentations by these authors showed that the stringent response decreases the gene expression of the mazEF TA couple. Under experimental conditions and after abrupt increases in ppGpp (and thus an abrupt drop of GTP), only 15% of the cells survived. Moreover, the mazEF gene seems to be present in most procaryotes (Gerdes 2000).

Based on this metabolic model and because the mRNA transcription rate depends on the stringent response, the active toxin concentration in the cell should depend on the growth rate. Thus, cellular death would be regulated inversely to the growth rate, as stated by Mikkola and Kurland (1991).

However, the target of the toxin MazF is not well known, and thus the objective of this mechanism is poorly understood. A debate on the real effect of this toxin is still open. However, according to Yarmolinsky (1995), the DNA-gyrase is converted into a DNA-damaging agent by the toxin of the TA CcdA/CcdB, and could damage the DNA. Also, according to Yarmolinsky, some restriction enzymes and methylase belong to the toxin/antitoxin family. So, under stringency, restriction enzymes could cut DNA and cause damages. According to Yarmolinsky, cumulative damages would cause cell death.

The stringent response also induces SOS response (repair of DNA damage) (Nyström 1998). The SOS response is a mutagenesis-inducible response. The induction of the SOS response seems to be proportional to the number of lesions. Damage to DNA may give rise to mutations through the SOS response, or lead to cell death (Walker 1984).

A new hypothesis proposes the coupling of these two mechanisms. With damage to (by toxin) and repair of (by SOS response) DNA, the objective of the TA-SOS mechanism could be the production of stochastic mutations and cells that are better adapted to the new conditions. The cost of this mechanism is the death of many cells. Accordingly, a high number of mutations in cell cultures and mutants growing on dying cells are often observed at the onset of the stringent response (Huisman et al. 1996; Zambrano et al. 1993). These mutants seem to be well adapted for survival over long periods of starvation (Huisman et

al. 1996). Varying environmental conditions favour the rise of mutants showing an increase of fitness (Huisman et al. 1996; Hill and Gray 1988).

Moreover, cells with DNA injured by toxin, could maintain their enzymatic activity, but could be incapable of cell division. These cells could be VBNC. Under favourable conditions, DNA repair could regenerate the culturability of these cells.

Also, at the onset of stringent response, the cell downregulates synthesis of RNA, peptidoglycan, lipids, and proteins, and induces proteolysis and synthesis of the proteins that are required for stress adaptation and long-time survival (Nyström 1998). With the stringent response, the decrease of the specific activity and the toxin theory could explain the four states of the cell's viability (viable, dormant, VBNC, dead) that are observed in the literature (Masson et al. 1986).

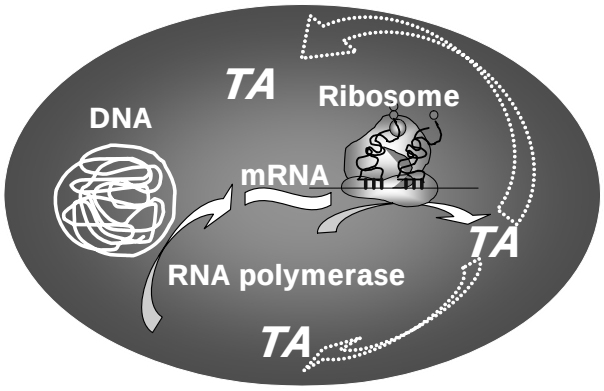

a) Production of the toxin-antitoxin couple during growth

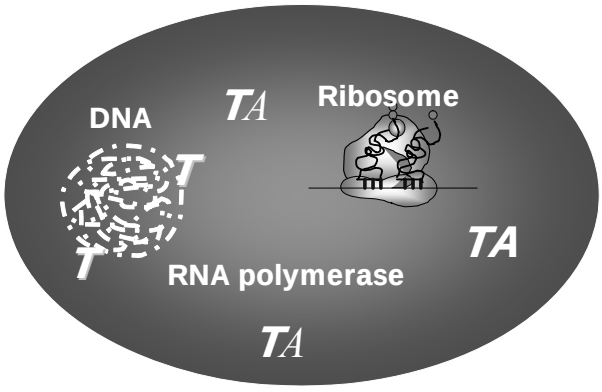

b) action of toxin during starvation

Figure 2-4 Regulation of toxin actions

These observations could reconcile the death school and the dormancy school. At the onset of starvation, the toxin becomes active, and causes mutations and cell death. With the onset of the stringent response network, the cell adapts by synthesizing survival proteins and mutating. When the concentration of toxin has decreased, the adapted cells might survive long periods of starvation. Further studies are required to validate this hypothesis.

In the proposed model, the production of a TA couple is included (Figure 2-4). In Figure 2-4.a, the cell is growing and produces TA. Under these conditions, the antitoxin is present and inhibits the toxin. In Figure 2-4.b, the cell is in an endogenous phase. The concentration of antitoxin decreases, and the toxin exerts its bactericidal effect. The fit of the model to the data should validate the hypothesis. However, as mutation is a stochastic process, it would be difficult to model the appearance of cells that are better adapted to the new conditions.

2.6.2 Maintenance energy

Survival over long starvation periods implies that, under these circumstances, energy expenditures for maintenance become almost negligible. McGrew and Mallette (1962) reviewed the opinions of microbiologists pertaining to cell energy needs. They defined maintenance energy as the energy required to compensate for the wear and tear caused by the action of physical and chemical agents in the cell, i.e. to maintain the status quo.

According to several authors (Pearson et al. 1991; Verduyn et al. 1991; Chudoba et al. 1992) the most significant specific energy expenditure (moles of ATP per 10^{-4}g of cells) is related to protein synthesis. Their data show that close to 70% of the energy expended for macromolecule replacement would be for protein synthesis. According to this theory, maintenance energy would increase with the protein level in the cell.

Kurland et al. (1996) also present a model showing that translation fidelity would depend on the elongation process rate and that the error percentage would increase exponentially above an optimal translation rate. However, Mikkola and Kurland (1991) do not establish a relationship between cellular growth rate and the energy expended to maintain translation fidelity. These authors established a relationship between the maximum growth rate and the

rate of the PSS, but they did not observe any relationship with translation errors. Also, during exponential growth, cells seem to maintain good translation fidelity (Nyström 1994).

Based on a model that relies on an ATP balance during various chemostat tests, Pearson et al. (1991) estimated the turnover rate of *E. coli* macromolecules at about 50% of the synthesis rate. Based on these observations, van den Berg (1998) proposes a model describing maintenance using a protein synthesis-decline process (turnover or active breakdown). In this model, the turnover rate of proteins increases with their expression level.

The stringent control network plays a role in maintaining the precision of the genetic transcription, this confirms the idea that metabolic changes occurring during a deficiency mainly target the maintenance of functional proteins (Nyström 1998).

Tempest and Neijssel (1984) consider that maintenance energy is associated largely with the maintenance of the ionic cellular potential. They consider that the renewal of various macromolecular components of the cell is only a small part of the energy required to maintain metabolic activity. According to them, maintaining the driving force of various ions through the membrane could represent a significant part of the maintenance energy. According to Stouthammer and Bettenhaussen (1977), leakages of protons through the membrane and the active transfer would "de-energize" the membrane (without consideration for ATP generation). They also note that proton leakages are less significant and active transfer can be associated mainly with growth activities. We would thus be in a position to believe that the energy spent under aerobic conditions for the renewal of macromolecules would be the main part of the macromolecule maintenance catabolism when there is no uncoupling between anabolism and catabolism.

A diminishing of carbon limitation would generate a loss in efficiency in cellular metabolism (Neissel et al. 1996). The accumulation of certain metabolites would favour the induction of futile cycles (or energy-dissipating processes) and hence the uncoupling between anabolism and catabolism. In fact, several hypotheses were postulated to explain the loss in efficiency of cellular metabolism during an exponential growth phase. Chang et al. (1993) noted an increase in the maintenance/growth ratio when measuring respiration

and CO_2 production in exponential growth cultures ($S_0/X_0>20$). A few authors (Liu et al. 1999; Liu 1999) propose equations to model the consumption of substrate associated with futile cycles. The Liu (1999) model adequately reflects some values found in the literature, but it does not explain the underlying metabolic processes.

On the other hand, Nilsson et al. (1984) showed that, for a given growth rate, the level of mRNA of some constitutive proteins was nine times the level observed for a growth rate that was five times lower. So, as the level of mRNA changes with growth rate, the maintenance of this component could change accordingly. This component should have an impact on maintenance because it has a high turnover.

In short, we can say that under stringent control maintenance is proportional to the mRNA and protein level of the cell. After release of the stringent control, futile cycles would significantly increase maintenance. In a first attempt, the proposed model could include a maintenance term proportional to the protein level in the cell. Futile cycles would be included in the model after further studies.

2.7 Extracellular factors

Some external factors can modify the evaluation of the actual growth rate of the active cells. They can include the population evolution in mixed cultures, and grazing by protozoa or higher life forms, e.g. nematodes.

2.7.1 Population changes

It is a well-known fact that selection phenomena occur in a continuous culture system at both the species and the mutation levels (Dykhuizen and Hartl 1983). So, in mixed culture systems, the variation of loading is generally accompanied by changes in population structure (Cassell et al. 1966; Grady et al. 1996). Obviously, modifications of kinetic parameters of the biomass are associated with these population changes (Grady et al. 1996; Kovárová-Kovar and Egli 1998).

According to Kovárová-Kovar and Egli (1998), the metabolic capacity (C) of a mixed population is the product of the sum of the number of organisms ($\sum N_i$) responsible for

substrate degradation, and their respective induction intensity (I_i). Thus, from a mathematical standpoint, if we are able to model the variation in induction intensity, only one variable ($\sum N_i$) would allow the representation of the variation in population structure. Werker and Hall (2001) used microbial fatty acids as an indicator of the population dynamics in activated sludge. Using the variation of the relative distribution of microbial fatty acids, they deduced a single variable to quantify the biomass activity variation. This shows that choosing a suitable model, makes it possible to model the population dynamics with a single variable. If the induction of cells is modeled, one part of the growth rate variation would be associated with the induction variation, and another part would be associated with the variation of the population structure. The part of the growth rate variation caused by the population structure variation would be modeled using a single variable as proposed by Werker and Hall (2001).

According to Dykhuizen and Hartl (1983), for a population composed of two bacterial species each one having one level of activity, the ratio of the two populations varies according to the following equation:

$$\ln\left[X_1(t)/X_2(t)\right] = \ln\left[X_1(0)/X_2(0)\right] + (\mu_{obs1} - \mu_{obs2}) \cdot t \qquad [2.1]$$

So, the evolution of a biocenosis, i.e. a biomass composed of several bacterial species, would depend on the difference of the observed growth rates and its composition would depend on the initial composition of the various species. In fact, the normalized sum of the differences of the observed growth rate could constitute a single variable representing the biocenosis evolution rate. However, the literature review did not reveal data that would permit the deduction of trends. Moreover, according to equation [2.1], a single cell might be able to become dominant given enough time. A single cell has little influence on the overall rate in an activated sludge. But after some time, a single cell could multiply and her daughters, which would grow more numerous could have a significant influence on the overall rate. Thus, long-term prediction of the biocenosis and rate of evolution will need continuous data acquisition to take into account the unquantifiable components as a single cell or small differences in the rates that would dominate eventually.

Clearly, further studies are required to find a mathematical formulation for a single variable that reflects or mimics the evolution of the maximal growth rate of a mixed population.

2.7.2 Predation

In activated sludge systems, protozoan growth may contribute to a significant part of the biomass decay rate (van Loosdrecht and Henze 1999). Protozoans and metazoans may constitute 10 to 20% (w/w) of the biomass (Madoni 1994) and exercise a significant part of respiration (Griffiths 1997). These protozoans and metazoans can directly consume the substrate, consume dead or live bacteria or, as the case may be, other protozoans (Gerardi et al. 1990; Atlas and Bartha 1998).

A bacterial population would develop in a completely different manner if protozoans were not present. From an ecological standpoint, the selective pressure exerted by protozoans modifies the population structure. It seems that the predation of protozoans on free or suspended bacteria favours the growth of flocculent species or at least the flocculation of species present (Ratsak et al. 1996; Pike and Curds 1971).

Predation induces cyclic variations in population density (Atlas and Bartha 1998). Protozoan predation is often defined by a Lotka-Voltera type relationship, but experiments rarely support this model (Atlas and Bartha 1998). So, one can ask how to model predation on a flocculated biomass composed of various bacteria, protozoan, and metazoan species that are found in activated sludge. Predation and growth of protozoans appear to be neglected aspects in modeled processes. Knowledge of these organisms represents a field of expertise to be developed. The ASMs simply used an overall decay rate including cell death and predation (van Loosdrecht and Henze 1999). Thus, when the time constant of the transient studied is shorter than the time constant of the variation induced by the predation process, a constant predation rate can be used.

2.8 Conclusion

Current models assume that cells or biomass have only a single level of expression of specific activity. The experimentally determined parameters are therefore inherently dependent on operating conditions and the configuration of the system studied (Henze et al.

2000). Actually, engineers use standard design rules and their knowledge to choose the process configuration or to optimize of the operation of a particular plant. Models are more often used, but in such cases, ASM are only of some assistance because they do not take into account the metabolic adjustment of the active biomass and subsequent variation of the parameters. Also, nucleic acid probes are now used more and more often in studies of wastewater treatment processes and microbial ecology (Amann and Ludwig 2000; Wilderer et al. 2002). So, quantification of active cells with probes will require models with further refinement in the description of active biomass because the variation of specific activity would then be taken into account. Thus, a new model would help in the understanding the transient behaviour of the activated sludge process and in the design and the operational optimization of the process. With such a model, it should be possible to find the intrinsic value of parameters defining the growth rate of the biomass on a given substrate.

Information from the literature review has been used to create a conceptual model which is presented in Figure 1-1 and Figure 2-2. The model included the main metabolic pathways as substrate transport, formation of endogenous reserve, formation of products, and protein synthesis. The model is a simplified view of cell metabolism, but it can produce good trends and was fitted on data of transient behaviour found in the literature (Lavallée et al. 2005a).

Here, the aim of the proposed model is to predict the varying growth rate of the active cells. The cell is separated into different components : endogenous substrate, endogenous reserves as glycogen or PHA, and some proteins or enzymes.

To complete the model, the metabolic state of the active biomass is introduced via a simplified representation of the PSS (see Figure 2-2). Modeling of ribosome, RNA polymerase, and mRNA levels within the cell could be a first step of a proposed model. In this representation, mRNA is produced by RNA polymerase and is used by ribosomes to produce proteins or enzymes. These enzymes produce the metabolites used by the cell for growth. As discussed earlier, the state of the PSS will set the rate of macromolecule elongation and thus the growth rate of bacteria. These components will model the limitation of the growth rate by transcription under stringency and by translation under fast growth rate conditions.

This description used by Lavallée et al. (2005a) fits quite well with the data related to the transients of fast- and slow-growing biomass.

CHAPITRE 3 MODÈLES À BIOMASSE STRUCTURÉE

La problématique consiste à trouver une représentation mathématique caractéristique du métabolisme des microorganismes, et donc à intégrer au modèle des constantes cinétiques à valeur intrinsèque, caractéristiques des voies métaboliques utilisées par les microorganismes lors des processus de dégradation du substrat et de croissance.

Un modèle à biomasse structurée doit être une représentation de différents composants qui ont une incidence sur la cinétique de croissance des micro-organismes, tout en étant une représentation simplifiée des modèles biochimiques complexes. Dans ces modèles, la cellule est représentée par plusieurs composants dont les interrelations modulent la variation des taux (Bailey et Ollis, 1986). Le nombre de composants requis dans le modèle dépend de leur temps de relaxation respectifs, et donc de leur influence sur la cinétique réactionnelle relativement à l'échelle de temps considérée. Ainsi, tel que proposée par Ramkrihsna (1983), l'approche est basé sur une stratégie invariable, définie par les interrelations entre les composants, plutôt que sur une cinétique invariable, tel que proposé dans les modèles classiques.

Daigger et Grady (1982a) ont fait une revue de littérature afin d'établir une description simple et structurée qui décrit les mécanismes de croissance de la biomasse qui concorderait avec l'ensemble des observations rapportées dans la littérature. Ces deux auteurs divisent les comportements transitoires de la biomasse en deux catégories, soit la réponse en stockage (storage response) et la réponse de croissance (growth response).

La réponse en stockage de la biomasse est relativement bien caractérisée et les modèles ASM 2 et 3 ont été proposés pour en faire la simulation. Toutefois la réponse en croissance de la biomasse caractérisée par Daigger (1979) est moins bien définie, et aucun des modèles utilisés en traitement des eaux usées ne décrit la cinétique observée.

3.1 Les modèles cybernétiques

Les modèles cybernétiques ont tout d'abord été proposés par Ramkrishna (1983) pour simuler la croissance sur de multiples substrats. Ces modèles ont été utilisés subséquemment par Ramkrishna et ses collaborateurs (Kompala et al., 1986; Turner et al., 1989; Baloo and Ramkrishna, 1991) pour modéliser la réponse transitoire d'une biomasse en croissance rapide dans un chemostat dont le taux de dilution était varié rapidement.

Dans les modèles cybernétiques, un ou des enzymes de transport du substrat (e_G) limitent la croissance. La cinétique d'accroissement des enzymes est régulée par d'autres composants cellulaires tel qu'une variable (R) qui représente l'ARN des cellules.

Le taux de croissance est défini par (Baloo et Ramkrishna, 1991) :

$$\mu = \mu_{\max} * \frac{e_{EG}}{e_{EG}^{\max}} * \frac{S}{K_S + S} \qquad [3.1]$$

ou e_{EG} représente la densité d'enzyme par unité de biomasse pour un état métabolique donné, et e_{EG}^{max} la densité d'enzymes à μ_{max}. Ainsi μ varie avec la concentration du substrat mais aussi selon un descripteur de l'état métabolique de la biomasse (e_{EG}/e_{EG}^{max}).

La vitesse à laquelle la biomasse va changer d'état métabolique (de_{EG}/dt) dépend d'une variable que les auteurs ont nommé ressource (R) et de la disponibilité du substrat. Aussi, les taux de croissance de R, de même que la croissance de l'enzyme e_{EG} seront définis par les équations 3.2 et 3.3.

$$r_R = \alpha_R * \frac{e_R}{e_R^{\max}} * \frac{S}{K_S + S} \qquad [3.2]$$

$$r_{EG} = r_{ER} = \alpha^{*}_{EG} + \alpha_{EG} * \frac{S}{K_S + S} * \frac{R}{K_R + R} \qquad [3.3]$$

Ainsi, le taux de croissance de la biomasse (μ) varie selon l'évolution de la concentration des enzymes limitants (e_G) qui dépend de l'évolution de la concentration des ressources R, qui dépend à son tour de l'évolution de la concentration de l'enzyme e_R (ou e_G par égalité dans l'équation 3.3). Puisque la cinétique donnée par la description mathématique dépend principalement de l'évolution de la densité de l'enzyme e_G, la réponse du modèle décrit principalement la cinétique induite par l'évolution de la densité des enzymes de transport du substrat.

Toutefois, lorsque le substrat est disponible en grande quantité, la biomasse a tendance à accumuler des réserves pour se donner un avantage compétitif (van Loosdrecht et al., 1997). Dans ces circonstances, le taux de transport du substrat est plus grand que la capacité anabolique de la biomasse et par conséquent ne constitue pas l'étape limitante de la croissance cellulaire.

Une autre structure que celle proposée dans les modèles cybernétiques doit donc être étudiée afin de décrire la réponse en croissance d'une biomasse capable d'accumuler le substrat sous formes de réserves.

3.2 Modèle proposé

L'article qui suit a été publié en 2005 dans la revue Journal of Environmental Engineering and Science, volume 4: 517–532.

MODELING THE METABOLIC ADAPTATIONS OF THE BIOMASS UNDER RAPID GROWTH AND STARVATION CONDITIONS IN THE ACTIVATED SLUDGE PROCESS

Lavallée B.[*], Lessard P.[*] and Vanrolleghem P. A.[†]

*Département de Génie Civil, Faculté des Sciences et de Génie, Université Laval, Québec, Canada, G1K 7P4.

[†]BIOMATH, Department of Applied Mathematics, Biometrics and Process Control, Ghent University, Coupure Links 653, B-9000 Gent, Belgium

Abstract: For wastewater treatment, the activated sludge models (ASMs) 1, 2, and 3 of the International Water Association (IWA) are accepted as industrial standard. However, many authors have observed that the kinetic parameters of these models depend on the type of substrate, process configuration, and sludge age. Some publications showed that the kinetic parameters of ASMs could be influenced by regulation of enzyme production. Therefore, an engineer aiming to make some modifications to a specific system is not able to predict the response of the real system after the modifications and choose the right configuration or modifications with the same set of parameters. On the other hand, cybernetic models are proposed for modeling cell growth and focus, among other things, on regulation of enzyme production, that is to say on induction. Thus, the objective of this paper is to present an activated sludge model that mimics the enzymatic induction of active biomass within the framework of ASMs. In the proposed model, process rates are modulated according to the environmental conditions and cell history. The model is fitted on the basis of data found in the literature. All data collected from short and long transient experiments were fitted with the same set of parameters, which was not possible with other models. The proposed model gives a more realistic picture of active biomass and of its specific activity under highly varying process conditions, but further research is required to support the model with experimental data.

Key words: activated sludge models (ASMs), activity, biomass, enzymes, induction, model, parameter, rate, regulation, sludge, transient.

Résumé : Les modèles de boues activées 1, 2 et 3 de l'International Water Association (IWA) sont acceptés comme la norme dans l'industrie du traitement des eaux usées. Toutefois, plusieurs auteurs ont remarqué que les constantes cinétiques de ces modèles dépendent du type de substrat, de la configuration du procédé et de l'âge des boues. Certains articles ont indiqué que les constantes cinétiques des modèles de boues activées pourraient être influencés par la régulation de la production d'enzymes. Ainsi, un ingénieur cherchant à modifier un système spécifique ne peut prédire la réponse du système réel une fois les modifications apportées, ni choisir la bonne configuration ou les bonnes modifications avec le même ensemble de constantes cinétiques. Aussi, des modèles cybernétiques sont proposés pour modéliser la croissance cellulaire et portent, entre autres, sur la régulation de la production d'enzymes, c'est-à-dire sur l'induction. L'objectif du présent article est donc de présenter un modèle de boues activées qui imite l'induction enzymatique de la biomasse active dans le cadre des modèles de boues activées. Dans le modèle proposé, les taux de réaction sont ajustés aux conditions environnementales et à l'historique cellulaire. Le modèle est calé sur les données trouvées dans la littérature. Les données colligées lors d'expériences transitoires à court et à long terme ont toutes été calées avec le même ensemble de constantes cinétiques, ce qui n'était pas possible avec les autres modèles. Le modèle proposé offre ainsi un regard plus réaliste de la biomasse active et de son activité spécifique sous des conditions de procédé hautement variables, mais une recherché plus poussée est requise pour soutenir le modèle avec des données expérimentales.

Mots clés : modèles de boues activées, activité, biomasse, enzymes, induction, modèle, paramètre, taux, régulation, boues, transitoire.

3.2.1 Introduction

During the last decade, many models were used to describe behaviour of wastewater treatment plants using activated sludge processes (e.g. Henze et al. 2000). In these models, kinetic parameters that depict the activity of biomass in the processes are assumed constant. The representation of active biomass can therefore be regarded as a static picture of its particular metabolic state. Authors of these models stated that these constant kinetic

parameters depend on the type of substrate, process configuration and sludge age (Henze et al. 2000).

However, the cell's metabolism is the result of a large number of biochemical reactions. These reactions are coordinated and regulated by different inhibitors and inducers. Thousands of enzymes exist, and hundreds could be involved in the active metabolism of the cell (Bailey et Ollis, 1986). Consequently, cells have a variable level of specific activity. For instance, Grady et al. (1996) showed that the value of the maximum growth rate of a particular sludge is linked to its metabolic state, and is dependent among other on the dilution rate in a chemostat. Many authors also showed that the maximum growth rate value will change with the applied substrate to biomass ratio S_0/X_0 in batch experiments (Chudoba et al. 1992; Daigger and Grady 1982a; Sin 2004). Furthermore, it was also shown that evaluation of kinetic parameters could be influenced by enzymatic induction (a mechanism inducing the production of a specific enzyme) (Çinar and Grady 2001; Grady et al. 1996; Lavallée et al. 2002; Sin 2004; Vanrolleghem et al. 1998).

Thus, variation in operating conditions of a treatment plant, or modifications made on the system, will induce variation in the specific activity of cells, but the model (with its constant parameters) will give a deviation from the response of the real system. For instance, it is well known that μ_{Hmax}, the maximum growth rate of heterotrophic biomass will change according to culture conditions (Daigger and Grady, 1982a). Also, K_{STO}, a parameter of the storage process in ASM3, is not universal, and its value changes with environmental conditions (Hanada et al. 2001). Variation of the process configuration or the operation mode changes the induction time of particular enzymatic chains. Thus, this changes the specific activity level of the biomass and the dependant parameters. A detailed literature review on process induction is given in a separate paper (Lavallée et al. 2005b). Therefore, an engineer aiming to optimize the configuration of a system, or to modify a specific system, is not able to predict the response of the real system after the modifications and choose the right configuration or modifications. Hence, further refinement of current models is desirable for process design and retrofitting.

To model enzymatic induction and metabolic adaptation, biochemical models have already been proposed in the literature (Jensen and Pedersen 1990; Zhang et al. 2002). In these

models, the protein synthesis system (PSS) will grow and decay with substrate availability or starvation. The state of the PSS will set the rate of protein formation and thus the growth rate of bacteria (Jensen and Pedersen 1990; Zhang et al. 2002).

Ramkrishna and co-workers (Baloo and Ramkrishna 1991; Kompala et al. 1986; Turner et al. 1989) proposed cybernetic models to mimic enzymatic induction of fast-growing bacteria. In these models, a structured representation of cells is adopted to mimic the growth and decay of some PSS components, called resource machinery. The cybernetic approach is based on an invariant strategy rather than an invariant kinetic response which is implicit in the framework of kinetic models (Ramkrishna 1983). Mathematical functions are used to model some induction mechanisms in addition to the usual kinetic functions. In these models, the enzymatic pool and resource machinery fluctuate with substrate availability and the history of the microorganisms. These models fit quite well to data collected in chemostat cultures with step variations of dilution rate. Liu et al. (1998) used a cybernetic model to describe the diauxic behaviour of activated sludge in the denitrification process. The significance of this short transient and influence of the induction time (the unaerated volume fraction) in the denitrification process was shown by Lee et al. (2004) using the model proposed by Liu et al. (1998). However, in this cybernetic model, only one component having a short time constant is used to mimic the PSS. Modeling longer transients as growth rate fluctuations (Frigon et al. 2002b) requires an additional component having a larger time constant (to mimic the stable RNA). To this end, different metabolic states of cells, that is to say, the adaptation speed of the cells to new conditions (Daigger and Grady 1982b) will be described using these two components (for a review see Lavallée et al. 2005b). Obviously, the real cellular processes are much more complex than the chosen representation, and several steps and components are not included in the model.

Thus, the objective of this paper is to present a model that mimics the variation of the specific activity of active biomass within the frame of the ASM models. The modifications done to ASM3 aim to model the variation of the process rates (defined in ASM3), and increase the prediction capabilities for a variety of process configurations. With a model able to mimic the regulation of the growth rate, it should be possible to access the intrinsic value of parameters defining the growth rate of biomass. As a consequence, it would be

possible to predict the response of continuous systems, or semi-continuous systems and batch processes with the same set of parameters. Hence, recalibration of the model to each process configuration would not be required as for ASMs. This will minimise the experimental work. Thus, after the model is calibrated with an effluent data set, it is conceivable that this mathematical tool can be used to perform design optimisation or plant retrofit.

In the proposed model, the biomass description is limited to heterotrophic biomass exposed to aerobic conditions. Extension of the model to anoxic conditions or inclusion of nitrifying biomass and phosphate accumulating organisms will need additional components and process descriptions. This will be topics of future work.

3.2.2 The chosen picture of biomass

It is difficult to choose the representation of biomass when one is building a model. Here, the aim of the proposed model is to describe the varying growth rate of the active cells. The only constituent that does not vary with growth rate is the mass of one nucleus. Obviously, growing cells could have more than one copy of the nucleus, but the mass of the nucleus could be used as a reference (Bremer and Dennis 1996). According to the data presented by Bremer and Dennis (1996) for *Echerichia coli* and Daigger and Grady (1982b) for *Pseudomonas putida*, the ratio of *structural proteins* (total proteins minus ribosomal proteins) to DNA remains constant for all growth rates. Also, Schaechter et al. (1958) suggested that the ratio of cell wall and membrane per nucleus remains constant for all growth rates. Their hypothesis is based on their observations that the ratio "surface areas of cell wall/nucleus" remains virtually constant. The same assumption is taken in the proposed model, and the cells will be represented by X_H, the mass of structural components built of one nucleus, and the corresponding amount of cell membrane and cell wall. Because the ratio of these structural components is assumed to be constant, the evaluation of active cells should be performed by measurement of the DNA concentration. Obviously, the model will not describe the various growth rates of a distributed population of bacteria, and it will model the mean growth rate of all cells.

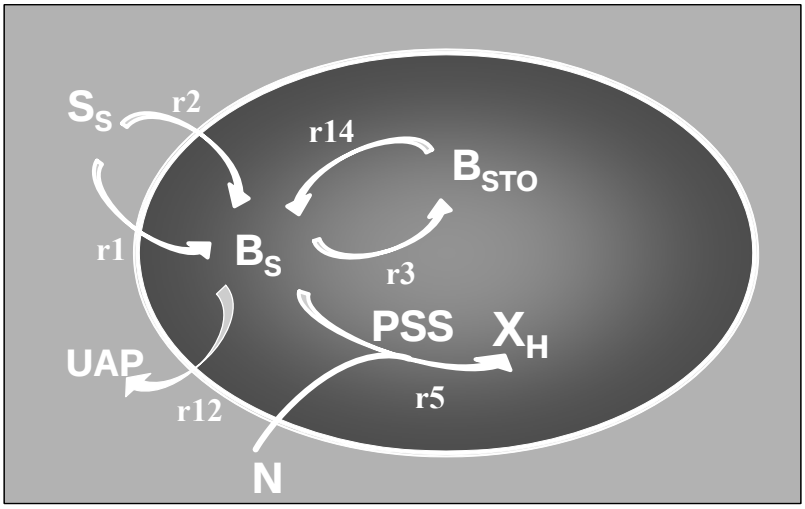

Figure 3-1 Diagram of the structured biomass

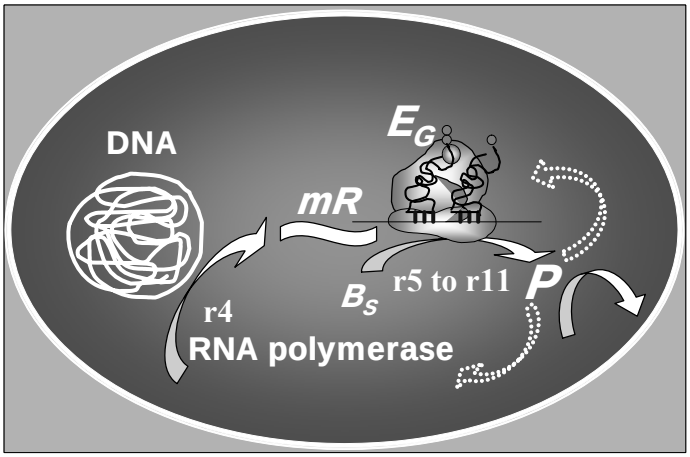

Figure 3-2 Details of the PSS

Different components are used to structure the chosen representation of biomass. The biomass chemical oxygen demand (COD) consists of endogenous substrate, endogenous reserves as glycogen or PHA, a simplified representation of the PSS and structural component. Specific model components are used to describe particular enzymes and their associated rates. The enzymes produce the metabolites used by the cell for growth and are those describing the reactions shown in Figure 3-1. A similar representation was initially proposed by Dircks et al. (2001) and was adapted by Lavallée et al. (2005b). In Figure 3-1, substrate (S_S) is taken up by the cell to form an intracellular substrate (B_S). The cell can grow on this endogenous substrate, make stored products (B_{STO}) or produce utilization associated products (UAP). The numbers (rX) close to the arrows in Figure 3-1 are the process numbers corresponding to the Peterson matrix (Table 3-3).

Proteins make up the main part of cell mass (Bremer and Dennis 1996; Daigger and Grady 1982a ; Herbert 1976). Thus, exponential growth could be seen as an increase in proteins (Zhang and al. 2002). This implies that growth and growth regulation is coupled to the state of the PSS which sets the rate of proteins formation (Zhang et al. 2002). In short, three components, i.e. messenger RNA (mRNA), ribosome (or rRNA) and RNA polymerase, make up the PSS. Proteins are synthesized in two steps. During the first step, the transcription step, the RNA polymerase transcribes the DNA code to produce mRNA. In the second step, the translation step, ribosomes translate the mRNA to produce proteins. During exponential growth, the number of ribosomes (the part of the PSS that assembles the proteins) shows a linear relationship with the growth rate of the cells (Bremer and Dennis 1996). Therefore, in the proposed model, the metabolic state of the active biomass is introduced via a simplified representation of the PSS (Lavallée et al. 2005b). The PSS representation is given in Figure 3-2. Transcription and translation are two key steps in protein synthesis (Zhang et al. 2002). The RNA polymerase limits the rate of transcription, i.e. synthesis of mRNA (Zhang et al. 2002), and its expression is regulated proportionally to the amount of ribosome proteins (Berlyn et al. 1996). Messenger RNA (mRNA) has a short half life, while rRNA which constituted a fixed fraction of the ribosomes, has a longer half life. Thus in the model, it is assumed that mRNA is modeled by the short half-life component of the PSS, *mR,* and stable rRNA is modeled by the growth enzyme E_G. Because RNA polymerase is coexpressed with ribosome proteins, it is modeled with the variable E_G too. Hence, in the model, mRNA is produced by E_G (RNA polymerase), and the latter is required as ribosomes for protein (P) or enzyme production.

The modeled processes are descriptions of the real processes. Therefore, the value of parameters should be chosen within the range of the values found in the literature with respect to time constants.

3.2.3 The proposed model

In the following paragraphs, the processes in Figs 3.1 and 3.2 are presented in a mathematical formulation. A complete mathematical description of the model is given in Table 3-3 to Table 3-5 using the Peterson matrix notation. In the proposed model, the

notation X refers to suspended materials, and S refers to soluble material as in ASM models. The notation B refers to endogenous material, as building blocks, E refers to an enzymatic structure. The concentrations of these are expressed as *X*, *S*, *B* and *E*, respectively, and are given in milligrams per litre. When the enzymatic component is expressed in specific value, the notation is expressed as E/X_H. The variable mR is used to mimic some components of the PSS, such as mRNA and is equivalent to an enzymatic structure. In the text, r*X* refer to the process rates in Table 3-3. Also, in the text saturation terms for O_2 and NH_4^+ are omitted from most of the equations. However, when required these terms are included in the equations of Table 3-3.

3.2.3.1 Modeling the growth rate fluctuations

In the proposed model, growth of heterotrophic organisms is regulated by concentrations of *mR*, E_G, and B_S. The concentration of ribosomes (rRNA) is mimicked by the variable E_G. So, the relative concentration of ribosomes within the cell is given by the ratio E_G/X_H. As shown in eq. [3.4], the ratio E_G/X_H is added to the growth rate equation proposed by Monod (1949). The ratio E_G/X_H reflects the metabolic state of the active biomass. It will change the growth rate of heterotrophic organisms, μ_H, according to the ribosomes concentration and to RNA theory (Lavallée et al. 2005b). As mRNA (mR) is required for the maximal rate of translation by ribosomes, a Michaelis–Menten equation is inserted in the proposed equation, too (Lavallée et al. 2005b). The saturation equation including mR will change the μ_H value according to the availability of mRNA (Lavallée et al. 2005b; Roels 1982; Vanrolleghem et al. 1998). This term will mimic the specific translation rate of ribosome. BS is the representation of the endogenous substrate or metabolites and building blocks.

$$\mu_H = \mu_{H\max}^{\text{int}} \cdot \frac{E_G}{X_H} \cdot \frac{mR/X_H}{K_{mR} + mR/X_H} \cdot \frac{B_S/X_H}{K_{BS} + B_S/X_H} \qquad [3.4]$$

The production rate of E_G (process r5 in Table 3-3) is described by equation 3.5 when O_2 and NH_4^+ are at saturation level. As shown in Figure 3-1, it is assumed that the ribosome (E_G) production is dependent on the rate of translation (Lavallée et al. 2005b), or in other words, of the E_G/X_H and $[mR]/X_H$ levels. Accordingly the E_G/X_H ratio and saturation equation for [mR] are introduced in equation 3.5. The parameter φ_{E_G} is a stoichiometric

coefficient related to the correlation between the growth rate and the protein production. The dependency on the availability of amino acids is mimicked by including the endogenous substrate B_S term.

$$r5_{(E_G)} = \varphi_{EG} \cdot \mu_{H\max}^{\text{int}} \cdot \frac{E_G}{X_H} \cdot \frac{mR/X_H}{K_{mR} + mR/X_H} \cdot \frac{B_S/X_H}{K_{BS} + B_S/X_H} \cdot X_H \qquad [3.5]$$

$$r4 = \alpha_{mR} \cdot \frac{E_G}{X_H} \cdot \frac{B_S/X_H}{K_{BS} + B_S/X_H} \cdot X_H \qquad [3.6]$$

In eq. [3.6] the α_{mR} parameter is the maximal production rate of the mR components. The expression of mR (or its rate of production r4) is completely inductive, and changes with the B_S and E_G concentrations. The RNA polymerase concentration is represented in eq. [3.6] by the ratio E_G/X_H . The number of RNA polymerases per nucleus is proportional to the amount of ribosome, and this for all growth rates (Bremer and Dennis 1996). Thus, the specific RNA polymerase concentration will be mimicked by the variable E_G and the ratio E_G/X_H. The activity of the RNA polymerases is different to the ribosome activity and is therefore modeled by the rate α_{mR}. In the model, the variable E_G has COD units. Hence, the active biomass COD is now composed of an amount of structural component (X_H) and a variable fraction, the biosynthetic constituent (E_G). The constituent E_G is endogenous; thus the mathematical description of biomass becomes (X_H+E_G). This description agrees with the description of biomass proposed by Masson et al. (1986) and van den Berg (1998). Thus, in the model, the specific COD of active biomass (COD/X_H) will rise and fall with E_G. The decay of E_G (process r15) and mR (process r19) are endogenous processes described as first-order reactions characterized by the "endogenous" rate constants β_{EG} and β_{mR}. This formulation is similar to the one used by Baloo and Ramkrishna (1991) for the decay of endogenous enzymes.

3.2.3.2 Modeling the substrate uptake rate

It was observed by several authors that the specific substrate uptake rate varies with growth conditions (Ferenci 1999; Kovárová-Kovar and Egli 1998). It was also observed that the rate of substrate uptake and storage in ASM3, is not universal, and the value of this

constant changes with environmental conditions (Hanada et al. 2001). It was furthermore shown that the substrate uptake rate is dependent on the concentration of several transport enzymes in the cell wall (Ferenci 1999). In the model, readily biodegradable organic substrate (S_S) is taken up by the transport enzyme (E_{BS}) to yield endogenous substrate (B_S). The accumulation rate is regulated by enzyme and substrate concentration. In this process, the variation of the specific substrate uptake rate will be mimicked by the ratio E_{BS}/X_H in eq. [3.7] (processes r1 and r2 in Table 3-3). Modeling of the production of transport enzymes will be done with an equation similar to the one proposed for production of E_G. The constant $k_{B_S}^{\max}$ is the maximum specific activity of the enzyme.

$$r1\ or\ r2 = k_{BS}^{\max} \cdot \frac{E_{BS(ha\ or\ la)}}{X_H} \cdot \frac{S_S}{K_{S(ha\ or\ la)} + S_S} \cdot \frac{S_O}{K_O + S_O} X_H \qquad [3.7]$$

However, the K_S constant could change with substrate, substrate concentration and growth conditions (Ferenci 1999; Kovárová-Kovar and Egli 1998). Ferenci (1999) showed that the level of expression of various transport enzymes of glucose is regulated by the substrate concentration. At low substrate concentrations, a transport enzyme with a high substrate affinity would be induced at a higher intensity than a second transport system with a low substrate affinity which is favoured at high glucose concentrations. Thus, the model includes two transport systems (process r1 and r2) with respective enzymes (E_{BSha} and E_{BSla}) and saturation constants (K_{Sha} and K_{Sla}). According to Ferenci (1999), in the model E_{BSha} production will be subject to catabolite repression at high substrate concentration.

3.2.3.3 Modeling the formation of endogenous reserves

It is well known that in some conditions, cells store substrate in the form of glycogen or PHB. Cells able to quickly use and store substrate possess a selective advantage over cells that cannot (van Loosdrecht et al. 1997).

Modeling of storage product formation (process r3) is done as suggested by Dircks et al. (2001) for glycogen and Beun et al. (2000) for PHB. Storage products (B_{STO}) are synthesized from endogenous substrate (B_S) through a single reaction.

$$r3 = \left(k_{STO}^{\max} \cdot \frac{E_{STO}}{X_H} \cdot \frac{B_S / X_H}{K_{BSla} + B_S / X_H} \right) \cdot X_H \qquad [3.8]$$

Also, as shown on Figure 3-1 degradation of storage product is modeled by a single reaction, and this process produces B_S. According to the expression of glycogen enzymes, the enzymes that synthesize and depolymerize B_{STO} are coexpressed by the same operon (Lavallée et al. 2005b). Therefore, these two enzymes should be modeled by the variable E_{STO} and the respective two rates k_{STO}^{max} and δk_{STO}^{max}. Obviously, depolymerization of B_{STO} (process 14) is regulated by its concentration and inhibited by high levels of B_S, as shown in equation 3.9.

$$r14 = \left(\delta k_{STO}^{\max} \cdot \frac{E_{STO}}{X_H} \cdot \frac{B_{STO} / X_H}{K_{STO} + B_{STO} / X_H} \cdot \frac{K_{Sha}}{K_{Sha} + S_S} \right) \cdot X_H \qquad [3.9]$$

The process rates are modulated by the ratio E_{STO}/X_H. Similar to E_G, production of E_{STO} is regulated at the transcription level. Consequently, the rate of formation or degradation of endogenous reserves will be modulated according to environmental conditions, as observed by Hanada et al. (2001).

3.2.3.4 Modeling the formation of soluble microbial products

In addition to the storage process, release of metabolites by the cell is often observed (Grady et al. 1972; Hao and Lau 1988; Huang and Cheng 1987). Utilization associated product formation may be significant, and the TOC or COD mass balance should take it into account.

Equation 3.10 models this process (r12).

$$r12 = k_{RBS}^{\max} \cdot \frac{B_S / X_H}{K_{RBS} + B_S / X_H} \cdot X_H \qquad [3.10]$$

In this equation, the constant $k_{RBS}^{\max}$ mimics the outward diffusion of metabolites through the cell membrane. A saturation equation is used to model this process. Thus, diffusion of metabolites through the cell membrane will be negligible at low B_S concentrations and

proportional to high B_S concentrations. The B_S diffusion will increase according to an exponential function relative to the growth rate. The half-saturation coefficients K_{BS} used in the growth equation could be set at a lower value than K_{RBS} used in equation 3.10. Thus, an excess of endogenous substrate will not significantly increase the growth rate, but it will induce an increasing release of B_S in the bulk liquid (Figure 3-3). This relation is in accordance with the exponential relation proposed by Hao and Lau (1988) for modeling UAP in a chemostat. Obviously, the real process is more complex than this representation, but for modeling convenience, a single step formulation is adopted as it was also done for storage formation. Moreover, because nitrogen is required for growth and is not required for UAP formation, this representation presents the opportunity to model the UAP formation under nitrogen limiting conditions. Also, a balance evaluation of storage on UAP formation is possible because the two processes are in competition for B_S utilization.

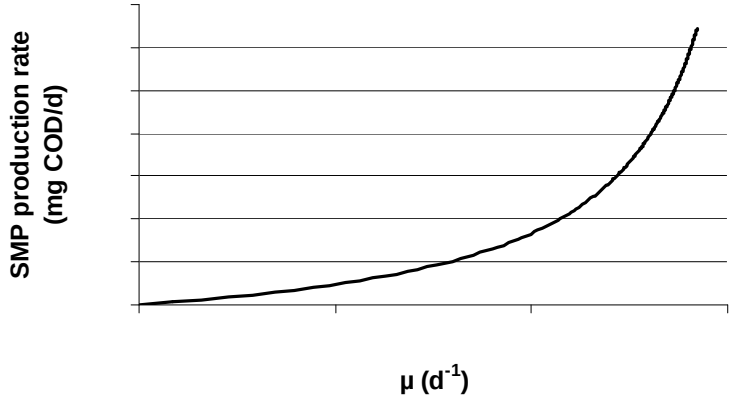

Figure 3-3 SMP production rates

The formation of soluble biomass associated products, which are released after exhaustion of the substrate, has not been modeled yet. However, this process has a significant impact on the COD concentration in the effluent and it will be included in the model after completion of further modeling studies.

3.2.3.5 Modeling the maintenance process

The decay of E_G (β_{EG}) is a continuous process, and thus occurs during both starvation and growth. Therefore, the biomass (E_G+X_H) uses substrate to maintain ribosome

concentrations at the desired level. The renewal of these enzymes will use the COD and a part will be used for respiration. This will be assumed to be the maintenance process. Thus, the E_G production and decay are a cycling process quite similar to the maintenance process proposed by Pirt (1965). According to Pirt (1965), maintenance is the use of substrate for other purposes than growth. Thus, in the model, the maintenance is proportional to the macromolecules turnover as proposed by some authors (Chudoba et al. 1992; van den Berg 1998). Then, oxygen used in the energy production process is coupled to the production of enzymes and the growth of active biomass. The decaying macromolecule E_G is used for energy production and leads to endogenous respiration and a loss of specific activity. Thus, the exogenous and endogenous respiration of active biomass are regulated as proposed by some authors (Beeftink et al. 1990; Nicolaï et al. 1991), with the model combining the Herbert (1958) and Pirt (1965) formulations of endogenous and maintenance metabolism, respectively.

Additionally, some energy could be spent in futile cycles as metabolites are released (Hao et Lau 1988). In this process, the constant $k_{RBS}{}^{max}$ mimics the outward diffusion of metabolites through the cell membrane. Thus, with the combination of the substrate uptake process and the release process, energy is spent in substrate uptake and release cycling.

Several additional processes could be included in the maintenance process (Lavallée et al. 2005b), but only some are included in the proposed equations to keep the complexity of the model at a reasonable level.

3.2.3.6 Modeling decay and death of active cells

As explained below, the proposed model makes a distinction between endogenous respiration and death of active biomass. The usual concept of active biomass decay includes grazing (process r24) and the influence of other external factors on cells (external decay as proposed by van Loosdrecht and Henze (1999)). Predation is a complex phenomenon that could be modeled with simple processes as in *River Water Quality Model No. 1* (Reichert et al. 2001). However, there is a general lack of information in the literature on kinetic description of grazing by protozoa in activated sludge. Future work will focus on DNA

extraction, as done by Brands et al. (1994), and inhibition of protozoa to give some information on the kinetics of cell death.

In the model, microfauna are modeled as a whole. They graze on active bacteria and cause decrease in the active biomass. Initially, a Lotka-Voltera equation form is adopted for modeling of microfauna growth (process r24). The microfauna component (X_{MF}) is associated with COD used and respiration. Also, the nitrogen fraction is assumed to be the same in microfauna as in active biomass. Therefore, respiration of micro fauna releases nitrogen in proportion to (1-Y_{MF}). Decay of X_{MF} is modeled by a simple fist order reaction (process r25).

On the other hand, the concept of cell death is proposed here (process r23 in Table 3-3); it consists of lysis and other internal factors affecting the cell. Death of active biomass can be induced by a toxin-antitoxin couple (TA) (Yarmolinsky 1995). The TA is produced by an inductive process that depends on the substrate concentration in the mixed liquor. The antitoxin (E_A) is produced by the cell during growth at a higher rate than the toxin, and neutralizes the effect of the toxin (E_T). However, antitoxin has a shorter half life than the toxin as shown by Aizenman et al. (1996). Thus, as suggested by Aizenman et al. (1996), only a short time after substrate depletion, the toxin could turn on its bactericidal effect (b_{XT}^{max}) (for a review see Lavallée et al. 2005b). E_A and E_T are functional components required for modeling, but not directly identifiable chemically. In the model, the toxin exerts its bactericidal effect when the E_A/X_H ratio is low as described by the Michaelis-Menten term in equation 3.12.

The rates of production of the toxin and its antitoxin (processes r10 and r9, respectively) are described as inductive processes dependent on endogenous substrate B_S and of the PSS state. Their decay is a simple first order process with different specific rates to account for the differences in half life. Modeling of antitoxin (equation 3.11) or toxin production will be done with an equation similar to the one proposed for production of E_G.

$$r9 = \alpha_{EA} \cdot \frac{E_G}{X_H} \cdot \frac{mR/X_H}{K_{mR} + mR/X_H} \cdot \frac{B_S / X_H}{K_{BS} + B_S / X_H} \cdot X_H \qquad [3.11]$$

Modeling of TA action on active biomass (process r23) is done with the following equation for the toxin induced death:

$$r23 = b_H^{\max} \cdot \frac{E_T}{X_H} \cdot \frac{K_{iT}}{K_{iT} + E_A / X_H} \cdot X_H \qquad [3.12]$$

In this equation, K_{iT} is the half-saturation coefficient of the toxin-induced death that is inhibited by the presence of the antitoxin.

3.2.3.7 Modeling the hydrolysis process

Previously, it was shown that variation of the hydrolysis process could be significant in evaluation of the COD fraction of the influent (Haïder et al. 2000). Here, for the same wastewater, the hydrolysis activities and COD fractions were found to be highly dependent on the sludge activity levels and the food to micro-organisms ratio. On the other hand, Frigon et al. (2002a) showed that different populations (the *Acinetobacter spp*. and an actinomycete) within the sludge could use different substrates (as S_S and X_{SS}) for growth. Therefore, a model should mimic the variable ability of sludge to hydrolyse suspended substrate (X_{SS}).

In the model, the hydrolysis rate (process r13) will change according to the specific density of hydrolytic enzymes E_h (equation 3.13). Indeed, hydrolytic enzyme expression is regulated by the substrate or substrate derivatives (Priest 1992). In the model it is assumed that the X_{SS} concentration (thus the derivatives) induces the production of hydrolytic enzymes. On the other hand, hydrolytic enzyme expression is subject to catabolite repression (Priest 1992). Hence, a switching function is added in the hydrolytic enzymes synthesis rate equation to mimic catabolic repression. Thus, enzymes will be produced only when the soluble substrate concentration, and thus the observed growth rate, is low (equation 3.14 and process r11). In addition, hydrolytic enzymes will only be produced when the necessary substrate concentrations are high. They are exogenous enzymes and are not affected by growth rate or decay of active biomass.

$$r13 = k_h^{\max} \cdot \frac{X_{SS}}{K_{XSS} + X_{SS}} \cdot E_h \qquad [3.13]$$

$$r11 = \alpha_{E_h} \cdot \frac{E_G}{X_H} \cdot \frac{mR/X_H}{K_{mR} + mR/X_H} \cdot \frac{X_{SS}}{K_{XSS} + X_{SS}} \cdot \frac{K_{Sha}}{K_{Sha} + S_S} \cdot \frac{B_S/X_H}{K_{BS} + B_S/X_H} \cdot X_H \qquad [3.14]$$

In equation 3.13, the substrate saturation function is adopted because Goel et al (1998) showed that hydrolysis of cellulose is dependent mainly on the enzyme concentration in the mixed liquor. Also these authors showed that the hydrolysis process is independent of the electron donor. Finally, E_h/X_H models the enzyme density per cell or flock surface used in ASM, as shown in equation 3.15.

$$k_h^{max} \cdot E_h = k_h^{max} \cdot \frac{E_h}{X_H} \cdot X_H \qquad [3.15]$$

The surface saturation function adopted in the ASM should be considered as a specific application of the more general representation chosen here.

3.2.4 Estimation of parameters

A number of new parameters are proposed in the model which includes 17 state variables and 41 parameters. This is seven state variables and 20 parameters more than used in ASM3 for description of heterotrophic biomass in aerobic conditions. Hence, new methods are required for evaluation of state variables and parameter identification. They are proposed in the following paragraphs. These new methods are based on transient behaviour data. These data are usually discarded when using ASMs because it is not possible to fit the response of the models to these data. Transient behaviour data give additional information compared with the steady state or the usual dynamic data. With these information rich data a multi-step identification procedure can be used to identify parameters one by one. Each parameter can be identified on a particular transient behaviour according to the transient time constants. Thus identification of each parameter can be done independently.

3.2.4.1 Evaluation of the active biomass

As proposed by Schaechter et al. (1958), in the model the ratio of cell wall to cell membrane per nucleus remains constant for every growth rate. The active biomass will be represented by X_H, i.e. the mass of structural components built of one nucleus, cell

membrane and cell wall. As the ratio of these structural components is assumed constant, evaluation of active cells as X_H can be performed by measurements of DNA concentration using a COD/DNA ratio.

According to the model assumptions, during exponential growth, the decay of active cells is not significant. Therefore in such experiment, the COD of suspended solids is equivalent to the COD of the cells (X_H+E_G+B_{STO}). The concentration of active cells (X_H+E_G) will be given by the COD of suspended solids minus the B_{STO} component. Also, the increase in growth rate is linked to an increase of E_G/DNA. The increase of COD per active cells ([X_H+E_G]/DNA) will give the increase of COD of E_G/DNA. The concentration of active cells (X_H+E_G) minus the COD of E_G will give the COD/DNA of X_H. Thus, with a DNA measurement, the X_H concentration expressed as COD should be available.

3.2.4.2 Evaluation of kinetic coefficients

Identification of parameters is done most easily by taking advantage of differences in relaxation times, or time constants. According to Roels (1982), the mass action law (substrate saturation) operates within milliseconds, mRNA control in a matter of minutes, enzyme production in a matter of hours, and selection within a population in a matter of days. It is possible to turn these time constants to our advantage, and make some simplifications in methods used for parameter evaluation. For instance, it is possible to choose an experimental design for evaluation of a particular coefficient, and make the assumption that variables changing with larger realxation time have constant value.

It is well known that the saturation of enzymes is reached within a few seconds, and usually this relaxation time is set to zero. According to the relaxation time as proposed by Roels (1982), in a batch experiment, the observable variables will increase or decrease along a sequence as explained below. The first one to increase will be the DNA transcript (Oerther et al. 2002; Cangelosi and Brabant 1997). This first increase of mRNA (mR in the model) induces a rapid increase of the growth rate. After the initial increase, the growth rate and RNA concentration per cell remain constant for at least 2 h (Kjeldgaard et al. 1958). Daigger and Grady (1982a) called this first increase of the growth rate, "the available reaction potential". The second observable variable is the stable rRNA concentration (E_G in

the model) which showed a slow and gradual increase (Cangelosi and Brabant 1997; Muttray et al. 2001; Oerther et al. 2002). This increase of stable rRNA concentration is correlated to the increase of the growth rate (Muttray et al. 2001). According to data presented by Daigger and Grady (1982a), this slow increase of the growth rate could take several hours, and is preceded by a lag phase. The length of the lag phase is dependent on the initial growth conditions, i.e. on the induction level of the sludge (the initial ratio E_G/X_H in the model). In the model, as the synthesis rate of E_G is dependent on its own concentration, the duration of this lag phase will be dependent on the initial concentration of E_G. Hence, the model is in agreement with the "unifying theory" proposed by Daigger and Grady (1982a).

Also, within biomass grown in a chemostat, by definition, different species of bacteria have the same growth rate. As discussed by Lavallée et al. (2005b), selection within a population will take place with the difference between the growth rates of these species. Thus, during the first few hours of a batch culture, the differential growth rate is small, and selection should not occur to a significant level.

Therefore, in a batch experiment, parameters can be identified done one at a time on a simple curve fit with adequate measurements. Albertson et al. (1990) observed an increase of the translation rate and a corresponding increase of the respiration after a substrate step-increase in batch experiments. Thus, DNA should be measured to estimate $\mu_{H,}$ and respiration rate for identification of parameters associated with mR and E_G/X_H. As mR has a short half life, a quick variation of μ_H will be caused by mR dynamics. A slow variation of μ_H will be caused by E_G/X_H variation as it has a greater half-life. As discussed by Lavallée et al. (2005b), during exponential growth, the death of active biomass (caused by toxin) is close to zero. Hence, independent identification of the growth rate of X_H and the production rate of E_G and mR is possible.

Obviously, during a batch experiment, release of substrate and storage could influence the growth curve. Hence, if glucose is used as soluble substrate, the glucose concentration and soluble COD concentration will have to be measured. Accordingly, the specific substrate uptake rate can be evaluated. A curve fit will give the uptake enzyme concentration (E_{BS}/X_H) when the specific rate reaches a constant value. A curve fit on the increase rate of

the specific substrate uptake rate, will give the production rate of the uptake enzyme (α_{EBS}). Similar methods can be used for identification of the production rates of other enzymes.

The decay of enzymes can be studied during starvation in a batch experiment. Biomass should be starved for several days. According to the time constants, biomass samples should be taken at constant intervals to build a time series. Consequently the decline of the growth rate or of the specific activity could be evaluated by performing pulse substrate addition experiments as done by Vanrolleghem et al. (1998). The half-life of mRNA is in the order of a few minutes, and the half life of stable rRNA or proteins is a few hours. The decline of the specific respiration rate during starvation should give the decay rate of *mR* (at the beginning of starvation with an interval of minutes) and of E_G (during the first day of starvation with an interval of hours).

Identification of the decay rate of active biomass should be performed by measurement of the decay rate of the endogenous DNA concentration.

Y_H will be obtained with the usual method for ASM calibration (Henze at al. 2000). As the time constant of the stable rRNA is in the order of hours, one could assume that the variation of rRNA will be limited during short experiments. The heterotrophic yield can then be determined from equations 3.16 and 3.17. Here, equation 3.16 is written two ways but both expressions have the same meaning. The substrate used should contain only soluble organic matter. If the substrate uptake and storage process occur simultaneously, equation 3.16 could be used. At the end of substrate uptake, the yield on stored product could be assessed with equation 3.17. B_S is assumed to be negligible at the beginning and the end of the experiment.

$$Y_{B_S} = \frac{(\Delta\, suspended\ \ solids\, COD - \Delta B_{STO}) \Big/ Y_H + \Delta B_{STO} + rO_{2\,maintenance} \Big/ Y_H \cdot \Delta t}{\Delta\, soluble\, COD} \qquad [3.16]$$

$$Y_{B_S} = \frac{\Delta\left[(X_H + E_G) \Big/ Y_H\right] + \Delta B_{STO} + (1 - Y_H) \Big/ Y_H \cdot E_G \cdot \beta_{EG} \cdot \Delta t}{\Delta\, soluble\, COD}$$

After exhaustion of soluble substrate one can evaluate the actual growth yield on B_S.

$$Y_H = \frac{\Delta(E_G + X_H) + (1 - Y_H) \cdot E_G \cdot \beta_{EG} \cdot \Delta t}{\Delta B_{STO}} \quad [3.17]$$

However, it is assumed that no respiration is associated with the synthesis of storage product ($Y_{BSTO/BS}$=1). As discussed by Dircks et al. (2001), a gap of only 4% is observed between the yield of biomass on internal substrate and the yield of biomass on storage product. This simplification is required for the easy independent identification of the yield constant Y_{BS} and Y_H.

The kinetic constants of the hydrolysis process can be identified from a curve fit on data from batch experiments (as carried out by Orhon et al. (1999) and Goel et al. (1998)). With sludge taken from chemostats operated at different dilution rates, the batch experiments will give different initial k_h values for the different sludges. The increase of the k_h rate along the experiment will give the α_{Eh} value. k_h^{max} will be found from a curve fit on the k_h variation and the corresponding value of E_h.

The variation of the structure of the population remains unknown. However, it is known that selection within a population can take more than days or weeks, and the relaxation time of this process is large (Roels 1982). Therefore, short experiments can be performed in which the population structure is assumed to be constant. Further research is required to obtain a formulation of this function.

3.2.5 Fitting the model to data

The value of a model is often expressed by its capacity to fit data. Therefore, data found in the literature were fitted with the model. It was built on GPS-X© using the spreadsheet utility Model Developper (Hydromantis Inc., Canada).

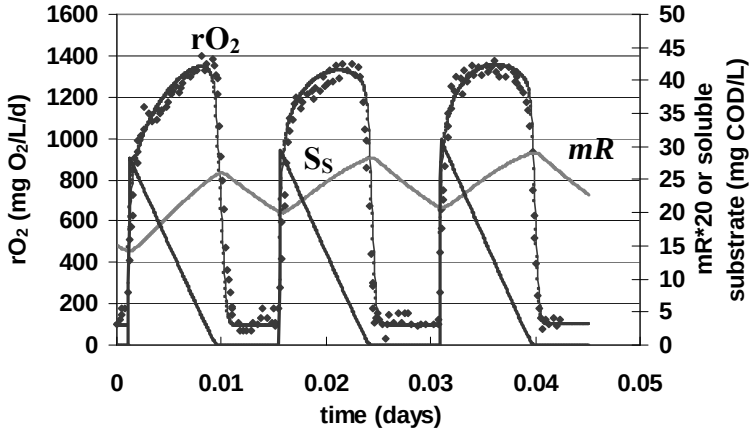

Figure 3-4 OUR start-up phenomenon observed when 3 pulses of S_S are dosed (data from Vanrolleghem et al. 1998)

Under aerobic conditions, the oxygen uptake rate (OUR) can be associated with the active biomass concentration and its specific activity. Some specific activity fluctuations (or specific growth rate fluctuations) are related to "endogenous variables" such as the mR and E_G levels. This complex behaviour can be observed in the data of Vanrolleghem et al. (1998) for OUR start-up phenomena when sludge starved for 12 h was dosed with three pulses of S_S with 22 minutes interval (Figure 3-4). The start-up phenomenon could be explained as following. The growth process induces an increase of the specific activity and starvation induces a loss of specific activity, resulting in a rise and a drop in growth rate and in OUR, respectively (Albertson et al. 1990). Albertson et al. (1990) observed a rapid increase of the transcription rate in the first 60 seconds. After the first minute the translation rate increased and within the first 10 min it reached 5 times the initial rate. This was accompanied by a proportional increase of the respiration rate. This observed behaviour is similar to that observed by Vanrolleghem et al. (1998). With the model, this behaviour is simulated as follows. Because mR has a short half-life, a decrease of the mR pool occurs during the 12 hours starvation period and after the exhaustion of the substrate. The available substrate is used for reconstruction of the mR pool, raising the specific OUR, as shown in the two first substrate pulses in Figure 3-4. After the second pulse, the mR concentration reaches the saturation level, and the decline of the specific activity associated with a decay of the mR concentration is not observed on the third pulse. The proposed

analysis is a simplified view of time-varying PSS activity, but the fit of the model with this experiment gives good agreement with the data.

Table 3-1 Identified parameters on experiment of Vanrolleghem et al. (1998).

Parameter	Symbol	units	Value
Maximal heterotrophic growth rate	μ_H	d^{-1}	30
Yield coefficient	Y_{BS}	COD/COD, g/g	0.92
Half saturation constant	K_{Sha}	COD, mg/L	0.2
Half saturation constant	K_{BS}	mg/mg/L	0.0015
Half saturation constant	K_{mR}	mg mg^{-1} L^{-1}	0.007
Ratio of production rate of E_G and μ_H	φ_{EG}	mg mg^{-1}	1.3
Production rate of *mR*	α_{mR}	d^{-1}	0.75
Production rate of E_{BSha}	α_{EBSha}	d^{-1}	15
Maximum specific activity of substrate uptake enzyme (high affinity)	k_{BSha}^{max}	COD, g g^{-1} d^{-1}	41
Decay rate of *mR*	β_{mR}	h^{-1}	2.083

With this simple experiment it is possible to identify β_{mR} and also α_{mR} since the time constant of E_G is larger. Indeed, the fit was quite sensitive to α_{mR} and β_{mR}. No storage occurred as no tailing of OUR was observed. The calculated level of internal substrate was always less than 5 mg COD /L (of bulk liquid) and this value is in agreement with those observed in the literature (Chassagnole et al. 2002; Vanrolleghem et al. 2004). Moreover, it was not possible to model the observed variation using only substrate uptake and storage without using the dynamics of the variable *mR*. Also, the identified value of β_{mR} gives a half-life of 20 minutes. This value is of the same magnitude as the half life of mRNA found in literature (Östling et al. 1993). Thus, the proposed mathematical formulation seems to be in agreement with the real processes. The parameters identified using this experiment are given in Table 3-1. The parameters identified in the fitting on data of Vanrolleghem et al. (1998) and additional parameters representing slow processes that are given in Table 3-2 were used to fit data first presented by Chiu et al. (1973). In these experiments, bacteria were cultivated in chemostats with imposed dilution rates, and the cells were taken out of the chemostats and put in batch reactors. Daigger and Grady (1982a) re-examined these data and showed that, an increase of growth rate took place within a few hours after the shift up and that the lag phase was dependent on the initial growth conditions.

To obtain the fit shown on Figure 3-5, only the initial values of state variables as X_H, E_G, [mR] and E_{BSha} and E_{BSla} were changed. The set of parameters used, is given in Table 3-2. The parameters related to the uptake process (in r2 and r8) were identified using the substrate concentration data from the Chiu et al.'s (1973) batch experiments (data not showed). To minimize the number of degrees of freedom, only the substrate uptake and the growth and storage processes were modeled. The other processes (r9 to r13, and r20 to r25) were set to zero. Additional data are required to identify the parameters included in these processes. In the fit of Vanrolleghem et al.'s (1998) data shown in Figure 3-4, the K_{Sha} = 0.2 mg/L was used. To perform the fit of Chiu et al.'s (1973) data, the K_{Sla} value was set close to 40 mg/L. These different values are of the same order of magnitude as those obtained by Chiu et al. (1973) in steady-state culture with dilution rates of 0.022 h^{-1} and 0.6 h^{-1}, respectively, or by Ferenci (1999) for two transport enzymes. The batch experiment favours the induction of an uptake system with low affinity and high capacity and therefore increases the specific substrate uptake rate and the observed K_S value, as seen in these fits. The observed K_S value and the specific substrate uptake rate change according to the relative induction of the two transport systems. The values of β_{EA}, and enzymes decay (β_{EX}) were chosen according to literature values (Aizenman et al. 1996; Cozzone 1981). Finally, all the data shown were fitted with the single set of parameters identified. Thus, with the same set of parameters, the model is able to describe short and long transients. It is not possible to fit all these data with the usual ASM without changing the values of the parameters because μ_{Hmax} varies during these experiments. With Chiu et al.'s (1973) data, ASMs will simply give straight lines with the same slope. With Vanrolleghem et al.'s (1998) data, ASM1 will give three square waves and ASM3 will give three identical waves with tailing.

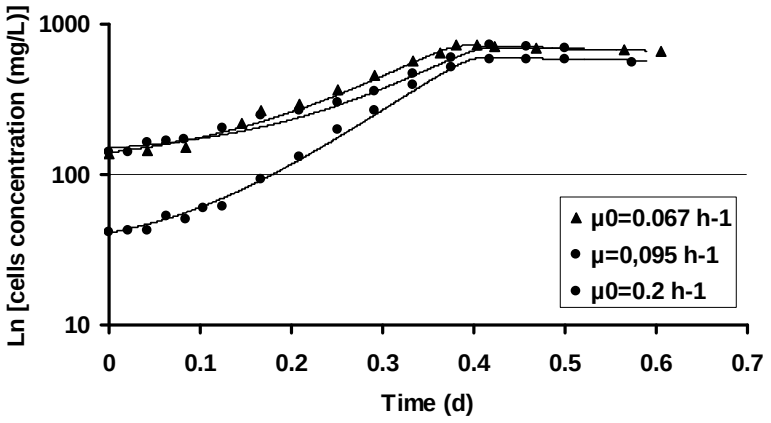

Figure 3-5 Fit of lag phase (data from Chiu et al. 1973)

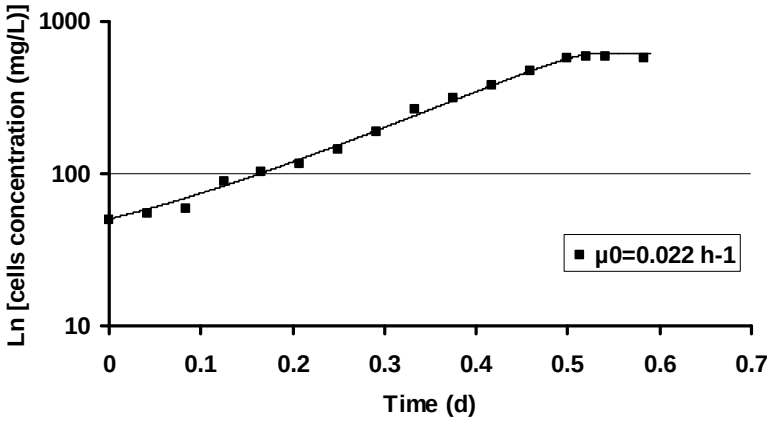

Figure 3-6 Fit of a lag phase (data from Chiu et al. 1973)

To model the data presented in Figure 3-6, the yield value (Y_H) used to perform the fit was lower (Y_H=0.66) than the one used for modeling of the other experiments (Y_H=0.73). In Figure 3-6, one sees that the initial growth rate was 0.022 h^{-1} and lower than those in Figure 3-5. The lower yield might be justified by an uncoupling between the growth process and the oxidation process under a critical growth rate (Daigger and Grady 1982b). The uncoupling phenomenon is not modeled here. Hence, it was necessary to modify the yield coefficient to perform the fit with a low initial growth rate. To perform the fit with a Y_H of 0.73 (Figure 3-6), some trials were done using several values of E_G turnover; however, a higher turnover of this component had a significant impact on the growth process but only a small one on the observed yield. Alternatively, an increase in soluble microbial products

production was modeled with the B_S release process. This process had a significant impact on the substrate concentration but still only a small one on the observed yield. This deficiency in the description of the biomass is a limitation in the application of the model. Perhaps futile cycles should be included in the model to enlarge the application range of the model.

Table 3-2 Additional parameters used to perform the fits of Chiu et al. (1973).

Parameter	**Symbol**	**units**	**Value**
Yield coefficient	Y_H	COD, g/g	0.73
Half saturation constant	$K_{S(2)}$	COD, mg/L	40
Maximum specific activity of substrate uptake enzyme (high affinity)	k_{BSha}^{max}	COD, g g^{-1} d^{-1}	10
Maximum specific activity of substrate uptake enzyme (low affinity)	k_{BSla}^{max}	COD, g g^{-1} d^{-1}	26
Maximum specific activity of storage enzyme	k_{STO}^{max}	COD, g g^{-1} d^{-1}	8
Maximum specific activity of degradation enzyme of storage product	δk_{STO}^{max}	COD, g g^{-1} d^{-1}	5
Half saturation constant of E_{STO} for B_{STO}	K_{STO}	mg mg^{-1} L^{-1}	0.7
Production rate of E_{BSla}	α_{EBSla}	d^{-1}	51
Production rate of E_{STO}	α_{ESTO}	d^{-1}	43
Decay rate of E_G	β_{EG}	d^{-1}	1.44
Decay rate of E_{BSha}	β_{EBSha}	d^{-1}	1.44
Decay rate of E_{BSla}	β_{EBSla}	d^{-1}	1.44
Decay rate of E_{STO}	β_{ESTO}	d^{-1}	1.44

Nevertheless, the turnover of E_G had some impact on the yield. Figure 3-7 shows the typical variation of the yield during the batch experiment. In the first phase of the experiment, the growth rate is low, and the maintenance of E_G uses a greater fraction of the substrate taken up. As the growth rate increases, the percentage of substrate used for the maintenance process decreases and the yield increases. Thus, in steady-state culture, the maintenance process decreases the observed yield as discussed by Pirt (1965). Also, although the death of active cells was set to zero, after the substrate exhaustion the growth rate is negative as discussed by Herbert (1958). For a starving biomass, the turnover of E_G (β_{EG} = 0.06 h^{-1}) gave a respiration close to that of the usually observed endogenous respiration (2 to 5 mg of O_2 per hour per gram of volatile suspended solids) of activated

sludge or that calculated with the decay rate default value in ASM (Avcioglu et al. 1998; Henze et al. 2000; Lavallée et al. 2002).

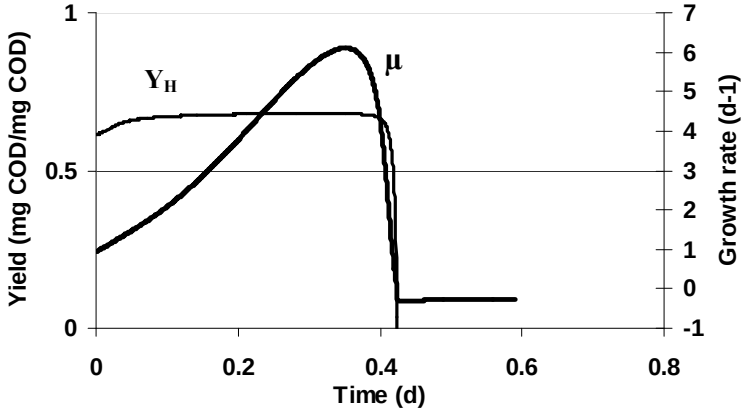

Figure 3-7 Simulated variation of cell characteristics during a batch experiment (μ_0=0.095 h^{-1})

The relative concentration of E_G and X_H and the growth rate are shown in Figure 3-8. The cell components are expressed as a ratio to the initial concentration. In this figure one can see that between 0 and 0.17 d, the growth rate increases faster than the E_G component indicating that the [mR] variable has an influence on the growth rate. Between 0.17 d and 0.27 d the growth rate increases at the same rate as E_G indicating that E_G is rate limiting according to the RNA-limiting theory (Daigger and Grady 1982b). After 0.27 d the growth rate increases slower than E_G indicating that another process has become rate-limiting. The exogenous substrate concentration becomes rate limiting ($S_S<2K_{Sla}$) only after 0.37 d, and according to the calibration procedure, in such circumstances the substrate uptake is rate-limiting. This analysis is in agreement with the analysis done by Daigger and Grady (1982b) on RNA, proteins and DNA production rate in similar experiments. Hence, the use of the proposed model could help in the understanding of transient behaviours occurring in activated sludge under organic shock loads for instance. Obviously this should be done with care, and several validation steps of the model on appropriate data remain to be performed.

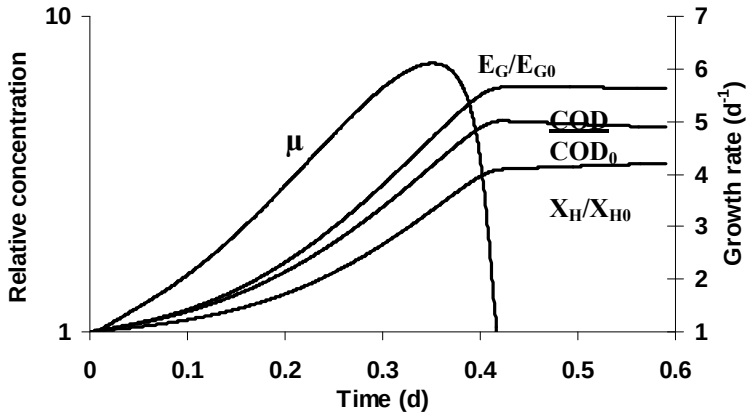

Figure 3-8 Simulated relative concentrations of components during a batch experiment (μ_0=0.095 h^{-1})

3.2.6 Conclusion

The proposed model gives a more realistic picture of active biomass and of its specific activity, but further research is required to support the model with experimental data. This model allows fitting of several data sets found in the literature with a single set of parameters. It therefore improves the quality of the kinetic information obtained by parameter estimation. Also, through the use of DNA measurements to estimate active biomass, it will be possible to assess specific values of parameters. This will help to increase our understanding of processes occurring within cells under transients. If the specific activity description of biomass gives a good description of the real behaviour of the active biomass under transient, the proposed formulation will make the kinetic constant evaluation a procedure that is independent of sludge age and of the process configuration. Thus, after substrate characterization, a single set of values for kinetic parameters would fit the response of different processes. This will eventually make the model a helpful tool for research and understanding of treatment processes.

The formulation of the proposed model opens several topics of further research. Thus, considerable work is still to be done to explore these new areas. Several validation steps of the model on appropriate data remain to be performed.

Table 3-3 Processes description

Rates	Description	Processes
r1	**Production of B_S**	$k_{BSha}^{\max} \cdot \frac{E_{BSha}}{X_H} \cdot \frac{S_S}{K_{Sha} + S_S} \cdot \frac{S_O}{K_O + S_O} \cdot X_H$
r2	**Production of B_S**	$k_{BSla}^{\max} \cdot \frac{E_{BSla}}{X_H} \cdot \frac{S_S}{K_{Sla} + S_S} \cdot \frac{S_O}{K_O + S_O} \cdot X_H$
r3	**Production of B_{STO}**	$k_{STO}^{\max} \cdot \frac{E_{STO}}{X_H} \cdot \frac{B_S / X_H}{K_{BS} + B_S / X_H} \cdot X_H$
r4	**Production of mR**	$\alpha_{mR} \cdot \frac{E_G}{X_H} \cdot \frac{B_S / X_H}{K_{BS} + B_S / X_H} \cdot \frac{S_O}{K_O + S_O} \cdot \frac{S_{NH}}{K_{NH} + S_{NH}} \cdot X_H$
r5	**Growth of heterotrophs and production of E_G**	$\mu_{H\max}^{\text{int}} \cdot \frac{E_G}{X_H} \cdot \frac{mR/X_H}{K_{mR} + mR/X_H} \cdot \frac{B_S / X_H}{K_{BS} + B_S / X_H} \cdot \frac{S_O}{K_O + S_O} \cdot \frac{S_{NH}}{K_{NH} + S_{NH}} \cdot X_H$
r6	**Production of E_{STO}**	$\alpha_{ESTO} \cdot \frac{E_G}{X_H} \cdot \frac{mR/Xh}{K_{mR} + mR/Xh} \cdot \frac{B_S / X_H}{K_{BS} + B_S / X_H} \cdot \frac{S_O}{K_O + S_O} \cdot \frac{S_{NH}}{K_{NH} + S_{NH}} \cdot X_H$
r7	**Production of E_{BSha}**	$\alpha_{EBSha} \cdot \frac{E_G}{X_H} \cdot \frac{mR/X_H}{K_{mR} + mR/X_H} \cdot \frac{S_S}{K_{Sha} + S_S} \cdot \frac{B_S / X_H}{K_{BS} + B_S / X_H} \cdot \frac{S_O}{K_O + S_O} \cdot \frac{S_{NH}}{K_{NH} + S_{NH}} \cdot \frac{K_{Sla}}{K_{Sla} + S_S} \cdot X_H$
r8	**Production of E_{BSla}**	$\alpha_{EBSla} \cdot \frac{E_G}{X_H} \cdot \frac{mR/X_H}{K_{mR} + mR/X_H} \cdot \frac{S_S}{K_{Sla} + S_S} \cdot \frac{B_S / X_H}{K_{BS} + B_S / X_H} \cdot \frac{S_O}{K_O + S_O} \cdot \frac{S_{NH}}{K_{NH} + S_{NH}} \cdot X_H$
r9	**Production of E_A**	$\alpha_{EA} \cdot \frac{E_G}{X_H} \cdot \frac{mR/X_H}{K_{mR} + mR/X_H} \cdot \frac{B_S / X_H}{K_{BS} + B_S / X_H} \cdot \frac{S_O}{K_O + S_O} \cdot \frac{S_{NH}}{K_{NH} + S_{NH}} \cdot X_H$
r10	**Production of E_T**	$\alpha_{ET} \cdot \frac{E_G}{X_H} \cdot \frac{mR/X_H}{K_{mR} + mR/X_H} \cdot \frac{B_S / X_H}{K_{BS} + B_S / X_H} \cdot \frac{S_O}{K_O + S_O} \cdot \frac{S_{NH}}{K_{NH} + S_{NH}} \cdot X_H$
r11	**Production of E_h**	$\alpha_{Eh} \cdot \frac{E_G}{X_H} \cdot \frac{mR/X_H}{K_{mR} + mR/X_H} \cdot \frac{X_{SS}}{K_{XSS} + X_{SS}} \cdot \frac{K_{Sha}}{K_{Sha} + S_S} \cdot \frac{B_S / X_H}{K_{BS} + B_S / X_H} \cdot \frac{S_O}{K_O + S_O} \cdot \frac{S_{NH}}{K_{NH} + S_{NH}} \cdot X_H$
r12	**Release of B_S**	$k_{RBS}^{\max} \cdot \frac{B_S / X_H}{K_{BSof} + B_S / X_H} \cdot X_H$

Table 3-3 Processes description (continuation)

Rates	Description	Processes
r13	**Hydrolysis**	$k_h^{\max} \cdot \frac{X_{SS}}{K_{XSS} + X_{SS}} \cdot E_h$
r14	**Degradation of B_{STO}**	$\delta k_{STO}^{\max} \cdot \frac{E_{STO}}{X_H} \cdot \frac{B_{STO}/X_H}{K_{STO} + B_{STO}/X_H} \cdot \frac{K_{Sha}}{K_{Sha} + S_S} \cdot X_H$
r15	**Decay of E_G**	$\beta_{EG} * E_G$
r16	**Decay of E_{STO}**	$\beta_{ESTO} * E_{STO}$
r17	**Decay of E_{BSha}**	$\beta_{EBS} * E_{BSha}$
r18	**Decay of E_{BSla}**	$\beta_{EBS} * E_{BSla}$
r19	**Decay of mR**	$\beta_{mR} * mR$
r20	**Decay of E_A**	$\beta_{EA} * E_A$
r21	**Decay of E_T**	$\beta_{ET} * E_T$
r22	**Decay of E_h**	$\beta_{Eh} * E_h$
r23	**Death of biomass cause by toxin**	$b_H^{\max} \cdot \frac{E_T}{X_H} \cdot \frac{K_{IT}}{K_{IT} + E_A/X_H} \cdot X_H$
r24	**Aerobic growth of protozoa**	$\mu_{MF\max} \cdot \frac{X_H/X_{MF}}{K_{X/MF} + X_H/X_{MF}} \cdot \frac{S_O}{K_{MFO} + S_O} \cdot X_{MF}$
r25	**Decay of protozoa**	$b_{MF} * X_{MF}$

Table 3-4 Stoichiometry of intracellular, soluble and particulated components

Rates	E_G	B_{STO}	B_S	S_S	So	S_{NH}	X_H	X_{MF}	X_{ii}	X_{SS}
Units:	**gCOD/m^3**	**gCOD/m^3**	**gCOD/m^3**	**gCOD**	**gCOD**	**gN**	**gCOD**	**gCOD**	**gCOD**	**gCOD**
r1			Y_{BS}	-1	$-(1-Y_{BS})$					
r2			Y_{BS}	-1	$-(1-Y_{BS})$					
r3		1	-1							
r4										
r5	φ_{EG}		$\frac{-(1+\varphi_{EG})}{Y_H}$		$\frac{-(1+\varphi_{EG})*(1-Y_H)}{Y_H}$	$-(1+\varphi_{EG})*inx$	1			
r6										
r7										
r8										
r9										
r10										
r11										
r12			-1	1						
r13				1		inx				-1
r14		-1	1							
r15	$-(1-Y_H)$				$-(1-Y_H)$	$inx*(1-Y_H)$				
r16										
r17										
r18										
r19										
r20										
r21										
r22										
r23	$\frac{-E_G}{X_H}$	$\frac{-B_{STO}}{X_H}$	$\frac{-B_S}{X_H}$	$\frac{(B_S+B_{STO})}{X_H}$			-1		$\frac{fu*(X_H+E_G)}{X_H}$	$\frac{(1-fu)*(X_H+E_G)}{X_H}$
r24	$\frac{-E_G}{(X_H*Y_{MF})}$	$\frac{-B_{STO}}{(X_H*Y_{MF})}$	$\frac{-Bs}{(X_H*Y_{MF})}$		$\frac{-(1-Y_{MF})*(X_H+E_G+B_S+B_{STO})}{(Y_{MF}*X_H)}$	$\frac{(1-Y_{MF})*(X_H+E_G)*ixb}{(Y_{MF}*X_H)}$	$\frac{-1}{Y_{MF}}$	$\frac{(1-fu)*(X_H+E_G+B_S+B_{STO})}{X_H}$	$\frac{fu*(X_H+E_G+B_S+B_{STO})}{XH}$	
r25								-1		1

Table 3-5 Stoichiometry of enzymatic components

Rates Units:	E_{STO} unit/L	E_{BSha} unit/L	E_{BSla} unit/L	mR unit/L	E_A unit/L	E_T unit/L	E_h unit/L
r1							
r2							
r3							
r4				*1*			
r5							
r6	*1*						
r7		*1*					
r8			*1*				
r9					*1*		
r10						*1*	
r11							*1*
r12							
r13							
r14							
r15							
r16	*-1*						
r17		*-1*					
r18			*-1*				
r19				*-1*			
r20					*-1*		
r21						*-1*	
r22							*-1*
r23	$\frac{-E_{STO}}{X_H}$	$\frac{-E_{BSha}}{X_H}$	$\frac{-E_{BSla}}{X_H}$	$\frac{-mR}{X_H}$	$\frac{-E_A}{X_H}$	$\frac{-E_T}{X_H}$	
r24	$\frac{-E_{STO}}{(X_H * Y_{MF})}$	$\frac{-E_{BSha}}{(X_H * Y_{MF})}$	$\frac{-E_{BSla}}{(X_H * Y_{MF})}$	$\frac{-mR}{(X_H * Y_{MF})}$	$\frac{-E_A}{(X_H * Y_{MF})}$	$\frac{-E_T}{(X_H * Y_{MF})}$	
r25							

CHAPITRE 4 MÉTHODE EXPÉRIMENTALE

Tel que déjà mentionné, le modèle proposé est une représentation synthétique des modèles biochimiques présentés dans la revue de littérature. Il s'agit d'une représentation structurée des micro-organismes, qui vise à décrire différents mécanismes d'adaptation des microorganismes présents dans les systèmes de traitement des eaux usées.

La description des microorganismes comprend plusieurs composants intracellulaires, et la description des cinétiques d'adaptation fait appel à des constantes cinétiques dits '*intrinsèques*', c'est-à-dire dépendantes du métabolisme des microorganismes, et indépendantes des facteurs abiotiques ou '*extrinsèques'* (Grady et al., 1996).

Ainsi, une calibration du modèle doit être effectuée afin d'obtenir une simulation précise de la réponse du système de traitement. Le modèle doit donc être calibré sur l'évolution des composants extra et intracellulaires qui sont ciblés dans la structure proposée du modèle, plus précisément sur les rapports stoechiométriques et sur les taux de production ou de dégradation des différents composants.

Dans un premier temps, il a été nécessaire de développer une méthode expérimentale en mesure d'évaluer l'évolution des divers composants ciblés. Ceux-ci sont le substrat, la biomasse active, les réserves intracellulaires, la respiration, l'azote ammoniacal et les produits microbiens solubles.

4.1 Méthode de mesure de l'ADN

Selon les hypothèses formulées précédemment, le rapport ADN/(structure cellulaire) demeure constant. Le but visé par ce protocole est d'isoler l'ADN afin de quantifier la biomasse active par fluorométrie. La fluorométrie n'exige pas un degré de pureté très élevé étant donné la spécificité du fluorochrome utilisé (Paul et Myers, 1982).

Le fluorochrome Hoescht 33258 réagit spécifiquement avec l'ADN (Paul et Myers, 1982).

4.1.1 Courbe de calibration

Afin de déterminer par fluorométrie la concentration d'ADN dans un échantillon, il est nécessaire de définir une courbe de calibration. La courbe de calibration a été préparée avec le fluorochrome Hoescht 33258 et de l'ADN pure suivant le protocole recommandé dans le bulletin technique no. MB-590 du fabriquant (Anonyme, 1998). Le protocole détaillé de même que la courbe de calibration sont présentés à l'annexe 1.1.

4.1.2 Protocole d'échantillonnage

Avant de procéder à l'extraction de l'ADN, il est nécessaire de stabiliser les échantillons durant l'entreposage.

Le gel des échantillons a été rejeté puisqu'il était nécessaire de conserver l'intégrité de la membrane cellulaire pour effectuer l'extraction de l'exo-ADN et l'extraction de l'endo-ADN en deux étapes différentes. Le gel-dégel peut être utilisé comme technique de lyse des cellules (Trevors et al., 1992).

Il a donc été nécessaire d'inhiber les ADNases présents dans les cellules. Quelques protocoles recommandent d'utiliser directement le EDTA comme agent chélateur. Le EDTA séquestre les métaux, ce qui inhibe l'activité de l'ADNase (Wallace, 1987 ; Picard et al, 1992). Cette méthode a été retenue.

Il a aussi été nécessaire d'inhiber la croissance cellulaire afin d'obtenir une image instantanée de l'état de la culture au moment du prélèvement. La norfloxacine est un inhibiteur de l'ADN gyrase chez les bactéries gram+ ou gram-, et est utilisé comme agent bactériostatique (Ito et al., 1980 ; Shen et al., 1989). Certains isothianozoles

semblent inhiber rapidement l'initiation de la réplication de l'ADN (Collier et al. 1990). L'efficacité de ces deux inhibiteurs a été vérifiée dans le cadre de ce protocole.

4.1.3 Protocole d'extraction

On retrouve une quantité significative d'ADN dans les exo polymères de cultures cellulaires (Catlin et Cunningham, 1958; Sponza, 2002). L'extraction des exo polymères peut être effectuée à l'aide de crown éther sans entraîner une lyse significative des cellules (Wurtz et al, 2001). L'extraction de l'exo-ADN à l'aide de crown éther a donc été effectuée au cours de la première étape d'extraction.

La lyse cellulaire peut être effectuée efficacement à l'aide de sodium dodecyl sulphate (SDS) et un battage sur billes (beadbeating) (Moré et al., 1994).

Les composés comme les sucres, les protéines ou l'ARN ont peu d'effets sur la fluorescence générée par le fluorochrome Hoescht 33258 (Van Lancker et Gheyssens, 1986). Il semble donc que la quantification de l'ADN peut être effectuée directement sur l'extrait cellulaire (Sambrook, 2001). Il est toutefois préférable d'utiliser des détergents pour dissocier l'ADN des protéines car l'association de protéines avec les acides nucléiques inhibe leur association avec les fluorochromes (Canino et Caldarone, 1995).

L'extraction avec le SDS (1%) semble simple, efficace et reproductible pour dé-protéiner les acides nucléiques (Blumberg, 1987 ; Bukley et al., 1999) sans nécessiter l'utilisation d'étapes de purification au phénol-chloroforme (Bukley et al., 1999). Si la quantification de l'ADN est faite directement sur l'extrait brut, cette méthode génère une extinction et une fluorescence de fond associée à d'autres composés (Lancker et Gheyssens, 1986 ; Canino et Caldarone, 1995). Le SDS comme les autres détergents anioniques, émet de la fluorescence lorsque exposée à certaines longueur d'ondes (Canino et Caldarone, 1995).

Pour palier à ce problème, une étape de purification de l'ADN est requise. Il semble qu'une purification par précipitation sélective peut atteindre un degré de pureté suffisant pour utiliser des techniques comme l'hybridisation (Yu et Mohn, 1999 ; Muttray et al, 2001). La méthode de lyse et purification par précipitation sélective proposée par Yu et Mohn (1999) a donc été retenue.

Afin d'augmenter le taux de récupération de faibles quantités d'ADN lors de la précipitation dans l'éthanol, le glycogène est souvent utilisé comme agent transporteur (Sambrook, 2001).

Le détail du protocole d'extraction et de purification est présenté à l'annexe 1.1.

Selon Bukley et al. (1999), la précision et la fiabilité du protocole d'extraction et de quantification devraient être vérifiées.

4.1.4 Vérification de la limite de détection de la méthode

La limite de détection de la méthode a été déterminée à partir de la variance de duplicatas obtenus sur une longue période d'évaluation, conformément au Standard Methods (1998) et au protocole pour la validation d'une méthode d'analyse en chimie recommandé par le Centre d'expertise en analyse environnementale du Québec (Anonyme, 2002). La variance est déterminée selon l'équation suivante :

$$Var = \frac{\sum_{i}^{j}(x_{ij} - \mu_j)^2}{n-1} \qquad [4.1]$$

Selon cette méthode, la concentration des duplicatas utilisés pour déterminer la limite de détection doit se situer entre 5 et 7 fois la limite de détection calculée. Les résultats obtenus au cours des expérimentations se situant à l'intérieur de ces limites ont été retenus pour faire l'analyse. En tout, trente six échantillons ont été analysés en trois ou quatre duplicatas pour un total de 116 aliquotes sur une période de quatre mois. Les résultats sont présentés à l'annexe 1.1.

La variance ainsi calculée est de 1600 ng d'ADN/ml. Les limites de détection et de quantification obtenues sont de 120 ng d'ADN/ml et 400 ng d'ADN/ml respectivement.

4.1.5 Vérification de la linéarité du protocole en proportion de la quantité de biomasse

Afin de vérifier si la méthode est quantitative, un test de linéarité a été effectué. Le volume de l'aliquote de biomasse prélevé a été varié, afin de vérifier la proportionnalité de la mesure.

Tableau 4-1 Vérification de la linéarité de la méthode

Volume de biomasse	Quantification ADN	Volume de biomasse	Quantification ADN
ml	ng/ml	ml	ng/ml
1	4479	0.2	949
1	4313	0.2	811
1	4255	0.2	913
1	3846	0.2	935
0.5	2288	0.1	365
0.5	1947	0.1	321
0.5	2006	0.1	314
0.5	1899	0.1	329

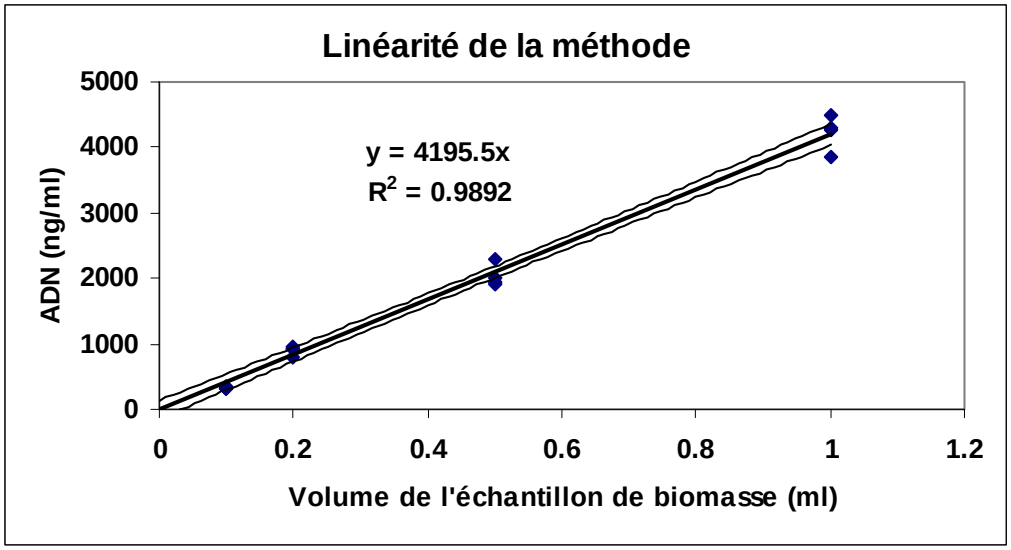

Figure 4-1 Linéarité du protocole d'extraction de l'ADN

Les résultats donnés au Tableau 4-1 et la Figure 4-1 démontrent que la quantité d'ADN extrait était proportionnelle au volume de l'aliquote prélevé. Le protocole d'extraction est demeuré linéaire entre 300 et 4300 ng d'ADN/ml. L'intervalle de confiance à 95% varie de 143 à 89 puis à 164 ng d'ADN/ml de part et d'autre de la droite de régression pour un volume d'échantillon de 0, 0,5 et 1 ml respectivement.

La linéarité de la méthode démontre que la méthode est quantitative dans la gamme étudiée.

4.1.6 Vérification du taux de récupération de l'ADN.

Afin de vérifier le pourcentage de récupération de l'ADN présent dans un échantillon, le protocole d'extraction a été appliqué à des duplicatas d'ADN standard. Une dose de 500 ng (5 µl d'une solution standard à 100 µg d'ADN /ml) a été ajoutée à 1 ml d'une

solution de lyse. Le protocole d'extraction et de purification a été appliqué à chacun des duplicatas. La quantité d'ADN du duplicata a ensuite été déterminée par fluorométrie. Le pourcentage de récupération est le rapport entre la quantité mesurée et la concentration initiale. Les résulats obtenus sont données au Tableau 4-2.

Selon cette méthode de vérification, le taux de récupération de l'ADN a été de approximativement 37%. La littérature consultée ne rapporte pas de taux de récupération pour d'autres protocoles. Ce taux de récupération semble faible mais tel que discuté précédemment, la méthode demeure quantitative. Compte tenu de la répétabilité des résultats obtenus, la méthode a été jugée acceptable.

Tableau 4-2 Taux de récupération de l'ADN

	Dose ADN	Quantification ADN/ml	Récupération
Duplicata	**ng/ml**	**ng/ml**	**%**
1	500	161	32%
2	500	212	42%
3	500	175	35%
4	500	183	37%
moy		183	37%
écart type		21	4%

4.1.7 Vérification de l'efficacité de l'extraction de l'exo-ADN

Sponza (2002) a observé que dans les procédés de boues activées, les exo-polymères peuvent contenir entre 6±2 et 13±4 mg ADN/g de matières volatiles en suspension. Cette auteure a démontré que la fraction d'ADN dans les exo-polymères varie selon la nature de l'effluent à traiter et selon le mode d'opération du réacteur biologique. Ces observations démontrent qu'il est opportun d'effectuer l'extraction de l'exo-ADN afin d'obtenir une image représentative de la biomasse active dans le procédé de traitement.

L'efficacité du protocole d'extraction de l'exo-ADN a été vérifiée en mesurant la concentration d'ADN dans des aliquotes bruts de biomasse, et dans les aliquotes traités selon la procédure de solubilisation de l'exo-ADN du protocole d'extraction détaillé à l'annexe 1.1. Tel qu'indiqué au Tableau 4-3 les mesures ont été effectué en quatre duplicatas.

Le rapport de distribution des variances a été vérifié afin de tester l'hypothèse de similarité des variances. Suite à ce premier test, la similarité des moyennes obtenues sur les duplicatas a été évaluée en comparant la valeur critique des tables de Students ($t_{\alpha/2}$) avec la valeur t' calculée (Walpole et Myers, 1985). L'hypothèse vérifiée (H_0) était qu'il n'existe aucune différence entre les moyennes.

Il est possible de conclure que les moyennes sont différentes (H_1) lorsque l'hypothèse H_0 est rejetée, et que la puissance du test est suffisante (Walpole et Myers, 1985). Le test a été effectué avec un intervalle de confiance de 95% (α=0,05) réparti sur les deux cotés de la distribution de la moyenne et une puissance de 95% (β=0,05).

Selon le rapport entre l'écart observé entre les moyennes et les écarts types (δ/σ) ainsi que le nombre de duplicatas, la puissance du test est suffisante pour faire une distinction entre les moyennes obtenues. Selon le test de similarité effectué, la concentration d'ADN dans les duplicatas sans extraction de l'exo-ADN est différente de celle obtenue dans les duplicatas avec extraction de l'exo-ADN.

Tableau 4-3 Extraction de l'exo-ADN

Duplicata	Exo-ADN+ADN Quantification ADN ng/ml	ADN Quantification ADN ng/ml
1	5000	4192
2	5417	4050
3	5750	4042
4	5625	4100
moy	5448	4096
écart type	329	69

L'écart entre les moyennes obtenues est d'environ 30%. Si on assume un rapport stoechiométrique de 0,09 mg DCO/µg ADN (voir la discussion sur les résultats) et un rapport stoechiométrique de 1,48 mg DCO/mg MVES, on obtient un taux d'extraction de exo-ADN de 5 mg ADN/g de matières volatiles en suspension. Sponza (2002) rapporte des valeurs du même ordre de grandeur.

4.1.8 Vérification de l'efficacité de l'inhibiteur

L'efficacité de l'inhibiteur a été vérifiée en mesurant la concentration d'ADN dans des aliquotes d'un mélange de biomasse et de substrat, au temps zéro et après 24 heures d'incubation au réfrigérateur. Les mesures ont été effectuées en quatre duplicatas.

Le rapport de distribution des variances a été vérifié afin de tester l'hypothèse de similarité des variances. Suite à ce premier test, la similarité des moyennes obtenues sur les duplicatas a été évaluée en comparant la valeur critique des tables de Students ($t_{\alpha/2}$) avec la valeur t' calculé (Walpole et Myers, 1985). L'hypothèse vérifiée (H_0) était qu'il n'existe aucune différence entre les moyennes.

Il est possible de conclure que moyennes sont différentes (H_1) lorsque l'hypothèse H_0 est rejetée, et que la puissance du test est suffisante (Walpole et Myers, 1985). Le test a été effectué selon un intervalle de confiance de 95% (α=0,05) réparti sur les deux cotés de la distribution de la moyenne et une puissance de 95% (β=0,05).

4.1.8.1 Inhibiteur : Norfloxacine

La Norfloxacine (1-ethyl-6-fluoro-1,4dihydro-4-oxo-7-(1-piperazinyl)-3-quinolinecarboxilic acid; $C_{16}H_{18}FN_3O_3$) est un antibiotique utilisé contre les infections urinaires (Hirai et al., 1981). Cet antibiotique inhibe l'activité de l'enzyme ADN-gyrase, et donc inhibe la réplication de l'ADN (Shen et al., 1989). Une dose de 0,42 µg/ml semble inhiber toute croissance de cultures en suspension de bactéries Gram-positives ou Gram-négative (Ito et al., 1980).

Un volume de 0,5 ml d'une solution inhibitrice concentrée à 125 µM de Norfloxacine a été ajouté à chaque alicot de 1 ml de biomasse. La dose appliquée de Norfloxacine était donc de 13,3 µg/ml.

Selon les résultats présentés au Tableau 4-4, le test de similarité effectué indique que la concentration d'ADN dans les duplicatas témoins (Témoins 0h) est inférieure à celle obtenue pour les duplicatas avec substrat et l'inhibiteur Norfloxacine et incubés 24 heures. Selon le rapport entre l'écart observé entre les moyennes et les écarts types (δ/σ) ainsi que le nombre de duplicatas, la puissance du test est suffisante pour faire une distinction entre les moyennes obtenues.

L'inhibiteur Norfloxacine ne semble pas suffisamment efficace dans le cadre du protocole proposé.

Tableau 4-4 Test d'inhibition par la Norfloxacine

Duplicata	**Témoin 0 h** - subst. - inhib. **ADN ng/ml**	**Inhib. 24h** + subst. + inhib. **ADN mg/ml**
1	3000	3700
2	3208	3417
3	3250	3333
4	2583	3583
moy	3010	3508
écart type	305	165

4.1.8.2 Inhibiteur : Katlon®

Le Katlon® est utilisé comme agent bactériostatique en laboratoire ou au niveau industriel. Ce produit inhibe l'initiation de la réplication de l'ADN. Une concentration de 0,5 µg/ml semble inhiber toute croissance ou recroissance de la bactérie *Escherichia coli* ATCC 8739 (Collier et al., 1990). La concentration recommandée par le fabricant pour totalement inhiber la croissance microbienne est de 6 à 15 ppm (Anonyme, 1996).

Un volume de 0,1 ml d'une solution inhibitrice concentrée à 240 mg/L de Katlon® a été ajouté à un volume de 1 ml de biomasse et 0,5 de solution TRIS-HCl pH 8. La dose appliquée de Katlon® était donc de 15 mg/L.

Tableau 4-5 Test d'inhibition par le Katlon®

Duplicata	**Inhib. 0h** + subst. + inhib. **ADN ng/ml**	**Inhib. 24h** + subst.+ inhib. **ADN ng/ml**	**Témoin 24h** + subst. **ADN ng/ml**
1	2500	2500	
2	2417	2575	2858
3	2217	2675	2950
4	2442	2683	2842
moy	2393	2608	2883
écart type	123	87	58

Selon les résultats présentés au Tableau 4-5, le test de similarité effectué indique que la concentration d'ADN observée dans les duplicatas non incubés (Inhib. 0h) et dans les duplicatas incubés avec l'inhibiteur Katlon® (Inhib. 24h) est inférieure à celle observée dans les duplicatas témoins incubés sans inhibiteurs (Témoin 24h). Selon le rapport entre l'écart observé entre les moyennes et les écarts types (δ/σ) ainsi que le nombre de duplicatas, la puissance du test est suffisante pour faire une distinction entre les moyennes obtenues.

La concentration d'ADN dans les duplicatas témoins non incubés (Inhib. 0h) semble inférieure à celle obtenue dans les duplicatas incubés 24 heures avec l'inhibiteur (Inhib. 24h), mais la puissance du test n'est pas suffisante pour déterminer si les deux moyennes sont différentes.

Comme on peut le constater à l'examen du Tableau 4-6, ces observations indiquent que l'inhibiteur Katlon® semble inhiber la réplication de l'ADN mais que son efficacité n'est pas complète ou instantanée. L'inhibiteur Katlon a été jugé suffisamment efficace dans le cadre du protocole proposé.

Tableau 4-6 Comparaison de la validité des hypothèses

Duplicata		Hypothèse			Puissance
		H_o	H_1	$t' < -t_{\alpha/2}$	
Série 1	Série 2	$\mu_1=\mu_2$	$\mu_1\neq\mu_2$	$\mu_1<\mu_2$	
Inhib. 0h	**Témoin 24h**	Faux	Vrai	Vrai	Suffisante
Inhib. 24h	**Témoin 24h**	Faux	Vrai	Vrai	Suffisante
Inhib. 0h	**Inhib. 24h**	Faux	Vrai	Vrai	Insuffisante

On peut donc conclure que le protocole proposé permet de stabiliser les échantillons prélevés pour une période d'entreposage de 24 heures, que la méthode demerue quantitative entre 300 et 4300 ng ADN/ml.

4.2 Méthode de mesure du glucose

Les méthodes colorimétriques à l'anthrone ou au phénol sont largement utilisées pour quantifier les carbohydrates totaux (Daniels et al., 1994; Herbert et al., 1971).

La méthode au phénol donne une réaction similaire pour tous les types de carbohydrates. La méthode à l'anthrone donne une réaction plus faible pour les pentoses

(5C) ou les heptoses (7C), et une réaction plus forte pour les hexoses (6C) (Herbert et al., 1971). Le glucose utilisé comme substrat pour la culture est un hexose. La méthode à l'anthrone a donc été retenue pour quantifier les carbohydrates solubles.

Pour mesurer la fraction soluble, les échantillons du bouillon de culture sont filtrés sur 0,45µm immédiatement au moment du prélèvement. L'analyse des carbohydrates est ensuite effectuée sur le filtrat.

La description détaillée du protocole d'échantillonnage et de la méthode à l'anthrone de même que la courbe standard sont données l'annexe 1.2. L'intervalle de confiance sur la courbe standard est l'ordre de 0,7 mg de glucose/L.

4.2.1 Vérification de la limite de détection de la méthode

La limite de détection de la méthode a été déterminée à partir de l'écart type sur douze duplicatas, conformément au Standard Methods (Standard Methods, 1998) et au protocole pour la validation d'une méthode d'analyse en chimie recommandé par le Centre d'expertise en analyse environnementale du Québec (Anonyme, 2002).

Selon cette méthode, la concentration des duplicatas utilisés pour déterminer la limite de détection doit se situer entre 4 et 10 fois la limite de détection calculée. Les résultats sont présentés à l'annexe 1.2.

L'écart type calculé sur les duplicatas est de 0,23 mg de glucose/L. Les limites de détection et de quantification obtenues sont de 0,7 mg de glucose/L et 2,3 mg de glucose/L respectivement.

4.3 Méthode de mesure du glycogène

Lorsque le substrat est disponible en grande quantité, les microorganismes ont tendance à accumuler des réserves pour se donner un avantage compétitif (van Loosdrecht et al., 1997). Les bactéries hétérotrophes cultivées sur du glucose peuvent accumuler préférentiellement des glycogènes aux autres formes de réserves intracellulaires (Dircks et al., 2001).

Les glycogènes peuvent être extrait de la masse cellulaire par digestion au KOH, puis précipités avec de l'éthanol, et ensuite quantifiés avec la méthode à l'anthrone ou au phénol (Daniels et al., 1994; Herbert et al., 1971).

Selon Herbert et al. (1971), la méthode proposée pour quantifier les carbohydrates totaux est insensible aux interférences causées par les protéines, et peu être appliquée directement à l'extrait cellulaire brut. Toutefois, dans la littérature, la quantification des glycogènes est effectuée après le processus d'extraction et précipitation (Daniels et al., 1994; Wang et al., 2001; Makinoshima et al., 2003). D'autres sucres comme les acides nucléiques peuvent interférer sensiblement. Comme la méthode à l'anthrone est moins sensible à ces sucres que la méthode au phénol (Herbert et al., 1971), la méthode à l'anthrone a été retenue.

Afin d'inhiber la formation ou la dégradation de glycogènes durant la période d'entreposage des échantillons, quelques gouttes de formaldéhyde ont été ajoutées à l'échantillon (Dircks et al., 2001).

La description détaillée du protocole d'échantillonnage et de la méthode à l'anthrone de même que la courbe standard sont données à l'annexe 1.3.

4.3.1 Vérification du taux de récupération du glycogène.

Une dose de 50 µg (50 µl d'une solution standard de glycogène à 1000 µg /ml) a été ajoutée à trois tubes de digestion. Une dose de 100 µg (100 µl d'une solution standard de glycogène à 1000 µg /ml) a été ajoutée à trois autres tubes de digestion. Le protocol d'extraction par digestion au KOH a été appliqué à chacun des échantillons. La quantité de glycogène du duplicatas a ensuite été évaluée avec la méthode à l'anthrone. Le pourcentage de récupération est le rapport entre la quantité mesurée et la concentration initiale.

Selon les résultats présentés au Tableau 4-7, cette méthode de vérification, le taux de récupération du glycogène a été de approximativement de 93%. Ce taux de récupération apparait acceptable.

Tableau 4-7 Taux de récupération du glycogène

Duplicata	Dose ng/ml	Lecture luminosité	Mesure mg/l	% recup
1	50	0.272	45	91%
2	50	0.283	47	94%
3	50	0.242	40	81%
4	100	0.555	93	93%
5	100	0.609	102	102%
6	100	0.603	101	101%
moy				93%
écart type				8%

4.4 Méthode de mesure de l'azote ammoniacal

La méthode de Nesslerisation directe 4500-NH_3 C du Standard Methods (Standard Methods, 1998) est une méthode de mesure standardisée et largement utilisée pour quantifier l'azote ammoniacal dans les eaux usées. La compagnie Hach^{MC} commercialise des produits prêts à l'usage pour effectuer la Nesslerisation.

Pour mesurer la concentration de l'azote ammoniacal, les échantillons du bouillon de culture sont filtrés sur un filtre de 0,45µm immédiatement au moment du prélèvement. L'analyse est ensuite effectuée sur le filtrat.

Selon le Standard Methods (Standard Methods, 1998), la méthode Nessler est généralement appliquée à un volume d'échantillon de 50 ml. L'utilisation d'un volume de 50 ml en triplicata requiert donc un volume significatif de bouillon de culture. La méthode a donc été adaptée au volume de 3 ml des cuvettes utilisées pour faire la lecture au spectrophotomètre. La description détaillée du protocole d'échantillonnage et de la méthode Nessler de même que la courbe standard sont données à l'annexe 1.4.

La méthode Nessler utilisée demeure linéaire entre 0 et 5 mg N/L. L'intervalle de confiance sur la droite de régression est de l'ordre de 0,03 mgN/L.

4.5 Méthode de mesure de la demande chimique en oxygène

La méthode de mesure à reflux fermé et par titration de la demande chimique en oxygène (DCO) 5220 C du Standard Methods (1998) est une méthode de mesure standardisée et largement utilisée pour quantifier la DCO dans les eaux usées.

La compagnie Hach^{MC} commercialise des tubes de digestion à reflux fermé prêts à l'usage pour effectuer la mesure de la DCO. Les tubes Hach^{MC} utilisés était de la gamme de 0 à 1500 mg DCO/L. Un volume de 2 ml de l'échantillon dilué si requis doit être ajouté au tube avant la digestion à 150°C durant deux heures.

Une fois le tube refroidi, un indicateur de potentiel rédox, une solution à la ferroine, doit être ajouté au tube avant la titration. La titration est effectuée avec une solution de sulphate d'ammonium ferreux (FAS). Le Standard Methods (1998) recommande de préparer la solution de titration à une concentration de 0,10M, mais la solution de titration a été préparée à une concentration de 0,02M afin d'obtenir davantage de précision.

La DCO particulaire a été définie par la soustraction de la DCO filtrée de la DCO totale. La DCO filtréee était mesurée sur le filtrat d'échantillons du bouillon de culture filtrés immédiatement au moment du prélèvement sur un filtre de 0,45µm.

Au cours des expérimentations effectuées dans ce travail, la variance des 81 triplicatas pour les mesures de plus de 500 mg DCO/L a donnée un écart type moyen de l'ordre de 10 mg DCO/L. Pour les mesures inférieures à 300 mg DCO/L la variance sur les 33 triplicatas a donné un écart type moyen de l'ordre de 4 mg DCO/L. Les limites de détection et de quantification de la méthode seraient donc inférieures à 12 mg DCO/L et à 41 mg DCO/L respectivement. Pour l'ensemble des mesures inférieures à 300 mg DCO/L, un ratio de conformité de 17 a été obtenu. Pour définir avec plus de précision les limites de détection et de quantification de la méthode, il aurait été nécessaire d'effectuer des mesures de l'ordre de 50 mg DCO/L afin d'obtenir un ratio de conformité entre 5 et 7 (Anonyme, 2002). Cette évaluation n'a pas été jugée utile puisque toutes les mesures étaient supérieures à 150 mg DCO/L, c'est-à-dire, plus de trois fois la limite de quantification estimée.

4.6 Méthode de mesure de la respiration des microorganismes

La majorité des essais de respirométrie ont été effectués en cellule fermée sur les gaz et ouverte sur les liquides conformément à la méthode proposée par Spérandio (1999). La température de la cellule était maintenue à 20°C grâce à une double enveloppe thermostatée par un cryostat. La liqueur mixte à l'intérieur de la cellule est agitée grâce

à un barreau aimanté et un agitateur magnétique ajusté à 700 tpm. Une sonde galvanique était insérée dans la cellule pour mesurer la concentration en oxygène dissous. L'oxymètre était relié à un ordinateur qui procédait à l'acquisition des données durant la manipulation.

Tableau 4-8 Description des respiromètres fermés sur les gaz

Instrumentation	Culture exponentielle	Culture 3 pulses
Réacteur		
Volume	10 L	2,25 L
Agitateur	Modèle 134-2 RPM 1000-12000 Talboy Laboratory Stirrer	RW 16 basic IKA
Aération	Diffuseur poreux Régulateur pneumatique 14R113FC Parker Pneumatic	Diffuseur poreux Rotamètre
Cryostat	Modèle VWR Scientific Product PolyScience	Neslab RTE-7D Thermo^{MC}
Sonde	WTW-Cellox 325	WTW Triomatic 701
Oxymètre	WTW OXY 340i	WTW OXY 296
Cellule respirométrique		
Volume	250 ml	410 ml
Pompe péristaltique	EasyLoad 7518-00	EasyLoad 7518-00
Système d'acquisition		
Carte d'acquisition	SN 1701 Cal 1994 Workmate© 1991 Strawberry Tree Inc	Respiromètre Bios R INSA Toulouse
Logiciel d'acquisition	DASYlab® V 5.50.00 National Instruments Ireland Ressources Ltd	Bios-R
Enregistrement des données	Digital PC Gelemnis GL Pentium	Digital PC 3000 Pentium 2
Intervalle d'enregistrement	2 secondes	2 secondes

La cellule respirométrique était reliée au réacteur aérobie par des conduits flexibles de type Tygon^{MC}. La liqueur mixte était renouvelée dans la cellule respirométrique à toutes les 3 minutes et 30 secondes. Le bouillon de culture était recirculé durant une minute au

taux de 1610 ml par minute à partir du réacteur par une pompe péristaltique Easyload 7518-00 de Masterflex. À l'arrêt de la pompe, la concentration en oxygène dissous était enregistrée à toutes les deux secondes après une période de stabilisation de 30 secondes. Une description détaillée des deux respiromètres utilisés au cours des travaux est donnée au Tableau 4-8.

Dans ce type de respiromètre, la décroissance de la concentration en oxygène dissous (dC/dt) est proportionnelle au taux de respiration des microorganismes (rO_2) (Spanjer et al., 1998).

$$\frac{dC}{dt} = rO_2 \qquad [4.2]$$

Le taux de respiration a été déduit de la pente de la droite de régression des points enregistrés.

Afin de déterminer le coefficient de rendement de biomasse sur le substrat exogène, des essais de respirométrie ont été effectués en cellule de type ouverte sur les gaz et fermée sur les liquides. La cellule était installée dans un incubateur maintenu à 20°C. La liqueur mixte était maintenue en suspension par un agitateur mécanique ajusté à environ 120 tpm. Une sonde galvanique était insérée dans la cellule pour mesurer la concentration en oxygène dissous. L'oxymètre était relié à un ordinateur qui procédait à l'acquisition des données durant la manipulation. Le Tableau 4-9 donne une description des équipements qui constituaient ce respiromètre.

Tableau 4-9 Description du respiromètre ouvert sur les gaz.

Sonde	WTW-Cellox 325
Oxymètre	WTW OXY 340i
Système d'acquisition	
Carte d'acquisition	SN 1701 Cal 1994 Workmate© 1991 Strawberry Tree Inc
Logiciel d'acquisition	DASYlab® V 5.50.00 National Instruments Ireland Ressources Ltd
Enregistrement des données	Digital PC Gelemnis GL Pentium
Intervalle d'enregistrement	1 secondes

Dans ce type de respiromètre, le taux de respiration de la biomasse (rO_2) est proportionnel à la variation de la concentration en oxygène dissous (dC/dt) corrigée par le taux de transfert d'oxygène du système ($K_La(C'_S-C)$), ou C'_S est la concentration à saturation de l'oxygène dissous dans la phase liquide (Spanjer et al., 1998).

Comme la cellule est fermée sur les liquides, le bilan sur les gaz s'établit de la façon suivante :

$$\frac{dC}{dt} = K_L a'(C'_S - C) - rO_{2endo} \qquad [4.3]$$

Or, lorsque la concentration d'oxygène se stabilise dans le réacteur en respiration endogène (dC/dt = 0), on assume que rO_{2endo} est constante, alors à l'équilibre on a $rO_{2endo} = K_L a'(C'_S - C_S^*)$, ou C^*_S est la concentration de saturation apparente lors de la respiration endogène. Après réarrangement, on obtient l'équation suivante :

$$\frac{dC}{dt} = K_L a'(C_S^* - C) \qquad [4.4]$$

La concentration d'oxygène dissous dans le réacteur était abaissée par la respiration endogène lors d'un arrêt de l'aération. Au démarrage de l'aération, la courbe de ré-aération jusqu'à la saturation apparente était utilisée pour déterminer le facteur K_La (C.T.G.R.E.F., 1981).

L'aération était ajustée afin de maintenir l'oxygène dissous entre 3 et 8 mg O_2/L. Par la suite, un bilan de l'oxygène consommé a été effectué par différences finies (Δt=1 sec.) après l'addition d'une quantité connue de substrat afin de déterminer le coefficient de rendement de la biomasse.

4.7 Culture de la biomasse

Une culture de microorganismes a été effectuée dans un réacteur alimenté de façon semi-continue. Cette culture a été maintenue au cours d'une période de plus de vingt quatre mois avant la phase expérimentale des travaux. Elle a été utilisée pour constituer la biomasse initiale (X_{H0}) des expériences en cuvées. La culture de microorganismes a

été inoculée avec de la biomasse prélevée à la station d'épuration municipale de l'arrondissement de St-Nicolas de la ville de Lévis.

Le réacteur décrit au Tableau 4-10 avait un volume de 3,25 litres et était alimenté au rythme de 8 fois par jour de 40 à 70 ml par dose, selon le temps de rétention visé. Chaque dose était administrée en 3 minutes par une pompe à diaphragme. L'effluent était déversé par un trop-plein. La biomasse y était maintenue en suspension par un agitateur mécanique. L'oxygène dissous était maintenu approximativement à 8 mg O_2/L à l'aide d'un diffuseur poreux alimenté en air par le réseau d'air comprimé de l'université. La pression du réseau était réduite par deux détenteurs de pression installés en série et suivis d'un humificateur afin de réduire l'évaporation dans le réacteur.

Tableau 4-10 Description du réacteur semi-continu

Réacteur semi-continu	
Instrumentation	
Volume	3,250 L
Agitateur	Modèle RZR 1 35-250/280-2200 rpm Caframo Ltd.
Aération	Régulateur pneumatique 14R113FC Parker Pneumatic Diffuseur poreux
Incubateur	Modèle 805 5 à 50°C Precision Scientific General Electric
Pompe d'alimentation	Modèle Concept CON b 0803NE1 000D000 Metering rate 3,4 L/h 8 bars Prominent
Minuterie de l'alimentation	Modèle 61-1065 Digital timer 7 days 8on/8off Radio Shack

4.8 Description du substrat

Afin de minimiser l'influence de facteurs extérieurs aléatoires, le substrat utilisé lors des expériences est un substrat synthétique, entièrement soluble. Tel qu'indiqué aux

Tableau 4-11 et 4-12, il était composé d'une solution minérale (Grady et al., 1989) et d'une source de carbone constituée principalement de glucose (Dircks et al., 2001).

Tableau 4-11 Description du substrat glucosé

Produit	Qte (g.)
Glucose	4.5
NH_4Cl	0.91
K_2HPO_4	7.47
KH_2PO_4	1.435
$MgSO_4.7H_2O$	1.095
Cycloheximide	0.6
Colchicine	0.3
Éléments trace	12 ml
H_2O	Compléter à 3 L

Tableau 4-12 Description de la solution des éléments trace

Produit	Qte (g.)
EDTA	12.5
$ZnSO_4.7H_2O$	5.5
$CaCl_2.7H_2O$	2.963
$MnCl_2.4H_2O$	1.265
$FeSO_4.7H_2O$	1.248
$(NH_4)6Mo_7O_{24}.4H_2O$	0.275
$CuSO_4.5H_2O$	0.3925
$CoCl_2.6H_2O$	0.4025
KOH	Ajuster pH à 6.0
H_2O	Compléter à250 ml

La concentration de la DCO a été ajustée afin d'obtenir une concentration de biomasse adéquate dans le réacteur semi-continu. Comme aucun appareil de contrôle de pH n'était disponible, un tampon phosphate a été ajouté à la solution (Grady et Williams, 1975). Pour inhiber la nitrification de l'ATU peut être ajouté régulièrement dans le réacteur (Dircks et al., 2001). Pour inhiber la croissance des protozoaires, de la cycloheximide (inhibiteur de la synthèse de protéines chez les eucaryotes) et de la colchicine (inhibiteur de la polymérisation de la tubuline) ont été ajoutés (Maurines-Carboneill et al, 1998).

4.9 Expérimentations

Afin de valider la structure du modèle proposé, deux expériences ont été effectuées.

Dans un premier temps, une expérience de croissance exponentielle a été effectuée. Cette expérience visait à produire une accélération de la croissance des microorganismes. Au préalable, trois essais ont été étudiés à l'aide de la respirométrie afin de s'assurer de la répétabilité du comportement transitoire de la biomasse. La description du bouillon de culture de chacun des essais est donnée au Tableau 4-13.

Le profil respirométrique des quatre essais est relativement semblable. Aux figures 4-2 à 4-5, on peut observer une baisse rapide de la respiration, suivie d'une période de croissance lente, qui est alors suivie d'une accélération de la croissance. Pour trois de ces essais, le taux de croissance observé a plus que triplé.

Tableau 4-13 Description du bouillon de culture des essais en cuvée

	Essai no.			
	201204	080105	120105	140205
NH_4Cl (g)	3,033	2,00	2,00	2,00
K_2HPO_4 (g)	24,88	24,90	24,88	24,88
KH_2PO_4 (g)	12,17	4,78	12,17	12,70
$MgSO_4.7H_2O$ (g)	3,65	3,65	3,65	3,65
Cycloheximide (g)	2,00	2,00	2,00	2,00
Colchicine (g)	1,00	1,00	1,00	1,00
Éléments trace (ml)	40	160	40	40
Biomasse				
Volume (L)	1	1 [1]	1	1,5
ADN (µg/L)	2840	n.d.	5264	4478
Temps de rétention hydraulique (jours)	9,9	6,4	5,6	5,7
H_2O (L)	8,960	8,840	8,960	8,960
pH	n.d.	7,2	7,0	7,0
Période d'acclimatation (heures)	20	10	20	22
Glucose (g)	8,00	8,00	8,00	6,00
Rapport S_0/X_{H0} (mg DCO/mg DCO)[2]	31	n.d.	16,7	9,9

[1] Pour cet essai, l'effluent du réacteur semi-continu qui avait été accumulé dans un réservoir a été utilisé.

[2] Un rapport stoechiométrique de 0,09 mg DCO/µg ADN a été utilisé pour définir X_{H0}.

Pour effectuer les essais, un échantillon de biomasse était placé dans le réacteur du respiromètre fermé sur les gaz et ouvert sur les liquides. Le volume était complété à 10 litres avec la base du substrat (sans la source de carbone) afin de minimiser le choc

osmotique. Le respiromètre était démarré pour une période d'acclimatation. Au temps zéro, la source de carbone était ajouté au réacteur sous forme de glucose afin d'induire une croissance de type exponentielle de la biomasse active. Le rapport S_0/X_{H0} était supérieur à 10 dans les quatres essais.

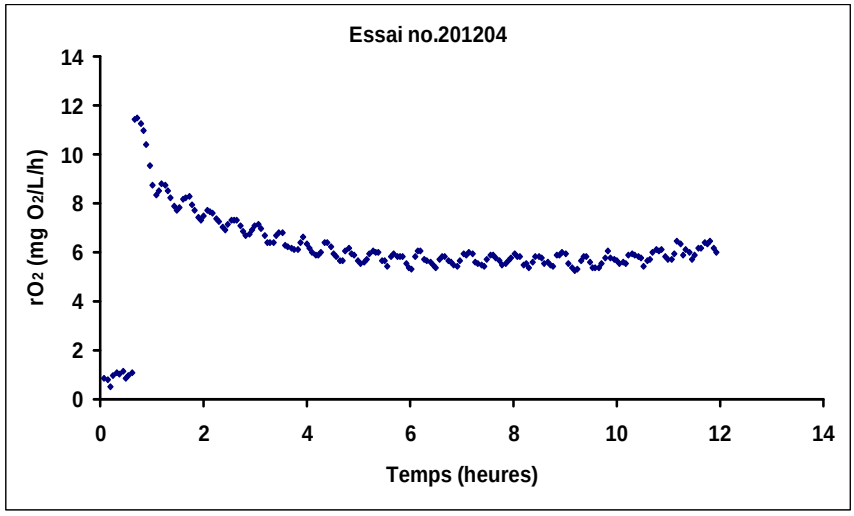

Figure 4-2 Profil respirométrique de l'essai no. 201204.

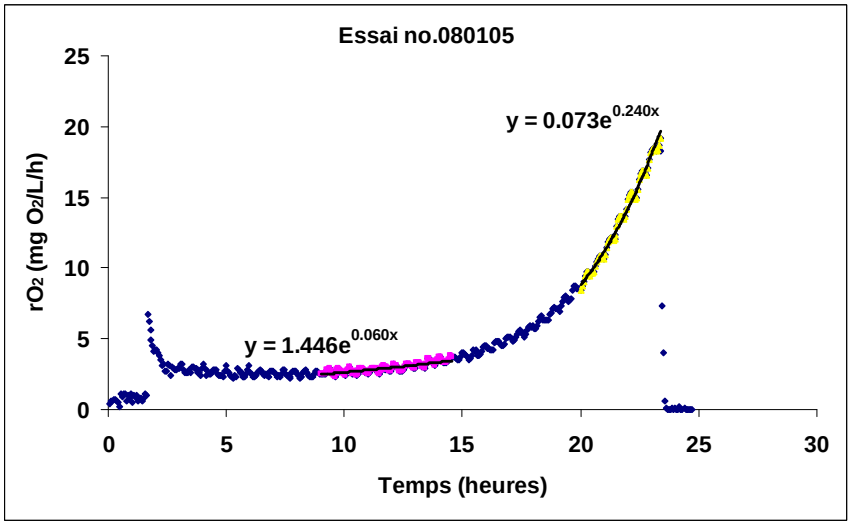

Figure 4-3 Profil respirométrique de l'essai no. 080105

Dans un deuxième temps, un essai à alimentation pulsée a été effectué. Trois doses de substrat ont été injectées dans un réacteur en cuvée. Cette expérience visait à produire un comportement transitoire induit par la saturation des voies métaboliques des microorganismes. Au préalable, un essai a été étudié à l'aide de la respirométrie afin de s'assurer de la répétabilité du comportement transitoire de la biomasse. Les profils

donnés par les mesures respirométriques ont été considérés semblables, ce qui indique que l'essai peut être répété.

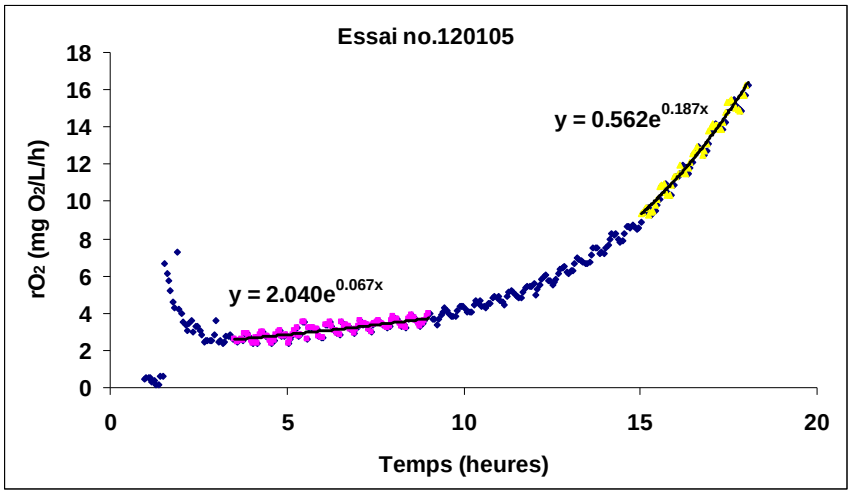

Figure 4-4 Profil respirométrique de l'essai no. 120105

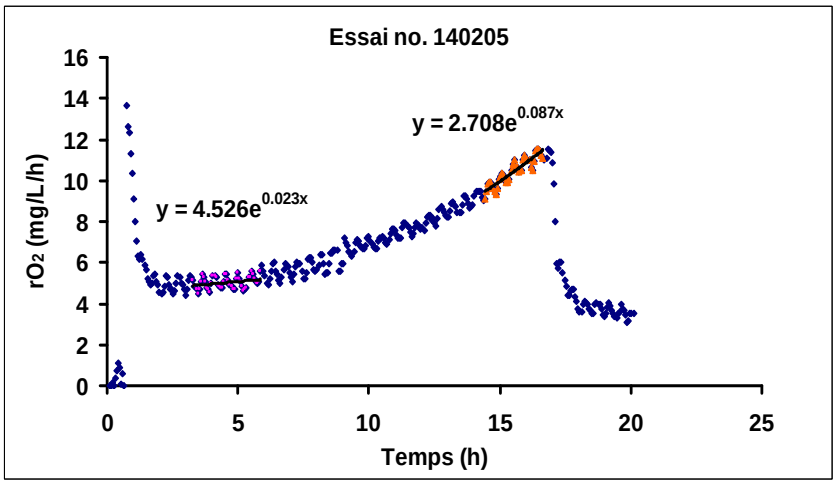

Figure 4-5 Profil respirométrique de l'essai no. 140205

Un échantillon de biomasse de 0,5 litres a été placé dans le réacteur du respiromètre fermé sur les gaz et ouvert sur les liquides. Le volume a été complété à 2,5 litres avec la base du substrat (sans la source de carbone) afin de minimiser le choc osmotique. La DCO de la biomasse active estimée selon les résultats expérimentaux obtenus (X_{H0}) était d'environ 54 mg/L. Tel qu'indiqué au Tableau 4-14, un premier essai a été effectué à la mise en route du respiromètre. Après 12 heures de stabilisation, le respiromètre a été réinitialisé et un second essai a été effectué. Au temps 1,5 heures, 4,2 heures et 5,25 heures, 85, 115 et 183 mg de DCO/L ont été ajoutés respectivement au réacteur sous

forme de glucose afin d'induire une saturation des voies métaboliques des microorganismes. Chaque dose de substrat a été ajoutée après que la dose précédente eut été entièrement consommée par les microorganismes.

Tableau 4-14 Description du bouillon de culture de l'essai par doses de substrat

		Essai no.	
		1	2
Glucose (g)		0,150 0,150 0,200	0,200 0,200 0,300
Rapport S_0/X_{H0} (mg DCO/mg DCO)[1]		1,1 1,1 1,5	1,5 1,5 2,2
NH_4Cl (g)		0,375	
K_2HPO_4 (g)		4,976	
KH_2PO_4 (g)		2,540	
$MgSO_4.7H_2O$ (g)		0,730	
Cycloheximide (g)		0,00	
Colchicine (g)		0,00	
Éléments trace (ml)		16	
Biomasse			
	Volume (L)	0,5	
	ADN (µg/L)	2954	
	θ (jours)	6,9	
H_2O (L)		2,00	
pH		7,0	

[1] Un rapport stoechiométrique de 0,09 mg DCO/µg ADN a été utilisé pour définir X_{H0}.

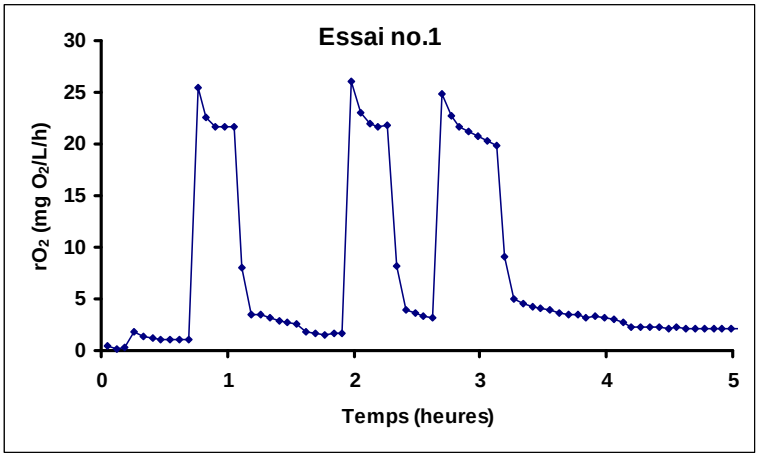

Figure 4-6 Profil respirométrique de l'essai par doses de substrat no. 1

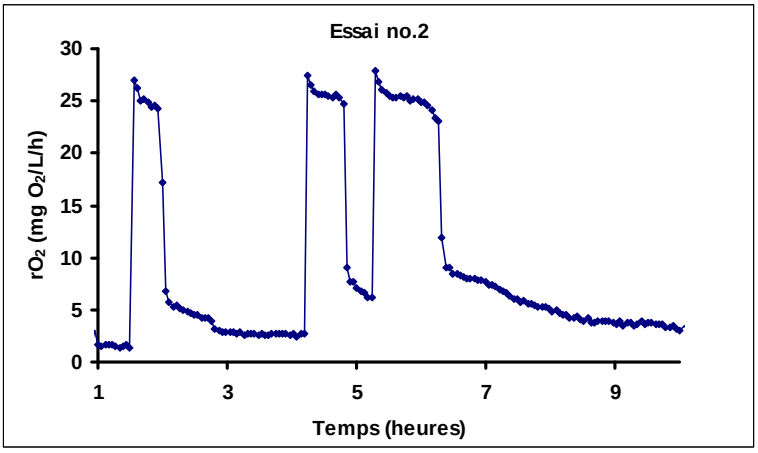

Figure 4-7 Profil respirométrique des essais par doses de substrat no. 2.

Au cours de ces expériences, l'ADN, les carbohydrates solubles (glucose), les carbohydrates particulaires (glycogènes), l'azote ammoniacal, la DCO soluble et la DCO totale, ainsi que le taux de respiration ont été mesurés afin de caractériser les différents composants inclus dans le modèle proposé. Le compte de la micro-faune a été aussi effectué afin de caractériser, si il y avait lieu, l'influence de celle-ci sur les cinétiques observées.

Les produits microbiens solubles (SMP) ont été définis par la soustraction de la DCO du glucose (selon un rapport stoechiométrique DCO/glucose égal à 1) de la DCO soluble.

CHAPITRE 5 MODÉLISATION DES COMPORTEMENTS TRANSITOIRES OBSERVÉS DE LA BIOMASSE

Selon l'objectif visé lors de l'éboration du modèle proposé, une seule série de constantes cinétiques serait nécessaire pour décrire l'évolution des divers composants lors de diverses conditions alors qu'une recalibration des modèles classiques serait requise pour décrire chacune de ces conditions.

Le modèle proposé a donc été calibré sur les différentes expériences effectuées dans le cadre de ce travail. Plusieurs simplifications et modifications sont proposées au modèle présenté au chapitre 3 afin d'établir une concordance entre le modèle et la méthode expérimentale, tout comme avec les résultats obtenus.

MODELING OF ACTIVATED SLUDGE TRANSIENT BEHAVIOUR INDUCED BY REGULATION OF CARBON AND NITROGEN METABOLISM

Lavallée B.*, Lessard P.* and Vanrolleghem P. A. *

*Département de Génie Civil, Faculté des Sciences et de Génie, Université Laval, Québec, Canada, G1K 7P4.

ABSTRACT

An experimental protocol to evaluate the structured biomass model proposed by Lavallée et al. (2005b) is presented. The protocol was devised to induce transient behaviour and characterize the evolution of several internal biomass components. The proposed model is based on biochemical principles, and fitted to the collected data. In these experiments, it was observed that filling the storage capacity of cells leads to special transient behaviour, including a temporarily reduced metabolic activity. The model-based interpretation of the results showed that the observed transient behaviour can be explained by cross-regulation of carbon and nitrogen metabolism. Hence, according to an extensive literature review, the cross-regulation of carbon and nitrogen can be used to model some observed transient behaviours and regulation of the storage process in activated sludge.

KEYWORDS: Accumulation capacity, activated sludge, mathematical modelling, metabolic model, nitrogen regulation, structured biomass model, transient behaviour.

5.1 Introduction

Increasingly, RNA-based molecular techniques are used in wastewater treatment process monitoring and microbial ecology studies (Saikaly et al., 2005). The quantification of active cells by the use of probes thus allows the development of refined models regarding the description of active biomass because the variation of their specific activity can then be taken into account. Such models would help in

understanding the transient behaviour of the activated sludge process and in the design and the operational optimization of the process. With such a structured biomass model, it should also be possible to find the intrinsic value of parameters (Grady et al., 1996) defining the growth rate of the biomass on a given substrate.

Literature has shown that the rRNA-level correlates with the specific growth rate (Bremer and Dennis, 1996; Muttray et al., 2001). However, Daigger and Grady (1982b) showed that the RNA-limiting theory of transient response is incomplete and must be expanded. Alternatively, some authors stated that the description of substrate transport by peripheral enzymes and ribosome synthesis are sufficient to model most of the transients related to diauxic growth in pure cultures (Gupta et al., 2005).

Based on an extensive literature review (Lavallée et al., 2005b), Lavallée et al. (2005a) thus proposed a structured biomass model including peripheral enzymes and ribosome (or rRNA-level) regulation to model fluctuations of the maximal growth rate and the resulting transient behaviour of mixed cultures.

However, among several types of transients observed in activated sludge, it was observed that filling the cell's accumulation capacity leads to a decrease of its metabolic activity (Cech and Chudoba, 1983). When cells are exposed to high substrate concentrations, Chang et al. (1999) observed that cells appear to exhibit saturation of their anabolic fluxes, suggesting a kinetic limitation for precursor metabolite production downstream of the carbon incorporation into cell mass. These authors observed also that poly-β-hydroxybutyrate (PHB) production could restore the balance between metabolic fluxes.

Similarly, Aon and Cortassa (2001) observed that under various C:N ratios, *Saccharomyces cerevisiae* appear to exhibit a saturation of anabolic fluxes and observed that an imbalance between metabolic fluxes induces ethanol production when using a substrate with a carbon limitation. These authors concluded that the onset of the aerobic fermentation is not associated with the saturation of the respiratory activity, but that it is rather associated to the limited nitrogen availability through the supply of N-carrying molecules. A slow incorporation rate of nitrogen limits the glutamate synthesis and induces an oversupply of precursors as α-ketoglutarate and metabolites of the tricarboxylic acid cycle (TCA cycle).

In the literature, pathways of carbon and nitrogen metabolism are well described. Glutamate and glutamine are the key nitrogen donors for biosynthetic reactions (Merrick and Edwards, 1995). Both are synthesized by the addition of an amine group to α-ketoglutarate, a metabolite of the TCA cycle. Hence, the carbon assimilation into cell constituants is linked to nitrogen incorporation through the TCA cycle and glutamate synthesis. When organic substrate and nitrogen are available in high concentrations, a high carbon consumption rate is observed, and the lower rate of nitrogen supply induces a limitation in anabolism. However, the substrate uptake rate and metabolism can be balanced by fermentation or storage processes.

Such conditions can be found in SBR and in EBPR processes where substrate is fed in batch to promote glycogen, PHB or polyphosphate accumulation. In an anaerobic-aerobic sequencing batch reactor (SBR), it was suggested that nitrogen limitation could induce polyphosphate metabolism (Harper and Jenkins, 2003; Harper et al., 2005). However, there is no nitrogen limitation in most wastewater treatment plants and even then the enhanced biological phosphorus removal (EBPR) process functions well (van Loosdrecht, 2007).

Given current knowledge, induction and regulation of the carbon uptake and storage by C/N imbalance in cells seems well understood from a biochemical point of view in pure culture. However, no model has yet been suggested to describe the behaviour of activated sludge cells in such conditions. Hence, in this work, the hypothesis that the induction of the storage process and the substrate uptake rate can be regulated by a saturation of anabolic fluxes was tested by modelling observed transient behaviour of mixed cultures of cells.

A new structured biomass model is thus proposed in this paper; it is based on the Lavallée et al. (2005a) model and on biochemical regulation principles proposed for single species in aerobic processes. The aim of the model is to simulate transient behaviour induced in semi-batch and batch reactors. A transient that got particular attenttion was the unexpected reduced metabolic activity observed after substrate oversupply. Unbalanced uptake rates of carbon and nitrogen were suspected to induce a saturation of the anabolic flux. The transients were modeled using the cross-regulation pattern of carbon and nitrogen metabolism proposed in literature for pure cultures of

bacteria. Also proposed is an experimental protocol to validate the underlying assumptions and support the calibration of such a model.

5.2 Material and methods

5.2.1 Experiments

The mixed culture was grown in a semi-continuous reactor for an adaptation period of more than 24 months. The reactor was inoculated with sludge from a municipal SBR wastewater treatment plant located in Lévis (Qc, Canada). The culture was maintained in suspension with a mechanical mixer and the dissolved oxygen concentration close to 8 mg/L with porous diffusers. The reactor volume was 3.25 L and the hydraulic and sludge residence time close to 6 days. The mixed liquor overflowed to the effluent.

Substrate was added within 3 minutes every 3 hours. The substrate used was made of: glucose (4.5 g), NH_4Cl (0.91 g), $KHPO_4$ (7.47 g), KH_2PO_4 (1.435 g), $MgSO_4.7H_2O$ (1.095 g), 12 ml of trace elements solution (Vishignac and Santer, 1975) and distilled water (completion to 3 L). Nitrification was inhibited in the reactor by periodically adding allylthiourea doses of 100 mg/L (Dircks et al., 2001). Inhibition of nitrification was required to performed balance on ammonia and nitrogen consumption by growing biomass. The phosphate buffer maintained the pH of the mixed liquor close to 6.9±0.1. Growth of protozoa was inhibited by applying an anaerobic period of 3 hours daily (van Dongen et al., 2001). In one culture, growth of protozoa was inhibited by adding cycloheximide (0.6 g) and colchicine (0.3 g) to the substrate solution (Maurines-Carboneill et al, 1998). However, microscopic observations showed that the inhibition was only efficient during a limited period of time and regrowth of protozoa was observed. Internal decay of active cell and predation were then non distinguishable.

To perform a validation of the model under different experimental conditions, an initial S_0/X_0 ratio of 9,9 was first used in a batch experiment to ensure exponential growth, and in a subsequent experiment, S_0/X_0 ratios of 1.5, 1.5 and 2.2 in three consecutive substrate pulses were used. For these two batch experiments, 1.5 and 0.5 litre of mixed liquor volume respectively was taken from the semi-continuous reactor and mixed with the substrate solution. Glucose and nitrogen quantities were adjusted to the required concentrations and glucose was added at time zero in the exponential growth experiment and at time 1.50, 4.20, 5.25 hours respectively in the three pulses

experiment. As in the semi-continuous reactor, the biomass was maintained in suspension with a mechanical mixer and the dissolved oxygen concentration was maintained close to 8 mg/L. The temperature of all reactors was regulated at 20.0±0.1°C.

The exponential growth batch experiment was conducted four times using various glucose substrates, and proved the observed transient behaviour to be reproducible. The three pulse experiment was conducted twice and the oxygen uptake rate pattern was the same in both. Hence, it was concluded that the observed transient behaviours were repeatable and were not induced by some unknown inhibitor.

5.2.2 Analysis

The cells concentration (X_H) was quantified by DNA analysis which was chosen as an arbitrary unit for cell number. The assumption was that the ratio of cell structure (surface of cell wall) per nucleus remains constant and independent of growth rate, as proposed by Schaechter et al. (1958). This unit of cell wall membrane bound proteins and nuclei was used as a basic unit of cell's structure. Hence, the COD of the cell's structure (X_H) was evaluated using a constant X_H/DNA ratio (mg of COD/µg of DNA). Using this assumption, it was then possible to assess the mass of pool material, similarly to Schaechter et al. (1958).

Aliquots were taken in four replicates, and EDTA was added to inhibit DNAse (Picard et al. 1992) and norfloxacine and Katlon® was added to inhibit DNA gyrase (Shen et al., 1989). The stabilised samples were stored at 4°C until DNA was extracted and quantified in each replicate. Exogenous DNA was extracted using Crown-ether (Wurtz et al., 2001) before cell lysis. Then, the replicates were centrifuged at 16000g during 10 minutes at 4°C. For cell lysis, the pellets were beadbeated continuously during 5 minutes at 4800 cycles/minute in a 3% SDS solution. The SDS extraction of DNA, ammonium acetate purification and ethanol precipitation was performed according to Yu and Mohn (1999). DNA quantification was performed by fluorescence using the Hoescht 33258 fluorochrome (Paul and Myers, 1982). Fluorescence was measured using a Sequoia-Turner model 450 fluorometer, and filters of 360 and 450 nm. The full width-half maximum of the bandpass was ±10 nm and the precision of the central wavelength was ± 2nm. The DNA concentration was obtained from a calibration curve

constructed with pure calf thymus DNA (Sigma DNA standard D.4810). The confidence interval of the standard curve varied between 1 and 4 ng DNA/ml for low and high DNA concentrations respectively. The extraction and purification method were applied to pure DNA aliquots. The percentage of DNA recovery was only 37% but the method remained linear for various aliquot volumes. The detection limit of the method applied to biomass was 45 ng DNA/ml. The standard deviation of the extracted DNA varied between 10 and 20% of the replicate's mean.

The total COD and soluble COD were measured by using the Close reflux and titration method described in Standard Methods (1998). Analyses were done on three replicates. Commercially prepared 1500 COD Hach^{TM} tubes were used. For soluble COD measurements, samples were filtered on superposed fibre glass 934 AH filters and 0.45 μm polycarbonate HTTP filters of Millipore. The standard deviation of total and soluble COD triplicates was less than 1% of the mean. The particulate COD was obtained by subtracting the soluble COD from the total COD value.

The Nessler method was used for NH_4^+ measurement on filtered samples (Standard Methods, 1998). Hach^{TM} commercially prepared solutions were used. The filtration method was the same as for COD. The method was adapted to 3 ml samples and measurements were performed directly in polymetacrylate dishes after dilution, and read at 425 nm. The standard deviation of triplicates was always lower than 0.7 mg/L.

Soluble carbohydrates (standing for glucose) and particulate carbohydrates (standing for glycogen) were measured using the anthrone method (Daniels et al., 1994; Herbert et al., 1971). Filtered samples were stored at 4°C in sterilized vials until analysis. The filtration method was as used for COD. A few drops of formaldehyde were added to unfiltered aliquots to inhibit glycogen metabolism (Dircks et al., 2001). Unfiltered aliquots were centrifuge for 10 minutes at 16000g and particulate carbohydrates were extracted from pellets by KOH digestion and ethanol precipitation (Daniels et al., 1994; Wang et al., 2001; Makinoshima et al., 2003). The 95% confidence interval on the calibration curve was smaller than 2 mg/L. During experiments, some noisy triplicates gave a standard deviation close to 5 mg/L.

As the substrate used for the experiments was glucose, the expected soluble microbial by-product (SMP) was acetate. Hence, acetate concentration in filtered and diluted

samples was measured by ion chromatography. However, acetate concentration in diluted samples was always low and the data were noisy. Hence, SMP was estimated by subtracting the concentration of glucose COD from the soluble COD concentration (Hao and Lau, 1988; Grady et al., 1972).

Protozoan and metazoan populations were quantified by individual count under a dark field microscope at a 100X magnification (Védry, 1996). Each count was performed in triplicate as well. The mean count was close to 1E+06 org./L, hence ten times lower than the values reported for the activated sludge process (Ratsak et al., 1996). Sixty six percent of the population consisted of saccodine, and 30% of the observed micro fauna were fixed ciliates. The inhibition method did not work well and seems to simply shift the population of free ciliates and rotifers to a less evident type as saccodine. Thus, it was assumed that the decay of the bacteria population included internal and external decay (van Loosdrecht and Henze, 1999).

During each batch experiment, the oxygen uptake rate (OUR) evaluation was performed with a LLS-type respirometer (Spanjers et al., 1998) according to Spérandio (1999). Mixed liquor was recycled from the batch reactor to the 250 ml closed respirometer with a peristaltic pump. Every 3 minutes and 30 seconds, the pump was running during 1 minute to renew at least 3 times the volume in the respirometer. The oxygen concentration was recorded every 2 seconds after a 30 seconds period of stabilization. After the pump stopped, the OUR was deduced from the slope of the regression curve of the dissolved oxygen (DO) data collected in the respiration chamber. The oxygen probe used was a WTW Cellox 325 and was connected to a data acquisition system.

For assessment of yields, the oxygen uptake rate evaluation was performed with a flowing gas-static liquid (LFS) respirometer (Spanjers et al., 1998). Oxygen concentration was recorded every second. A first order filter was used to reduce noise in the signal (Press et al., 2002). The mass balance was performed by time integration of the data.

5.3 Experimental results

Figure 5-1 shows the increase of cell mass and DNA in the experiment. The cell mass was assessed by subtracting inert material and glycogen from the particulate COD. In the batch experiment, the cell mass and the DNA increased accordingly. However, in

the substrate pulse experiment, an increase of cell mass is observed, but no significant increase in DNA.

Figure 5-2 presents the amount of nitrogen used for the production of cell constituents compared to the DNA increase. In the batch experiment (Figure 5-2a.), the slope of the regression line gives a specific nitrogen to cell DNA ratio (0.010 mgN/µgDNA).

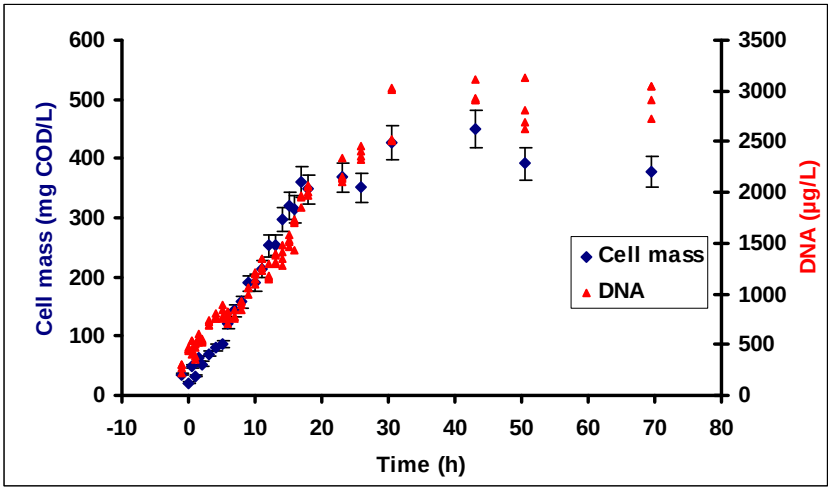

a) Batch experiment

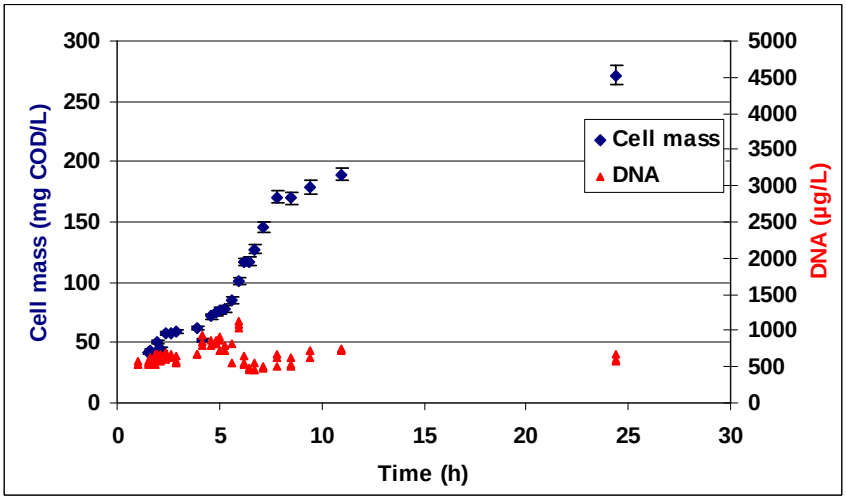

b) Substrate pulse experiment

Figure 5-1 DNA and cell mass accumulation during the experiments

However, no correlation was observed between nitrogen utilization and the DNA in the substrate pulse experiment (Figure 5-2b. It was assumed that carbon and nitrogen were used for amino acid or proteins synthesis (here called precursors) which accumulated in the cells.

As shown in Figure 5-3, the observed cell mass (COD)/DNA ratio increased from 0.09 to 0.22 mg COD/µg DNA in the batch experiment. After the exhaustion of substrate, this ratio decreased again to 0.14±0.03 mg COD/µg DNA and keeps decreasing slowly for the following 50 hours. Hence, it was assumed that the specific COD of cells was the minimal observed value of 0.09 mg COD/µg DNA. Accordingly, the value of the COD/DNA ratio exceeding the basic value of 0.09 mg COD/µg DNA was assumed the COD of the precursors. The relative error on precursor assessment was lower than 25% for each triplicate, with a mean value of 15% for each data set for both experiments.

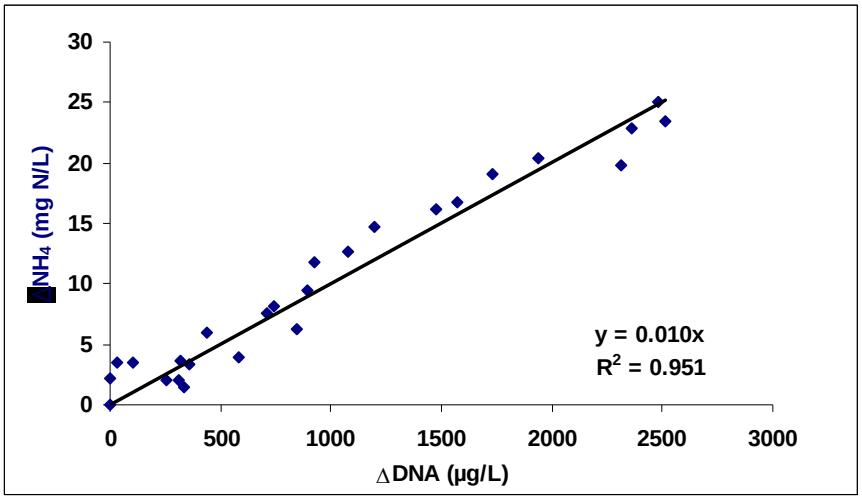

a) Batch experiment

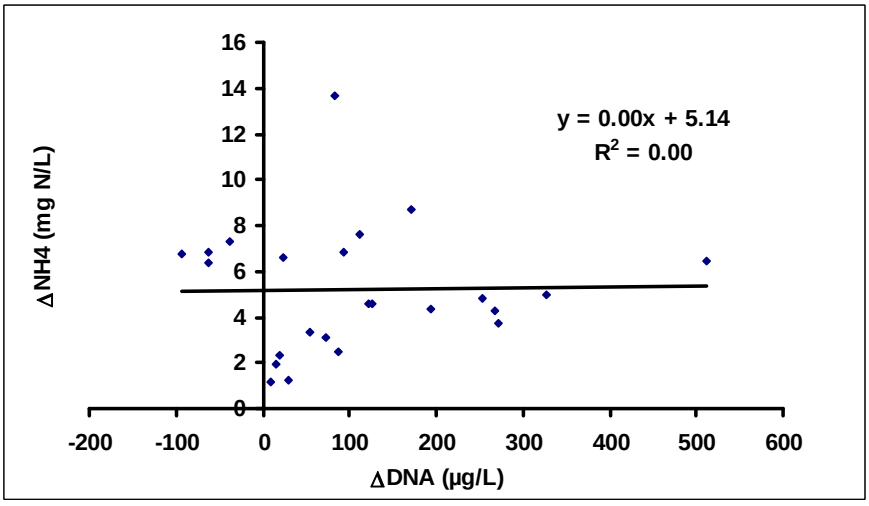

b) Substrate pulse experiment

Figure 5-2 Nitrogen used and increase in DNA concentration

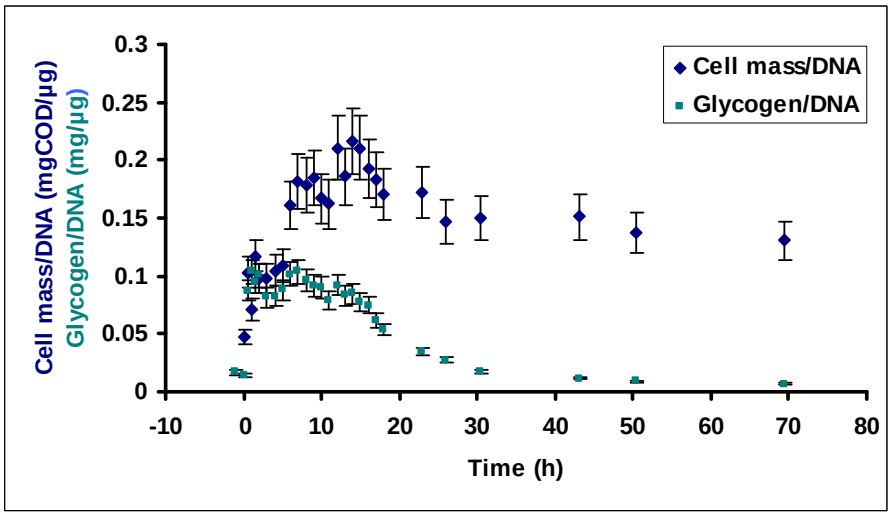

a) Batch experiment

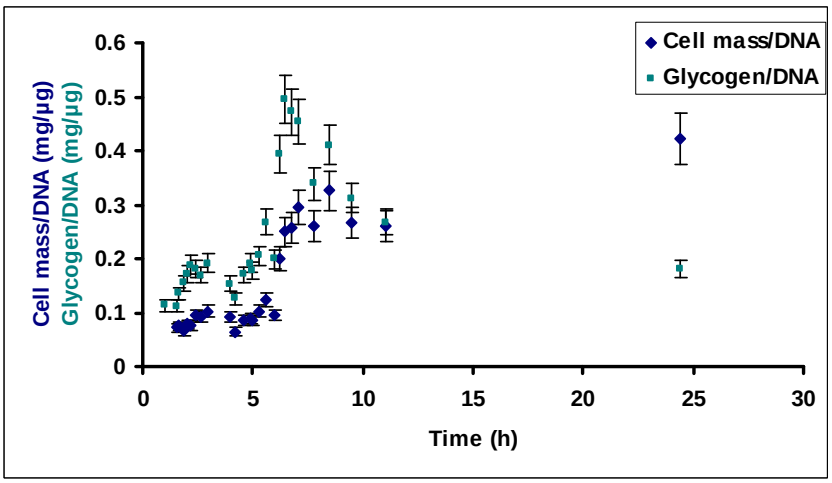

b) Substrate pulses experiment

Figure 5-3 Variation of the cell mass/DNA ratio and glycogen/DNA ratio

The ratio of nitrogen (0.010 mgN/µgDNA) and COD (0.14 mg COD/ µg DNA) used per µg of DNA at the substrate exhaustion in the batch experiment gives the nitrogen fraction into cells. The observed ratio (i_{NX}) was 0.07 mg N/mg COD. This value is consistent with the default value of the biomass nitrogen content, i_{NBM}=0.07, used in ASM3 (Henze et al., 2000).

The COD of the population X_H was then assessed using the DNA concentration and a conversion factor of 0.09 mg COD/µg DNA. This ratio seems high compared to a theoretical value of 0.03 mg COD/µg DNA based on 3% of DNA per cell mass (Bremer and Dennis, 1996). Considering the efficiency of the extraction protocol, the conversion factor is in agreement with the theoretical percentage of DNA in cells.

Figure 5-4a shows that at the start of the batch experiment, the oxygen uptake rate was high and unexpectedly, decreased sharply after a few minutes. Then, the oxygen uptake rate increased again until exhaustion of the substrate and dropped again as expected.

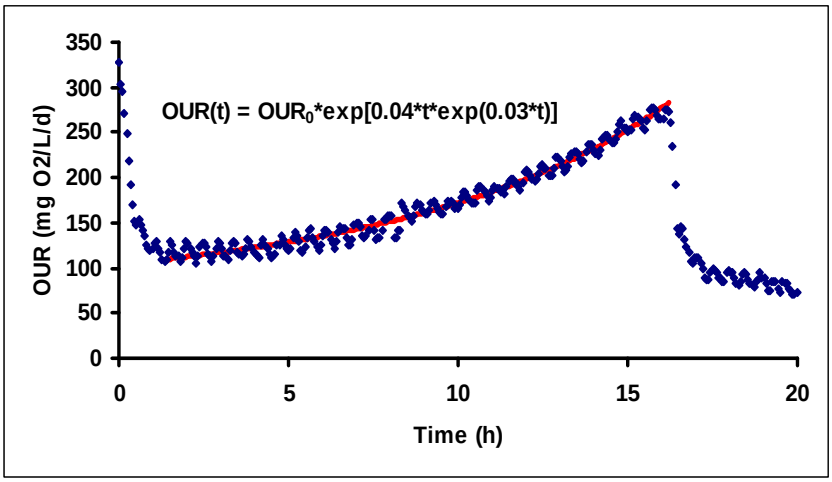

a) Increase of oxygen uptake rate

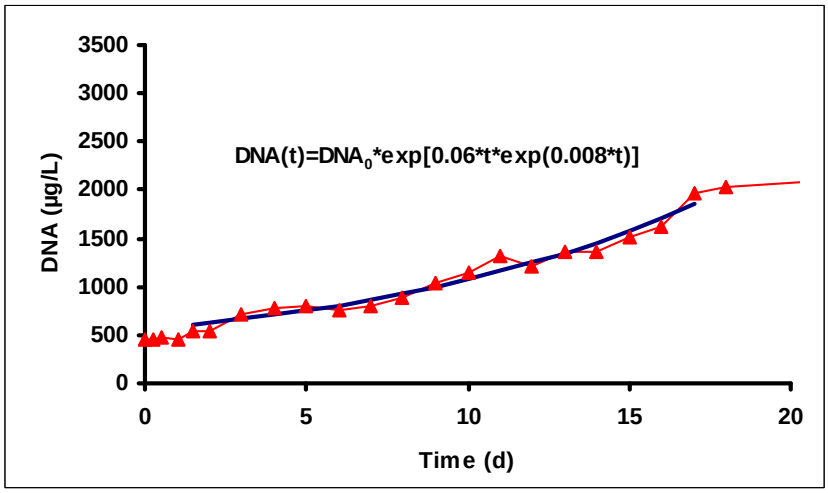

b) Increase of DNA

Figure 5-4 Growth rate assessment for the batch experiment

The growth rate was assessed using the evolution of the oxygen uptake rate and the DNA concentration during the exponential growth phase (Figure 5-4b). However, the analysis of OUR residuals stressed that the exponential relationship did not fit the data well (Figure 5-5). The growth rate was assessed on time intervals of 3 hours, and it increased fourfold during the exponential phase.

Keener and Nomura (1996b) showed that the RNA level is positively correlated with the growth rate. They state that since the ribosome production is an autocatalytic

reaction, in an unrestricted growing culture, the rate of ribosome accumulation (and rRNA), i.e. the increase of the growth rate, will increase with the square of the growth rate. Since the growth of a bacterial population is an autocatalytic reaction as is the rate of ribosome accumulation, then the RNA level theory predicts that after the removal of the carbon limitation on a slow growing culture, the increase of the population will follow a double exponential growth curve, as showed in Figure 5-4b. The residuals of this model fit are shown on Figure 5-5b.

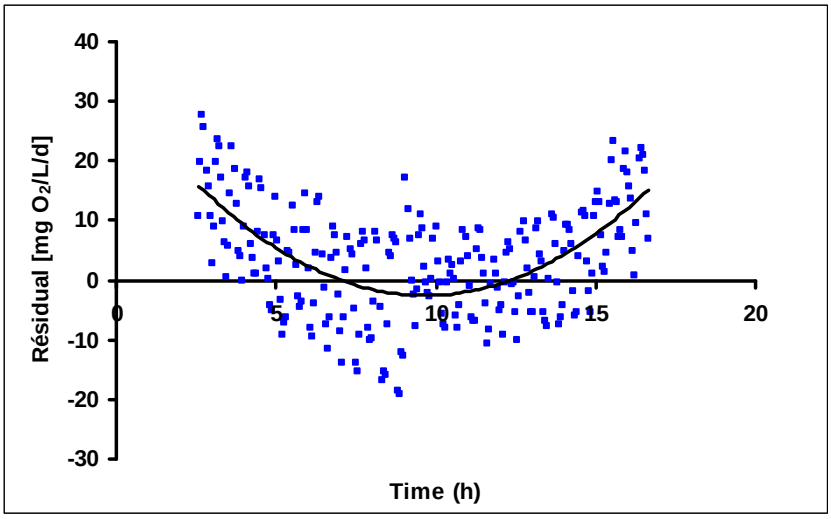

a) Residuals of exponential model

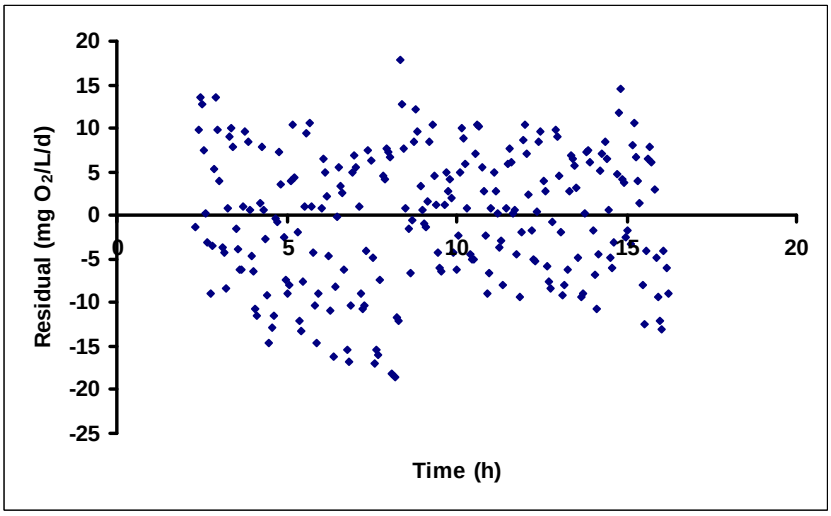

b) Residuals of the double exponential model

Figure 5-5 Residuals distribution of the growth models

On Figure 5-6, one can see that, after a first drop, the specific oxygen uptake rate (OUR/DNA) decreased slightly throughout the exponential growth phase. This observation is not in agreement with results found in literature (Daigger and Grady,

1982b) or to the RNA level theory. It raises questions about the need to model the RNA level for slow growing biomass. With this in mind, the growth rate obtained from the OUR and from the DNA data were compared. The ratio of the equations of the two regression curves on Figure 5-4 gives a parabolic curve with a minimum near the twelfth hour. Thus it was assumed that the downregulation of the OUR observed in the first hour of the experiment was extending and decreasing for several hours. It was concluded that until the twelfth hour, the increase of the specific OUR caused by the increase of the growth rate was masked by the down regulation observed in the first few hours.

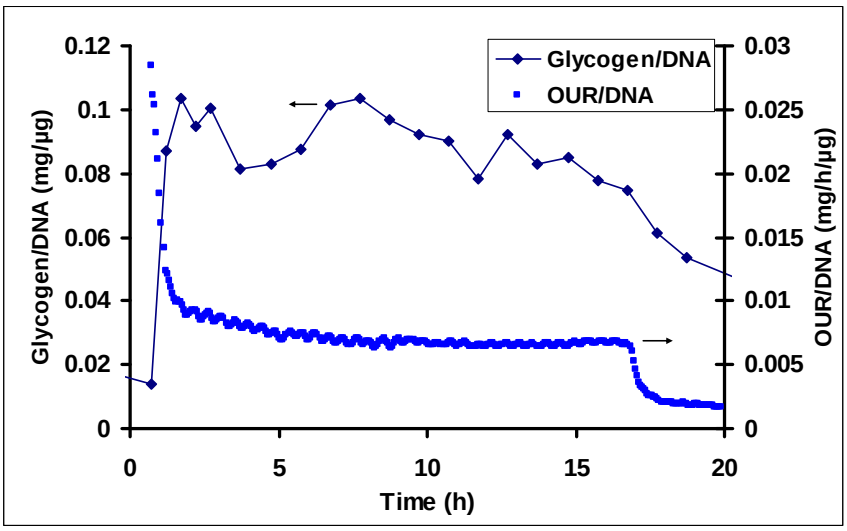

Figure 5-6 Fluctuation of the specific oxygen uptake rate and glycogen accumulation in the batch experiment

The sharp decrease of OUR at the beginning of the experiment was a reproducible transient behaviour. The peak in oxygen uptake rate corresponds to the high rate of substrate uptake and glycogen formation. In the first hour of the experiment Figure 5-6 shows that the glycogen/DNA ratio in cells increased sharply while the OUR/DNA ratio decreased quickly, and then remained constant until exhaustion of the substrate. The accumulation capacity of the cells was evaluated by time integration of the OUR curve during the first hour, as proposed by Cech and Chudoba (1983). Using this method, the initial accumulation capacity was estimated to be 0.09 mgCOD/µgDNA. This value fits the sharp increase of glycogen at the start of the experiment. It was concluded that the cells stored substrate as glycogen until the storage capacity was fully used, and then the substrate uptake rate seems governed by the anabolic rate. Hence, the OUR drop

observed at the beginning of the experiment seems correlated with the drop of the substrate uptake rate.

In Figure 5-3 one can observe that the COD of the precursors increased after having completed the glycogen accumulation capacity. The accumulation of precursors indicates a saturation of the anabolic fluxes. This observation is in agreement with the previous observation that the substrate uptake rate is first governed by the storage rate and afterwards by the anabolism rate.

The accumulation of precursors supports the assumption that the RNA level limits the growth rate when cells are suddenly exposed to high substrate concentrations. On the other hand, the nitrogen incorporation didn't seem to be limiting for cell growth as precursors were accumulated after the storage capacity had been filled completely. However, the rate of precursor accumulation was lower than the maximal carbon uptake rate. Hence, as in these conditions the carbon fluxes should not be the bottleneck of the growth process, nitrogen assimilation could be a candidate limiting process, as proposed in the introduction. Consequently, according to Chang et al. (1999) and Harper and Jenkins (2003), it was assumed that storage would be induced by an imbalance between the rates of assimilation of carbon and nitrogen. Therefore, for the purpose of modeling, accumulation of intracellular substrate caused by the imbalance in the uptake of carbon and nitrogen was used to describe the observed transient behaviours.

The resulting specific rates (r/DNA) and cell's composition (C/DNA) provide an assessment of the metabolic status of the population. This information should be used to assess the intrinsic values of parameters (Grady et al., 1996) in model development and calibration.

5.4 The proposed model

Figure 5-7 shows the simplified model of carbon and nitrogen metabolism adopted here. In this figure, the capital letter S stands for soluble components, the capital B stands for intracellular material, and X for particulate material. The soluble substrate is modeled by the S_S component, the utilisation associated soluble microbial products by S_{MP}, and the ammonia by S_{NH}. In the figure, intracellular substrates like G6P or pyruvate are modeled by B_S, while the amino acids and precursors are modeled by the B_P component, and the cell structure by X_H. The units of all these components are in mg/L.

In Figure 5-7, the arrows stand for enzymatic reactions. One arrow could stand for a sequence of several enzymatic reactions. In the model, the notation "E" refers to an enzymatic structure, and its units are in mg/L. When the enzymatic component is expressed as a specific value, the notation is expressed as "E/X_H" and its units are in mg/mg.

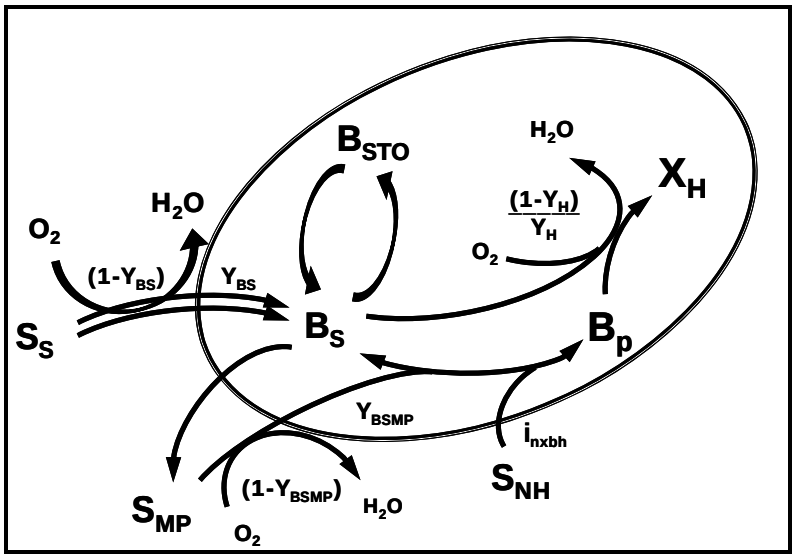

Figure 5-7 Schematic of metabolism

In Figure 5-7, two substrate transporter systems, the phosphoenolpyruvate transferase system (PTS) and a non-PTS system are modeled. According to Chang et al. (1999), the phosphoenolpyruvate transferase system (PTS) has a high capacity and is expressed at high substrate concentrations. The PTS consumes phosphoenolpyruvate (PEP) and produces an excess of pyruvate, which in turn inhibits the PTS (Liao et al., 1996). The excess of pyruvate is then transformed in utilization associated soluble microbial products that are excreted (Aon and Cortassa, 2001; Wolfe, 2005). The non-PTS system is subject to catabolic repression and it is only present at lower growth rates (Death and Ferenci, 1994). Chen et al. (1997) showed also that the non-PTS has a lower capacity than the PTS, and Chang et al. (1999) observed that the non-PTS leads to a more balanced flux of carbon and nitrogen.

Amino acid synthesis uses glutamate and metabolites of the tricarboxylic acid cycle (Merrick and Edwards, 1995). Hence, nitrogen assimilation and glutamate availability positively regulate incorporation of carbon in the tricarboxylic acid cycle.

Hence, in the model the B_P and the B_S components are used in saturation functions to mimic the regulation of the carbon uptake by the intracellular nitrogen availability or the excess of carbon and the saturation of the flux.

After exhaustion of the soluble substrate S_S, the excreted S_{MP} are taken up again but at a different branch point of the metabolism than S_S. They are then transformed in B_P.

A complete mathematical description of the model is given under matrix form in Tables 5-1 to 5-4. The arrows of Figure 5-7 are translated in their mathematical formulation.

To perform a validation of the proposed metabolic model, simple model versions were tested on the experimental data presented in this paper. Only the model versions which include the intracellular precursor component shown in Figure 5-7 allowed describing the down-regulation of substrate uptake and nitrogen incorporation into the cells. The proposed model is the simplest one tested that can describe all components and rates shown in the two comprehensive experimental data sets. The COD and nitrogen mass balance is modeled with 19 processes and 14 components (5 of which are virtual enzymes) and the rate fluctuations are modeled with the increase and decay of the virtual enzymes. In comparison, the ASM3 model uses 5 processes and 8 components to model the COD and nitrogen mass balance of heterotrophic biomass in aerobic conditions, but no modulation of the kinetic rate expressions is possible. Hence, the proposed model mainly introduces the modulation of the rates at the substrate uptake enzyme levels and at the rRNA synthesis level.

Table 5-1 Processes description

Rate	Process rate description	Process rate equation:
r1	increase of B_S (high affinity system)	$k_{Bsha}^{max}*E_{Bsha}*M_{Ssha}*M_{So}$
r2	increase of B_S (low affinity system)	$k_{Bsla}^{max}*E_{Bsla}*M_{Ssla}*I_{bs}$
r3	increase of B_{STO}	$k_{sto}^{max}*E_{STO}*M_{Bsto}*M_B^{max}$
r4	uptake of S_{MP}	$k_{BSMP}^{max}*E_{Bs(SMP)}*M_{SMP}*I_{ssha}$
r5	increase of B_P	$k_{Bp}^{max}*M_{NH}*M_{Bs}*X_H$
r6	aerobic growth of heterotrophs and E_G	$\mu_{Hmax}^{int}/f_{PSS}^{max}*B_{PSS}/X_H*M_{So}*M_{Bs}*M_{Bp}*X_H$
r7	aerobic growth of B_{PSS}	$k_{PSS}*B_{PSS}*M_{So}*M_{Bs}*M_{Bp}$
r8	increase of E_{STO}	$\alpha E_{sto}*B_{PSS}*M_{Bsof}*M_{So}*M_{Bs}*M_{Bp}$
r9	increase of E_{Bsha}.	$\alpha E_{Bsha}*B_{PSS}*M_{Ssha}*M_{So}*M_{Bs}*M_{Bp}*I_{Ssla}$
r10	increase of E_{Bsla}.	$\alpha E_{Bsla}*B_{PSS}*M_{Ssla}*M_{So}*M_{Bs}*M_{Bp}$
r11	increase of $E_{Bs(SMP)}$	$\alpha E_{BSMP}*B_{PSS}*M_{SMP}*I_{Ssha}*M_{So}*M_{Bs}*M_{Bp}$
r12	release of S_{MP}	$kr_{Bs}^{max}*M_{Bsof}*B_S$
r13	degradation of B_{STO}	$\delta k_{sto}^{max}*E_{STO}*M_{STO}*I_{Ssla}$
r14	decay of B_P	$b_{Bp}*B_P$
r15	decay of B_{PSS}	$b_{PSS}*B_{PSS}$
r16	decay of E_{STO}	$\beta_{Esto}*E_{STO}$
r17	decay of E_{Bsha}.	$\beta_{Ebs}*E_{Bsha}$
r18	decay of E_{Bsla}	$\beta_{Ebs}*E_{Bsla}$
r19	decay of $E_{Bs(SMP)}$	$\beta_{EBSMP}*E_{Bs(SMP)}$
r20	decay of X_H	$b_H*I_{ssla}*X_H$

Table 5-2 Description of Saturation and Inhibition Functions

Description of Saturation and Inhibition Functions
$M_{Bs} = (B_S/X_H)/(K_{Bs} + (B_S/X_H))$
$M_{Bp} = B_P/X_H/(K_{Bp}+B_P/X_H)$
$M_{SMP} = S_{MP}/(K_{SMP} + S_{MP})$
$M_{Ssha} = S_S/(S_S + K_{Ssha})$
$M_{Ssla} = S_S/(S_S + K_{Ssla})$
$M_{NH} = S_{NH}/(K_{NH} + S_{NH})$
$M_{So} = S_O/(S_O + K_O)$
$M_{Bsto} = (B_S/X_H)*(B_S/X_H)$
$M_{STO} = (B_{STO}/X_H)/(K_{STO} + B_{STO}/X_H)$
$I_{bs} = (K_{ibs}/(K_{ibs} + B_S/X_H))$
$I_{Ssha} = K_{Ssha}/(K_{Ssha} + S_S)$
$I_{Ssla} = (K_{Ssla}/(S_S + K_{Ssla}))$
$M_{Bsof} = (B_S/X_H)/(K_{bsof} + (B_S/X_H))$
$M_B^{max} = ((f_{STO}^{max}-B_{STO}/X_H)/(K_{isto}+f_{STO}^{max}-B_{STO}/X_H))$

Table 5-3 Stoechiometry of enzymatic components

Rate	B_{PSS}	E_{STO}	E_{BSha}	E_{BSla}	$E_{BS(SMP)}$
Units:	g/g	g/g	g/g	g/g	g/g
r1					
r2					
r3					
r4					
r5					
r6					
r7	1				
r8		1			
r9			1		
r10				1	
r11					1
r12					
r13					
r14					
r15	-1				
r16		-1			
r17			-1		
r18				-1	
r19					-1
r20	$-B_{PSS}/X_H$	$-E_{STO}/X_H$	$-E_{BSha}/X_H$	$-E_{BSla}/X_H$	$-E_{BS(SMP)}/X_H$

Table 5-4 Stoichiometriy of intracellular, soluble and particulate components

Rate Units:	S_O gCOD/m^3	S_S gCOD/m^3	B_S gCOD/m^3	B_{STO} gCOD/m^3	S_{NH} gN/m^3	B_P gCOD/m^3	X_H gCOD/m^3	S_{MP} gCOD/m^3	X_{ii} gCOD/m^3
r1	$-(1-Y_{BS})$	-1	Y_{BS}						
r2	$-(1-Y_{BS})$	-1	Y_{BS}						
r3			-1	1					
r4	$-(1-Y_{SMP})$				$-i_{nx}*Y_{SMP}$	Y_{SMP}		-1	
r5			-1		$-i_{nx}$	1			
r6	$-(1-Y_H)/Y_H$		$-(1-Y_H)/Y_H$			-1	1		
r7									
r8									
r9									
r10									
r11			-1					1	
r12			1	-1					
r13			1		i_{nx}	-1			
r14									
r15									
r16									
r17									
r18									
r19	$-(1-fu)*(1+B_S/X_H+B_{STO}/X_H+B_P/X_H)$		$-B_S/X_H$	$-B_{STO}/X_H$	$(1-fu)*i_{nx}*(1+B_P/X_H)$	$-B_P/X_H$	-1		$fu*(1+B_S/X_H+B_{STO}/X_H+B_P/X_H)$

In Table 5-1, several process rates are modulated by the enzymes concentration (E) and are regulated by the concentration of the enzyme's substrates. The ratio B_{PSS}/X_H in process 6 (r6) reflects the metabolic state of the active biomass. It will change the μ_H value according to the ribosome level in the cells following the RNA limiting theory. Since the synthesis of ribosomes is an autocatalytic process, the increase of the B_{PSS} component is modeled by using the B_{PSS} component and its *intrinsic* increase rate k_{PSS} in r7 (Table 5-3). The dependency on the availability of amino acids is mimicked by including the B_P intracellular precursors term.

The messenger RNA (mRNA) is not considered in this model. As it has a half-life close to 2 minutes, it quickly reaches a quasi steady state concentration (Gupta et al. 2005).

In the model, the variable B_P has COD units. Hence, the active biomass COD is now composed of an amount of structural component (X_H) and a variable fraction, the "biosynthetic constituent" (B_P). The constituent B_P is intracellular, and the mathematical description of biomass then becomes $(X_H+B_P+B_S)$. This description agrees with the description of biomass proposed by Masson et al. (1986) and van den Berg (1998). Thus, in the model, the specific value of the biomass COD ($(X_H+B_P+B_S)/X_H$) will rise and fall with B_P. Accordingly, in this paper, the storage capacity is the maximal B_{STO}/X_H ratio, and the accumulation capacity is the maximal $(B_{STO}+B_P+B_S)/X_H$ ratio.

The decay of B_P (β_{BP}) is a continuous process, and will thus occur both during growth and starvation. During starvation, the active biomass (X_H) will use B_P to produce the energy required for growth on this component. The B_P component is then transformed in B_S and S_{NH}. The cycling of this component will use a part of the COD for respiration. This will be assumed to be the maintenance process. It will increase with the size of B_P.

In the literature it is recognized that cell death of most prokaryotes can be induced by the action of a toxin–antitoxin couple (TA) (Gerdes, 2000; Hochman, 1997; Nyström, 1998; Yarmolinsky 1995). The TA is produced by cells during growth, and the antitoxin counteracts the toxin effect. Only a short time after substrate depletion, the antitoxin is depleted and the toxin can turn on its bactericidal effect. In the proposed model the decay rate of active cells (r19) depends on the availability of substrate. Thus, cellular death would

be regulated inversely to the growth rate, as stated by Mikkola and Kurland (1991). The decay process leads mainly to endogenous respiration.

The production of the enzymes is modeled by including a dependency on B_{PSS} and B_P components. The decay of B_{PSS} and enzyme components (processes r14 to r18) are endogenous processes described as first order reactions characterized by the "endogenous" rate constants *b*. This formulation is similar to the one used by Baloo and Ramkrisna (1991) for the decay of enzymes.

Modeling of storage (process r3) is done through a single reaction as suggested by Dircks et al. (2001) for glycogen and Beun et al. (2000) for PHB. As proposed by these authors, a maximal fraction ($f_{STO}^{\max}$) of B_{STO} in the cell is included in the regulation of the process. This fraction parameter is also included in the saturation function as proposed in ASM2 (Henze et al., 2000) for polyphosphate.

Soluble microbial product (SMP) formation was significant during the experiments performed, and the COD mass balance would take it into account. In the process r11, the constant $k_{RBS}^{\max}$ therefore mimics the outward diffusion of metabolites through the cell membrane.

5.5 Assessment of yields

A number of new parameters is proposed in the model. Hence, new methods were required for parameter identification of yields. These yields were estimated in three steps. In the first step, the yield of intracellular substrate on exogenous substrate (Y_{Bs}) has been calculated from a COD mass balance during a substrate pulse (Vanrolleghem et al., 1999). The oxygen consumption was assumed as negative COD.

As discussed by Vanrolleghem et al. (1999), in this short pulse experiment all glucose was stored as glycogen. The following equation was applied to assess the yield of intracellular substrate on exogenous substrate Y_{Bs}:

$$Y_{Bs} = 1 - \frac{\int rO2(t)dt}{\Delta COD_{consumed}} \qquad [5.1]$$

The experiment was repeated three times, and the mean value was close to 0.9 g COD/g COD.

Then, in the second step, the yield of cell constituents on intracellular substrate ($Y_{H/Bs}$) has been estimated from a COD mass balance on the batch experimental data over the exponential growth phase. Regrowth and respiration on dead cells was not taken into account since the cell death can be assumed negligible under the exponential growth phase, as discussed before. The equation proposed by Vanrolleghem et al. (1999) to model the respiration on readily biodegradable substrate was modified to take into account the respiration associated to substrate that is taken up and is accumulated as intracellular materials. The following equation was applied to evaluate Y_H:

$$Y_H = \frac{\left[1 - \frac{\int rO2(t)dt - (\Delta B_{STO} + \Delta B_P) * (1 - Y_{Bs}) / Y_{Bs}}{\Delta COD_{consumed} - \Delta B_{STO} - \Delta B_P}\right]}{Y_{Bs}} \qquad [5.2]$$

The overall yield of X_H on exogenous substrate was $Y_{Bs}*Y_H$=0.6 g COD/g COD. Thus, the Y_H found on data of the batch experiment was 0.67 g COD/g COD. For a biomass growing on glucose, Dircks et al. (2001) observed similar values.

Finally, in the third step the yield of intracellular precursors on S_{MP} (Y_{SMP}) was chosen according to the Y_{STO} default value in ASM3 (Henze et al., 2000). The yield of B_P on S_{MP} was set to 0.8 g COD/g COD. The value for the uptake rate of S_{MP} was then chosen to fit the model output on the S_{MP}, B_P and OUR data.

5.6 Fitting the model to data

The model was implemented in GPS-X© using the Model Developer of Hydromantis Inc. The Figure 5-8 to5-11 show the fit of the model to the data.

For the batch experiment, the mean deviation between the model response and the data is lower than 6% of the COD for the total biomass (X) and also for the COD for the soluble substrate (S_S). The total biomass is the sum of the active biomass (X_H), the intracellular

materials (B_S, B_{STO}, B_P) and the inert material (X_{ii}). The mean difference between the model prediction and data was lower than 9% for the active biomass (X_H), lower than 12% for glycogen (B_{STO}) and substrate (S_S) lower than 15% for the OUR and lower than 6% for the nitrogen component (S_{NH}). Obviously, the deviation between the model response and the data becomes large when the data decreases to low values.

The mean deviations observed between the model output and the data in the substrate pulse experiment were of the same magnitude, albeit larger for the OUR and the active biomass (X_H). The larger deviation of the OUR was ascribed to the lack of synchronisation between the model output and the data at the sharp increase or drop off of the OUR. The deviation on the active biomass was blamed to the variation of the data since no growth of X_H was observed during this experiment.

As can be seen on Figure 5-9 and Figure 5-11, the deviation between the model response (B_P and S_{MP}) and the endogenous precursor and soluble microbial product data is large. These two components were not assessed directly with experimental measurements but after some manipulation of the COD data. Still, the model outputs represented the trends observed in the data.

5.7 Discussion

The proposed model is based on biochemical concepts. Thus, the main objective of the modelling exercise was to perform a validation of the experimental methods and the proposed model make-up. For modeling of pure cultures, Narang and coworkers (Gupta et al., 2005; Shoemaker et al., 2003) used dry weight as basic unit to assess cell density. This is not possible in wastewater treatment since various kinds of particulate materials are coming with the influent and materials arising from decay of cells are accumulated in the system. In this paper, DNA was used as a basic unit to assess active biomass (X_H). Exogenous DNA, resulting of decay of biomass was removed from suspended solids using crown ether. The «*intracellular* DNA» was then extracted and converted in COD using a stoichiometric coefficient. Note that another extraction protocol of DNA will probably give a different efficiency of extraction and thus a different stoichiometric coefficient.

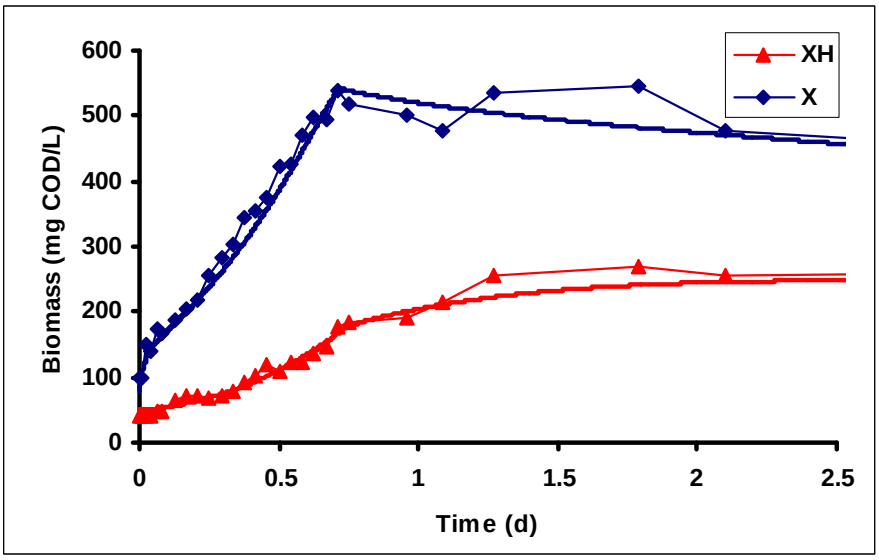

a) Batch experiment

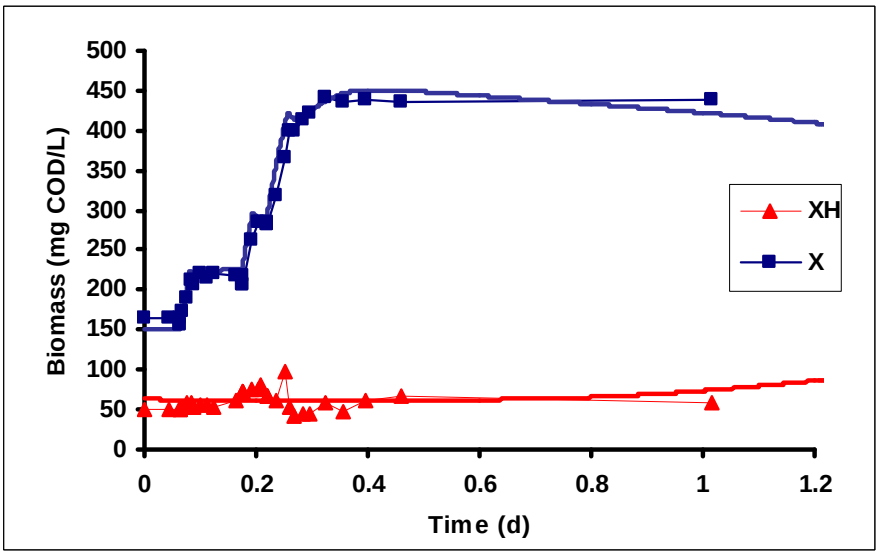

b) Substrate pulses experiment

Figure 5-8 Increase of active biomass (X_H) and total biomass (X) during the experiments.

Figure 5-8 shows that the used yields allow to adequately predict the active biomass (X_H) and total biomass (X) evolution. The stoichiometric coefficient of 0.09 mg COD/µg DNA seems to give a consistent evaluation of the active population of cells all along the experiments even the population increased fivefold.

On the other hand, no increase of the population was observed during the substrate pulse experiment as confirmed by the DNA data and the maximal oxygen uptake rate. Still, the substrate added to the mixed liquor in the substrate pulse and the batch experiments was

430 mg COD/L (doses of 108, 115 and 207 mg/L) and 630 mg COD/L respectively for an initial concentration of biomass of 50 and 63 mg COD/L respectively. In the substrate pulse experiment, most of the substrate COD was accumulated in storage product and precursor materials, and a no growth period of twenty four hours was also observed. In the batch experiment, exponential growth occurred during the same period as COD was converted in active cell material.

In Figure 5-10, it is evident that the inhibition of the OUR was quite larger in the batch experiment than in the substrate pulse experiment. The substrate uptake rates decrease with the same patern. In the batch experiment, the initial OUR and substrate uptake rate are at least fourfold higher than the rates after the inhibition. In the substrate pulse experiment, the initial OUR and substrate uptake rate are only 15% higher than the rates after the inhibition.

In the simulation of the batch experiment, the PTS (r2 in Table 5-1) was highly expressed and the non-PTS (r1 in Table 5-1) was expressed at a low level. After the PTS was inhibited, the transport rate was low and balanced with the growth rate of cells. In the simulation of the substrate pulse experiment, the non-PTS (r1) was highly expressed and the PTS (r2) was expressed at a lower level. After the PTS was inhibited, the non-PTS transport rate was high and not in balance with the growth rate of the cells. Then B_P was accumulated in the biomass of the substrate pulse experiment, and remained at a low level in the sludge of the batch experiment, as also observed in the experimental data.

Also, it was not possible to fit the model on the data of these two experiments using a single set of parameters without modeling the RNA-level with the B_{PSS} component.

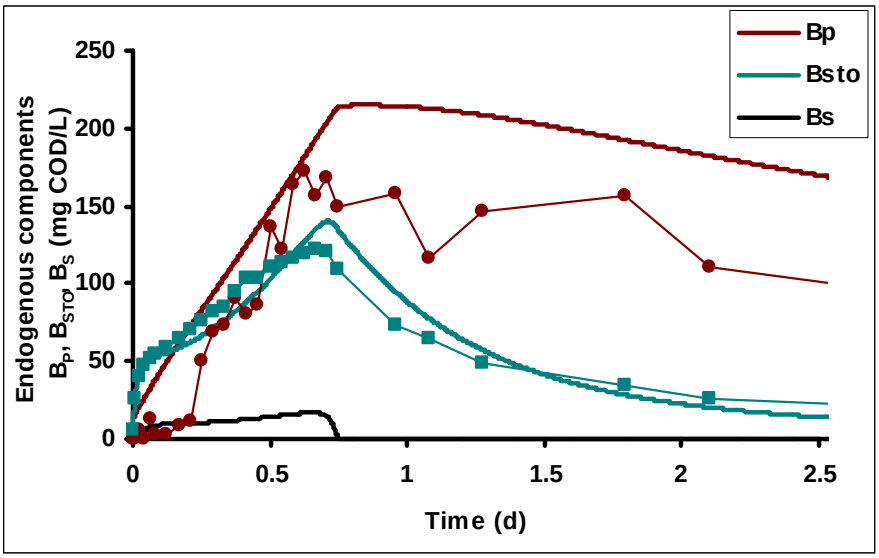

a) Batch experiment

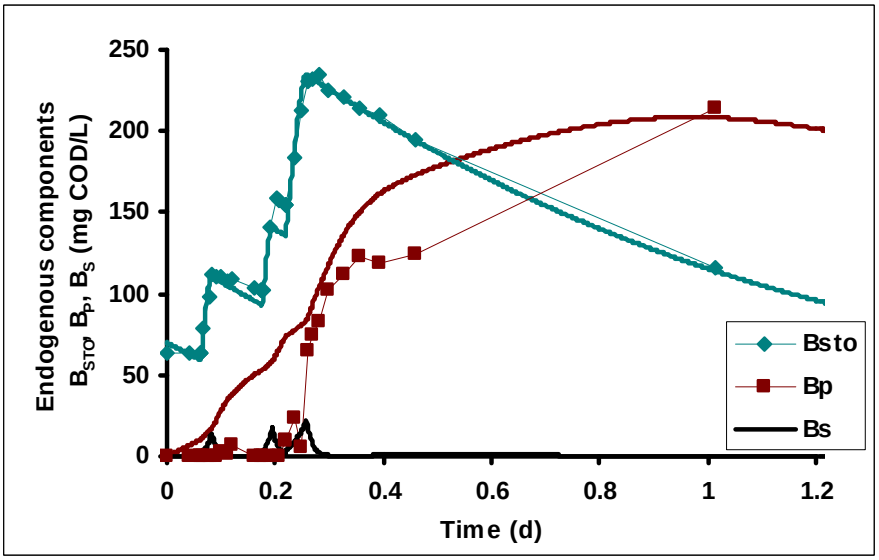

b) Substrate pulses experiment

Figure 5-9 Evolution of intracellular components

At the end of the substrate pulse experiment, the glycogen/DNA ratio was five times the maximal fraction observed in the batch experiment. Dircks et al. (2001) proposed a detailed metabolic model for glycogen accumulating organisms, but the authors set the glycogen fraction as a fixed value. In the experiments presented in this paper, short rest periods in between substrate pulses increased the maximal storage capacity of the biomass. This adaptation of cells was not taken into account in the model. Thus, the maximal fraction ($f_{STO}^{\max}$) of storage material had to be adjusted to fit the two experiments. The mechanism

regulating the maximal value of the glycogen fraction could not be elucidated in this study. Further research is required to understand how this biomass characteristic is regulated.

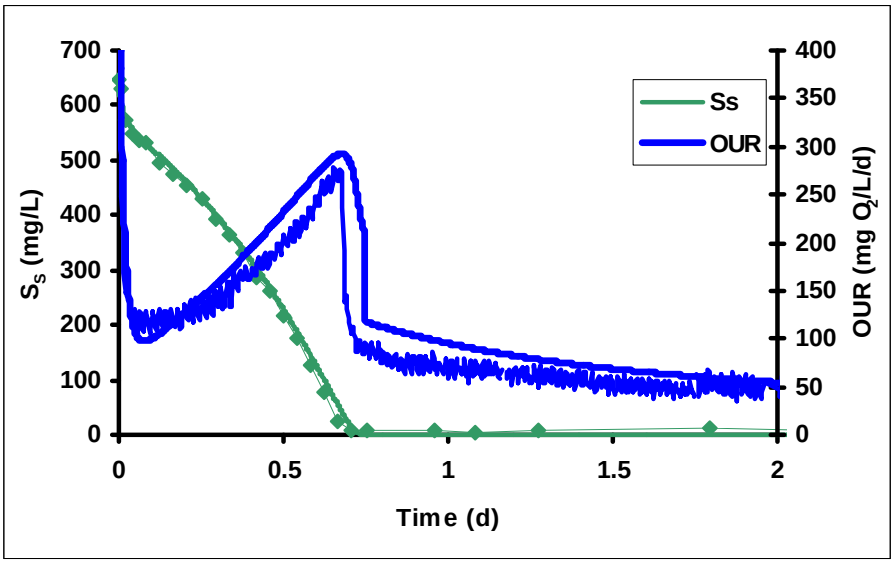

a) Batch experiment

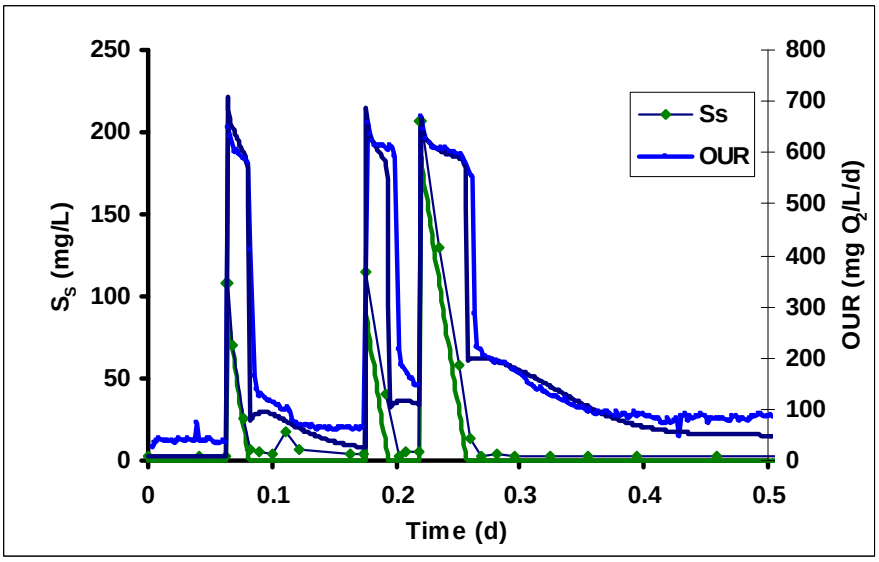

b) Substrate pulses experiment

Figure 5-10 Evolution of soluble substrate and OUR.

As discussed earlier, in addition to the B_{STO} component, the data of the substrate pulse experiment showed that a nitrogenous component was accumulating in the cells (Figure 5-9.b). Moreover, in Figure 5-11.b, the data of this experiment reveal a production of S_{MP} when B_P increased. This is confirmed by the finding that accumulation of intracellular metabolites favours release of SMP (Barker and Stuckey 1999).

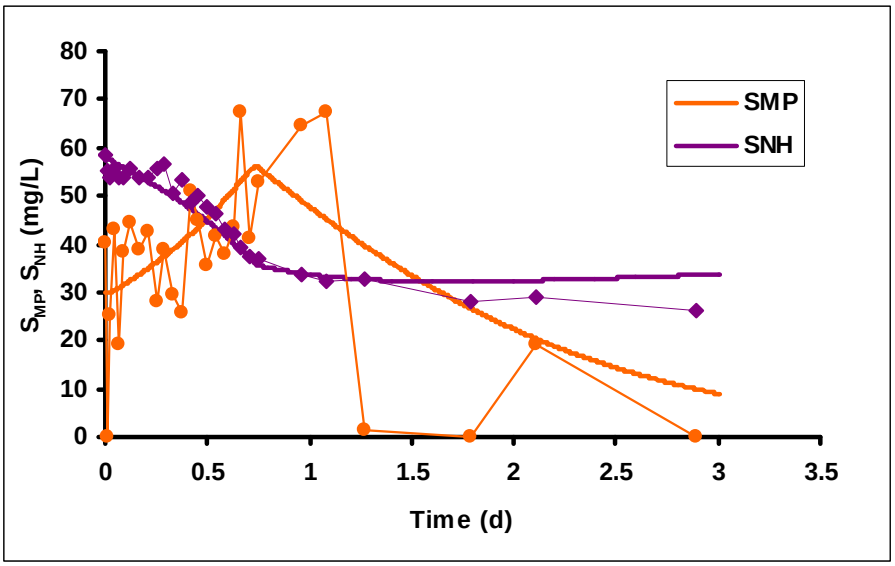

a) Batch experiment

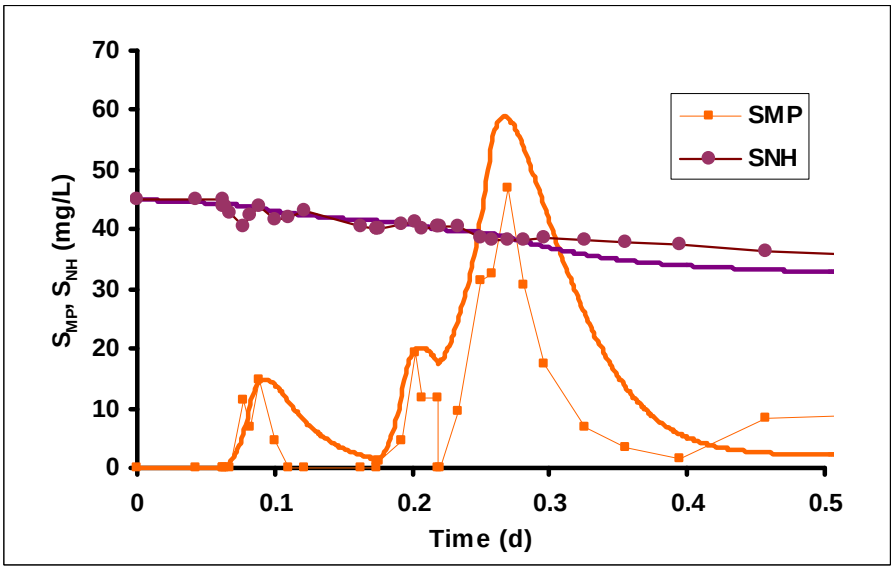

b) Substrate pulses experiment

Figure 5-11 Evolution of soluble microbial products and ammonia.

To our opinion, the filling of the glycogen storage capacity followed by the accumulation of the nitrogenous component, and afterward by the release of soluble microbial products indicates a saturation of the anabolic flux.

The saturation of the flux is modeled using the B_P/X_H ratio. In the model, the production rate of B_P can be higher than the growth rate and lower than the substrate uptake rate. In such conditions, when substrate is taken up, the B_P/X_H and the B_S/X_H ratio increase. The

B_S/X_H ratio is used in saturation functions for regulation of the S_S uptake processes and this in turn affects the saturation of the anabolic flux.

However, from the various conditions applied in these two experiments, it could be concluded that the S_{MP} production was not proportional to the substrate taken up or to the biomass concentration, and moreover it was not correlated to the growth rate. Therefore, it appears that the regulation dynamics of this process is complex and a Luedeking–Piret type relationship as proposed by Chang and Rittmann (1989), or an exponential relationship of the growth rate as proposed by Hao and Lau (1988) were found insufficient to describe the observed dynamics of the S_{MP} production.

In the proposed model the rate of S_{MP} production was assumed to be a diffusion process through the cell membrane proportional to the B_S concentration. However, the diffusion coefficient had to be changed to fit the batch and the substrate pulse experiment. Simulation of the varying SMP production could be improved by modeling an enzyme-catalyzed process as suggested by Saunders (2005; cited by Oehmen et al., 2007). The initial concentration of this enzyme would then be adjusted to fit the rate of the process on each experiment, but more information is needed on the regulation mechanisms of this process.

After short starvation periods, all substrate of a pulse was found to be taken up by the biomass. After a short peak, the OUR decreased and remained constant until exhaustion of the substrate (Figure 5-10). The storage product (B_{STO}) increased steadily until exhaustion of the substrate (Figure 5-9.b). Unlike the batch experiment, the initial peak of OUR cannot be associated to the regulation of the storage process rate. Therefore, in the substrate pulse experiment, in addition to the storage process, another mechanism must be regulating the substrate uptake. The short peaks of OUR observed after each substrate pulse were thus associated to saturation of the metabolic flux. This hypothesis is supported by the discussion on the unbalanced uptake of carbon and nitrogen and is confirmed by the accumulation of the precursor component B_P and by the observed production of S_{MP}.

The tailing of the OUR after the substrate pulses was correlated to the re-uptake of soluble microbial products (S_{MP}). Indeed, the decrease of the storage materials B_{STO} and B_P was not

sufficient to explain the tailing of the OUR. On the other hand, simulations of the S_{MP} uptake gave good agreement with the data.

Additionally, even by using the data from the two experiments, it was not possible to extract information about the production of the enzymes. The objective of using enzyme concentrations in the model was to be able to take into account the history of the biomass. The counterpart of this is that simulations were sensitive to initial enzyme concentrations, and that gave additional degrees of freedom to fit the data. Therefore, the model was run to fit data of a start-up experiment which ran over 25 days (data not shown). Using the parameter values given in tables 5-6 to 5-8, the model described the evolution of the COD all along the experiment. The simulations were not sensitive to the initial concentrations of enzymes but to the production rate (α_E) of the enzyme. This means that in the proposed model, simulations could be done according to the history of the biomass to determine the initial level of the enzymes for the starting point of a given experiment. It can be concluded that more information is needed to enhance the modeling of transients induced by process induction.

5.8 Conclusion

The proposed experimental method seems to give a reliable evaluation of the model components and the model structure presents a consistent assessment of the process dynamics. The components/DNA and rate/DNA ratios could be used to assess the metabolic status of the biomass, and this rich information allows assessing levels of intracellular components which could not be assessed in another way.

The data demonstrated the accumulation of precursors (B_P) when the biomass was exposed to large pulses of substrate. This supports the assumption that the RNA-level limits the growth rate when cells are exposed to high substrate concentrations.

Modeling the imbalance of the uptake rate of carbon and nitrogen gave good results in the simulation of the observed transient behaviours. The model parameters were calibrated on the observed data and the paper shows that the observed transient behaviours can be

explained with the proposed metabolic network. Thus, the fit of the model on the experimental data supports the proposed regulation pattern and the tested hypothesis.

The model needs some improvements to properly model some phenomena observed during the experiments. Further studies are required to understand how the maximal fraction of storage material a cell can hold is regulated. Also, simulation of the SMP production should be enhanced by modeling of an enzyme catalyzed process, but more information is needed on the induction of the processes.

On the other hand, some simplification to the model can be proposed if the simulations aim to describe the behaviour of the biomass when the storage capacity is not completely used. From the data observed in the performed experiments, when the storage capacity is not completely used, saturation of the anabolic flux does not seem to be observable and modeling of the component B_S, B_P and S_{MP} is then not useful.

Further investigations using RNA-based techniques are required to support the proposed protocol and assumptions. These techniques could be used to validate the proposed component to model the r-RNA level and the maximal growth rate fluctuations as proposed by Frigon et al. (submitted). Also, more information is needed to enhance the modeling of transients induced by induction of processes like substrate uptake, soluble microbial product formation and storage.

Table 5-5 Definition of symbols

Symbol	*Definition*
S_O	Soluble oxygen (mg COD/L)
S_S	Soluble substrate (mg COD/L)
S_{MP}	Soluble microbial products (mg COD/L)
S_{NH}	Ammonia (mg N/L)
B_S	Intracellular substrate (mg COD/L)
B_{STO}	Storage material (mg COD/L)
B_P	Intracellular precursors (mg COD/L)
X_H	Heterotrophic biomass (mg COD/L)
X_{ii}	Inert suspended organic matter (mg COD/L)
B_{PSS}	Growth enzyme (ribosome) (mg / L)
E_{STO}	Storage enzyme (mg / L)
E_{Bsha}	High affinity uptake enzyme of soluble substrate (mg / L)
E_{Bsla}	Low affinity uptake enzyme of soluble substrate (mg / L)
$E_{Bs(SMP)}$	Uptake enzyme of soluble microbial products (mg / L)

Table 5-6 Value of kinetic coefficients

Symbol	*Definition*	*Value*
μ^{int}_{max}	Intrinsic value of growth rate (d^{-1})	15
β_{XH}	Decay rate of biomass (d^{-1})	0.09
k_{Bp}^{max}	Synthesis rate of precursors (d^{-1})	0.084
β_{Bp}	Decay rate of precursors (d^{-1})	0.9
kr_{Bs}^{max}	Release rate of soluble material (d^{-1})	3 (88[1])
k_{Bsha}^{max}	Specific activity of substrate uptake enzyme with high affinity (d^{-1})	1
k_{Bsla}^{max}	Specific activity of substrate uptake enzyme with low affinity (d^{-1})	95
k_{Bsto}^{max}	Specific activity of storage enzyme (d^{-1})	35
δk_{Bsto}^{max}	Specific activity of hydrolysis enzyme of stored material (d^{-1})	1
k_{BSMP}^{max}	Specific activity of SMP uptake enzyme (d^{-1})	1
αE_{Bsha}	Increase rate of substrate uptake enzyme with high affinity (mg*mg COD^{-1}*d^{-1})	1.5
αE_{Bsla}	Increase rate of substrate uptake enzyme with low affinity (mg*mg COD^{-1}*d^{-1})	20
αE_{BSMP}	Increase rate of SMP uptake enzyme (mg*mg COD^{-1}*d^{-1})	3
αE_{sto}	Increase rate of storage enzyme (mg*mg COD^{-1}*d^{-1})	1
β_{Ebs}	Decay rate of substrate uptake enzyme (d^{-1})	0.06
β_{EBSMP}	Decay rate of SMP uptake enzyme (d^{-1})	0.06
b_{PSS}	Decay rate of B_{PSS} (d^{-1})	0.5
β_{Esto}	Decay rate of E_{STO} (d^{-1})	0.6

[1] Value used in the substrate pulses experiments (see discussion).

Table 5-7 Value of saturation constants

Symbol	*Definition*	*Value*
K_{SMP}	Soluble microbial products half saturation coefficient (mg COD/L)	40
K_{Ssha}	Soluble substrate half saturation coefficient for high affinity enzyme (mg COD/L)	0.40
K_{Ssla}	Soluble substrate half saturation coefficient for low affinity enzyme (mg COD/L)	20
K_{NH}	Ammonia half saturation coefficient (mg N/L)	2
K_O	Oxygen half saturation coefficient (mg /L)	0.20
K_{Bs}	Intracellular substrate half saturation coefficient (mg COD/(mg COD)	0.0004
K_{Bp}	Intracellular precursors half saturation coefficient (mg COD/(mg COD)	6
K_{STO}	Storage material half saturation coefficient (mg COD/(mg COD)	0.6
K_{ibs}	Intracellular substrate inhibition coefficient for substrate uptake process (mg COD/(mg COD)	0.01
K_{bsof}	Intracellular substrate half saturation coefficient for the SMP production(mg COD/(mg COD)	0.0005
K_{isto}	Intracellular substrate inhibition coefficient for hydrolysis enzyme of storage material (mg COD/(mg COD)	5

Table 5-8 Values of stoichiometric ratios and yields

Symbol	*Definition*	*Value*
f_{PSS}	PSS fraction in active biomass (g/g COD)	0.68
Y_{BS}	Yield of intracellular substrate on soluble substrate (g/g)	0.88
Y_{BSMP}	Yield of intracellular substrate on soluble microbial products(g/g)	0.8
Y_H	heterotrophic yield on intracellular substrate (g/g)	0.66
f_{STO}^{max}	Maximal fraction of storage material (g/g)	1 (7[1])
i_{nx}	Nitrogen fraction of active biomass (g N/g COD)	0.068
f_u	Fraction of biomass leading to particulate products (g/g)	0.20

[1] Value used in the substrate pulses experiments (see discussion).

CHAPITRE 6 RÉPONSE DU MODÈLE PROPOSÉ EN CONDITIONS EXPÉRIMENTALES STABLES

Un des objectifs de ce travail consistait à affranchir le modèle et les constantes cinétiques de l'histoire de la biomasse et de la configuration du procédé. Or, tel que mentionné précédemment, la modélisation de la production et du dépérissement des enzymes visait à décrire l'état métabolique de la biomasse à un instant donné en fonction de son historique.

Au chapitre précédent il a été mentionné que les expériences effectuées ne permettainet pas d'extraire de informations sur les taux de production d'enzymes (α_E) et que cela laissait disponible des degrés de liberté pour effectuer le calage du modèle sur les données.

Ainsi afin de réduire le nombre de degrés de liberté disponibles, le modèle a été calé sur une expérience de longue durée qui a mis en évidence la sensiblilité du modèle au taux de production des enzymes de transport du substrat.

6.1 Description de l'expérimentation

Après que la biomasse ait été acclimatée au substrat et aux conditions d'opération, seulement une fraction de la liqueur mixte a été conservée dans le réacteur semi-continu. Le volume liquide a été complété avec la base du substrat (sans la source de carbone), et l'alimentation semi-continue a été démarrée au rythme de huit doses de 60 ml par jour pour obtenir un temps de rétention hydraulique de 6,5 jours.

La mesure de différents composants a été effectuée quotidiennement sur une période de 25 jours.

6.2 Niveau d'expression des enzymes de transport

En comparant la Figure 6-1avec la Figure 5-6, il est possible de constater que la respiration spécifique initiale de la biomasse était beaucoup plus faible lors de l'expérience pulsée, mais qu'après la réduction d'activité, la respiration spécifique était de l'ordre de 0,035 mg O_2/ADN/h dans les deux expériences. La réduction de la respiration semble encore une fois causée par la saturation des flux, mais le niveau de respiration initial (avant la saturation des flux) serait selon toute vraisemblance, limité par le taux de transport du substrat. L'écart de 0,07 mg O_2/µg ADN/h observé entre la respiration spécifique initiale de ces deux expériences constitue près de deux fois le taux de respiration initial de l'experience pulsée. Cet écart serait attribuable au temps de rétention plus long dans le réacteur semi-continu lors de la culture de la biomasse utilisée pour inoculer la cuvée de l'expérience pulsée. Le niveau d'expression des enzymes de transport du substrat serait donc sensible à l'âge des boues. Cette observation tombe sous le sens puisque les modèles cybernétiques ont été développés justement pour modéliser les processus induction des enzymes de transport de substrat en fonction des différentes conditions appliquées sur des réacteurs biologiques (Baloo et Ramkrishna, 1991).

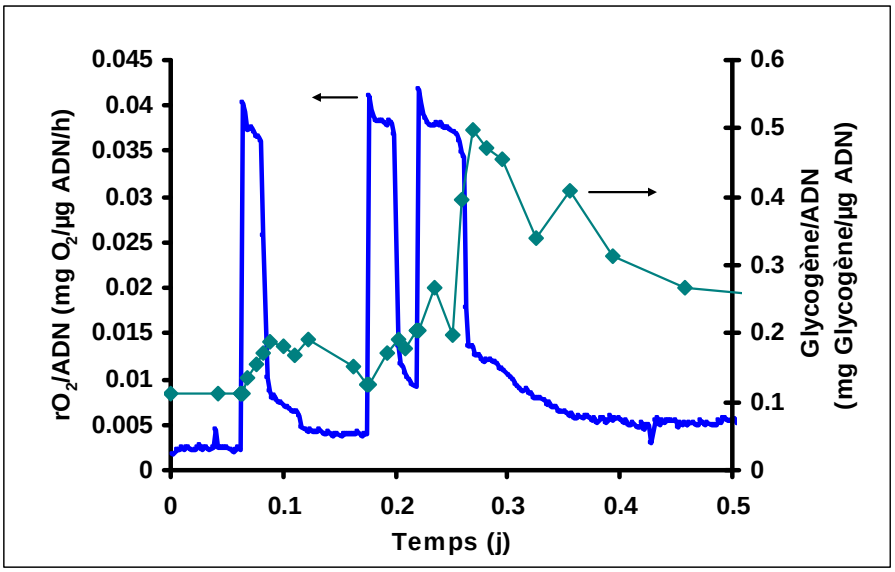

Figure 6-1 Variation de la respiration spécifique de la biomasse lors des pulses de substrat.

Les simulations effectuées sur les expériences de courte durée (moins de 24 h) ont démontré que la réponse du modèle était sensible à la concentration initiale d'enzyme. De

ce fait, le modélisateur dispose de degrés de liberté supplémentaires pour ajuster les taux lors de ces simulations.

Selon la structure du modèle proposé, la concentration d'enzymes dans la biomasse dépend du taux de production (αE) de ces derniers et du taux de dilution dans le réacteur de culture, c'est à dire de l'historique de la biomasse.

6.3 Réponse du modèle sur le démarrage du réacteur semi-continu

Afin de tenir compte du niveau d'expression des enzymes, le modèle a été calé sur des données obtenues lors d'une expérimentation qui s'est étendue sur une période de 25 jours. Les figures 6-2 à 6-6 montrent la réponse du modèle lors de la simulation du démarrage du réacteur à alimentation semi-continue. Encore une fois, la simulation a été effectuée avec les valeurs données aux tableaux 5-6 à 5-8.

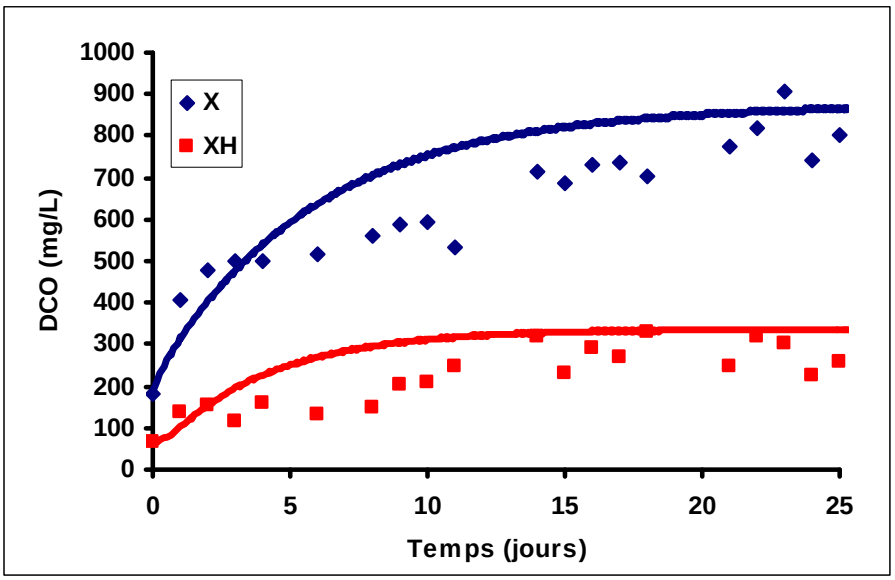

Figure 6-2 Évolution de la DCO lors du démarrage du réacteur

Le modèle prédit adéquatement l'évolution de la biomasse dans le réacteur. Lors de cette simulation, la réponse du modèle sur la biomasse était sensible au coefficient de rendement et au taux de dépérissement. Le taux de dépérissement a été ajusté à 0,09 j^{-1} pour que la réponse du modèle décrive adéquatement les données expérimentales dans les trois expériences.

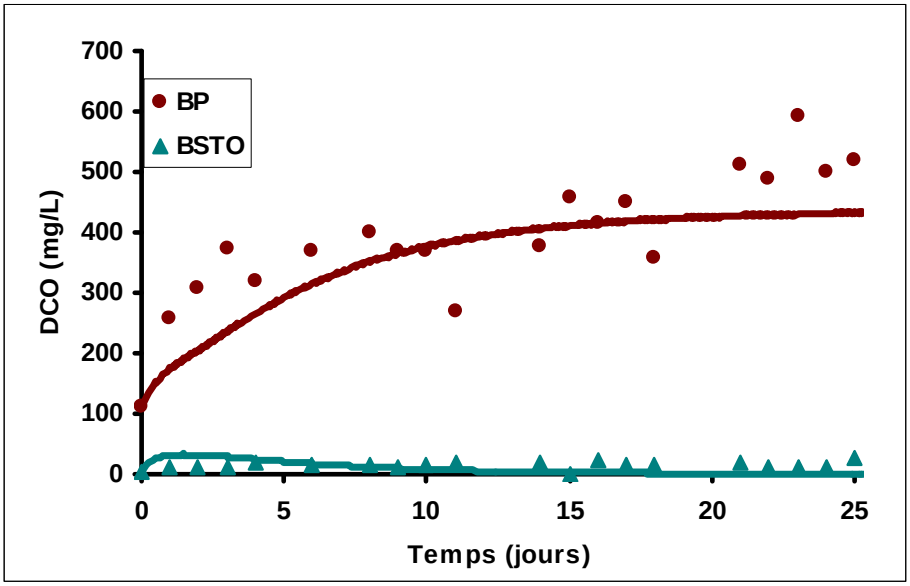

Figure 6-3 Évolution des réserves lors du démarrage du réacteur

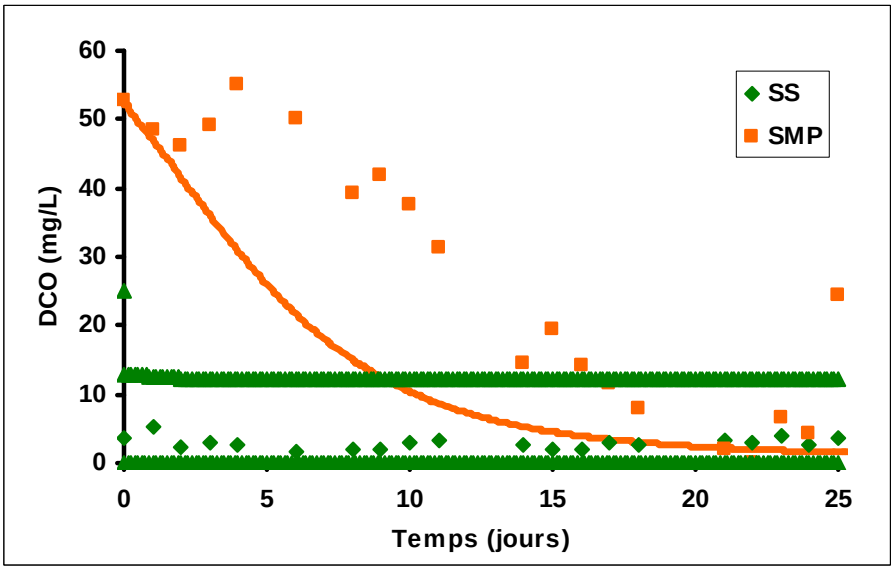

Figure 6-4 Évolution du substrat et des SMP lors du démarrage du réacteur

La concentration des glycogènes est demeurée à de faible valeurs tout au long de l'expérience contrairement aux matériaux constituants cellulaires. Lors de cette expérience la biomasse ne semble pas avoir développé une grande capacité d'accumulation des glycogènes.

Même si lors de cette simulation, la concentration initiale d'enzymes de consommation des SMP ($E_{BS(SMP)}$) a été fixée à zéro, le modèle ne décrit pas adéquatement le délai observé

dans les données expérimentales (Figure 6-4). Il y aurait lieu de préciser les mécanismes d'induction des enzymes d'hydrolyse.

Le modèle semble en mesure de prédire adéquatement la respiration maximale et la respiration endogène. Le taux de production α_{EBSla} de l'enzyme de transport E_{BSla} a été fixé à 50 g g^{-1} j^{-1} afin de caler la réponse du modèle sur la respiration maximale de la biomasse (Figure 6-5). Toutefois, lors de cette expérience, la respiration maximale correspond à la respiration mesurée à saturation par le substrat. Or, le modèle prédit une concentration maximale de substrat dans le réacteur de 11 mg DCO/L, ce qui est inférieur à la valeur de demi-saturation. Comme on peut le voir sur la Figure 6-6, la même simulation effectuée avec un taux de production d'enzyme α_{EBSla} de 20 g g^{-1} j^{-1} donne une respiration maximale inférieure à celle mesurée expérimentalement. Cette description devrait normalement correspondre davantage à la respiration qui aurait pu être observée dans le réacteur au moment de l'alimentation. Cette dernière n'a pas été mesurée. La valeur de 20 g g^{-1} j^{-1} a donc été retenue pour effectuer les autres simulations.

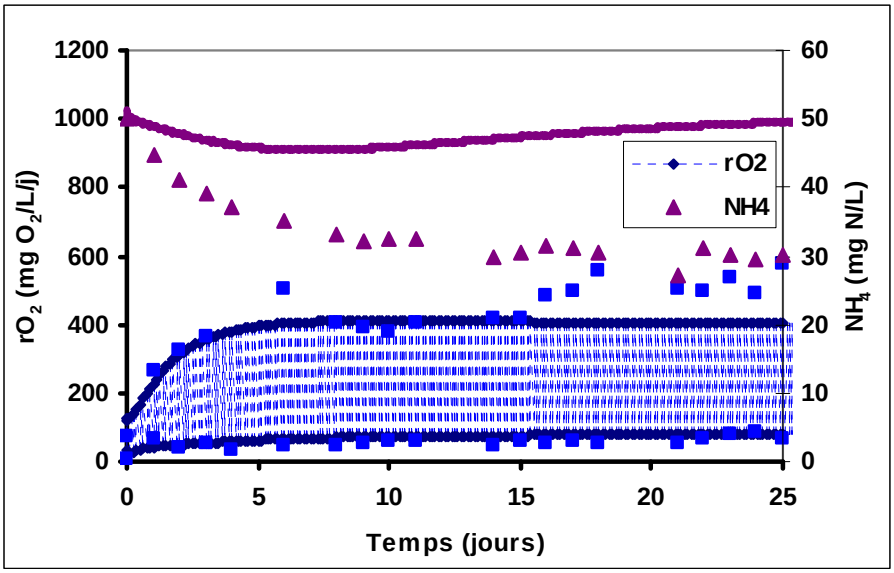

Figure 6-5 Évolution du taux de respiration et du NH_4^+ lors du démarrage du réacteur (α_{EBSla}=50 g g^{-1} j^{-1}).

Il apparaît donc que la réponse du modèle est sensible au taux de production d'enzyme à faible affinité pour la consommation du substrat (α_{EBSla}).

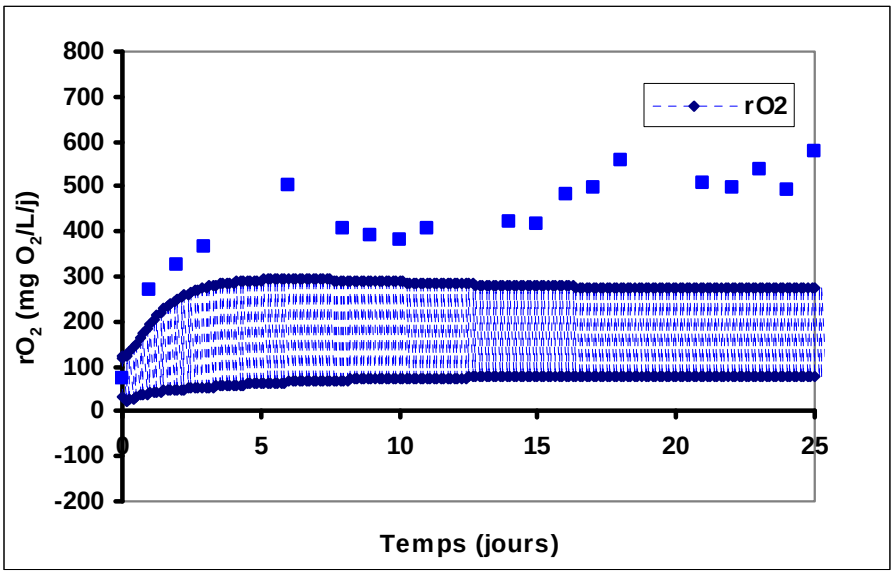

Figure 6-6 Modélisation du taux de respiration lors du démarrage du réacteur (α_{EBSla}=20 g g^{-1} j^{-1}).

Comme la biomasse prélevée pour effectuer les expériences de courte durée provenait du réacteur semi-continu, les conditions qui prévalaient dans ce réacteur constituaient les conditions qui définissaient l'état métabolique de la biomasse. Par conséquent, les concentrations d'enzyme données par le modèle devraient être retenues comme conditions initiales des expériences de courte durée.

Ainsi il apparaît qu'il est nécessaire de recalibrer le modèle sur ces expériences de longue durée représentatives des conditions initiales des expériences de courte durée pour définir les taux de production d'enzyme, ce qui fixe le niveau d'enzymes prédit par le modèle. Ensuite, il devient nécessaire de recalibrer les expériences de courte durée avec les concentrations d'enzymes prédites par le modèle lors des simulation des expériences de longue durée pour finalement trouver une seule valeur à chacune des constantes cinétiques du modèle.

Cette étape de la calibration du modèle n'a pu être effectuée. Dans les faits, la méthode de mesure de la respiration maximale utilisée lors du démarrage du réacteur semi-continu ne nous permet pas de calibrer le modèle adéquatement sur l'expérience de longue durée puisqu'elle ne décrit pas le taux de respiration observé dans le réacteur, mais le taux de

respiration à saturation par le substrat exogène. Il n'y a donc pas concordance entre la méthode expérimentale utilisée et la simulation.

D'autre part, la réponse du modèle sur l'évolution du NH_4^+ dans le réacteur dévie considérablement des données expérimentales. Cette observation révèle un problème structural dans la description mathématique du modèle. Selon la structure ce dernier, la respiration endogène des matériaux constituants cellulaires libère du NH_4^+ directement dans la phase liquide. Or, dans les modèles ASM1 et ASM2, la respiration endogène génère plutôt de l'azote organique qui doit par la suite être «ammonifiée». Cette étape a été négligée dans le modèle proposé. Par conséquent, lors de la simulation du dépérissement, le modèle prédit une concentration de NH_4^+ plus élevée que les mesures expérimentales. Il est possible d'observer ce phénomène aussi dans la Figure 5-11a lors de la phase endogène (après 1,25 jours). Plus le taux de dépérissement de la biomasse est élevé, plus la déviation de la réponse du modèle s'écarte des données expérimentales.

La structure du modèle devrait donc être modifiée pour tenir compte de la production d'azote organique et de l'ammonification.

CHAPITRE 7 MODÈLES AVEC STRUCTURES ARN-r

Selon la discussion effectuée précédemment, il semble que le modèle proposé soit en mesure de décrire adéquatement la réponse transitoire observée de la biomasse. Le modèle inclut une description des enzymes de transport du substrat en plus de la structure ARN-r qui décrit le système de synthèse des protéines (PSS).

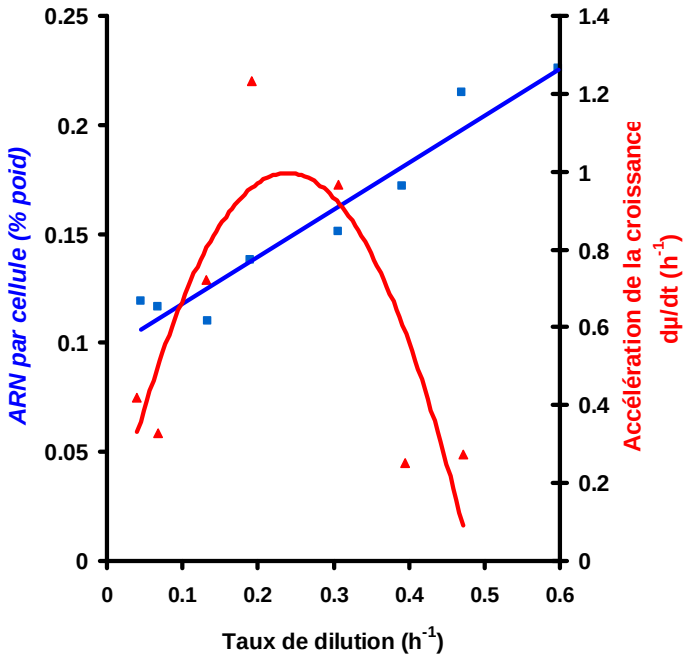

Figure 7-1 Variation de la fraction d'ARN et du taux de croissance

(Adapté de Daigger, 1979).

La structure ARN-r devrait permettre au modèle de décrire la variation du taux de croissance pour différentes situations. Selon la littérature, le taux de croissance semble corrélé linéairement avec la proportion d'ARN ribosomal (ARN-r) dans la masse cellulaire

(Bremer et Dennis, 1996; Daigger, 1979), mais tel qu'on peut l'observer sur la Figure 7-1, Daigger (1979) a démontré que la variation du taux de croissance ($d\mu/dt$) des bactéries *Pseudomonas putida* ne varie pas proportionnelement à la fraction d'ARN dans la masse cellulaire. Un modèle avec une structure ARN-r doit être en mesure de reproduire adéquatement l'accéleration de la croissance de la biomasse observée par ces auteurs.

Une analyse de sensibilité a donc été effectuée afin de vérifier la réponse du modèle à différents pourcentages d'ARN-r.

L'article qui suit a été publié en janvier 2009 dans la revue Water Science and Technology, volume 59(4), 661-671.

MODELLING USING R-RNA-STRUCTURED BIOMASS MODELS

Lavallée B.[*], Frigon D.[**], Lessard P.[*], Vanrolleghem P.A.[*], Yuan Z.[***] and van Loosdrecht M. C. M.[****]

[*]*Département de génie civil, Université Laval, Québec, QC, Canada, G1K 7P4 (email : bernard.lavallee.1@ulaval.ca, Paul.Lessard@gci.ulaval.ca, Peter.Vanrolleghem@gci.ulaval.ca).*
[**]*Department of Civil Engineering and Applied Mechanics, McGill University, Montreal, H3A 2K6. (email: Dominic.Frigon@mcgill.ca).*
[***]*Advanced Water Management Center (AWMC), The University of Queensland, St. Lucia, Queensland 4072, Australia (email: zhiguo@uq.edu.au).*
[****]*Environmental Biotechnology Group, Department of Biotechnology, Delft University of Technology, Delft, The Netherlands (email: m.c.m.vanloosdrecht@tudelft.nl).*

ABSTRACT

Models currently used have been developed to describe the storage response in the activated sludge process. In these models the distribution of the substrate flux between growth and storage is an empirical function. rRNA-structured biomass models are proposed to describe the metabolic status of cells in view of predicting the growth response (dμ/dt) of cells in the activated sludge process. The autocatalytic reaction rate of the synthesis of the PSS component (rRNA) can provide a mechanistic explanation for the growth response and the growth lag phase. The proposed models were able to describe and predict properly the growth response of the biomass in various types of reactor. Such models could be more widely applicable by using intrinsic model parameters. This would be a key improvement for as it would lead to improved models for design.

7.1 Introduction Overview of models and structuring in the models

Daigger and Grady (1982a) were the first authors to propose a structured approach to model the metabolic status of the biomass in activated sludge processes. They noted that the *inputs to most wastewater treatment systems are time-variant, indicating that steady-states*

are seldom achieved. Consequently, realistic prediction of the performance of biochemical unit processes requires that the dynamic response of the microbial culture be considered. They divided the transient phenomena into two general classes; the storage response and the growth response.

Since then, various models have been developed to describe the storage response in the activated sludge process. The main ones include the IWA Activated Sludge Model No.2d (ASM2d), ASM3 (Henze et al., 2000), ASM3-BioP (Ky et al., 2001; Rieger et al., 2001) and TUDelft model (TUDP) (van Veldhuizen et al., 1999).

For all these models, the values of the kinetic parameters are typically site-specific and calibration is usually required for accurate description of the actual process under study (Gernaey et al., 2004). Usually and fortunately, the calibration effort is limited to a few key parameters and some steps in the calibration procedure can be omitted depending on the aims (Gernaey et al., 2004).

In ASM, the biomass is separated into micro-organisms and different storage compounds. It is assumed that the various intracellular fractions (but storage) of the micro-organisms does not change according to the pseudo steady state hypothesis.

However, when the conditions in the process significantly change, the level of intracellular components as well as the rates and the metabolic status of bacterial cells will change. Hence, one pseudo steady state can not describe the old and the new situations. Then, recalibration of the kinetic parameters involved is usually required for accurate description of the process exposed to the new operational conditions or for accurate description of the new process configuration (Gernaey et al., 2004; van Loosdrecht et al., 2002).

The simplifications adopted in conceptual models of the metabolism are dependent on the experimental methods used to determine the parameter values, and therefore the conceptual models are empirical by nature and the parameters value are often site specific. Due to the site-specific nature of the calibration procedure, the parameters have been denoted as *extant* as opposed to universal parameters that would be *intrinsic* (Grady et al., 1996). By introducing the *extant/intrinsic* nomenclature, Grady and coworkers (1996) speculated that

most parameters are extant because the models fail to consider the metabolic status of the bacterial biomass, suggesting that considering the metabolism could allow the development of more widely applicable (intrinsic) model parameters. It appears that the metabolic status of the cell can be partly captured by considering the level of rRNA per cell (Daigger and Grady, 1982a).

Consequently, RNA-based models have been developed to describe the metabolic status of cells in view of performing simulations of the microbial adaptation and growth response of cells. Using a simplified RNA-based model, van Loosdrecht and Heijnen (2002) showed the overall trends of the model output for various values of specific enzyme (RNA) decay rates and operational conditions in an SBR. The simulation showed that the parameters had only a limited influence, but also that the model correctly predicted the PHB fractions and growth rates under various sludge retention times.

More recently, two quite similar approaches have been suggested to use molecular data for better description of transient behavior. A first approach uses stoichiometric modelling involving a carbon mass balance and RNA-based molecular techniques to model PHB accumulation and growth of biomass in SBR's (Frigon et al., submitted). The second one uses dynamic modelling involving a COD mass balance and DNA molecular techniques to model the transients induced by substrate pulses and batch experiments with high initial substrate to biomass ratio (Lavallée et al., in preparation). Both approaches proposed similar structures.

The discussion in this paper aims to expose these works in progress in order to extend the application range of the ASMs and TUDP to different processes configurations or to different steady states (including the modelling of the transient from one steady state to the other) without the need for recalibration. The objective is not to calibrate the models on a particular data set, but to indicate when a RNA-structured biomass model is needed.

7.2 Scope and objectives of rRNA-structured biomass models

Faced with different problems of the kind presented above, various authors attempted to develop model in which they structured the biomass COD in specific pools and specifically

described the COD conversion between these pools. A survey of activated sludge structured-biomass models indicates the following specific objectives for the developed models:

Implementing a fundamental metabolic yield coefficients (the ATP/NADH2 ratio in the oxidative phosphorylation) (Beun et al., 2000; Dirks et al., 2001; Smolders et al., 1994)

Predicting transient conditions under the dynamic conditions of activated sludge processes or batch tests (Daigger and Grady, 1982b; Smolders et al., 1995a, 1995b; Grady et al., 1996; Beun et al, 2000; Lavallée et al., 2002; Vanrolleghem et al., 2004; Frigon et al., 2006)

Predicting microbial activities in different processes (Oerther et al., 2001; Frigon et al., 2002a; 2002b; Stroot et al., 2005; Simpson et al., 2006)

Interfacing with microbial population dynamics results obtained by molecular techniques (Frigon et al., 2006; Gilbride et al., 2006)

RNA-based models have been developed with all these specific objectives in prospect.

S*toichiometric modelling* used to describe yields, and *kinetic modelling* used to describe dynamics, are two basic aspects of modelling. Though not independent, the considerations for both modelling approaches invoke different aspects of microbial metabolism and the contribution and promises of these two approaches will be described separately. rRNA models proposed by the authors include structured descriptions of the metabolism in both approaches.

7.3 Stoichiometric modelling

The approach proposed by the group at the Technical University of Delft was to model the EBPR microbial activity by describing the stoichiometry of the specific metabolic pathways involved. This metabolic description has the benefit of adding constraints to the model solution space by linking pathways through the production or consumption of energy (ATP) and reducing equivalent carriers (NADH). The external observed yield coefficients

for different cellular fractions are all dependent on one metabolic yield coefficient: the oxygen (or $NADH_2$) to ATP ratio. Consequently, assuming that the carriers do not accumulate in bacterial cells allows the expression of the substrate consumption and intracellular component formation rates with a reduced number of *independent* parameters. This property has made it possible to successfully describe full-scale domestic wastewater treatment plants of numerous configurations by adjusting only 3 or 4 parameters (Oehmen et al., 2007).

Note further that, since the pathways are all linked through the energy carriers, the successful calibration of such a model is by itself a validation of the proposed model structure.

7.4 Kinetic modelling – RNA-based approach

The cells' composition in relation to the growth rate has been studied by several authors (Daigger and Grady, 1982b; Esener et al., 1982; Herbert, 1958; Herbert, 1976; Bremer and Dennis, 1996). Herbert (1976) observed that when the carbon source is the limiting substrate, the elementary composition of cells is independent of the growth rate, but the fractions of the cell constituents vary.

Approximately 50% to 65% of the mass of fast growing bacterial cells is accounted for by proteins and 10 to 20% is accounted for by RNA. All RNA can be considered rRNA since it comprises approximately 85% of the cellular RNA at all growth rates (Bremer and Dennis, 1996) and all proteins are synthesized by ribosomes. The ribosome is the catalytic unit responsible of protein synthesis and its main catalytic constituent is rRNA. As a result, a major aspect of the metabolic status of bacterial cells is the level of rRNA, and its level is correlated with growth rate (Herbert, 1958; Keener and Nomura, 1996a; Koch, 1970).

Determination of the RNA/DNA ratio has been proposed to assess the nutritional condition of larval fish (Kaplan, 2001) and growth rates in marine bacteria (Dell'Anno et al., 1998; Kerkhof and Ward 1993) or in foodstuffs (Milner et al, 2001). Muttray et al. (2001) used the rRNA/rDNA ratio to characterize the metabolic activity of *Pseudomonas abietaniphila* in activated sludge.

Using a genetic knockout mutant Frigon et al. (2006) observed that the reactor configuration and the ability to produce PHB had an impact on the rRNA-level for a pure culture growing in an acetate-fed reactor. Because the intracellular concentration of rRNA varied with process configuration or with the loading as well as with the growth rate, these observations showed that one pseudo steady state can not hold for different process configurations or for different steady states (i.e. different maximal growth rates) when a mass balance around rRNA is not included, and then recalibration of the model is required.

RNA-based models have been developed to describe the metabolic status of cells with a view to perform simulation of microbial adaptation and transient behavior of cells (Frigon et al, 2002a; Frigon et al, submitted; Gupta et al., 2005; Lavallée et al., 2005a; Lavallée et al., in preparation; Turner and Ramkrishna, 1988; van Loosdrecht and Heijnen, 2002). In these models, the size of the component, here called the protein synthesis system (PSS, or rRNA), is used to describe the metabolic status of the cells. This component (X_{PSS}) denotes the rRNA-level in the cells and it is used to model the modulation of the specific growth rate. It catalyzes the cell constituent synthesis.

Most of these models suggest that the synthesis rate of rRNA is autocatalytic as its rate of synthesis is related to its own concentration (Figure 7-2). This provides a sigmoidal increase of rRNA-level after a switch in conditions. As a result, when the level of the rRNA is low, the rate of change of the transient response is slow; when the level is medium the rate of change of the transient becomes fast; and when the rRNA-level is high, its further increase is small and the response doesn't quite change. Accordingly, Daigger and Grady (1982b) observed that the rate of change of the transient response ($d\mu/dt$) of *Pseudomonas putida* increased with the growth rate to reach a maximal value near a growth rate of 0.2 h^{-1}, and then decreased as the growth rate increased. The autocatalytic reaction rate of the rRNA synthesis can provide a mechanistic explanation for the pattern of the growth rate adaptation observed by Daigger and Grady (1982b) and so for the lag phase occurring in a slow growing culture when the substrate limitation is removed.

All proposed models present a component (B_P) to mimic the level of the building blocks or precursors. The synthesis of the PSS and the structural component of the biomass (X_C) (mainly proteins, lipids and DNA) is rate-dependent on the building block level.

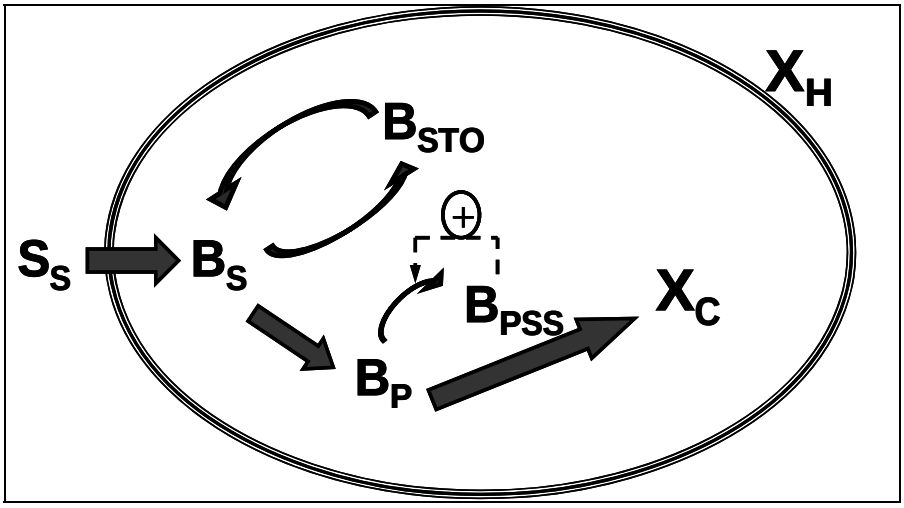

Figure 7-2 Common kinetic scheme of the models (symbols used may differ for the different models in literature). S_S: Soluble substrate; B_S: intracellular substrate or metabolites; B_P: Building blocs or precursor; B_{PSS}: protein synthesis system or rRNA; X_C: Structural component of cell or proteins; X_H: $B_S+B_{STO}+B_P+B_{PSS}+X_C$.

7.5 Interfacing the biomass composition with molecular techniques

van Loosdrecht and Heijnen (2002) first proposed a simplified model in an academic context. These authors explained that cells prioritize growth to storage. In order to describe the storage process, it is needed to define models with a variable amount of anabolic enzymes. They showed that the simplified model predicted fairly well the PHB fraction in biomass for various SRT.

Frigon et al. (submitted) proposed to use a carbon mass balance, PHB extraction, protein assay and RNA molecular techniques to model PHB accumulation and growth of biomass in SBR. These authors proposed a detailed description of the PSS and the structural components of biomass to provide an explicit link between molecular techniques and the model predictions.

Lavallée et al. (in preparation) on the other hand used a COD mass balance, glycogen and DNA extraction to model the response to substrate pulses and batch experiments with high initial substrate to biomass ratio. Lavallée et al. (in preparation) modelled the PSS using a component with zero mass to conserve a closed COD mass balance on the different components. These authors chose DNA for quantitative population assessment since the

DNA level per cell remains constant for all growth rates and can be used for quantitative interpretation of data for bacterial populations in activated sludge.

Table 7-1 summarizes the components considered by these authors for their RNA-structured biomass.

Table 7-1 Description of the RNA-structured biomass.

	Frigon et al.	Lavallée et al.	van Loosdrecht & Heijnen
Mass balance	Carbon	COD	COD
Substrate	Acetate	Glucose	Acetate
B_S	acetyl-CoA	G6P	None
B_P	amino acids, nucleic acids, lipids, other precursors.	amino acids, other precursors, soluble proteins, etc.	None
B_{STO}	PHB	Glycogen	PHB
B_{PSS}	$X_{PSS,R}$ = RNA $X_{PSS,P}$ = r-proteins $X_{PSS} = X_{PSS,R} + X_{PSS,P}$ $X_{PSS,P} = \frac{RNA}{\alpha} = \gamma * X_P$ (r_{PSS} = autocatalytic)	B_{PSS} = component with zero mass (r_{PSS} = autocatalytic)	X_{PSS} = component with zero mass (r_{PSS} = biomass dependent)
X_C	$X_{C,L}$ = lipids, non-proteins and non-RNA cell constituants X_P = proteins $X_C = X_{C,P} + X_{C,L}$ $X_{C,P} = (1-\gamma)*X_P$ $X_{C,L} = \beta*X_P$	X_C = proteins, lipids, cell wall, etc. $X_C = \frac{DNA}{f_{DNA}}$	X_C = proteins, lipids, cell wall, etc. $\Delta X_C = \frac{Y_{SP}}{Y_{SX}} * \Delta PHB$

The two last models were developed with an experimental perspective in view of developing activated sludge models that can be calibrated with *intrinsic* model parameters.

7.6 Common structures in proposed models

A simplified rRNA-structured model was formulated to evaluate the sensitivity of the output of a rRNA-structured model to the parameters of the rRNA synthesis and decay

models. Not all usual metabolic processes are included in the model here, since the aim was to explicitly determine the sensitivity of the proposed model structure.

The production of the PSS is an autocatalytic process since it depends on its own concentration. The production rate of the PSS is given by the net synthesis rate minus the decay rate of the PSS and minus the loss causes by cell decay.

$$r_{PSS} = k_{PSS} * B_{PSS} * M_i * M_{i+j} - b_{PSS} * B_{PSS} - b_{XC} * B_{PSS} \qquad [7.1]$$

where b_{PSS} and b_{XC} are the decay rate of B_{PSS} and X_C respectively, and M_i are saturation kinetic terms (e.g. Monod).

The B_{PSS} production will be in equilibrium with its decay and its dilution into new biomass. The balance equation for this component into the cell is described by :

$$\frac{df_{PSS}}{dt} = 0 = k_{PSS} * f_{PSS} * M_{B_P} * M_O - b_{PSS} * f_{PSS} - f_{PSS} * \frac{dX_C}{X_C * dt} \qquad [7.2]$$

In this equation, the right term represents reduction of f_{PSS} caused by dilution from growth of the cell population. At steady state, if we assumed the oxygen and the building blocks are not limiting, the equation can be rewritten:

$$k_{PSS} * f_{PSS} - b_{PSS} * f_{PSS} = \mu_C^{int} * f_{PSS} \qquad [7.3]$$

In this equation, μ_C^{int}, the intrinsic growth rate of active cells is equal to the specific production rate of the PSS.

The metabolic status of the cells is introduced in the model with the PSS level to describe the growth rate of the cell's structural material (X_C):

$$\mu_C = \mu_C^{int} * \frac{f_{PSS}}{f_{PSS}^{max}} = (k_{PSS} - b_{PSS}) * \frac{f_{PSS}}{f_{PSS}^{max}} \qquad [7.4]$$

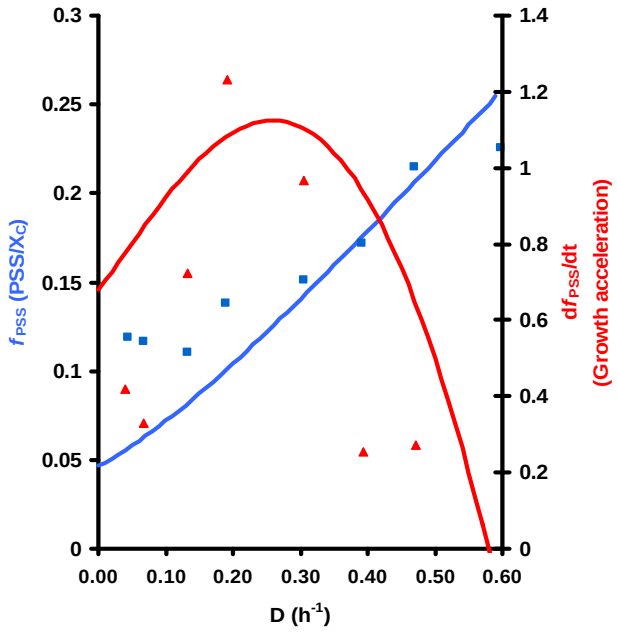

Figure 7-3 Variation of RNA fraction and growth acceleration.

D=μ-b. The decay rate was varied between 0.02 h^{-1} at D=0.6 to 0.13 h^{-1} at D=0.00.
(Data adapted from Daigger and Grady, 1982b)

As shown in Figure 7-3, using the autocatalytic process for the B_{PSS} production, it was possible to roughly describe the rate of change of the transient response (dμ/dt) of *Pseudomonas putida* observed by Daigger and Grady (1982b). The decay rate was varied unless f_{PSS} goes to zero with the dilution rate. From a metabolic point of view, several phenomena can have incidence on the f_{PSS} fraction at low dilution rate. Some authors report variable decay rate, variable maintenance, induction and repression of metabolic pathways etc (Lavallée et al., 2002; Lavallée et al., 2005a).

A complete mathematical description of the simplified model is given under a Petersen matrix form in table 7.2 to 7.4. In brief, the exogenous substrate is taken up by biomass to yield intracellular substrate (B_S). The intracellular substrate is used for building block (B_P) production, for storage (B_{STO}) and for energy expenditures (OUR) associated with biomass growth. It decreases with the endogenous respiration of biomass b_{XC}. The PSS (B_{PSS}) is a unit less component.

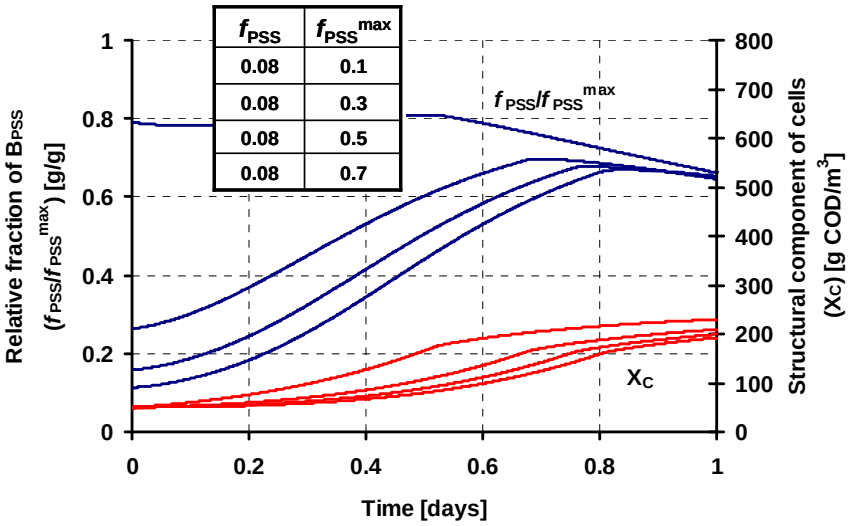

Figure 7-4 Batch reactor. $S_0/X_0 = 10$. Sensitivity analysis for initial values of f_{PSS}/f_{PSS}^{max} = 0.8; 0.27; 0.16; 0.11 units/g.

Figure 7-4 shows that the model response is sensitive to the initial f_{PSS} value. The output of the model is insensitive to f_{PSS} during the first few hours, but the discrepancy of the cell concentration (X_C) between the different simulations increased all along the batch simulation according to the f_{PSS} used.

The lower the initial f_{PSS} was, the longer the lag phase. Since the rRNA-level is correlated to the growth rate at steady-state, a culture growing more slowly will have a lower f_{PSS}/f_{PSS}^{max} ratio and the lag phase will therefore stretch over a longer period, as predicted by the model.

Figure 7-5 shows the output of the model after an up-shift of the flow rate into a reactor. The cells concentration (X_C) and the f_{PSS}/f_{PSS}^{max} reached the same values for every value of f_{PSS}^{max}. The simulation shows that after 12 days, the f_{PSS}/f_{PSS}^{max} ratio always reaches the same value and the model is thus insensitive to f_{PSS}^{max} at steady state. Again, during the transient induced by the flow rate up-shift, the model was sensitive to the initial f_{PSS}/f_{PSS}^{max} fraction. This indicates that the growth response of the model varies with the f_{PSS} fraction, that is to say, with the history of the cell components.

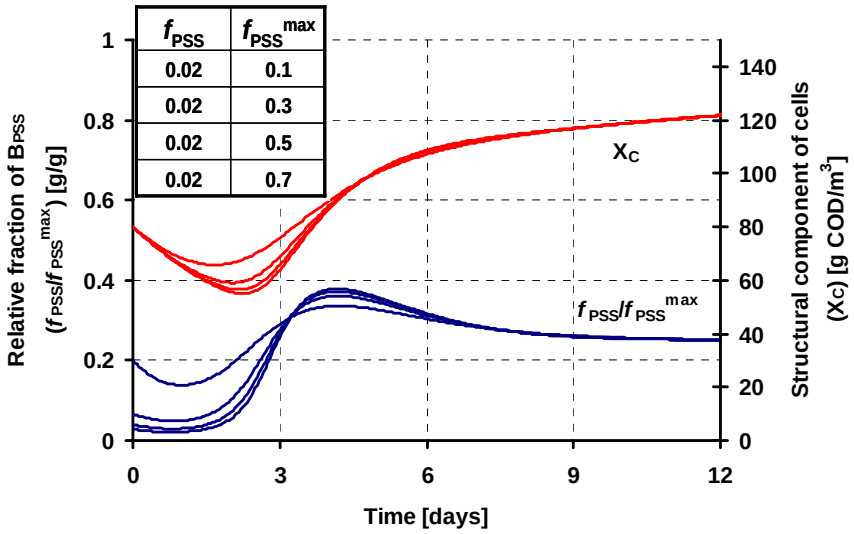

Figure 7-5 Sensitivity of the model during the start-up of a continuous-flow stirred reactor (HRT= 6.5 days).

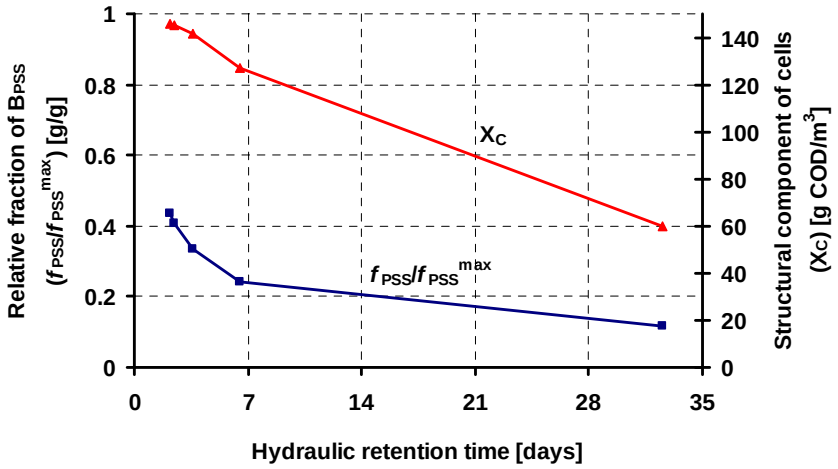

Figure 7-6 Semi-continuous-flow stirred reactor. Sensitivity of the model to hydraulic retention time (f_{PSS}^{max} = 0.5 units/g).

Additionally, a phase analysis shows that at steady state, the B_{PSS} level increases when the hydraulic retention time is decreased (Figure 7-6). The growth response will change accordingly, as well as the transient behaviour after a modification of the retention time.

Hence, a rRNA model would reflect the specific growth rate level of microorganisms, according to the conditions prevailing in the reactor.

In ASMs, the specific heterotrophic oxygen uptake rate can be described by the following equation:

$$\frac{OUR}{X_H} = \mu_H \frac{(1-Y_H)}{Y_H} \qquad [7.5]$$

In this equation, μ_H and Y_H are two parameters. Because μ_H does not reflect the variations of the specific activity associated to variations of the rRNA-level, recalibration of the model will be required when the conditions prevailing in the reactor are significantly different from those prevailing during the preceding calibration exercise.

In a rRNA model, on the other hand, the specific heterotrophic oxygen uptake rate related to the growth process is given by:

$$\frac{OUR_G}{X_C} = \frac{\mu_C^{\max}}{f_{PSS}^{\max}} * \frac{B_{PSS}}{X_C} * \frac{(1-Y_C)}{Y_C} \qquad [7.6]$$

The parameter Y_C is the yield of biomass on intracellular substrate B_S. This equation reflects the variation of the specific activity of microorganisms and thus recalibration will no longer be required. The calibration procedure would remain similar to those used with ASM, but the reference unit used in the description of the specific respiration would be the PSS:

$$\frac{OUR_G}{B_{PSS}} = \frac{\mu_C^{\max}}{f_{PSS}^{\max}} * \frac{(1-Y_C)}{Y_C} \qquad [7.7]$$

In light of this analysis, it can be concluded that a rRNA-structured model is sensitive to the history of the B_{PSS} component, to the process configuration and to the operation conditions. However, the model is not sensitive to the f_{PSS} fraction at steady state. Thus, identification of the $f_{PSS}^{\max}$ value must be done under transient conditions. Since the model is sensitive to

the relative fraction f_{PSS}/f_{PSS}^{max}, an explicit link between measured and predicted rRNA-level can been made.

7.7 Mass balance during transient period

Lavallée et al. (in preparation) used DNA as basic unit for biomass quantification. The maximal growth rate of cells (μ_C^{max}) was then determined by monitoring the evolution of the DNA concentration in a batch experiment with a high initial S_0/X_0 ratio. The DNA measurements were converted to COD by using a measured DNA/COD ratio (f_{DNA}). Hence, using the COD of the suspended solids minus the COD of glycogen, these authors were able to observe variations of the intracellular COD fractions ($f_{BS}+f_{BP}$). Considering the nitrogen assimilation and the N/COD ratio (i_{nx}), they observed that f_{BS} was negligible and most of the intracellular fraction was under the f_{BP} form. Using this method for a batch experiment, a significant increase of the f_{BP} fraction was observed as soon as the storage capacity of the biomass was fully utilized, and its decrease after the substrate was exhausted. Since a COD mass balance was used, the nature of the f_{BP} could not be determined. It was assumed that the product was an aminated storage component (e.g. amino acids, intracellular soluble proteins, etc). After exhaustion of the substrate, growth occurred on the basis of a breakdown of glycogen and X_B. With this in mind, Lavallée et al. suggested that a model assuming a constant cell size ($B_S+B_P+X_C$ = Cte) can be used as long as the storage capacity of the biomass is not fully used. These authors proposed to use a mass balance on the B_P component to model large transients.

Frigon et al. (submitted) used a carbon mass balance and proposed to describe the X_{PSS} into two subset pools, the $X_{PSS,R\ (RNA)}$ and the $X_{PSS,P}$ (protein) in order to explicitly link measured and predicted rRNA-levels. The ratio between these two components was assumed constant since these components are tightly co-regulated by cells (Nomura, 1999).

Hence, by combining the methods proposed by the authors of these two papers (adapted to the units used) it will be straightforward to determine the f_{PSS}^{max} by using the equation [7.7], knowing the actual rRNA concentration, the OUR_G and the yield Y_C. Intracellular levels of the component B_P can be determined by using a mass balance of carbon (or COD)

and nitrogen around biomass. It follows that a calibration of the model conversion rates is possible on the basis of the above mentioned data.

7.8 Biodiversity and RNA-structured biomass model

Proper interpretation of the rRNA-level in terms of the cell's metabolic status clearly needs further research. For example, Frigon et al. (2002b) determined the diurnal variations of rRNA-levels of a population of *Acinetobacter* and of a population of *Gordonia* in the mixed liquor of a full-scale wastewater treatment plant, and observed two different profiles: The variations for the first population followed variations in the influent loading, while the rRNA of the second population remained stable throughout the day. Using a model-based analysis, they suggested that the ecological function of the populations may be responsible for the observed trends. Muttray et al. (2001) suggested it cannot be assumed that the positive linear relationship between growth rate and RNA:DNA ratio holds for all microorganisms, and also observed that a direct deduction of actual growth rates in batch cultures from the RNA:DNA ratio measured at steady-state may not always be possible.

Additionally, it is increasingly recognized that advances in wastewater treatment processes will require description of the biodiversity of microorganisms present in these systems, and of their diverse biochemical and metabolic activities. With the advent of ribosomal RNA (rRNA)-based molecular techniques, it has become possible for environmental engineers and scientists to accurately assess the bacterial diversity in activated-sludge systems (Saikaly et al., 2005; Yuan and Blackall, 2002). No wonder that the last decade one saw the publication of several studies describing bacterial diversity in activated sludge process through phylogenetic analysis (evolutionary-based analysis of marker genes), mainly of the 16S rRNA gene. Using rRNA terminal restriction fragment analysis, some indices were proposed to model the fingerprint of a bacterial community structure, that were correlated to influent variables and performance indicators (Gilbride et al., 2006).

7.9 Conclusion and perspective

Structured biomass models are by nature less empirical than unstructured biomass models. While increasing model complexity, they simplify the model calibration effort because they

replace extant by intrinsic parameters. Development of molecular techniques has created a deeper insight in the microbial diversity and activity level of microbial populations in activated sludge and, with this insight, RNA-based models are currently under development.

An explicit link between molecular techniques and the model structures have been proposed. It has become possible to determine the rRNA to biomass ratio to accurately assess the metabolic status of microbial populations in activated-sludge systems. The autocatalytic process proposed to model the rRNA component dynamics can describe the rRNA evolution, the growth rate adaptation ($d\mu/dt$) and the growth lag phase observed by Daigger and Grady (1982 a and b) and observed by the authors in their own experiments (Frigon et al., submitted; Lavallée et al., in preparation). Further studies are needed to provide a proper interpretation of rRNA-levels in terms of metabolic status.

A simple rRNA-structured model has been presented here. By combining the methods proposed by the authors, and knowing the actual rRNA concentration, the OUR_G and the yield Y_C, it will be straightforward to determine the f_{PSS}^{max} by using the equation [7.7]. To model large transients, the intracellular concentrations of the component B_P need to be determined by mass balancing the carbon (or COD) around the biomass. A calibration of the remaining model parameters can then be done by using available data. However, the regulation of the transformation reaction rates of the components are not yet well defined, and it has great influence on the model output. Further studies are therefore need for validation of such a model.

Results from this kind of metabolic modelling exercises and from the TUDP EBPR metabolic model suggest that it may be possible to develop activated sludge models calibrated by *intrinsic* and not *extant* model parameters.

For the time being, however, the rRNA-structured biomass models remain restricted to research. Though, the driving force for that kind of model currently remains low in treatment of wastewater, they present the potential of key improvements that practitioners would benefit from as they would lead to improved reliability of activated sludge models.

Water professionals that develop strategies to control microbial populations would clearly take advantage of such models too.

Table 7-2 Stoichiometriy of intracellular, soluble and particulated components

Rates	**B_{PSS}**	**S_O**	**S_S**	**B_S**	**B_P**	**B_{STO}**	**S_{nh}**	**X_C**	**X_{ii}**
Units:	g/g	$gCOD/m^3$	$gCOD/m^3$	$gCOD/m^3$	$gCOD/m^3$	$gCOD/m^3$	gN/m^3	$gCOD/m^3$	$gCOD/m^3$
r1		$-(1-Y_S)$	-1	Y_S					
r2				-1		1			
r3				-1	1		$-i_{nx}$		
r4		$-(1-Y_C)/Y_C$		$-(1-Y_C)/Y_C$	-1			1	
r5	1								
r6				1		-1			
r7				1	-1		i_{nx}		
r8	-1								
r9	$-B_{PSS}/X_C$	$-(1-fu)*(1+B_S/X_C+B_{STO}/X_C+B_P/X_C)$		$-B_S/X_C$	$-B_P/X_C$	$-B_{STO}/X_C$	$(1-fu)*(B_P/X_C+1)*i_{nx}$	-1	$fu*(1+B_S/X_C+B_{STO}/X_C+B_P/X_C)$

Table 7-3 Processes description

Rates	**Process**	**Description**	**units**
r1	**Substrate uptake**	$k_S*Mss*Mso*I_{Bs}*X_C$	gCOD/m3/d
r2	**Substrate storage**	$k_{STO}*Mssto*Msto^{max}*X_C$	gCOD/m3/d
r3	**increase of B_P**	$k_P*Mnh*M_{BS}*Mso*X_C$	gCOD/m3/d
r4	**aerobic growth of X_C**	$\mu_C^{int}/f_{PSS}^{max}*B_{PSS}/X_C*Mso*M_{BS}*M_{BP}*X_C$	gCOD/m3/d
r5	**aerobic growth of B_{PSS}**	$k_{PSS}*B_{PSS}*Mso*M_{BS}*M_{BP}$	units/m3/d
r6	**degradation of Bsto**	$dksto*Msto*X_C$	gCOD/m3/d
r7	**degradation of Bp**	$b_{Bp}*B_P$	gCOD/m3/d
r8	**decay of B_{PSS}**	$b_{PSS}*B_{PSS}$	units/m3/d
r9	**decay of X_C**	b_C*X_C	gCOD/m3/d

Table 7-4 Description of Saturation and Inhibition Functions

Function	Description
Mss	$S_S/(S_S+Kss)$
Mso	$S_O/(S_O+Ko)$
I_{BS}	$Ki_{Bs}/(Ki_{Bs}+B_S/X_C)$
Mnh	Snh/(Knh + Snh)
M_{BS}	$(B_S/X_C)/(K_{BS}+B_S/X_C)$
M_{BP}	$(B_P/X_C)/(K_{BP}+B_P/X_C)$
Mssto	$(B_S/X_C)/(K_{BS,STO}+B_S/X_C)$
$Msto^{max}$	$(f_{sto}^{max}-B_{STO}/X_C)/(Kisto+f_{sto}^{max}-B_{STO}/X_C)$
Msto	$(B_{STO}/X_C)/(Ksto+B_{STO}/X_C)$

CONCLUSION

La valeur des constantes cinétiques utilisées dans un modèle pour décrire un système de traitement donné, est dépendante des conditions d'opération et de la configuration du dit système. Puisque la valeur de ces constantes cinétiques dépend de facteurs abiotiques, celles-ci sont dites «extrinsèques».

Ces constantes cinétiques «extrinsèques» révèlent donc le caractère empirique des modèles mathématiques généralement utilisés en traitement des eaux usées, tel les modèles ASM. Conséquemment, ces derniers donnent une image statique dépendante des conditions prévalentes au moment de la calibration, et spécifiques au procédé de traitement.

Le choix qui a été fait dans cette thèse a plutôt été de représenter la biomasse elle-même avec un modèle à caractère plus fondamental à l'aide de constantes cinétiques qui représentent la nature «intrinsèque» du métabolisme des microorganismes, pour ainsi affranchir le modèle et les constantes cinétiques de l'histoire de la biomasse et de la configuration du procédé.

Le principal objectif visé de la thèse était donc de construire un modèle mathématique qui donne une description de certains mécanismes de régulation de l'activité spécifique de la biomasse, et ainsi obtenir une information «intrinsèque» lors de l'évaluation des constantes cinétiques. Cet objectif visait à développer un modèle qui tienne compte de l'histoire de la biomasse, et qui serait donc capable de prévoir la réponse dynamique d'un système exposé à de larges transitoires, ou de prévoir la réponse du système de traitement pour différentes configurations sans avoir recours à des pilotes pour calibrer la réponse du modèle pour chacune de diverses conditions d'opération ou pour chacune des différentes configurations étudiées.

Afin d'obtenir une information à caractère intrinsèque, il devient nécessaire de définir des descripteurs du niveau d'expression du métabolisme des microorganismes. Le protocole

expérimental développé cherchait donc à déterminer le niveau d'activité des microorganismes en les exprimant en valeur spécifique sur une mesure de référence. Le choix de la valeur de référence devient donc critique puisqu'elle ne doit pas avoir d'incidence sur les niveaux d'activité mesurés.

Ainsi, dans le cadre de cette thèse il a été nécessaire de développer un protocole expérimental qui permet de quantifier la biomasse active présente dans la boue activée, et de définir divers descripteurs de son niveau d'activité comme les taux spécifiques, et des descripteurs de son état métabolique comme les niveaux spécifiques de métabolites ou de réserves. L'expression des taux et des niveaux en valeur spécifique constitue un nouveau type d'information associée au caractère intrinsèque du métabolisme des microorganismes.

L'ADN a été sélectionné comme unité de base pour quantifier les microorganismes puisque ce composant constitue une fraction relativement constante de la masse structurale des cellules. Le protocole d'extraction est apparu quantitatif puisque la mesure est demeurée proportionnelle au volume de l'aliquote analysé. La DCO de la fraction structurale de la biomasse active (X_C) était déterminée à l'aide d'un ratio stoechiométrique de 0,09 mg DCO/µg ADN. Ce ratio correspond relativement bien aux valeurs rapportées dans la littérature compte tenu du taux de récupération de l'ADN obtenu avec la méthode. Le rapport stoechiométrique utilisé a permis de décrire adéquatement l'évolution de la fraction structurale de la biomasse active et des divers composants de la biomasse au cours d'une croissance exponentielle et de maintenir l'écart entre les prédictions du modèle et les mesures expérimentales à des valeurs moyenne de l'ordre de 10%. Ceci démontre que l'hypothèse posant un rapport stoechiométrique constant entre la fraction structurale et l'ADN de la biomasse a été respectée au cours de cette expérience. On peut donc en conclure que le protocole proposé permet d'évaluer la quantité de microorganismes présents dans une boue activée, et de suivre l'accroissement ou la chute de la population globale.

La méthode proposée s'est montrée efficace puisqu'elle a permis de définir des indicateurs de l'état métabolique des microorganismes comme les taux spécifiques de même que de préciser l'état des réserves de matériaux intracellulaires au cours de comportements

transitoires de la biomasse. L'étude de l'évolution dynamique de ces divers indicateurs a permis d'obtenir une meilleure compréhension de l'état métabolique des microorganismes et de placer ces indicateurs en relation avec la description des mécanismes de production des macromolécules étudiée au chapitre 2.

En plus de la méthode expérimentale, un modèle mathématique a donc été développé pour décrire la variation du taux de croissance de la biomasse active (dμ/dt) ainsi que les divers comportements transitoires de la biomasse observés au cours des expériences.

Les équations mathématiques proposées pour décrire l'évolution du système de synthèse des protéines donnent une réponse cinétique de type autocatalytique. Cette description permet de modéliser la réponse en croissance de la biomasse observée par Daigger et Grady (1982). Le choix du modèle est basé sur les mécanismes biochimiques présentés dans la littérature pour décrire l'évolution du système de synthèse des protéines. La réponse cinétique obtenue donne une explication mécanistique de la variation du taux de croissance et de la phase de latence notée par ces auteurs. La description de la croissance d'une population de cellule devient alors une double exponentielle. Selon ce constat, une première exponentielle décrit l'accroissement du taux de croissance, et une seconde décrit l'accroissement de la population. Naturellement, lorsque l'accroissement du taux de croissance (dμ/dt) demeure faible, une simple exponentielle décrit l'accroissement de population adéquatement.

La sensibilité du modèle aux taux de production des différentes structures semble dépendre des conditions dans lesquelles l'évaluation est effectuée. Par exemple, en conditions stables, le modèle montre peu de sensibilité à la fraction relative du composant qui représente le système de synthèse des protéines (f_{PSS}/f_{PSS}^{max}), alors qu'il montre une sensibilité à cette fraction relative en conditions dynamiques. On observe la situation inverse pour le taux de production des enzymes de transport du substrat. La sensibilité variable du modèle démontre que la calibration de ce dernier doit nécessairement être effectuée sur des expériences dynamiques et des expériences statiques. Par conséquent, une fois calibré, le modèle proposé serait en mesure de décrire l'état métabolique de la

biomasse compte tenu de son historique, ce qui constituait l'objectif principal de cette thèse.

Le modèle a donc été validé par un processus de calibration sur diverses expériences conçues pour induire des comportements transitoires de la biomasse active. Les différentes hypothèses formulées lors de l'élaboration du modèle ont été vérifiées avec la nouvelle information intrinsèque obtenue à l'aide de la méthode expérimentale.

Les données expérimentales montrent que les matériaux constituants intracellulaires (B_P) s'accumulent dans les cellules lorsque la biomasse est exposée à des doses de substrat qui dépassent la capacité de stockage en glycogène des microorganismes. Cette accumulation de produits aminés démontre que les flux de carbone et d'azote ont été supérieurs aux besoins métaboliques. Conséquemment, l'incorporation du carbone et de l'azote n'ont pas été des processus limitants la croissance des microorganismes lors des expériences. L'accumulation de produits aminés (B_P) démontre que le taux de croissance des microorganismes, en terme de nombre d'individus ou de nucléus constituait le processus limitant de la croissance. Puisque la littérature, tout comme les expériences effectuées, indique que d'une part, la croissance des microorganismes est balancée au cours de la phase exponentielle, et que d'autre part, le taux de croissance des microorganismes est proportionnel à la fraction d'ARN-r de la masse cellulaire, ceci démontre que l'hypothèse voulant que le niveau d'expression du système de synthèse des protéines peut constituer l'élément limitant de la croissance cellulaire en certaines circonstances.

Toutefois, il faut noter que le taux de croissance initial observé dans les expériences exponentielles est de l'ordre de dix fois celui imposé dans le réacteur à alimentation semi continue d'où a été prélevé la biomasse initiale. On peut en déduire que dans le réacteur à alimentaiton semi continue, le niveau d'expression du système de synthèse des protéines ne constituait l'élément limitant de la croissance. Puisque dans ce réacteur le substrat était dirigé vers le stockage avant d'être dirigé vers les voies anaboliques, on peut présumer que dans un réacteur à croissance lente, la cinétique de croissance est limité par le taux de dégradation des réserves ou la disponibilité des métabolites intracellulaires. En conséquence, pour modéliser la variation du taux de croissance des microorganismes, il

devient nécessaire de modéliser les flux de métabolites intracellulaires tel que cela a été proposé dans le cadre de cette thèse.

L'accumulation successive des glycogènes puis des matériaux constituants cellulaires, et suivi par la production de produits microbiens solubles, indique une saturation des flux métaboliques au cours des expériences. Cette saturation des flux métaboliques, couplée à une réduction significative de la respiration, tend à démontrer que l'activité métabolique des microorganismes est régulée par l'équilibre des flux de carbone et d'azote dans la cellule, ceci conformément aux observations relevées dans la littérature. Cette information de nature «intrinsèque» a été utilisée pour valider les structures du modèle qui décrivent l'inhibition du transport de substrat et le relargage de produits microbiens solubles.

Selon les observations effectuées, le taux de respiration maximal spécifique varie aussi selon le niveau d'expression du système de transport du substrat. Ceci constitue une vérification de l'hypothèse voulant que l'historique de la biomasse ait une incidence sur le niveau d'expression des enzymes et sur le niveau d'activité spécifique de la biomasse. De ce fait, il apparaît pertinent de modéliser cette variation d'activité par une description de la production d'enzymes. Ceci indique qu'il pourrait être difficile de modéliser uniquement l'évolution du système de synthèse des protéines sans tenir compte de l'expression des autres systèmes enzymatiques.

Toutefois, la nature du substrat peut avoir une incidence sur l'expression de certains systèmes enzymatiques. Le choix du substrat s'avère donc un facteur important pour la caractérisation de la biomasse et l'identification des constantes cinétiques. Le glucose favorise l'expression d'un système de transport du substrat à grande capacité ce qui a une forte influence sur les transitoires observées. L'acétate est généralement considéré comme une fraction importante du substrat observé dans les eaux usées. Ce substrat ne semble pas induire l'expression de systèmes de transport à grande capacité, mais certaines recherches démontrent l'existence de perméases à haute affinité pour l'acétate (Wolfe, 2005). Ceci permettrait de simplifier la description du système de transport du substrat par une seule enzyme de transport. Le choix de l'acétate plutôt que le glucose s'avèrerait donc un choix plus pertinent pour la validation des structures proposées dans le modèle.

On peut conclure que la cohérence de la réponse du modèle sur trois expériences différentes indique que la méthode expérimentale et les structures proposées dans le modèle semblent suffisantes pour modéliser correctement différents comportements transitoires de la biomasse qu'il est possible d'observer dans un procédé par boues activées (à l'exclusion des changements de structure dans la population de microorganismes).

Toutefois, une description de la production d'azote organique suivi d'une ammonification devrait être ajoutée au modèle afin de décrire correctement l'évolution du NH_4^+ lors du dépérissement de la biomasse active.

Le modèle a été calibré sur des expériences en cuvée de courte durée mais idéalement, il aurait été nécessaire de le calibrer aussi sur des expériences de longue durée représentatives des conditions initiales des expériences en cuvée afin de recalibrer l'ensemble des expériences avec les concentrations d'enzyme prédites par le modèle lors des simulations des expériences de longue durée. Cette procédure permettrait valider la description des structures enzymatiques et de trouver une seule valeur à chacune des constantes cinétiques du modèle. Les constantes cinétiques calibrées avec cette méthode présenteraient un caractère intrinsèque affranchi de l'histoire de la biomasse. Le modèle serait alors en mesure de prédire le comportement de divers systèmes de traitement opérés sous différentes conditions.

Cette étape constituerait la suite logique de ce travail. Afin de poursuivre dans cette direction, des données expérimentales devraient être colligées à différents taux de croissance afin de déterminer les niveaux d'expression et d'en déduire des taux de production d'ARNr et d'enzymes et calibrer le modèle sur les valeurs expérimentales obtenues.

De nouvelles méthodes devraient être développées pour faciliter l'étape de calibration du modèle sur de multiples expériences séquencées. Les outils d'optimisation utilisés au cours de cette thèse ne permettaient d'optimiser qu'une seule série de données à la fois. De plus comme il n'existait pas de lien direct entre les différentes expériences effectuées, il n'était pas possible d'automatiser l'optimisation des valeurs des constantes cinétiques à l'aide du

solutionneur utilisé. La procédure de calibration consistait alors à calibrer en séquence les constantes cinétiques par ordre croissant de temps de relaxation sur une expérience à la fois, puis de recommencer le cycle chaque fois qu'une nouvelle constante était calibrée. La calibration cyclique du modèle par étapes successives sur chacune des expériences jusqu'à convergence des valeurs des différentes constantes cinétiques s'avère un processus laborieux qui gagnerait à être simplifié et automatisé. Il serait nécessaire d'utiliser un outil d'optimisation qui permettrait d'optimiser la valeur des constantes cinétiques sur plusieurs séries de variables et plusieurs expériences à la fois.

En bref, cette thèse propose un modèle métabolique capable de décrire des cinétiques transitoires grâce à des descripteurs de l'état métabolique de la biomasse. La méthode expérimentale est basée sur une quantification de la population de microorganismes présents dans la biomasse afin de définir en valeur spécifique ces descripteurs de l'état métabolique, et en tirer une information à caractère intrinsèque. Grâce à l'information trouvée dans la littérature, et grâce à l'information intrinsèque obtenue lors des expériences effectuées, il a été possible de redéfinir et valider la description mathématique de la croissance d'une population des microorganismes présents dans une boue activée. En preuve, la réponse du modèle proposé a été cohérente avec les cinétiques transitoires observées durant les expériences effectuées.

Bibliographie

Aizenman E., Engelberg-Kula H. et Glaser G. (1996). An *Escherichia coli* chromosomal «addiction module» regulated by guanosine 3',5'-bispyrophosphate : a model for programmed bacterial cell death. Proceedings of the National Academy of Science, USA, **93**: 6059-6063.

Akesson M., Karsson E. N. et Hagander P. (1999). On-line detection of acetate formation in Escherichia coli cultures using dissolved oxygen responses to feed transients. Biotechnology and Bioengineering, **64**: 590-598.

Albertson N. H., Nyström T. et Kjelleberg S. (1990). Macromolecular synthesis during recovery of the marine *Vibrio* S14 from starvation. Journal of Genetical Microbiology, **136** : 2201-2207.

Amann R. et Ludwig W. (2000). Ribosomal RNA-targeted nucleic acid probes for studies in microbial ecology. FEMS Microbiological Review, **24**: 555-565.

Aon J. C. et Cortassa S. (2001). Involvement of nitrogen metabolism in the triggering of ethanol fermentation in aerobic chemostat cultures of *Saccharomyces cerevicae*. Metabolic Engineering, **3**: 250-264.

Anonyme (1996). Katlon® CG/ICP and CG/ICP II preservatives, T797002A Data Sheet, Sigma-Aldrich Co., SUPELCO, Bellefonte, PA., 1 p.

Anonyme (1998). Technical bulletin No. MB-590, DNA quantification Kit – Fluorescence Assay, Product No. DNA-QF, SIGMA, Sigma-Aldrich, Saint-Louis Miss. USA, 4 p.

Anonyme (2002). Protocole pour la validation d'une méthode d'analyse en chimie, DR-12-VMC, EN V/2000/0049, Programme d'accréditation des laboratoires d'analyse environnementale, Centre d'expertise en analyse environnementale du Québec, Gouvernement du Québec, Québec, 27 p.

Arbidge M. et Chesbro W. R. (1982). Very slow growth of *Bacillius polymyxa* : Stringent response and maintenance energy, Archive of Microbiology, **132**: 338-344.

Atkinson D. E. (1977). Cellular energy metabolism and its regulation. Academic Press, Inc., London, UK., 293 p.

Atlas R. M. et Bartha R. (1998). Microbial ecology, Fundamentals and applications. Benjamin/Cummings Publishing Company, Menlo Park, Calif., 694 p.

Avcioglu E., Orhon D. et Sösen S. (1998). A new method for the assessment of heterotrophic endogenous respiration rate under aerobic and anoxic conditions. Water Science and Technology **38**(8-9) : 95-103.

Bailey J. E. (1983). Single-cell metabolic model determination by analysis of microbial populations. *Dans* Foundations of biochemical engineering : Kinetics and thermodynamics in biological systems, Les Éditions Blanch H. W., Papoutsakis E. T. et Stephanopoulos G., ACS symposium series 207, American Chemical Society.

Bailey J. E. et Ollis D. F. (1986). Biochemical engineering fundamentals. 2nd ed. McGraw-Hill, New York., 984 p.

Baloo S. et Ramkrishna D. (1991). Metabolic regulation in bacterial continuous cultures :1. Biotechnology and Bioengineering, **38** : 1337-1352.

Barker D. J. et Stuckey D. C. (1999). A review of soluble microbial products (SMP) in wastewater treatment systems. Water Research, **33**(14): 3063-3082.

Bazin M. J., Curds C., Dauppe A., Owen B. A. et Saunders P. T. (1983). Microbial predation dynamics. *Dans* Foundations of biochemical engineering : Kinetics and thermodynamics in biological systems, Les Édition Blanch H. W., Papoutsakis E. T. et Stephanopoulos G., ACS symposium series 207, American Chemical Society.

Beeftink H. H., van der Heijden R. T. J. M. et Heijnen J. J. (1990). Maintenance requirements : energy supply from simultaneous endogenous respiration and substrate consumption. FEMS Microbiology and Ecology, **73** : 203-210.

Berlyn M. K. B., Low K. B. et Rudd K. E. (1996). Linkage map of *Escherichia coli* K-12, Edition 9, In *Escherichia coli* and *Salmonella*, cellular and molecular biology. Vol. 2. Les Éditions F. C. Neidhardt, R. Curtiss, J. L. Ingraham, E. C. C. Lin, K. B. Low, B. Magasanik, W. S. Reznikoff, M. Riley, M. Schaechter and H. E. Umbarger, ASM Press, Washington, D. C., pp. 1715-1902.

Beun J. J., Paletta F., van Loosdrecht M. C. M. et Heijnen J. J. (2000). Stochiometry of poly-β-hydroxybutyrate metabolism in aerobic, slow growing, activated sludge cultures. Biotechnology and Bioengineering **67**: 379-389.

Björk G. R. (1996). Stable RNA modification. *Dans Escherichia coli* and *Salmonella*, Cellular and molecular biology, Les Éditions Neidhardt F. C., Curtiss R., Ingraham J. L., Lin E. C. C., Low K. B., Magasanik B., Reznikoff W. S., Riley M., Schaechter M. and Umbarger H. E., ASM Press, Washington, D. C. Vol. 2, pp. 861-886.

Blumberg D. D. (1987). Creating a ribonuclease-free environment. *Dans* Methods in enzymology, vol. 152; Molecular biology laboratory requirements, p. 20-24.

Borel J. P., Maquart F. X., Le Peuch C., Randoux A., Gillery P., Bellon G. et Monboisse J. C. (1997). Biochimie dynamique. Les Éditions De Boeck & Larcier s. a., Brussels, Belgique.

Brands E., Liebeskind M. et Dohmann M. (1994). Parameters for dynamic simulation of wastewater treatment plants with high-rate and low-rate activated sludge tanks. Water Science and Technololgy, **30**(4), 211-214.

Bremer H. et Dennis P. P. (1996). Modulation of chemical composition and other parameters of the cell by growth rate, *Dans Escherichia coli* and *Salmonella*, cellular and molecular biology. Vol. 2. Les Éditions F. C. Neidhardt, R. Curtiss, J. L. Ingraham, E. C. C. Lin, K. B. Low, B. Magasanik, W. S. Reznikoff, M. Riley, M. Schaechter and H. E. Umbarger, ASM Press, Washington, D. C., pp. 1553-1569.

Bukley L., Caldarone E. et Ong T.-L. (1999). RNA-DNA ratio and other nucleic acid-based indicators for growth and condition of marine fishes. Hydrobiologia, **401**: 265-277.

Cangelosi G. A. and Brabant W. H. (1997). Depletion of pre-16S rRNA in starved *Escherichia coli* cells, Journal of Bacteriology, **179**(14): 4457-4463.

Canino M. F. et Caldarone E. M. (1995). Modification and comparison of two fluorometric techniques for determining nucleic acid contents of fish larva. Fishery Bulletin **93** : 158-165.

Cassell E. A., Sulzer F. T. et Lamb J. C. (1966). Population dynamics and selection in continuous mixed cultures, Journal of the Water Pollution Control Federation, **38**(9) : 1398-1409.

Catlin B.W. et Cunningham L.S. (1958). Studies of extracellular and intracellular bacterial deoxiribonucleic acids. Journal of Genetical Microbiology, **19** :522-539.

Cech J.S. et Chudoba J. (1983). Influence of accumulation capacity of activated sludge microorganisms on kinetics of glucose removal. Water Research, **17**(6): 659-666.

Cesarone C.F. Bolonesi C. et Santi L. (1979). Improved microfluorometric DNA determination in biological material using 33258 Hoechst. Analytical Biochemistry, **100** : 188-197.

Chang J. Chudoba P. et Capdeville B. (1993). Determination of the maintenance requirement of activated sludge. Water Science and Technology, **28**(7) : 139-142.

Chang H. T. et Rittmann B. E. (1989). Transient responses incorporating products formation. Journal of Environmental Engineering (ASCE) **115** : 476-479.

Chang D. E., Shin S., Rhee J. S. et Pan J.-G. (1999). Acetate metabolism in a mutant of *Escherichia coli* W3110: importance of maintaining acetyl coenzyme A flux for growth and survival. Journal of Bacteriology, **181**(21) : 6656-6663.

Characklis W. G. (1978). Microbial reaction rate expressions. Journal of Environmental Engineering, (ASCE) **104**(EE3) : 531-534.

Characklis W. G. (1990). Energetics and stochiometry. *Dans* Biofilms, Les Éditions Charackils W. G. and Marhall K. C., Wiley-Interscience publication, John Wiley & Son, Inc., U.S.A., pp. 161-192.

Chassagnole C. Noisommit-Rizzi N., Schmid J. W., Mauch K. et Reuss M. (2002). Dynamic modeling of the central carbon metabolism of *Escherichia coli*. Biotechnology and Bioengineering, **79**(1) : 53-73.

Chen R., Yap W.M.G.J., Postma P.W. et Baley J.E. (1997). Comparative studies of Escherichia coli strains using different glucose uptake systems: Metabolism and Energetics. Biotechnology and Bioengineering, **56**(5) : 583-590.

Chiu S. Y., Kao I. C., Erickson L. E. et Fan L. T. (1973). ATP pool in activated sludge. Journal of the Water Pollution Control Federation, **45**(8), 1746-1758.

Chu K. H., van Veldhuizen H. M. et van Loosdrecht M. C. M. (2003). Respirometric measurement of kinetic parameters: effect of activated sludge floc size. Water Science and Technology, **48**(8): 61-68.

Chudoba P., Capdeville B. et Chudoba J. (1992). Explanation of biological meaning of the S_0/X_0 ratio in batch cultivation. Water Science and Technology, **26**(3-4): 743-751.

Çinar Ö. et Grady C.P.L. (2001). Aerobic and anoxic biodegradation of benzoate: Stability of biodegradative capability under endogenous conditions. Water Research, **35**(4) : 1015-1021.

Cole J. R. et Nomura M. (1986). Translational regulation is responsible for growth-rate-dependent and stringent control of the synthesis of ribosomal proteins L11 and L1 in *Escherichia coli*. Proceedings of the National Academy of Science USA., **83** : 4129-4133.

Collier P.J., Ramsey A.J., Austin P. et Gilbert P. (1990). Growth inhibitory and biocidal activity of some isothiasnozolone biocides. Journal of Applied Bacteriology, **69** : 569-577.

Contois D. E. (1959). Kinetics of bacterial growth : relationship between population density and specific growth rate of continuous culture. Journal of Genetical Microbiology, **21** : 40-50.

Cozzone A. J. (1981). How do bacteria synthesize proteins during amino acid starvation ?. Trends in Biochemical Sciences, **6**: 108-110.

C.T.G.R.E.F., 1981. Les performances des systèmes d'aération des stations d'épuration. Centre technique du génie rural des eaux et des forêts, Ministère de l'agriculture, Paris, France, 125 p.

Daigger G.T., 1979. The interaction of physiological adaptation and transient response for Pseudomonas putida and its implication for dynamic modeling of microbial growth, Ph. D. Thesis, Pudue University, West Lafayette, IN..

Daigger G.T. et Grady C.P.L. (1982a). The dynamics of microbial growth on soluble substrates : A unifying theory. Water Research, **16**: 365-382.

Daigger G.T. et Grady C.P.L. (1982b). An assessment of the role of physiological adaptation in the transient response of bacterial cultures. Biotechnology and Bioengineering, **24** : 1427-1444.

Daniels L., Hanson R. et Phillips J.A. (1994). Chemical analysis. *Dans* Methods for general and molecular bacteriology, Les Éditions P. Gerhardt, R. G. E. Murray, W. A. Wood et N. R. Krieg, American Society for Microbiology, Washington, D.C., pp. 512-554.

Davies D. G. (1999). Regulation of matrix polymer in biofilm formation and dispersion. *Dans* Microbial extracellular polymeric substances, Characterisation, structure and function, Les Éditions J. Wingender, T. R. Neu and H.-C. Flemming, Springer-Verlag Berlin Heidelberg, Germany, pp. 93-117.

Davis B. D., Luger S. M. et Tai P. C. (1986). Role of ribosome degradation in the death of starved *Escherichia coli* cells. Journal of Bacteriology, **166**(2): 439-445.

Dawes E. A. et Senior P. J. (1973). The role and regulation of energy reserve polymers in micro-organisms. Advance in Microbiological Physiology, **10** : 135-266.

Death A. et Ferenci T. (1994). Between feast and famine: Endogenous inducer synthesis in the adaptation of *Escherichia coli* to growth with limiting carbohydrates. Journal of Bacteriology, **176**(16): 5101-5107.

Dell'Anno A., Fabiano M., Duineveld G.C.A., Kok A. et Danovaro R. (1998). Nucleic acid (DNA, RNA) quantification and RNA/DNA ratio determination in marine sediments: Comparison of spectrophotometric, fluorometric, and high-performance liquid chromatography methods and estimation of detrial DNA. Applied Environmental Microbiology, **64**(9), 3238-3245.

de Smit M. H. et van Duin J. (1990). Secondary structure of the ribosome binding site determines translational efficiency: a quantitative analysis. Proceedings of the National Academy of Science, USA, **87**: 7668-7672.

De Souza Melo H. (1984). Contribution à la modélisation des processus de traitement biologique des effluents, Isolement et identification de métabolites inhibiteurs de la croissance bactérienne, 2ième partie : Étude des inhibiteurs. Thèse de doctorat, Institut National des Sciences Appliquées de Toulouse, Toulouse, France.

De Vuyst L., De Vin F., Vaningelgem F. et Degeest B. (2001). Recent developments in biosynthesis and application of heteropolysaccharides from lactic acid bacteria. International Dairy Journal, **11**: 687-707.

Dircks K., Beun J.J., van Loosdrecht M.C.M., Heijnen J.J. et Henze M. (2001). Glycogen metabolism in aerobic mixed cultures, Biotechnology and Bioengineering., **73**(2): 85-94.

Doelle H. W., Ewings K. N. et Hollywood N. W. (1982). Regulation of glucose metabolism in bacterial systems. Advance in Biochemical Engineering, **23** : 1-35.

Dold P. L., Ekama G. A. et Marais G. vR. (1980). A general model for the activated sludge process, Progress in Water Technology, **12** : 47-77.

Draper D. (1996). Translational initiation, *Dans Escherichia coli* and *Salmonella*, cellular and molecular biology. Vol. 1. Les Éditions F. C. Neidhardt, R. Curtiss, J.L. Ingraham, E.C.C. Lin, K.B. Low, B. Magasanik, W.S. Reznikoff, M. Riley, M. Schaechter and H.E. Umbarger, ASM Press, Washington, D. C., pp. 902-908.

Dunkan S. Farewell A. Ballestreros M.m Taddei F., Radman M. et Nyström T. (2000). Proteins are oxydatively carbonylated in response to reduced transcriptional or translational fidelity. Proceeding of the National Academy of Science, USA, **97** : 5746-5749.

Dykhuizen D. E. et Hartl D. L. (1983). Selection in chemostats. Microbiological Review, **47**(3): 150-168.

Esener A.A., Roels J.A. et Kossen N.W.F. (1982). Dependence of the elemental composition of *K. pneumoniae* on the steady-state specific growth rate. Biotechnology and Bioengineering, 24(6); 1445-1449.

Ferenci T. (1999). 'Growth of bacterial cultures' 50 years on: towards an uncertainty principle instead of constants in bacterial growth kinetics. Research in Microbiology, **150** : 431-438.

Flärdh K., Cohen P. S. et Kjelleberg S. (1992). Ribosomes exist in large excess over the apparent demand for protein synthesis during carbon starvation in marine *Vibrio* sp. Strain CCUG 15956. Journal of Bacteriology, **174**(21): 6780-6788.

Frigon D., Oerther D.B., Morgenroth E. et Raskin L. (2002a). Oligonucleotide probe hybridization and modeling results suggest that populations consuming readily degradable substrate have high cellular RNA levels. Water Science and Technology, **45**(6): 115-126.

Frigon D., Arnaiz E., Oerther D. B. et Raskin L. (2002b). Who eats what? Classifying microbial populations based on diurnal profiles of rRNA-levels, Water Science and Technology, **46**(1-2), 1-9.

Frigon D., Muyzer G., van Loosdrecht M.C.M. et Raskin L. (2006). rRNA and poly-b-hydroxybutyrate dynamics in bioreactors subjected to feast and famine cycles, Applied Environmental Microbiology, **72**(4), 2322-2330.

Frigon D., van Loosdrecht M.C.M. and Raskin L., (submitted). Mathematical model accounting for growth history and reactor conditions in predicting biomass formation and poly-β-hydroxybutyrate storage for bacteria submitted to feast and famine cycles.

Frostegard A., Courtois S., Ramisse V., Clerc S., Bernillon D., Le Gall F., Jeannin P., Nesme X. et Simonet P. (1999). Quantification of bias related to the extraction of DNA directly from soils. Applied and Environmental Microbiology, **65**(12) : 5409-5420.

Furumai H. et Rittmann B. E. (1992). Advanced modeling of mixed population of heterotrophs and nitrifiers considering the formation and exchange of soluble microbial products. Water Science and Technology, **26**(3-4): 493-502.

Gallant J. A. (1979). Stringent control in *E. coli*, Annual Review of Genetic, **13** :393-415.

Gerardi M. H. et al. (1990). Wastewater biology: The microlife, Special publication. Water Pollutution Control Federation Alexandria, Va.

Gerdes K. (2000). Toxin-Antitoxin modules may regulate synthesis of macromolecules during nutritional stress. Journal of Bacteriology, **182**(3): 561-572.

Gernaey K., van Loosdrecht M.C.M., Henze M., Lind M. et Jorgensen S.B. (2004). Activated sludge wastewater treatment plant modelling and simulation: State of the art. Environmental Modelling & Software, **19** : 763-783.

Gilbride K.A. Frigon D., Cesnik A., Gawat J. et Fulthorpe R.R. (2006). Effect of chemical and physical parameters on a pulp mill biotreatment bacterial community. Water Research, **40** : 775-787.

Goel R., Takashi M., Hiroyasu S. et Matsuo T. (1998). Comparison of hydrolytic enzyme systems in pure culture and activated sludge under different electron acceptor condition. Water Science and Technology, **37**(4-5) : 335-343.

Grady C.L.P., Dang J.S., Harvey D. M., Jobbagy A. et Wang X.-L., (1989). Determination of biodegradation kinetic through use of electrolytic respirometry, Water Science and Technology, **21** : 957-968.

Grady C.L.P., Harlow L.J. et Riesing R.R. (1972). Effects of growth rate and influent substrate concentration on effluent quality from chemostats containing bacteria in pure and mixed culture. Biotechnology and Bioengineering, **14**: 391-410.

Grady C.P.L., Smets B.F. et Barbeau D.S. (1996). Variability in kinetic parameter estimates: A review of possible causes and a proposed terminology. Water Research, **30**(3) :742-748.

Grady C.L.P. et Williams D.R. (1975). Effects of influent substrate concentration on the kinetics of natural microbial populations in continuous culture. Water Research, **9** : 171-180.

Griffiths P. (1997). The rate of death and predation in activated sludge systems incorporating anoxic zones. BNR3 Conference, Brisbane, Aust. pp. 85-93.

Gujer W., Henze M., Takahashi M. et Van Loosdrecht M. (1999). Activated sludge model no. 3, Water Science and Technology, **39**(1) : 183-193.

Gupta S., Pilyugin S.S. et Narang A. (2005). The dynamics of single-substrate continuous culture: The role of ribosomes. Journal of Theoretical Biology, **232** : 467-490.

Hanada S. Hiroyasu S. and Mino T., 2001. Measurement of microorganisms with PHA production capability in activated sludge and its implication in activated sludge model no. 3. Water Science and Technology, **45**(6): 107-113.

Haïder S., Vanrolleghem P.A. et Kroiß H. (2000) Low sludge age and its consequences for metabolisation, storage and adsorption of readily biodegradable substrate (Ss). *Dans* Proceedings 1st World Congress of the International Water Association. Paris, France, 3-7 July 2000 [CD-ROM].

Han K., Lim H. C. et Hong J. (1992). Acetic acid formation in *Escherichia coli* fermentation. Biotechnology and Bioengineering, **39** : 663-671.

Han L., Enfors S.-O., et Häggström L. (2002). Change in intracellular metabolite pools, and acetate formation in *Escherichia coli* are associated with a cell-density-dependant metabolic switch. Biotechnology Letters, **24** : 483-488.

Hanada S. Hiroyasu S. et Mino T. (2001). Measurement of microorganisms with PHA production capability in activated sludge and its implication in activated sludge model no. 3., Water Science and Technology, **45**(6), 107-113.

Hao O. J. et Lau A. O. (1988). Kinetics of microbial by-product formation in chemostat pure cultures, ASCE Journal of Environmental Engineering, **114**(5): 1097-1115.

Harper W.F., Moore T.L., Russel T.L. et Turnbull J.A. (2005). Using nitrogen limitation to reduce polyphosphate metabolism in engineered bioreactor. Journal of Environmental Engineering and Science, **4** : 497-503.

Harper W.F. et Jenkins D. (2003). The effect of an initial anaerobic zone on the nutrient requirements of activated sludge. Water Environment Research, **75**(3): 216-224.

Henze M. (1992). Characterization of wastewater for modelling of activated sludge process. Water Science and Technology, **25**(6) : 1-15.

Henze M., Gujer W., Mino T. et van Loosdrecht M.C.M. (2000). Activated sludge models ASM1, ASM2, ASM2d and ASM3. IWA Publishing, London, UK.

Heptinstall J. (2000). Total RNA isolation from bacteria, *Dans* The nucleic acid protocols handbook, Les Éditions Ralph Rapley, Humana Press, Totowa, N. J., p. 47-52.

Herbert D. (1958). Some principles of continuous culture. In: Recent progress in microbiology, Proceedings of the Symposium 7th International Congress of Microbiology, Les Édition Tunevall Almqvist and Wiksell, Stockholm, pp. 381–396.

Herbert D. (1976). Stoichiometric aspects of microbial growth, *Dans* Continuous culture 6: Applications and new field. Les Éditions Dean A. C. R., Ellwood D. C., Evans C. G. T., Melling J., Chichester and Horwood, 6: 1-30.

Herbert D., Phipps P.J. et Strange R.E. (1971). Chemical analysis of microbial cells. *Dans* Methods in microbiology, Les Éditions J. R. Norris et D. W. Ribbons, Academic Press, London et New York, p. 209-344.

Hill C. W. et Gray J. A. (1988). Effects of chromosomal inversion on cell fitness in *Escherichia coli* K-12, Genetics, **199** : 771-778.

Hirai K., Ito A., Abe Y, Suzue S., Irikura T., Inoue M. et Mitsuhashi S. (1981). Comparative activities of AM-715 and pipemidic and nalidixic acids against experimentally induced systemic and urinary tract infections. Antimicrobial Agents Chemotherapy, **19**(1) : 188-189.

Hochman A. (1997). Programmed cell death in prokaryotes. Critical Review in Microbiology, **23**(3): 207-214.

Huang J. Y. C. et Cheng M. D. (1987). Transient responses incorporating products formation. ASCE Journal of Environmental Engineering, **113**(4) : 868-880

Huisman G. W., Siegle D. A., Zambrano M. M. et Kolter R. (1996). Morphological changes during stationary phase. *Dans Escherichia coli* and *Salmonella*, cellular and molecular biology. Vol. 2. Les Éditions F. C. Neidhardt, R. Curtiss, J. L. Ingraham, E. C. C. Lin, K. B. Low, B. Magasanik, W. S. Reznikoff, M. Riley, M. Schaechter and H. E. Umbarger, ASM Press, Washington, D. C., pp. 1672-1682.

Ito A., Hirai K., Inoue M., Koga H., Suzue S., Irikura T. et Mitsuhashi S. (1980). In vitro antibacterial activity of AM-715, a new nalidixic acid analog. Antimicrobial Agent and Chemotherapy, **17**(2):103-108.

Jensen K. F. and Pedersen S. (1990). Metabolic growth rate control in *Escherichia coli* may be a consequence of subsaturation of the macromolecular biosynthetic apparatus with substrates and catalytic components. Microbiological Review, **54**(2) : 89-100.

Jones L. J., Yue S. T., Cheung C.-Y. et Singer V. L. (1998). RNA quantification by fluorescence-based solution assay: Ribogreen reagent characterisation. Analitical Biochemistry, **265**: 368-374.

Jöres L. et Wagner R. (2003). Essential steps in the ppGpp-dependent regulation in bacterial ribosomal RNA promoters can be explained by substrate competition. Journal of Biological Chemistry, **278**(19) : 16834-16849.

Kaplan L.A.E. (2001). The development of a rapid and sensitive, high-throughput protocol for RNA:DNA ratio analysis. Journal of Aquatic and Animal health, **13**, : 276-279.

Kaprelyants A. S., Gottschal J. C. et Douglas B. K. (1993). Dormancy in non-sporulating bacteria. FEMS Microbiological Review, **104** : 271-286.

Keener J. et Nomura M. (1996a). Modulation of chemical composition and other parameters of the cell by growth rate. *Dans Escherichia coli* and *Salmonella*, Cellular and molecular biology, Vol. 2, Les Éditions Neidhardt F.C., Curtiss R., Ingraham J.L., Lin E.C.C., Low K.B., Magasanik B., Reznikoff W.S., Riley M., Schaechter M. and Umbarger H.E., ASM Press, Washington, D.C., pp. 1447-1431.

Keener J. et Nomura M., (1996b). Regulation of ribosome synthesis. *Dans Escherichia coli* and *Salmonella*, Cellular and molecular biology, Les Éditions Neidhardt F. C., Curtiss R., Ingraham J. L., Lin E. C. C., Low K. B., Magasanik B., Reznikoff W. S., Riley M., Schaechter M. and Umbarger H. E., ASM Press, Washington, D. C., Vol. 1, pp. 1417-1431.

Kerkhof L. et Ward B.B. (1993). Comparison of nucleic acid hybridization and fluorometry for measurement of the relationship between RNA/DNA ratio and growth rate in a marine bacterium, Applied Environmental Microbiology, **59**(5) : 1303-1309.

Kessler B. et Witholt B. (2001). Factors involved in the regulatory network of polyhydroxyalkanoate metabolism. Journal Bacteriology, **86** : 97-104.

Kjeldgaard N. O., Maaloe O. et Schaechter M. (1958). The transition between different physiological states during balanced growth of *Salmonella typhimurium*. Journal of Genetical Microbiology, **19** : 607-616.

Koch A.L. (1970). Overall controls on the biosynthesis of ribosomes in growing bacteria. Journal of Theoretical Biology, **28** : 203-231.

Koch A. L. et Deppe C. S. (1971). In vivo assay of protein synthesis capacity of *Escherichia coli* from slowly growing chemostat cultures, Journal of Molecular Biology, **55** : 549-562.

Kompala D. S., Ramkrishna D., Jansen N. B. et Tsao G. T. (1986). Investigation of bacterial growth on mixed substrates: experimental evaluation of cybernetic models. Biotechnology and Bioengineering, **28** : 1044-1055.

Kovárová-Kovar K. et Egli T., 1998. Growth kinetics of suspended microbial cells : from single-substrate-controlled growth to mixed-substrate kinetics. Microbiology and Molecular Biology Reviews, **62**(3) : 646-666.

Kuzmic P., Sideris S., Cregar L. M., Elrod K. C., Rice K. D. et Janc J. W. (2000), High-throughput screening of enzyme inhibitors: Automatic determination of tight-binding inhibiton constants, Enzyme assays and analyses, Analytical Biochemistry, 281(1) : 45-50.

Krishna C. et van Loosdrecht M. (1999). Substrate flux into storage and growth in relation to activated sludge modeling. Water Research, **33**(14): 3149-3161.

Kuba T., van Loosdrecht M. C. M., Murnleitner E. et Heijnen J. J. (1997). Kinetics and stoichiometry in the biological phosphorus removal process with short cycle times. Water Research, **31** : 918-928.

Kurland C. G., Huges D. et Ehrenberg M. (1996). Limitations of translational accuracy, *Dans Escherichia coli* and *Salmonella*, cellular and molecular biology. Vol. 1. Les Éditions F. C. Neidhardt, R. Curtiss, J.L. Ingraham, E.C.C. Lin, K.B. Low, B. Magasanik, W.S. Reznikoff, M. Riley, M. Schaechter and H.E. Umbarger, ASM Press, Washington, D. C., pp. 979-1004.

Ky R.C., Comeau Y., Perrier M. et Takacs I. (2001). Modelling biological phosphorus removal from cheese factory effluent by an SBR. Water Science and Technology, **43**(3), 257-264.

Lagosky P. A. et Chang F. N. (1980). Influence of amino acid starvation on guanosine 5'-diphosphate 3'-diphosphate basal-level synthesis in *Escherichia coli*, Journal of Bacteriology, **144**(2) : 499-508.

Lancker et Gheyssens, 1986. A comparison of four frequently used assays for quantitative determination of DNA, Analytical letters, **19**(5-6), 615-623.

Lau A. O., Strom P. F. et Jenkins D. (1984). Growth kinetics of *Sphaerotilus natans* and a floc former in pure and dual continuous culture. Journal of the Water Pollution Control Federation, **56**(1) : 41-51.

Lavallée B., Lessard P. and Besser C. (2002). Decay rate variability of active heterotrophic biomass, Water Science and Technology, **46**(1-2) : 423-430.

Lavallée B., Lessard P. and Vanrolleghem P.A. (2005a). Modeling the metabolic adaptations of the biomass under rapid growth and starvation conditions in the activated sludge process. Journal of Environmental Engineering and Science, **4** : 533-548.

Lavallée B., Lessard P. and Vanrolleghem P.A. (2005b). Review of prokaryote metabolism in view of modeling microbial adaptation from fast growth to starvation conditions, Journal of Environmental Engineering and Science, **4** : 517-532.

Lavallée B., Lessard P. and Vanrolleghem P.A. (en préparation). Modeling of activated sludge transient behaviour induced by regulation of carbon and nitrogen metabolism.

Lee D.-U., Casasús-Zambrana A., Hamilton R., Svoronovos S., Lee S.-I. et Koopman B. (2004). Significance of denitrifying enzyme dynamics in biological nitrogen removal processes: a simulation study. Water Science Technology, **49**(5-6) : 265-274.

Lessard P. et Beck M. B. (1991). Dynamic modeling of wastewater treatment processes. Environmental Science and Technology, **25**(1) : 30-39.

Liao J.C., Hou S.Y. et Chao Y.P. (1996). Pathway analysis, engineering, and physiological considerations for redirecting central metabolism. Biotechnology and Bioengineering, **52** : 129-140.

Liu Y. (1999). Model of dissolved organic carbon distribution for substrate-sufficient continuous culture. Biotechnology and Bioengineering, **65**(4) : 474-479.

Liu Y., Chen G. H. et Rols J. L. (1999). A kinetic model incorporating energy spilling for substrate removal in substrate-sufficient batch culture of activated sludge. Applied Microbiology and Biotechnology, **52** : 647-651.

Liu P.-H., Zhan G., Svoronos S. A. et Koopman B. (1998). Diauxic lag from changing electron acceptors in activated sludge treatment. Water Research, **32**(11) : 3452-3460.

Lu S. G., Ukita M., Sekine M., Higuchi T. et Fukagawa M. (2001). A model for membrane bioreactor process based on the concept of formation and degradation of soluble microbial products. Water Research, **35**(8) : 2038-2048.

Madoni P. (1994). Microfauna biomass in activated sludge and biofilm. Water Science and Technology, **29**(7) : 63-66.

Majewski R. A. et Domach M. M. (1990). Simple constrained-optimisation view of acetate overflow in *E. coli*. Biotechnology and Bioengineering, **35**(7) : 732-738.

Maloy S. R., Cronan J. E. Jr. et Freifelder D. (1994). Microbial genetics, Jones et Bartlett Publishers, p. 128

Makinoshima H., Aizawa S.I., Hayashi H., Miki T., Nishimura A. et Ishihama A. (2003). Growth phase-couple alterations in cell structure and function of *Escherichia coli*. Journal Bacteriology, **185**(4) : 1338-1345.

Martinage V., 1999. Traitement biologique d'eaux résiduaires engendrant des variations du rapport C/N: analyse de la nitrification. Thèse de doctorat (527), Génie des procédés, Institut National des Sciences Appliquées de Toulouse, Toulouse, France.

Marr, 1991. Growth rate of *Escherichia coli*. Microbiological Reviews, **55**(2), 316-333.

Masson, C.A., Hamer, G., et Bryers, J.D. (1986). The death and lysis of microorganisms in environmental processes. FEMS Microcobiology Reviews, **39** : 373–401.

Maurines-Carboneill C., Pernelle J. J, Morin L., Sachon G. et Leblon G., 1998. Relevance of the INT test response as an indicator of ETS activity in monitoring heterotrophic aerobic bacterial populations in activated sludges. Water Research, **32**(4) : 1213-1221.

McGrew S. B. et Mallette M. F. (1962). Energy of maintenance in *Echerichia coli*, Journal Bacteriology, **83** : 844-850.

Merrick M.J. et Edwards R.A. (1995). Nitrogen control in bacteria. Microbiological Reviews, **59**(4) : 604-622.

Mikkola, R., et Kurland, C.G. (1991). Is there a unique ribosome phenotype for naturally occurring *Escherichia coli*?. Biochimie, **73** : 1061–1066.

Milner M.G. Saunders J.R. et McCarty A.J. (2001). Relationship between nucleic acid ratios and growth in Listeria monocytogenes. Microbiology, **147** : 2689-2696.

Molin S., von Meyenburg K., Maaloe O. Hansen M. T. et Pato M. L. (1977). Control of ribosome synthesis in *Echerichia coli*: Analysis of an energy source shift down. Journal of Bacteriology, **131**(1) : 7-17.

Monod J. (1949). The growth of bacterial cultures. Annual Review of Microbiology, **3** : 371-394.

Moré M.I., Herrick J.B., Silva M.C., Ghiorse W.C. et Madsen E.L. (1994). Quantitative cell lysis of indigenous microorganisms and rapid extraction of microbial DNA from sediment. Applied Environmental Microbiology, **60** : 1572-1580.

Muttray A.F., Yu Z. et Mohn W.W. (2001). Population dynamics and metabolic activity of Pseudomonas abietaniphila BKME-9 within pulp mill wastewater microbial communities assayed by competitive PCR and RT-PCR. FEMS Microbiology Ecology, **38** : 21-31.

Neissel O. M., De Mattos M. J. T., et Tempest D. W. (1996). Growth yield and energy distribution, *Dans Escherichia coli* and *Salmonella*, Cellular and molecular biology, Les Éditions Neidhardt F. C., Curtiss R., Ingraham J. L., Lin E. C. C., Low K. B.,

Magasanik B., Reznikoff W. S., Riley M., Schaechter M. and Umbarger H. E., ASM Press, Washington, D. C., Vol. 2, pp. 1683-1692.

Nelder J.A. et Mead R. (1965). A simplex method for function minimization. Computer Journal, 7: 308-313.

Nicolai B.M., Van Impe J.F., Vanrolleghem P.A. et Vandewalle J. (1991) A modified unstructured mathematical model for the penicillin G fed-batch fermentation. Biotechnology Letters, **13** : 489-494.

Nilsson G., Belasco J. G., Cohen S. N. et von Gabain A. (1984). Growth-rate dependent regulation of mRNA stability in *Escherichia coli*, Nature, **312** : 75-77.

Ninio J. (1986). Fine tuning of ribosomal accuracy, FEBS Letters, **196**(1) : 1-4.

Nomura M. (1999). Regulation of ribosome biosynthesis in *Escherichia coli* and *Saccharomyces cerevicae*: Diversity and common principles. Journal of Bacteriology, **181**(22) : 6857-6864.

Nyström T. (1994). The glucose-starvation stimulon of *Escherichia coli*: induced and repressed synthesis of enzymes of central metabolic pathways and role of acetyl phosphate in gene expression and starvation survival. Molecular Microbiology, **12**(5) : 833-843.

Nyström, T. (1998). To be or not to be: the ultimate decision of the growth-arrested bacteria cell. FEMS Microbiological Review, **21** : 283–290.

Nyström T. (2001). Not quite dead enough: on bacterial life, culturability, senescence, and death. Archive of Microbiology, **176** : 159-164.

Oehmen A., Lemos P.C., Carvalho G., Yuan Z., Keller J., Blackall L.L. et Reis M. (2007). Advances in enhanced biological phosphorus removal: From micro to macro scale, Water Research, **41** : 2271-2300.

Oerther D.B. De Los Reyes III F.L., de Los Reyes M.F. et Raskin L. (2001). Quantifying filamentous microorganisms in activated sludge before, during, and after an incident of foaming by oligonucleotide probe hybridizations and antibody attaining, Water Research, **35**(14) : 3325-3336.

Oerther D. B., van Loosdrecht M. C. M. et Raskin L., (2002). Quantifying the impact of wastewater micronutrient composition on in situ growth activity of *Acinetobacter* spp., Water Science and Technology, **46**(1-2) : 443-447.

O'Farrell P. H. (1978). The supression of defective translation by ppGpp and ist role in tne stringent response. Cell, **14** : 545-557.

Orhon D., Çokgör U. E. et Sözen S. (1999). Experimental basis for the hydrolysis of slowly biodegradable substrate in different wastewaters. Water Science and Technology, **39**(1) : 87-95.

Östling J., Holmquist L., Flärdh K., Svenblad B., Jouper-Jaan A. et Kjelleberg S. (1993). Starvation and recovery of *Vibrio*, in Starvation in bacteria, Les Édition S. Kjelleberg, Plenium Press, New York et London, p. 103-127.

Paul J.H. et Myers B. (1982). Fluorometric determination of DNA in aquatic microorganisms by use of Hoechst 33258. Applied Environmental Microbiology, **43**(6) : 1393-1399.

Pearson S. D., Ackeman R. A. et Seagrave R. C., 1991. The energetics of embryoni growth and developpement I. Oxygen consumption, biomass growth, and heat production. Journal of Theoretical Biology, **151** : 223-240.

Petersen B., Gerneay K., Henze M. et Vanrolleghem P.A. (2001). A comprehensive model calibration procedure for ASM1, Proceedings of Water Environment Federation 74th Annual Conference and Exposition, [CD-ROM], Atlanta, Ga.

Picard C., Ponsonnet C., Paget E., Nesme X., et Simonet P. (1992). Detection and enumeration of bacteria in soil by direct DNA extraction and polymerase chain reaction. Applied Environmental Microbiology, **58**(9) : 2717-2722.

Pike E. B. et Curds C. R. (1971). The microbial ecology of the activated sludge process. *Dans* Microbial aspects of pollution. The Society for Applied Bacteriology Symposium Series no. 1, Les Éditions Sykes G. and Skinner F. A., Academic Press, London, New York.

Pirt S. J. (1965). The maintenance energy of bacteria in growing cultures, Proceedings of the Royal Society of London, **163 B** : 224-231.

Pirt S. J. (1982). Maintenance energy : a general model for energy-limited and energy-sufficient growth. Archives of Microbiology, **133** : 300-302.

Press W.H., Teukoisky S.A., Vetterling W.T. et Flannery B.P. (2002). Numerical recipes in C++; The art of scientific computing, Cambridge University Press, New York, USA., pp. 655-660.

Priest F. G. (1992). Synthesis and secretion of extracellular enzymes in bacteria, Dans Microbial degradation of natural products, Les Éditions G. Winkelman, VCH Publisher Inc., New York. pp. 1-27.

Preiss J. (1996). Regulation of glycogen synthesis. *Dans Escherichia coli* and *Salmonella*, cellular and molecular biology. Vol. 1. Les Éditions F. C. Neidhardt, R. Curtiss, J.L. Ingraham, E.C.C. Lin, K.B. Low, B. Magasanik, W.S. Reznikoff, M. Riley, M. Schaechter and H.E. Umbarger, ASM Press, Washington, D. C., pp. 1015-1024.

Prescott L. M., Harley J. P. et Klein D. A. (1990). Microbiology. Wm. C. Brown Publishers, Dubuque, Iowa,.

Ramos A., Boels I., De Vos W. et Santos H. (2001). Relationship between glycolysis and exopolysaccharide biosynthesis in *Lactococus lactis*, Applied Environmental Microbiology, **67**(1) : 33-41.

Ramrishna D. (1983). A cybernetic perspective of microbial growth, in Foundation of biochemical Engineering - Kinetics and thermodynamics in biological Systems. Les Éditions Blanch H. W., Papoustakis E.T and Stephanopoulos G., ACS Symposium Series 207, American Chemical Society, 161-178.

Ratsak C.H., Maarsen K.A. et Kooijman S.A.L.M. (1996). Effect of protozoa on carbon mineralization in activated sludge. Water Research, **30**(1) : 1-12.

Record M. T., Reznikoff W. S, Craig M. L., McQuade K. L. et Schlax M. L. (1996). *Escherichia coli* RNA polymerase (Eσ70) promoters, and the kinetics of the steps of transcription initiation, *Dans Escherichia coli* and *Salmonella*, cellular and molecular biology. Vol. 1. Les Éditions F. C. Neidhardt, R. Curtiss, J.L. Ingraham, E.C.C. Lin, K.B. Low, B. Magasanik, W.S. Reznikoff, M. Riley, M. Schaechter and H.E. Umbarger, ASM Press, Washington, D. C., pp. 792-821.

Reichert P., Borchardt D., Henze M., Rauch W., Shanahan P., Somlyody L.et Vanrolleghem P.A. (2001). River Water Quality Model No.1, Scientific & Technical Report No. 12, IWA Publishing, London, U.K..

Rieger L., Koch G., Kühni M., Gujer W. et Siegrist H. (2001). The EAWAG Bio-P module for activated sludge model No. 3, Water Research, **35**(16) : 3887-3903.

Richardson J. P. et Greenblatt J. (1996). Control of RNA chain elongation and termination, *Dans Escherichia coli* and *Salmonella*, cellular and molecular biology. Vol. 1. Edited by F. C. Neidhardt, R. Curtiss, J.L. Ingraham, E.C.C. Lin, K.B. Low, B. Magasanik, W.S. Reznikoff, M. Riley, M. Schaechter and H.E. Umbarger, ASM Press, Washington, D. C., pp. 822-848.

Roels J. P. (1982). Mathematical models and the design of biochemical reactors. Journal of Chemical Technology and Biotechnology, **32** : 59-72.

Rojas A. M. et Ehrenberg M. (1991). How does ppGpp affect translational accuracy in the stringent response ?. Biochimie, **73** : 599-605.

Saikaly P.E., Stroot P.G. et Oerther D.B. (2005). Use of 16S rRNA gene terminal restriction fragment analysis to assess the impact of solids retention time on the bacterial diversity of activated sludge, Applied Environmental Microbiology, **71**(10) : 5814-5822.

Sambrook J., Fritsch E. F. et Maniatis T. (1989). Molecular cloning: A laboratory manual 3, Cold Spring Harbor Laboratory Press.

Sambrook J. et Russel D.W. (2001). Molecular cloning: A laboratory manual, 2ième edition, Cold Spring harbour Laboratory, Cold Spring Harbour, New York.

Sandén A. M., Prytz I., Tubulekas I., Förberg C., Le H., Hektor A., Neubauer P., Pragai Z., Harwood C., Ward A., Picon A., de Mattos J. T., Postma P., Farewell A., Nyström T., Reeh S., Pedersen S. et Larson G. (2002). Limiting factors in *Escherichia coli* fed-batch production of recombinant proteins. Biotechnology and Bioengineering, **81** : 158-166.

Schaechter M., Maaloe O. et Kjedgaard N.O. (1958). Dependency on medium and temperature of cell size and chemical composition during balanced growth of *Salmonella typhimurium*. Journal of general Microbiology, **19** : 592-606.

Schmid A. (2002). Increasing the microbial activity in activated sludge by the phenomenon of "biological resonance". Environmental Science and Pollution Research, **9**(4) : 227-229.

Schneider D. A., Gaal T. and Gourse R. L. (2002). NTP-sensing by rRNA promoters in *Escherichia coli* is direct. Proceedings of the National Academy of Science USA, **99**(13) : 8602-8607.

Shen L.L., Kohlbrenner W.E., Weigl D. et Baranowski J. (1989). Mechanism of quinolone inhibition of DNA gyrase, appearance of unique norfloxacin binding sites in enzyme-DNA complexes. Journal Biological Chemistry, **264**(5) : 2973-2978.

Shepherd N., Dennis P. et Bremer H. (2001). Cytoplasmic RNA polymerase in *Escherichia coli*, Journal of Bacteriology, **183**(8) : 2527-2534.

Shieh W.K. (1980). The effect of internal mass transfert resistance on the interpretation of substrate removal data in the suspended growth system. Water Res. **14** : 695-699.

Shoemaker J., Reeves G.T., Gupta S., Pilyugin S.S., Egli T and Narang A. (2003). The dynamics of single-substrate continuous cultures: the role of transport enzymes. Journal of Theoretical Biolology, **222** : 307-322.

Simpson J.M., Stroot P.G., Gelman S., Beydilli I., Dudley S. et Oerther D.B. (2006). 16S ribosomal RNA tools identify an unexpected predominance of *Paenibacillus*-like bacteria in an industrial activated sludge system suffering from poor biosolids separation. Water Environment Research, **78**(8) : 864-871.

Sin G. (2004). Systematic calibration of activated sludge models. Ph. D. Thesis, Gent University, Gent, Belgium.

Smolders G. J. F., van der Meij J. M., van Loosdrecht M. C. M. et Heijnen J. J. (1994). Stoichiometric model of the aerobic metabolism of the phosphorus removal process. Biotechnology and Bioengineerig, 44, 837-848.

Smolders G. J. F., Klop J. M., van Loosdrecht M. C. M. and Heijnen J. J. (1995a). A metabolic model of the biological phosphorus removal process: I. Effect of the sludege retention time. Biotechnology and Bioengineering, **48** : 222-233.

Smolders G. J. F., Bulstra D J., van Loosdrecht M. C. M. et Heijnen J. J. (1995b). A metabolic model of the biological phosphorus removal process: II. Validation during star-up conditions. Biotechnology and Bioengineering, **48** : 234-245.

Sohail M. (1998). A simple and rapid method for preparing genomic DNA from gram-positive bacteria. Molecular biotechnology, **10** : 191-193.

Spanjers H., Vanrolleghem P.A., Olson G. et Dold P.L. (1998). Respirometry in control of the activated sludge process: Principles. Scientific and technical report no. 7, IAWQ.

Spérandio M. (1999). Développement d'une procédure de compartimentation d'une eau résiduaire urbaine et application à la modélisation dynamique de procédés à boues activées. Thèse de doctorat, Génie des Procédés, INSA, Toulouse, France.

Sponza D.T. (2002). Extracellular polymer substrances and physicochemical properties of flocs in steady- and unsteady-state activated sludge system. Process Biochemistry, **37** : 983-998.

Standard Methods for the examination of water and wastewater (1998). 20^{ième} édition, American Public Health Association, American Water Work association, Water Environment Federation, Washington DC, USA.

Steward K. L. and Linn T. (1991). In vivo analysis of overlapping transcription units in the rplKAJLrpoBC ribosomal protein-RNA polymerase gene cluster of *Escherichia coli*. Journal of Molecular Biology, **218** : 23-31.

Stouthammer A. et Bettenhaussen C. (1973). Utilisation of energy for growth and maintenance in continuous batch culture of microorganisms. Biochimica et Biophysica Acta, **301** : 53-70.

Stouthammer A. et Bettenhaussen C. (1977). A continuous culture study of an ATPase-negative mutant of *Escherichia coli*, Archives of Microbiology, **113** : 185-189.

Stouthamer A. H. (1984). The realtion between biomass production and substrate consuption at very low growth rates. *Dans* Innovations in Biotechnology, Les Édition Houwink et van der Meer, Elsever Science Publisher, Amsterdam, Netherlands.p. 517-529.

Stroot P.G. Saikaly P.E. et Oerther D.B. (2005). Dynamic growth rates of microbial populations in activated sludge systems, Journal of Environmental Engineering, ASCE, **131**(12) : 1698-1705.

Stumm-Zollinger E. et Harris R. (1971). Kinetics of biologically mediated aerobic oxidation of organic compounds in receiving waters and in waste treatment. *Dans* Organic compounds in aquatic environments, Les Éditions S.D. Faust and J.V. Hunter. Marcel Dekker., New York. pp. 555-598.

Sutherland I. W. (2001). Microbial polysaccharides from gram-negative bacteria, International Dairy Journal, **11** : 663-674.

Templeton L.L. et grady C.L.P., 1988. Effect of culture history on the determination of biodegradation kinetics by batch and fed-batch techniques. Journal of Water pollution Control Federation, **60**, 651-658.

Tempest D. W. et Neijssel O. M. (1984). The status of Y_{ATP} and maintenance energy as biologically interpretable phenomena. Annual Review of Microbiology, **38** : 459-486.

Tchobanoglous G., Burton F.L. (1991). Wastewater engineering; Treatment, disposal, and reuse. Metcalf & Eddy, 3ième édition, É.U., 1334 p.

Trevors J.T., Lee H. et Cook S. (1992). Direct extraction od DNA from soil. Microbiology Releases Report, **1** : 111-115.

Trgovcich B., Kirsch E. D. et Grady C. L. P. (1983). Characteristics of activated sludge effluents before and after breakpoint chlorination. Journal of the Water Pollution Control Federation, **55**(7) : 966-976.

Turner B.G. et Ramkrishna D. (1988). Revised enzyme synthesis rate expression in cybernetic models of bacterial growth. Biotechnology and Bioengineering, **31**(1) : 41-43.

Turner B.G., Ramkrishna D. et Jansen N.B. (1989). Cybernetic modeling of bacterial cultures at low growth rates: Single-substrate systems. Biotechnology and Bioengineering, **34** : 252-261.

Vadeboncoeur C. (1991). Éléments de physiologie bactérienne. Notes de cours MBC-10022, Département de Biochimie, U. Laval., Québec, Canada.

van Aalst-van Leeuwen, M.A., Pot, M.A., van Loosdrecht, M.C.M. et Heijnen, J.J. (1997). Kinetic modeling of poly(β-hydroxybutyrate) production and consumption by dynamic substrate supply. Biotechnology and Bioengineering, **55** : 773-782.

van den Berg, H.A. (1998). A generic view of classic microbial growth models. Acta Biotheoretica, **46** : 117–130.

van Dongen L.G.J.M., Jetten M.S.M. et van Loosdredrecht (2001). The combined Sharon/Anamox process A sustainable method for N-removal from sludge water. IWA Publishing, 64 p..

van Gulik W. M. et Heijnen J. J. (1995). A metabolic network stokiometry analysis of microbial growth and product formation. Biotecnolology and Bioengineering, **48** : 681-698.

Van Lancker M. et Gheyssens L. C. (1986). A comparison of four frequently used assay for quantitaitve determination of DNA. Analytical Letters. **19** : 615-623.

van Loosdrecht M.C.M., 2007, Personal communication.

van Loosdrecht M.C.M. and Heijnen J.J. (2002). Modelling of activated sludge processes with structured biomass. Water Science and Technology, **45**(6) : 13-23.

van Loosdrecht M. C. M. and Henze M. (1999). Maintenance, endogenous respiration, lysis, decay and predation. Water Science and Technology, **39**(1) : 107-117.

van Loosdrecht M. C. M., Pot M. A. and Heijnen J. J. (1997). Importance of bacterial storage polymers in bioprocesses. Water Science and Technology, **35**(1) : 41-47.

Vanrolleghem P.A., Gernaey K., Petersen B., De Clercq B., Coen F. et Ottoy J.-P. (1998) Limitations of short-term experiments designed for identification of activated sludge biodegradation models by fast dynamic phenomena. In: Proceedings 7th IFAC Conference on Computer Applications in Biotechnology CAB7. Osaka, Japan, May 31 - June 4 1998. 567-572.

Vanrolleghem P. A., Sin G. et Gernaey K. (2004). Transient response of aerobic and anoxic activated sludge activities to sudden substrate concentration changes. Biotechnology and Bioengineering, **86**(3) : 277-290.

Vanrolleghem P.A., Spanjers H., Petersen B., Ginestet P., and Takacs I. (1999). Estimating (combinations of) activated sludge model no. 1 parameters and components by respirometry. Water Science and Technology, **39**(1) : 195-214.

Varner J. et Ramkrisna D. (1998). Application of cybernetic models to metabolic engineering : Investigation of storage pathways. Biotechnology and Bioengineering, **58**(2-3) : 282-291.

Védry B., 1996. Les biomasses épuratrices. Agence de l'eau, Seine-Normandie, France, 220 pp.

Verduyn C., Stouthamer A. H., Scheffers W. A. et van Dijken P. (1991). A theoretical evaluation of growth yields of yeast. Antonie van Leeuwenhoek, **59** : 49-63.

Vishignac W. et Santer M. (1975). The thiobacilli. Bacteriology Review, **21** : 195-213.

Walker G. C (1984). Mutagenesis and inducible responses to deoxyribonucleic acid damage in *Escherichia coli*, Microbiology Review, **48**(1) : 60-93.

Wallace D. M. (1987). Large ans small-scale phenol extraction, *Dans* Methods in enzymology, vol. 152, Guide to molecular cloning techniques, Edition de Berger S. L. et Kimmel A. R., Academic Press, New York, p. 33-48.

Walpole R. E. et Myers R. H. (1985). Probability and Statistics for Engineers and Scientists, Macmillan Publishing Compagny, New York, 639 p.

Wang J.C., Park J.K. et Whang L.M. (2001). Comparison of fatty acid composition and kinetics of phosphorus-accumulating organisms and glycogen-accumulating organisms. Water Environment Research, **73**(6) : 704-710.

Weddle C. L. et Jenkins D. (1971). The viability and activity of activated sludge. Water Research, **5** : 621-640.

Werker A. G. et Hall E. R. (2001). Quantifying population dynamics based on community structure fingerprints extracted from biosolids samples, Microbial Ecology, **41** : 195-209.

Wild D., von Schultness R. et Gujer W. (1994). Synthesis of denitrification enzymes in activated sludge: modelling with structured biomass. Water Science and Technology, **30**(6) : 113-122.

Wilderer P. A., Bungartz H.-J., Lemmer H., Wagner M., Keller J. et Wuertz S. (2002). Modern scientific methods and their potential in wastewater science and technology, Water Research, **36** : 370-393.

Wolfe A.J. (2005). The acetate switch. Microbiology and Molecular Biology Reviews, **69**(1) : 12–50

Wurtz S., Spaeth R., Hinderberger A., Griebe T., Flemming H.-C. et Wilderer P.A. (2001). A new method for extraction of extracellular polymeric substances from biofilms and activated sludge suitable for direct quantification of sorbed metals. Water Science and Technology, **43**(6) : 25-31.

Yarmolinsky M.B. (1995). Programmed cell death in bacterial populations. Science, **267** : 836–837.

Yu Z. et Mohn W.W. (1999). Killing two birds with one stone : simultaneous extraction of DNA and RNA from activated sludge biomass. Canadian Journal of Microbiology, **45** : 269-272.

Yuan Z. et Blackall L.L. (2002). Sludge optimization: A new dimension for the control of biological wastewater treatment systems. Water Research, **36** : 482-490.

Zambrano M. M., Siegele D. A., Almiron M., Tormo A. et Kolter R. (1993). Microbial competition : *Escherichia coli* mutants that take over stationary phase cultures. Science, **259** : 1757-1760.

Zhang X., Dennis P., Ehrenberg M. et Bremer H. (2002). Kinetic properties of rrn promoters in *Escheriachia coli*, Biochimie, **84** : 981-996.

ANNEXES

ANNEXE 1 MÉTHODE EXPÉRIMENTALE

ANNEXE 1.1 Quantification de l'ADN par fluorométrie

Quantification de l'ADN par fluorométrie

Protocole détaillé

Appareillage

Fluorimètre; modèle 450 de Sequoia-Turner,
Filtres à interference Edmund Industrial Optics: Longueur d'onde centrale : ± 2nm
Largeur de bande (FWHM) : ±10 nm
Blocage : ≤ 0,1 %
Agitateur; Mini-Beadbeater^{TM}, 25-48 cycles/sec., Biospec Product
Billes de verre 0,1 mm
Microcentrifugeuse; Biofuge Pico, Kendro Laboratory Products
Rotor Heraeus Instruments, PP 4/98 #3325
Agitateur ; Reciprocating shaker no. 6000 Eberbach, 1-1/2 stroke ; 60-120 oscillation/min.
Balance Mettler AE 200, 0,0000 g.

Acessoires
Cuvette de polyméthacrylate, UV-visible, 4,5 ml, 4clrside, (Fisherbrand 14-386-21).

Réactifs

ADN, DNA Standard 1 mg calf thymus /ml 10 mM Tris HCl (Sigma D4810)
Acide éthylènediaminetétraacétique (EDTA), $(HOOCCH_2)_2N(CH_2)_2N(CH_2COOH)_2$, grade ACS (BDH inc.)
Acétate d'ammonium, CH_3COONH_4, grade ACS, (BDH inc.)
Dicyclohexyl-18-crown-6 (Crown ether) (Sigma D-2637)
Éthanol 70 %, Les alcools de commerce Inc.
Fluorochrome Hoescht 33258 (2-[2-(4-hydroxyphenyl)-6-benzimidazole]-6-(1_methyl-4-piperazyl)-benzimidazole trihydrochloride) 10 mg/ml (Sigma B1302).
Glycogène Type VII de moules (Sigma G-1508)
HCl grade ACS (EM Science ; Merk)
Isopropanol 99+%, (Sigma I-9516)
Kathon® CG/ICP II Preservative 1.5%, 5-chloro-2-methyl-4-isothiazoline-3-one, (Supelco 48175-U).
NaCl grade ACS (Fisher scientific)
Sodium dodecyl sulphate (SDS) (Sigma L-4390)
Tris [hydroxymethyl] aminomethane (TRIZMA® Base, $NH_2C(CH_2OH)_3$) (Sigma T-6066)

Préparation

Solution inhibitrice :
200 mM TRIS-HCl pH 8, 20 mM EDTA, 40 µM norfloxacine.
Solution de Kathon :

4 ml de Kathon 1.5%, compléter à 250 ml avec de l'eau distillée.
Solution de crown ether:
50 mM TRIS, 30 mM crown ether dicyclohexyl-18-crown-6, pH 8.
Solution de lyse :
50 mM TRIS-HCl pH 8, 5 mM EDTA et 3% SDS.
Solution d'acétate d'ammonium10 M :
77,08 g d'acétate d'ammonium et compléter à 100 ml.
Solution de glycogène1000 µg/mL
100 mg de glycogène et compléter à 100 ml.
Tampon à fluorométrie :
TRIS 10 mM, pH 7,4, 1 mM EDTA, 1,5 mM Hoescht, 0,2 M NaCl.

Procédure d'échantillonnage

Dans un tube de lyse (*à bouchon vissé*) de 2 mL, placer 0,5 ml de solution inhibitrice (TRIS-EDTA-Nofloxacine) et 0,15 ml de solution Kathon.
Prélever 1 ml de biomasse et mélanger avec la solution inhibitrice.
Effectuer en triplicata.
Placer au frigo jusqu'à l'analyse.

Procédure de solubilisation de l'exo-ADN

Centrifuger la biomasse à 4°C durant 10 minutes à 16000g.
Disposer du surnageant.
Ajouter 1 ml de solution crown éther.
Placer sur la glace et agiter durant 3 heures à 60 oscillations par minutes.

Procédure de lyse (Adapté de Yu et Mohn, 1999)

Centrifuger la biomasse à 4°C durant 10 minutes à 16000g.
Disposer du surnageant.
Dans le tube de lyse contenant le culot, placer 0,5 g de billes de verres.
Ajouter 1,5 ml de solution de lyse.
Passer au *beadbeater* durant 5 minutes à 4800 cycles/min.
Centrifuger l'extrait cellulaire 5 minutes à 16000 g.
Réserver 1,0 ml de surnageant dans un tube *Eppendorf*.

Purification de l'ADN (Adapté de Yu et Mohn, 1999)

Ajouter 250 µl d'acétate d'ammonium 10 M pour obtenir une concentration finale de 2 M.
Mélanger.
Centrifuger à 16000g durant 15 minutes à 4°C.

Prélever 0,7 ml de surnageant dans un nouveau tube *Eppendorf*.
Ajouter 1 volume d'isopropanol (à -20°C) et 50 µL de la solution de glycogène (facultatif).
Centrifuger 20 minutes à 16000g à 4°C.
Disposer du surnageant.
Rincer le précipité en ajoutant un volume d'éthanol 75% (à -20°C).
Centrifuger de nouveau et disposer du surnageant.
Laisser sécher à l'air libre durant 2 minutes.
Dissoudre le culot d'ADN dans 0,5 ml de tampon à fluorométrie.
Passer au vortex durant 10 secondes.

Évaluation de la concentration de l'ADN (Cesarone et al, 1979)

Préparer une dose quotidienne de solution Hoescht 1,5 µM.
Ajouter 1,6 ml de la solution dans les cuvettes.
Ajouter 0,4 ml d'ADN purifié.
Placer au noir, et lire la fluorescence après 10 minutes.
Exciter le fluorochromes à une longueur d'onde de 360nm et lire la fluorescence à une longueur d'onde d'émission de 450nm.
Déterminer la concentration d'ADN dans l'échantillon prélevé suivant la courbe de calibration et le facteur de correction.

Courbe standard

Afin de déterminer par fluorométrie la concentration d'ADN dans un échantillon, il est nécessaire de définir une courbe de calibration. La courbe de calibration a été préparée suivant le protocole recommandé dans le bulletin technique no. MB-590 (Product No. DNA-QF, Technical bulletin No. MB-590, December 1998. DNA quantification Kit – Fluorescence Assay, SIGMA, Sigma-Aldrich, Saint-Louis, Miss., USA, 4 p.).

Préparation

Tampon à fluorométrie :

TRIS 10 mM, pH 7,4, 1 mM EDTA, 1,5 mM Hoescht, 0,2 M NaCl.

Solution standard d'ADN

TRIS 1 mM, ADN 10 µg/ ml.

TRIS 1 mM, ADN 100 µg/ ml

Solution dilué d'ADN

2,5 ng ADN/2 ml	8 ml de tampon à fluorométrie, 1 µl de solution standard à 10 µg d'ADN
5 ng ADN /2 ml	4 ml de tampon à fluorométrie, 1 µl de solution standard à 10 µg d'ADN
10 ng ADN /2 ml	2 ml de tampon à fluorométrie, 1 µl de solution standard à 10 µg d'ADN
20 ng ADN/2 ml	2 ml de tampon à fluorométrie, 2 µl de solution standard à 10 µg d'ADN
50 ng ADN /2 ml	2 ml de tampon à fluorométrie, 5 µl de solution standard à 10 µg d'ADN
100 ng ADN /2 ml	2 ml de tampon à fluorométrie, 10 µl de solution standard à 10 µg d'ADN
200 ng ADN /2 ml	2 ml de tampon à fluorométrie, 2 µl de solution standard à 100 µg d'ADN
500 ng ADN /2 ml	2 ml de tampon à fluorométrie, 5 µl de solution standard à 100 µg d'ADN
1000 ng ADN /2 ml	2 ml de tampon à fluorométrie, 10 µl de solution standard à 100 µg d'ADN

Évaluation de la concentration de l'ADN

Placer au noir durant 10 minutes, et lire la fluorescence.
Exciter le fluorochromes à une longueur d'onde de 360nm et lire la fluorescence à une longueur d'onde d'émission de 450nm.

Tableau A.1.1-1Construction de la courbe standard

ADN	Fluorescence
ng/mL	unitées
0	0
0	0
0	0
0	0
0	0
0	0
1,25	0
1,25	2
1,25	1
1,25	1
1,25	2
1,25	0
2,5	2
2,5	3
2,5	3
2,5	3
2,5	2
2,5	1
5	4
5	4
5	3
5	4
5	4
5	3
10	8
10	7
10	9
25	24
25	20
25	20
50	42
50	44
50	38
100	85,333
100	84,000
100	90,667
250	218,400
250	225,250
250	226,500
500	419,400
500	421,200
500	429,000

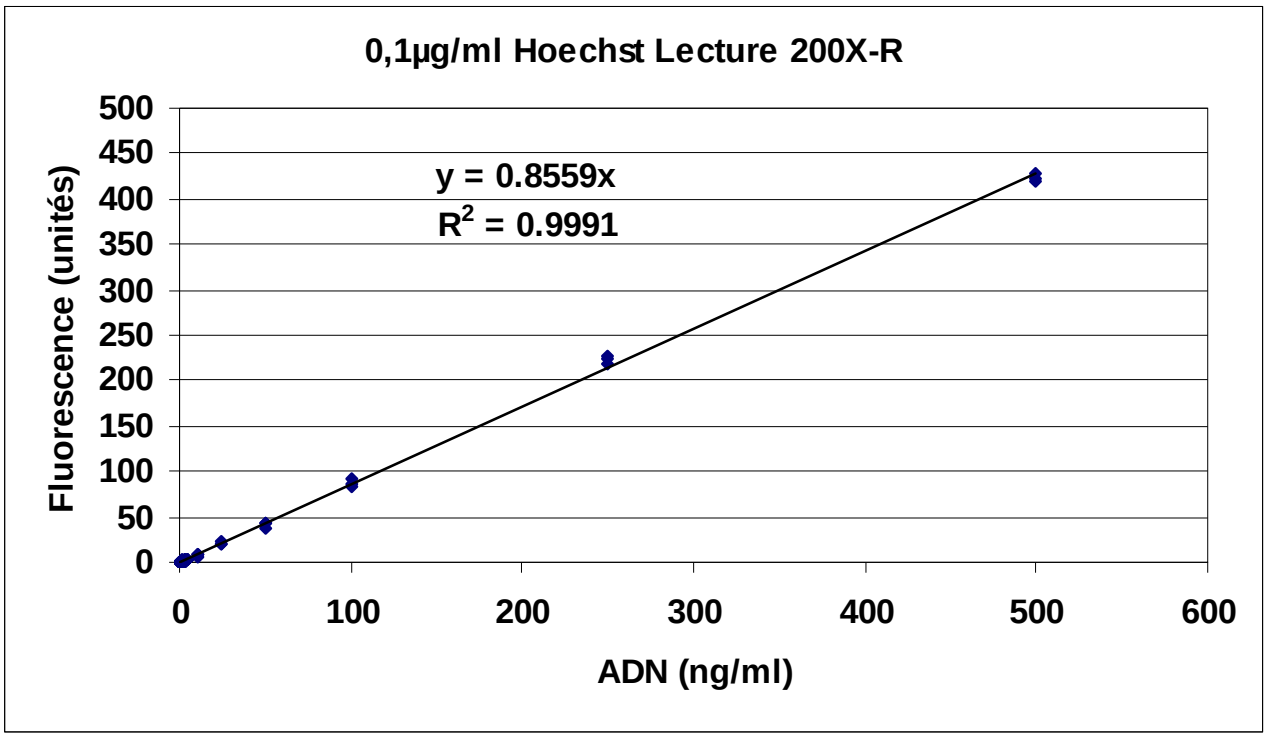

Vérification de l'interval de confiance sur la courbe standard

L'interval de confiance sur la droite de regression de la courbe standard a été determine selon la méthode de calcul décrite dans Walpole et Myers (1985).

Tableau A.1.1-2 Interval de confiance sur la courbe standard

Interval de confiance sur la courbe standard	x	y	
n	42	42	
moyenne	68,036	58,423	
$\Sigma(y-y_{moy})^2$		573131	
$\Sigma(x-x_{moy})^2$	782960		
$\Sigma(x-x_{moy})\ (y-y_{moy})$			669587
$t_{\alpha/2}$			2,000
y (unités)		0	420
Intervalle de confiance moy. (ng/ml)		1	4

Tableau A.1.1-3 Limites de detection et de quantification

	ADN x ng/ml	Moyenne µ ng/ml	$(x-\mu)^2$ ng/ml
1.1	535		263.3
1.2	584		1053.3
1.3	535		263.3
		551.7	
2.1	526		853.2
2.2	555		0.0
2.3	584		853.2
		555.0	
3.1	584		10.5
3.2	545		1274.5
3.3	613		1053.3
		580.9	
4.1	526		5571.9
4.2	613		168.5
4.3	662		3802.4
		600.4	
5.1	604		853.2
5.2	662		853.2
5.3	633		0.0
		632.9	
6.1	682		3802.4
6.2	584		1274.5
6.3	594		674.1
		619.9	
7.1	691		2696.4
7.2	594		2064.5
7.3	633		42.1
		639.4	
8.1	662		379.2
8.2	643		0.0
8.3	623		379.2
		642.6	
9.1	652		2696.4
9.2	584		263.3
9.3	565		1274.5
		600.4	
10.1	682		0.0
10.2	682		0.0
10.3	682		0.0
		681.5	
11.1	935		6583.1
11.2	837		263.3
11.3	789		4213.2
		853.6	

	ng/ml	ng/ml	ng/ml
12.1			
12.2	798		853.2
12.3	857		853.2
		827.6	
13.1	828		10.5
13.2	808		516.1
13.3	857		674.1
		830.8	
14.1	730		10785.7
14.2	915		6583.1
14.3	857		516.1
		834.1	
15.1			
15.2	720		1161.3
15.3	789		1161.3
		754.6	
16.1	925		2369.9
16.2			
16.3	828		2369.9
		876.3	
17.1	555		379.2
17.2	643		4645.0
17.3	526		2369.9
		574.4	
18.1	487		168.5
18.2	487		168.5
18.3	448		674.1
		473.8	
19.1	467		379.2
19.2	448		1516.7
19.3	545		3412.7
		486.8	
20.1	487		42.1
20.2	516		516.1
20.3	477		263.3
		493.3	
21.1	516		8257.8
21.2	682		5571.9
21.3	623		263.3
		606.9	
22.1	613		3802.4
22.2	526		674.1
22.3	516		1274.5
		551.7	

	ng/ml	ng/ml	ng/ml
23.1	711		674.1
23.2	720		1274.5
23.3	623		3802.4
		684.8	
24.1	740		42.1
24.2	740		42.1
24.3	720		168.5
		733.5	
25.1	584		1516.7
25.2	682		3412.7
25.3	604		379.2
		623.1	
26.1	458		23.7
26.2	438		213.3
26.3	448		23.7
26.4	467	452.7	213.3
27.1	535		2612.8
27.2	545		3703.0
27.3	409		5693.7
27.4	448	484.4	1333.1
28.1	351		6452.1
28.2	506		5693.7
28.3	477		2138.8
28.4	389	430.8	1712.3
29.1	604		2138.8
29.2	535		479.9
29.3	516		1712.3
29.4	574	557.4	290.3
30.1	526		213.3
30.2	555		213.3
30.3	535		23.7
30.4	545	540.4	23.7
31.1	682		716.9
31.2	730		479.9
31.3	682		716.9
31.4	740	708.3	1001.3
32.1	759		213.3
32.2	808		1161.3
32.3	779		23.7
32.4	750	774.0	592.5
33.1	837		592.5
33.2	886		5332.3
33.3	750		4005.1
33.4	779	813.0	1161.3

	ng/ml	ng/ml	ng/ml
34.1	818		2612.8
34.2	789		479.9
34.3	711		3134.2
34.4	750	766.7	290.3
35.1	779		53.3
35.2	779		53.3
35.3	837		2612.8
35.4	750	786.2	1333.1
36.1	925		1001.3
36.2	925		1001.3
36.3	886		53.3
36.4	837	893.3	3134.2
		Variance	1597.3
		σ	40
		LDM	120
		LQM	400

Taleau A.1.1-3 Vérification de la linéarité de la méthode

Volume de biomasse	Lecture	Quantification
ml	fluorescence Unité	ADN ng/ml
1	460	4479
1	443	4313
1	437	4255
1	395	3846
0,5	235	2288
0,5	200	1947
0,5	206	2006
0,5	195	1899
0,2	130	949
0,2	111	811
0,2	125	913
0,2	128	935
0,1	50	365
0,1	44	321
0,1	43	314
0,1	45	329

Tableau A.1.1-4 Calcul de l'interval de confinace sur le linéaire de la méthode

	volume ml	DNA ng/mL	(x-xmoy)	(y-ymoy)	(x-xmoy)*(y-ymoy)	
	0.1	314	-0.35	-1559	545.7	
	0.1	321	-0.35	-1552	543.1	
	0.1	329	-0.35	-1544	540.5	
	0.1	365	-0.35	-1508	527.8	
	0.2	811	-0.25	-1062	265.6	
	0.2	913	-0.25	-960	240.1	
	0.2	935	-0.25	-938	234.6	
	0.2	949	-0.25	-924	230.9	
	0.5	1899	0.05	26	1.3	
	0.5	1947	0.05	74	3.7	
	0.5	2006	0.05	133	6.6	
	0.5	2288	0.05	415	20.8	
	1	3846	0.55	1973	1085.1	
	1	4255	0.55	2382	1310.0	
	1	4313	0.55	2440	1342.1	
	1	4479	0.55	2606	1433.1	
n	16	16				
moy	0.45	1873				
Sxx			1.96			
Syy				35787030		
Sxy					8330.9	
s						164.1
$t_{\alpha/2}$			2.145			
x0			0			
x				1		
Interval de confiance (ng/ml)			143	164		

Tableau A.1.1-4 Taux de récupération de l'ADN

	Dose ADN	Lecture		Quantification	Récupération
		fluorescence	ADN/ml	ADN/ml	
Échantillon	**ng/ml**	**unité**	**ng/ml**	**ng/ml**	**%**
1	500	22	26	161	32%
2	500	29	34	212	42%
3	500	24	28	175	35%
4	500	25	29	183	37%
moy				183	37%
écart type				21	4%

Tableau A.1.1-5 Vérification de l'efficacité de l'extraction de l'exo-ADN

Échantillon	Exo-ADN+ADN		ADN	
	Lecture fluorescence unité	Quantification ADN ng/ml	Lecture fluorescence unité	Quantification ADN ng/ml
1	600	5000	503	4192
2	650	5417	486	4050
3	690	5750	485	4042
4	675	5625	492	4100
moy	654	5448	492	4096
écart type	39	329	8	69

Tableau A.1.1-6 Test d'égalité des variances (F-Test)

Ho=Les variances sont semblables

	Variable 1	*Variable 2*
Moyenne	653.75	491.5
Variance	1556.25	68.33
Observations	4	4
Degré de liberté	3	3
α	0.975	0,025
Valeur critique pour F (unilatéral)	0.065	15.439
F	22.774	
P(F<=f) unilatéral	0.014	0.014

Tableau A.1.1-7 Test de similarité des moyennes Exo-ADN+ADN et ADN

Ho=Les moyennes sont semblables

n1 =	4	
n2 =	4	
S1 =	39,45	
S2 =	8,27	
Degré de liberté =	3,26	
v =	3	
α =	0,05	
Valeur critique de + $t_{\alpha/2}$ =	**3,182**	selon tables de Students
moy1	654	
moy2	492	
t' =	**8,051**	
Ho	FAUX	
moy1	≠	moy2
σ_{12} =	28,50	

Tableau A.1.1.-8 Test de puissance Exo-ADN+ADN et ADN

Vérification bilatérale		
$\Delta = \lvert\delta\rvert/\sigma = \lvert \mu 1 - \mu 2 - do \rvert/\sigma_{12}$		
$\alpha =$	0,05	
$\beta =$	0,05	
$\Delta =$	5,69	
$n \geq$	**4**	selon tables statistiques
Puissance suffisante		

Tableau A.1.1-9 Test d'inhibition par la Norfloxacine

Échantillon	Témoin 0 h - subst. - inhib.		Inhib. 24h + subst. + inhib.	
	Lecture fluorescence unité	**Quantification ADN ng/ml**	**Lecture fluorescence unité**	**Quantification ADN mg/ml**
1	360	3000	444	3700
2	385	3208	410	3417
3	390	3250	400	3333
4	310	2583	430	3583
moy	361	3010	421	3508
écart type	37	305	20	165

Tableau A.1.1-10 Test de similarité des variances (F-test) Témoin 0h et Inhib. 24h.

Ho=Les variances sont semblables

	Variable 1	*Variable 2*
Moyenne	361.25	421
Variance	1339.58	390.67
Observations	4	4
Degré de liberté	3	3
α	0.95	0,05
Valeur critique pour F (unilatéral)	0.108	9,277
F	3,429	
P(F<=f) unilatéral	0,169	0,169

Tableau A.1.1-10 Test de similarité des moyennes Témoin 0h et Inhib. 24h.

Ho=Les valeurs (moyennes) sont semblables

n1 =	4	
n2 =	4	
S1 =	14,77	
S2 =	10,49	
Degré de liberté =	6	
$(\sigma_{12})^2$ =	865.125	
α =	0.025	
Valeur critique de $\pm$ $t_{\alpha/2}$ =	**2.447**	selon tables de Students
moy1	361.25	
moy2	421.00	
t' =	**-2.873**	
Ho	FAUX	
moy1	$\neq$	moy2

Tableau A.1.1-11 Test de puissance sur les moyennes Témoin 0h et Inhib. 24h.

Vérification bilatérale		
$\Delta = \lvert\delta\rvert/\sigma = \lvert \mu1 - \mu2 - do \rvert/\sigma_{12}$		
$\alpha =$	0,05	
$\beta =$	0,05	
$\Delta =$	-2,01	
$n \geq$	**6**	selon tables statistiques
Puissance insuffisante		

Tableau A.1.12 Test d'inhibition par le Katlon®

	Inhib. 0h + subst. + inhib.		Inhib. 24h + subst.+ inhib.		Témoin 24h + subst.	
Échantillon	**Lecture fluorescence unité**	**Quantif. ADN ng/ml**	**Lecture fluorescence unité**	**Quantif. ADN ng/ml**	**Lecture fluorescence unité**	**Quantif. ADN ng/ml**
1	300	2500	300	2500		
2	290	2417	309	2575	343	2858
3	266	2217	321	2675	354	2950
4	293	2442	322	2683	341	2842
moy	287	2393	313	2608	346	2883
écart type	28	123	10	87	7	58

Tableau A.1.1-10 Test de similarité des variances Inhib. 0h et Témoin 24h (F-test)

Ho=Les variances sont semblables

	Variable 1	*Variable 2*
Moyenne	287.25	346
Variance	218.25	49
Observations	4	3
Degré de liberté	3	2
α	0.95	0,05
Valeur critique pour F (unilatéral)	0.105	19,164
F	4,454	
P(F<=f) unilatéral	0,189	0,189

Tableau A.1.13 Test de similarité des moyennes Inhib. 0h et Témoin 24h

Ho=Les moyennes sont semblables

n1 =	4	
n2 =	3	
S1 =	14,77	
S2 =	7,00	
Degré de liberté =	5	
$(\sigma_{12})^2$ =	150.55	
α =	0.025	
Valeur critique de $\pm$ $t_{\alpha/2}$ =	**2.571**	selon tables de Students
moy1	287.25000	
moy2	346.00000	
t' =	**-6.269156**	
Ho	FAUX	
moy1	≠	moy2

Tableau A.1.14 Test de puissance sur les moyennes Inhib. 0h et Témoin 24h

Vérification bilatérale $\Delta = \lvert\delta\rvert/\sigma = \lvert\mu1 - \mu2 - do\rvert/\sigma_{12}$		
$\alpha =$	0,05	
$\beta =$	0,05	
$\Delta =$	-4,788	
$n \geq$	**4**	selon tables statistiques
	OK	

Tableau A.1.1-10 Test de similarité des variances Inhib. 24h et Témoin 24h (F-test)

Ho=Les variances sont semblables

	Variable 1	*Variable 2*
Moyenne	313	346
Variance	110	49
Observations	4	3
Degré de liberté	3	2
α	0.95	0,05
Valeur critique pour F (unilatéral)	0.105	19,164
F	2,245	
P(F<=f) unilatéral	0,323	0,323

Tableau A.1.15 Test de similarité des moyennes Inhib. 24h et Témoin 24h

Ho=Les moyennes sont semblables

n1 =	4	
n2 =	3	
S1 =	10,49	
S2 =	7,00	
Degré de liberté =	5	
$(\sigma_{12})^2$ =	85.6	
α =	0.025	
Valeur critique de $\pm$ $t_{\alpha/2}$ =	**2.571**	selon tables de Students
moy1	313.00	
moy2	346.00	
t' =	**-4.670019**	
Ho	FAUX	
moy1	$\neq$	moy2

Tableau A.1.16 Test de puissance sur les moyennes Inhib. 24h et Témoin 24h

Vérification bilatérale		
$\Delta = \lvert\delta\rvert/\sigma = \lvert\mu 1 - \mu 2 - do\rvert/\sigma_{12}$		
α =	0,05	
β =	0,05	
Δ =	-3,567	
n $\geq$	**3**	selon tables statistiques
	OK	

Tableau A.1.1-10 Test de similarité des variances 0h et Inhib. 24h (F-test)

Ho=Les variances sont semblables

	Variable 1	*Variable 2*
Moyenne	287.25	313
Variance	218.25	110
Observations	4	4
Degré de liberté	3	3
α	0.95	0,05
Valeur critique pour F (unilatéral)	0.108	9,277
F	1,984	
P(F<=f) unilatéral	0,294	0,294

Tableau A.1.17 Test de similarité des moyennes Inhib. 0h et Inhib. 24h

Ho=Les moyennes sont semblables

n1 =	4	
n2 =	4	
S1 =	14,77	
S2 =	10,49	
Degré de liberté =	6	
$(\sigma_{12})^2$ =	164.125	
α =	0.025	
Valeur critique de $\pm$ $t_{\alpha/2}$ =	**2.447**	selon tables de Students
moy1	287.25	
moy2	313.00	
t' =	**-2.842529**	
Ho	FAUX	
moy1	$\neq$	moy2

Tableau A.1.18 Test de puissance

Vérification bilatérale

$\Delta = |\delta| / \sigma = |\mu 1 - \mu 2 - do| / \sigma_{12}$

α =	0,05	
β =	0,05	
Δ =	-2,010	
n $\geq$	**6**	selon tables statistiques

Puissance insuffisante

ANNNEXE 1.2 Évaluation de la concentration de glucose

Évaluation de la concentration de glucose

Protocole détaillé

Appareillage

Spectrophotomètre Pharmacia, LKB Ultraspec III, UV/visible, lampe au tungsten, parcours de 1 cm.
Pompe à vide
Support à filtres.
Balance Mettler AE 200, 0,0000 g.

Accessoires

Filtres : 934 AH de fibre de verre
Filtres 0,4 µm : Millipores HTTP de polycarbonate
Cuvette de polyméthacrylate, UV-visible, 4,5 ml, 4clrside, (Fisherbrand 14-386-21).

Réactifs

Acide sulfurique, 95-98%, grade ACS, (Fisher Scientific).
Anthrone, $C_{14}H_{10}O$ (Sigma A 1631).
Benzoate de sodium ($C_6H_5CO_2Na$), Lab. Mat. Inc.
Éthanol 100%, Les alcools de commerce Inc.
Éthanol 75%, Les alcools de commerce Inc.
D-Glucose ($C_6H_{12}O_6$),

Préparation

Acide sulfurique 75%
50ml H_2O, 150 ml acide sulfurique concentré.
Solution de anthrone (préparation quotidienne)
100 mg d'anthrone, 2,5 ml éthanol 100%, compléter à 50 ml avec l'acide sulfurique 75%.
Standard de glucose
0,100 g de glucose, 0,150 g de benzoate de sodium, 100 ml H_2O

Procédure dchantillonge

Prélever et filtrer immédiatement un volume de bouillon de la culture sur les filtres superposés.
Prélever un alicot de 0,6 ml de l'échantillon filtré et conserver dans une éprouvette de 12 ml.
Effectuer en triplicata,
Réfrigérer les échantillons.
Analyser dans un délai de 24 h.

Évaluation de la concentration du glucose

Préparer un blanc avec 0,6 ml d'eau distillée.
Refroidir les échantillons et la solution d'anthrone dans un bain à 0°C.
Ajouter 3 ml de la solution d'anthrone tout en maintenant dans le bain de glace.
Laisser refroidir durant 3 minutes.
Vortexer durant 10 secondes.
Laisser refroidir de nouveau durant 2 minutes.
Transférer le tube dans un bain à 100°C durant 10 minutes.
Replonger les tubes dans le bain de glace à 0°C durant 5 minutes.
Mesurer l'absorbance dans le spectrophotomètre à 625 nm.
Soustraire l'absorbance du blanc.
Déterminer la concentration de glucose dans l'échantillon prélevé suivant la courbe de calibration et le facteur de correction.

Courbe standard

Afin de déterminer par coloriméttrie la concentration de glucose dans un échantillon, il est nécessaire de définir une courbe de calibration à l'aide d'échantillons standards. La courbe de calibration a été préparée suivant le protocole recommandé

Préparation

Standard de glucose

0,100 g de glucose, 0,150 g de benzoate de sodium, 100 ml H_2O

Solution dilué de glucose

10 mg de glucose/l	99 ml de H2O, 1 ml de solution standard à 1000 mg/l de glucose
20 mg de glucose/l	49 ml de H2O, 1 ml de solution standard à 1000 mg/l de glucose
40 mg de glucose/l	48 ml de H2O, 2 ml de solution standard à 1000 mg/l de glucose
50 mg de glucose/l	95 ml de H2O, 5 ml de solution standard à 1000 mg/l de glucose
80 mg de glucose/l	46 ml de H2O, 4 ml de solution standard à 1000 mg/l de glucose
100 mg de glucose/l	90 ml de H2O, 10 ml de solution standard à 1000 mg/l de glucose
150 mg de glucose/l	85 ml de H2O, 15 ml de solution standard à 1000 mg/l de glucose
200 mg de glucose/l	80 ml de H2O, 20 ml de solution standard à 1000 mg/l de glucose

Tableau A.1.2-1Construction de la courbe standard

Glucose mg/L	abs unitées	Glucose mg/L	abs unitées
0	0	50	0.397
0	-0.002	50	0.398
		50	0.41
10	0.089	80	0.641
10	0.078	80	0.643
10	0.076	80	0.643
20	0.156	100	0.797
20	0.155	100	0.807
20	0.15	100	0.801
40	0.321	200	1.56
40	0.319	200	1.579
40	0.32	200	1.566

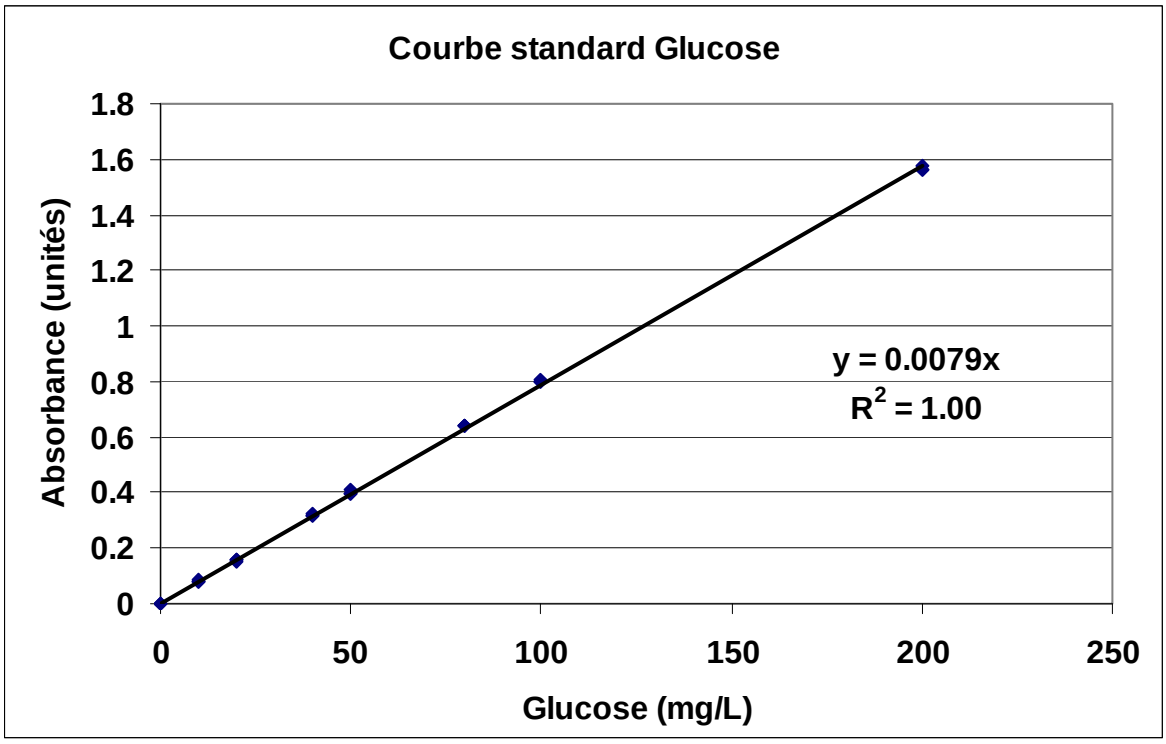

Tableau A.1.2-2 Interval de confiance sur la courbe standard

Interval de confiance sur la courbe standard	x	y	
n	23	23	
moyenne	65,2174	0,5176	
$\Sigma(y-y_{moy})^2$		5,266	
$\Sigma(x-x_{moy})^2$	85173,9		
$\Sigma(x-x_{moy})\ (y-y_{moy})$			669,6
$t_{\alpha/2}$			2,086
y (unité)		0	1,5
Intervalle de confiance moy. (mg/l)		0,7	1,1

ANNNEXE 1.3 Méthode d'évaluation des glycogènes

Évaluation des glycogènes

Protocole détaillé

Appareillage

Microcentrifugeuse, Biofuge Pico, Kendro Laboratory Products
Rotor Heraeus Instruments, PP 4/98 #3325
Spectrophotomètre Pharmacia, LKB Ultraspec III, UV/visible, lampe au tungsten, parcours de 1 cm.
Plaque chauffante.

Acessoires
Cuvette de polyméthacrylate, UV-visible, 4,5 ml, 4clrside, (Fishebrand 14-386-21).

Réactifs

Acide sulfurique, 95-98%, grade ACS, (Fisher Scientific).
Anthrone, $C_{14}H_{10}O$ (Sigma A 1631).
Éthanol 100%, (Les alcools de commerce Inc.).
Éthanol 75%, (Les alcools de commerce Inc.).
Formaldéhyde 36%, HCHO, ACS, (EM Science – Merck FX0410-1)
Glycogène, Type VII de moules, (Sigma G-1508).
KOH, ACS, (EMD PX1480-1).

Préparation

Acide sulfurique 75%
50ml H_2O, 150 ml acide sulfurique concentré.
Solution de anthrone
100 mg d'anthrone, 2,5 ml éthanol 100%, compléter à 50 ml avec l'acide sulfurique 75%.
Solution de KOH (50% p/v)
50 g de KOH, compléter à 100 ml.

Procédure d'échantillonnage

Dans un tube de lyse (*à bouchon vissé*) de 2 mL, placer 110 µl de formaldéhyde.
Prélever 1 ml de biomasse et mélanger avec la solution inhibitrice.
Effectuer en triplicata.
Placer au frigo jusqu'à l'analyse.

Procédure d'extraction des glycogènes

Centrifuger la biomasse à 4°C durant 10 minutes à 16000g.
Disposer du surnageant.

Ajouter 150 µl de solution KOH.
Placer dans un bain à 100°C durant 3 heures.
Refroidir le tube dans un bain de glace à 0°C.
Ajouter 1,1 ml d'éthanol 75%.
Centrifuger à 16000 g durant 10 minutes.
Disposer du surnageant et rincer le précipité avec de l'éthanol 75 %.
Centrifuger de nouveau et disposer du surnageant.
Laisser sécher à l'air libre durant 2 minutes.

Évaluation de la concentration des glycogènes

Ajouter 1,0 ml d'eau distillée aux tubes contenant le précipité.
Bien agiter pour dissoudre les glycogènes.
Préparer un blanc avec de l'eau distillée.
Transférer 0,6 ml de la solution dans un tube de 12 ml.
Refroidir l'échantillon et la solution d'anthrone dans un bain de glace à 0°C.
Ajouter 3 ml de la solution d'anthrone tout en maintenant dans le bain de glace.
Laisser refroidir durant 3 minutes.
Vortexer durant 10 secondes.
Laisser refroidir de nouveau durant 2 minutes.
Transférer le tube dans un bain à 100°C durant 10 minutes.
Replonger les tubes dans le bain à 0°C durant 5 minutes.
Mesurer l'absorbance dans le spectrophotomètre à 625 nm.
Soustraire l'absorbance du blanc.
Déterminer la concentration de glycogène dans l'échantillon prélevé suivant la courbe de calibration et le facteur de correction.

Tableau A.1.3-1 Construction de la courbe standard

Glycogène mg/L	abs unitées	Glycogène mg/L	abs unitées
0	0	75	0.544
0	0.001	75	0.548
0	-0.002	75	0.547
25	0.18	100	0.707
25	0.184	100	0.718
25	0.179	150	1.044
50	0.363	150	1.056
50	0.358	150	1.051
50	0.367		

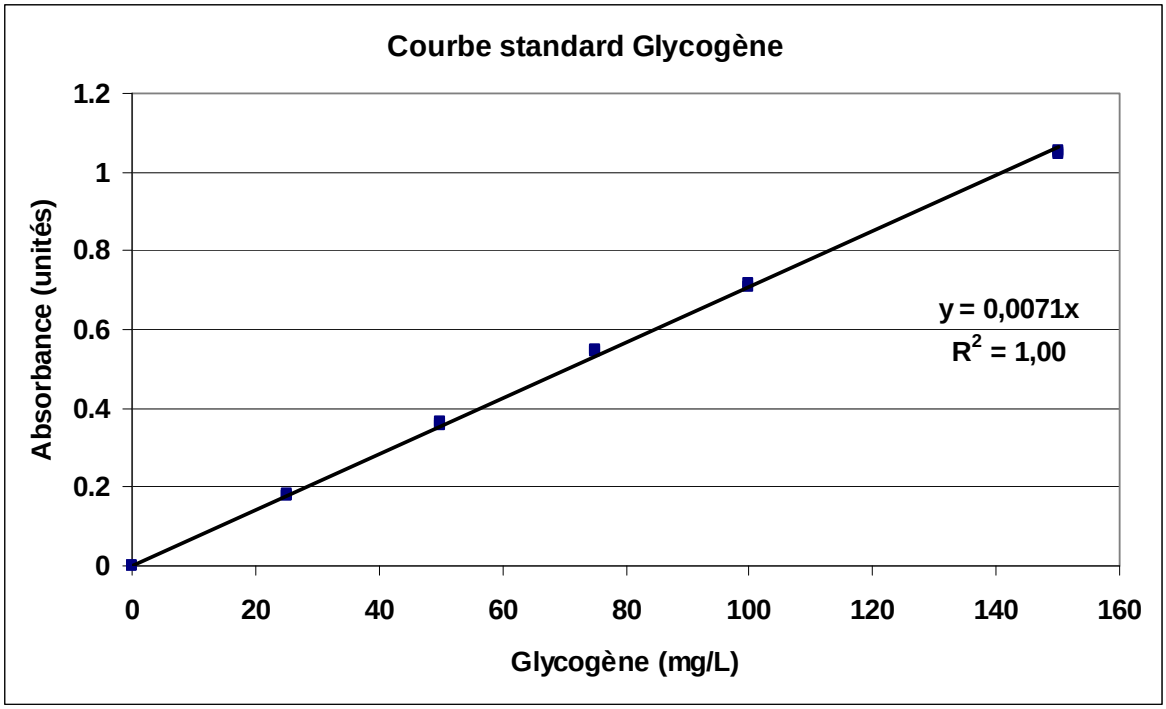

Figure A.1.3-1 Courbe de calibration du glycogène.

Tableau A.1.3-2 Interval de confiance sur la courbe standard

Interval de confiance sur la courbe standard	x	y	
n	14	14	
moyenne	66,667	0,472	
$\Sigma(y-y_{moy})^2$		2,1271	
$\Sigma(x-x_{moy})^2$	43750		
$\Sigma(x-x_{moy})\ (y-y_{moy})$			304,75
$t_{\alpha/2}$			2,12
y (unité)		0	1,05
Intervalle de confiance moy. (mg/l)		2,1	2,3

ANNEXE 1.4 Protocole détaillé de la mesure du NH_4^+

Évaluation de la concentration de NH_4^+

Protocole détaillé

Appareillage

Spectrophotomètre Jenway, 6405 UV/Vis.
Pompe à vide
Support à filtres.

Accessoires

Filtres : 934 AH de fibre de verre
Filtres 0,45 µm : Millipores, de nitrocellulose, 47 mmϕ.
Cuvette de polyméthacrylate, UV-visible, 4,5 ml, 4clrside, (Fisherbrand 14-386-21).

Réactifs

Réactif Nessler, (Hach ™ , 21194-49)
Solution de tartrate, tartrate de sodium et de potassium (Hach™, 23766-26).
Alcool de polyvinyle, (Hach ™, 23765-26).

Procédure d'échantillonnage

Prélever et filtrer immédiatement un volume de bouillon de la culturesur les filtres 934-AH et 0,45 µm superposés.
Prélever un alicot de 0,6 ml et compléter le volume à 1 ml.
Placer au frigo jusqu'à l'analyse.

Évaluation de la concentration du NH_4^+

Préparer un blanc avec de l'eau distillée.
Diluer 1ml de l'échantillon avec 9 volumes d'eau pure afin d'obtenir une concentration diluée inférieure à 5 mg/L.
Transférer 3 ml de l'échantillon dilué dans des cuvettes de méthacrylate.
Effectuer en triplicata.
Ajouter une goutte de solution tartrate aux échantillons.
Ajouter une goutte d'alcool de polyvinyle aux échantillons.
Agiter.
Ajouter 0,12 ml de la solution Nessler.
Agiter.
Laisser reposer durant 3 minutes.
Mesurer l'absorbance dans le spectrophotomètre à 425 nm.
Soustraire l'absorbance du blanc.
Déterminer la concentration de NH_4^+ dans l'échantillon prélevé suivant la courbe de calibration et le facteur de correction.

Tableau A-1.4-2 Construction de la courbe de standard

NH_4^+ mg N/L	abs unitées	NH_4^+ mg N/L	abs unitées
0	0	2	0.475
0.5	0.115	2	0.469
0.5	0.114	2	0.469
0.5	0.111	3	0.694
1	0.236	3	0.68
1	0.235	3	0.689
1	0.232	5	1.138
		5	1.138
		5	1.134

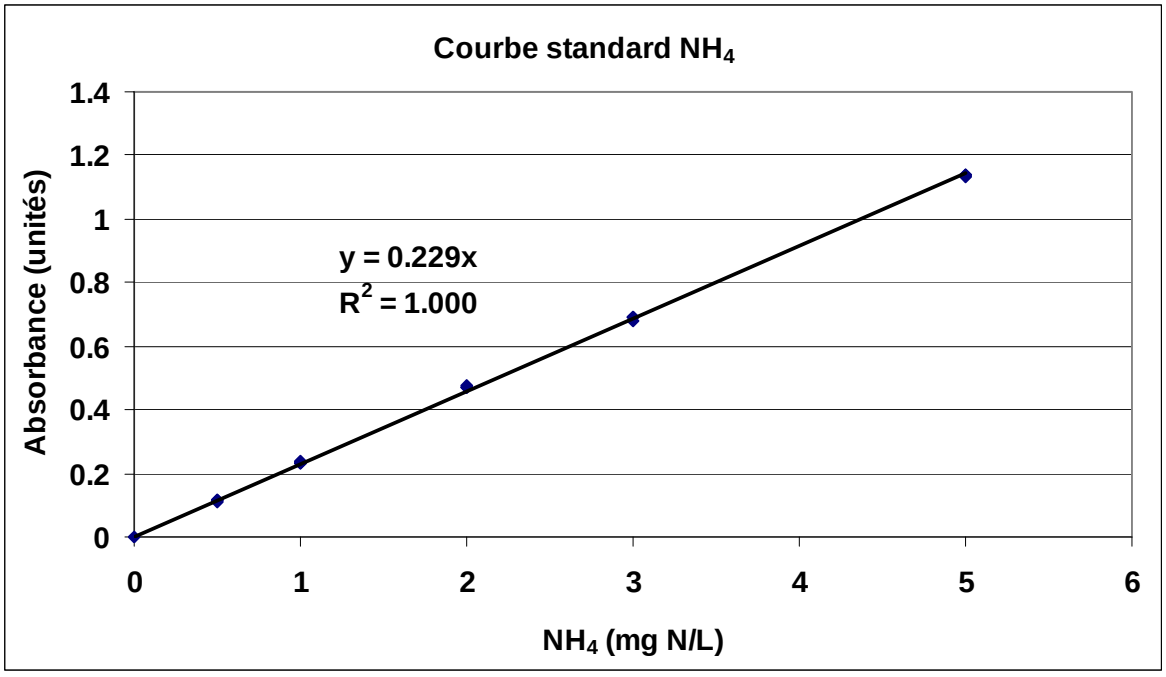

Figure A-1.4-1 Courbe standard de l'ammoniac

Tableau A-1.4-2 Interval de confiance sur la courbe standard

Interval de confiance sur la courbe standard	x	y	
n	16	16	
moyenne	2.1562	0.4956	
$\Sigma(y-y_{moy})^2$		2,234	
$\Sigma(x-x_{moy})^2$	43,359		
$\Sigma(x-x_{moy})\ (y-y_{moy})$			9,841
$t_{\alpha/2}$			2,179
y (unités)		0	1,13
Intervalle de confiance (mgN/L)		0,03	0,03

ANNEXE 1.5 Estimation de la limite de détection de la méthode de mesure de la DCO

Tableau A-1.5-1 Limite de détection de la méthode DCO

No.	Mesure (x) mg DCO/L	Moyenne (μ) mg DCO/L	$(x-\mu)^2$ mg DCO/L
1.1	245.8		12.8
1.2	249.4		0.0
1.3	253.0		12.8
		249.4	
2.1	291.3		22.4
2.2	280.6		35.1
2.3	287.7		1.4
		286.6	
3.1	243.4		30.1
3.2	256.6		58.9
3.3	246.7		4.8
		248.9	
4.1	223.7		4.8
4.2	223.7		4.8
4.3	217.1		19.2
		221.5	
5.1	230.3		4.8
5.2	233.6		30.1
5.3	220.4		58.9
		228.1	
6.1	229.8		6.7
6.2	229.8		6.7
6.3	222.1		26.7
		227.2	
7.1	226.0		6.7
7.2	218.2		26.7
7.3	226.0		6.7
		223.4	
8.1	148.7		15.1
8.2	152.6		0.0
8.3	156.5		15.1
		152.6	
9.1	234.1		26.8
9.2	249.6		107.1
9.3	234.1		26.8
		239.3	
10.1	222.5		0.0
10.2	226.3		15.1
10.3	218.6		15.1
		222.5	
11.1	191.4		1.7
11.2	191.4		1.7
11.3	187.5		6.7
		190.1	

Tableau A-1.5-1 Limite de détection de la méthode DCO (suite)

No.	Mesure (x) mg DCO/L	Moyenne (μ) mg DCO/L	$(x-\mu)^2$ mg DCO/L
12.1	164.3		6.7
12.2	172.0		26.8
12.3	164.3		6.7
		166.8	
13.1	172.0		1.7
13.2	172.0		1.7
13.3	175.9		6.7
		173.3	
14.1	164.3		6.7
14.2	152.6		82.0
14.3	168.1		41.8
		161.7	
15.1	160.4		1.7
15.2	160.4		1.7
15.3	164.3		6.7
		161.7	
16.1	148.7		1.7
16.2	152.6		26.8
16.3	141.0		41.8
		147.4	
17.1	156.5		15.1
17.2	148.7		15.1
17.3	152.6		0.0
		152.6	
18.1	272.9		15.1
18.2	265.1		15.1
18.3	269.0		0.0
		269.0	
19.1	195.3		6.7
19.2	206.9		82.0
19.3	191.4		41.8
		197.9	
20.1	175.9		1.7
20.2	172.0		6.7
20.3	175.9		1.7
		174.6	
21.1	172.0		6.7
21.2	164.3		26.8
21.3	172.0		6.7
		169.4	
22.1	350.5		1.7
22.2	350.5		1.7
22.3	354.4		6.7
		351.8	

Tableau A-1.5-1 Limite de détection de la méthode DCO (suite)

No.	Mesure (x) mg DCO/L	Moyenne (μ) mg DCO/L	$(x-\mu)^2$ mg DCO/L
23.1	296.2		15.1
23.2	288.4		15.1
23.3			
		292.3	
24.1	245.7		15.1
24.2	234.1		60.2
24.3	245.7		15.1
		241.9	
25.1	200.0		2.8
25.2	195.0		11.1
25.3	200.0		2.8
		198.3	
26.1	199.2		6.7
26.2	195.3		41.8
26.3	210.8		82.0
		201.8	
27.1	187.5		0.0
27.2	187.5		0.0
27.3	187.5		0.0
		187.5	
28.1	164.3		82.0
28.2	179.8		41.8
28.3	175.9		6.7
		173.3	
29.1	160.4		1.7
29.2	164.3		6.7
29.3	160.4		1.7
		161.7	
30.1	156.5		6.7
30.2	156.5		6.7
30.3	164.3		26.8
		159.1	
31.1	156.5		0.0
31.2	156.5		0.0
31.3	156.5		0.0
		156.5	
32.1	160.4		6.7
32.2	164.3		1.7
32.3	164.3		1.7
		163.0	
33.1	172.0		15.1
33.2	164.3		15.1
33.3	168.1		0.0
		168.1	

Tableau A-1.5-1 Limite de détection de la méthode DCO (suite)

n	33	98
Variance		16.6
s		4
LDM		12
LQM		41
moyenne		202.71
Ratio de conformité		**16.6**
Limite de détection		**12.2**
Limite de quantification		**40.8**

ANNEXE 1.5 Procédure d'échantillonnage

Procédure d'échantillonnage

Glycogènes
Dans un tube de lyse (*à bouchon vissé*) de 2 mL, placer 110 µl de formaldéhyde.
Prélever 1 ml de biomasse et mélanger avec la solution inhibitrice.
Effectuer en triplicata.
Placer au frigo jusqu'à l'analyse.

Glucose
Prélever et filtrer immédiatement un volume de bouillon de la culture sur les filtres superposés.
Prélever un alicot de 0,6 ml de l'échantillon filtré et conserver dans une éprouvette de 12 ml.
Effectuer en triplicata,
Réfrigérer les échantillons.
Analyser dans un délai de 24 h.

ADN
Dans un tube de lyse (*à bouchon vissé*) de 2 mL, placer 0,5 ml de solution inhibitrice (TRIS-EDTA-Nofloxacine) et 0,15 ml de solution Kathon.
Prélever 1 ml de biomasse et mélanger avec la solution inhibitrice.
Effectuer en triplicata.
Placer au frigo jusqu'à l'analyse.

NH_4^+
Prélever et filtrer immédiatement un volume de bouillon de la culturesur les filtres 934-AH et 0,45 µm superposés.
Prélever un alicot de 0,6 ml et compléter le volume à 1 ml.
Placer au frigo jusqu'à l'analyse.

rO_2
Prélever environ 350 ml de biomasse dans le réacteur.
Effectuer immédiatement la mesure du rO2 suivant le protocole.
Replacer l'échantillon dans le réacteur après la mesure.

DCO_{totale}
Prélever un volume suffisant de biomasse dans un bécher.
Bien homogénéiser la biomasse dans le bécher avant de prélever l'échantillon.
Pipeter 1ml dans un tube à DCO.
Ajouter 1 ml d'eau distillée.
Effectuer en triplicata.

$DCO_{filtrée}$
Prélever et filtrer immédiatement un volume sur les filtres 934-AH et 0,45 µm superposés.
Pipeter 1ml dans un tube à DCO.
Ajouter 1 ml d'eau distillée.
Effectuer en triplicata.

ANNEXE 2 Méthode statistique

A-2.1 Test d'égalité des variances

Le test effectué vise à determiner si la variance de deux échantillons est similaire. L'hypothèse à vérifier est:

$$H_0 : \sigma_1^2 = \sigma_2^2 \qquad \text{[A-2.1]}$$

La variance d'un échantillon d'une population est définie par:

$$S^2 = \frac{1}{n-1}\sum_{i=1}^{n}(X_i - \overline{X})^2 \qquad \text{[A-2.1]}$$

Selon un théorème de statistique, la distribution des variances d'échantillons d'une population suit une distribution Chi-deux avec (n-1) degrés de liberté. Ainsi :

$$\chi^2 = \frac{(n-1)S^2}{\sigma^2} \qquad \text{[A-2.1]}$$

Or, pour deux variables indépendantes, qui suivent une distribution Chi-deux, la statistique F est determinée par le rapport de ces deux variables divisées par leur degré de liberté respectif:

$$F = \frac{U/v_1}{V/v_2} \qquad \text{[A-2.1]}$$

Ainsi, pour deux échantillons issus de deux populations qui suivent une distribution normale, le rapport des distributions de variance (F) est défini par:

$$F = \frac{S_1^{\,2}/\sigma_1^{\,2}}{S_2^{\,2}/\sigma_2^{\,2}} \qquad \text{[A-2.1]}$$

Comme par hypothèse on a $\sigma_1=\sigma_2=\sigma$, la statistique F devient :

$$F = \frac{S_1^{\,2}}{S_2^{\,2}} \qquad \text{[A-2.1]}$$

Si la valeur calculée du rapport des distributions de variance (F) dépasse les valeurs critiques obtenues pour un risque d'erreur α d'une distribution F avec (n_1-1) et (n_2-1) degrés de liberté, l'hypothèse est rejettée.

Le résultat de ce test permet de tester l'égalité des moyennes.

A-2.2 Test d'égalité des moyennes

Le test d'hypothèse est le suivant:

$$H_0 : \mu_1 = \mu_2 \qquad \text{[A-2.1]}$$

Or, pour deux échantillons qui sont tirés de deux populations de moyenne μ_1 et μ_2 avec des variances de $\sigma_1$et σ_2, on sait que la difference entre les deux moyennes $\overline{X}_1$ et $\overline{X}_2$ suit une distribution normale et a une variance définie par:

$$\sigma^2_{\overline{X}_1-\overline{X}_2} = \frac{{\sigma_1}^2}{n_1} + \frac{{\sigma_2}^2}{n_2} \qquad \text{[A-2.2]}$$

Alors, la statistique Z suit une distribution normale.

$$Z = \frac{(\overline{X}_1 - \overline{X}_2) - (\mu_1 - \mu_2)}{\sqrt{{\sigma_1}^2/n_1 + {\sigma_2}^2/n_2}} \qquad \text{[A-2.3]}$$

A-2.3 Échantillons de variances égales

Si on peut assumer que $\sigma_1 = \sigma_2 = \sigma$, avec l'hypothèse H_0 la variable Z devient:

$$Z = \frac{(\overline{X}_1 - \overline{X}_2)}{\sigma\sqrt{1/n_1 + 1/n_2}} \qquad \text{[A-2.4]}$$

Lorsque le nombre n est inférieur à 30, S varie considérablement par rapport à σ et la statistique dévie d'une distribution normale. Lorsque n est inférieur à 30, la variable T suit la distribution de Student.

$$T = \frac{Z}{\sqrt{V/v}} \qquad \text{[A-2.5]}$$

Selon la définition d'une variable Chi-deux, la somme des variables Chi-deux de deux échantillons tirés d'une même population donne:

$$V = \frac{s_1^{\,2}(n_1 - 1) + s_2^{\,2}(n_2 - 1)}{\sigma^2} \qquad \text{[A-2.6]}$$

avec (n_1+n_2-2) degrés de liberté.

La statistique T devient:

$$T = \frac{\dfrac{(\overline{X}_1 - \overline{X}_2)}{\sigma\sqrt{1/n_1 + 1/n_2}}}{\sqrt{\dfrac{s_1^{\,2}(n_1 - 1) + s_2^{\,2}(n_2 - 1)}{\sigma^2(n_1 + n_2 - 2)}}} \qquad \text{[A-2.7]}$$

La variance $s_p^{\,2}$ de la population peut donc être estimée celle-ci avec:

$$s_p^{\,2} = \frac{s_1^{\,2}(n_1 - 1) + s_2^{\,2}(n_2 - 1)}{n_1 + n_2 - 2} \qquad \text{[A-2.8]}$$

et la statistique T devient:

$$T = \frac{(\overline{X}_1 - \overline{X}_2)}{\sigma_p^{\,2}\sqrt{1/n_1 + 1/n_2}} \qquad \text{[A-2.9]}$$

Si la valeur calculée de la variable T dépasse les valeurs critiques obtenues pour un risque d'erreur α de la table de Student avec (n_1+n_2-2) degrés de liberté, l'hypothèse est rejettée.

A-2.4 Échantillons de variances différentes

La variance exacte des deux population n'étant pas connue, on doit estimer σ_1 et σ_2 avec S_1 et S_2. Si on dispose d'échantillons de faible dimension (n<30), la statistique de Student s'applique, et selon l'hypothèse H_0 la variable T devient:

$$T = \frac{(\overline{X}_1 - \overline{X}_2)}{\sqrt{{s_1}^2/n_1 + {s_2}^2/n_2}} \qquad \text{[A-2.10]}$$

avec *v* degrés de liberté définis par l'équation:

$$v = \frac{\left({s_1}^2/n_1 + {s_2}^2/n_2\right)^2}{\left(\frac{\left({s_1}^2/n_1\right)^2}{n_1 - 1} + \frac{\left({s_2}^2/n_2\right)^2}{n_2 - 1}\right)} \qquad \text{[A-2.11]}$$

Le nombre *v* n'est pas toujours un nombre entier. Le nombre entier le plus près est acceptable.

Si la valeur calculée de la variable T dépasse les valeurs critiques obtenues pour un risque d'erreur α de la table de Student avec *v* degrés de liberté, l'hypothèse est rejettée.

A-2.5 Vérification de la puissance du test

La puissance d'un test est défini par la probabilité de rejetter l'hypothèse lorsqu'une alternative est vrai. La puissance du test est décrite par (1-β). Pour un risque d'erreur α, la puissance du test permet de vérifier si la grosseur de l'échantillon est suffisante pour que le test soit significatif.

Lorsque les variances ne sont pas connues, la statistique suivante ne suit pas une distribution de Student :

$$\frac{\overline{X} - (\mu_0 - \delta)}{S/\sqrt{n}}$$

Des tables statistiques sont présentées dans les manuels pour vérifier la puissance du test. Pour deux échantillons dont les variances ne sont pas connues mais assumées égales, la dimension $n_1=n_2=n$ requise pour vérifier la puissance $(1-\beta)$ d'un test avec un risque d'erreur α est définie dans les tables statistiques par la relation :

$$\Delta = \frac{|\delta|}{\sigma} = \frac{|\mu_1 - \mu_2 - d_0|}{\sigma}$$

Lorsque la puissance du test n'est pas suffisante, on ne peut rejetter l'hypothèse H_0.

ANNEXE 3 Résultats bruts

ANNEXE 3.1 Démarrage du réacteur semi-continu

Tableau A3.1-1 Mesures de la concentration d'ADN

Date	Temps	Lecture		ADN
	Jour	luminosité	ng/ml	ng/ml
28-juil	0	490	572	716
	0	506	591	739
	0	503	588	735
29-juil	1	201	235	1468
	1	213	249	1555
	1	211	247	1541
	1	205	240	1497
30-juil	2	224	262	1636
	2	196	229	1431
	2	253	296	1847
	2	266	311	1942
31-juil	3	191	223	1395
	3	183	214	1336
	3	40	47	
	3	158	185	1154
01-août	4	258	301	1884
	4	270	315	1972
	4	260	304	1899
	4	186	217	1358
03-août	6	190	222	1387
	6	225	263	1643
	6	222	259	1621
	6	176	206	1285
05-août	8	172	201	1256
	8	192	224	1402
	8	194	227	1417
	8	330	386	2410
06-août	9	286	334	2088
	9	444	519	3242
	9	153	179	1117
	9	367	429	2680
07-août	10	289	338	2110
	10	358	418	2614
	10	313	366	2286
	10	326	381	2381
08-août	11	377	440	2753
	11	329	384	2402
	11	418	488	3052
	11	381	445	2782
11-août	14	358	418	2614
	14	483	564	3527
	14	480	561	3505
	14	746	872	

Tableau A3.1-1 Mesures de la concentration d'ADN

Date	Temps	Lecture		ADN
	Jour	luminosité	ng/ml	ng/ml
12-août	15	237	277	1731
	15	112	131	
	15	462	540	3374
	15	169	197	
13-août	16	419	490	3060
	16	437	511	3191
	16	464	542	3388
	16	459	536	3352
14-août	17	240	280	1753
	17	367	429	2680
	17	214	250	1563
	17	652	762	4761
15-août	18	595	695	4345
	18	802	937	
	18	524	612	3826
	18	476	556	3476
18-août	21	356	416	2600
	21	450	526	3286
	21	240	280	
	21	300	351	2191
19-août	22	405	473	2957
	22	440	514	3213
	22	521	609	3804
	22	487	569	3556
20-août	23	544	636	3972
	23	424	495	3096
	23	526	615	3841
	23	430	502	3140
21-août	24	417	487	3045
	24	349	408	2548
	24	369	431	2695
	24	317	370	2315
22-août	25	408	477	2979
	25	196	229	
	25	477	557	3483
	25	307	359	2242

Tableau A3.1-2 Mesures de la DCO totale

Date	Temps Jour	Vol. blanc ml	F.A.S. molarité	Vol. ml	DCO mg DCO/L
28-juil	0	27	0.019	12.85	1075
	0	26.95	0.019	12.6	1094
	0	27	0.019	12.75	1082
	0	*26.983*	*0.019*		
29-juil	1	27	0.019	19.5	569
	1	26.95	0.019	19.3	584
	1	27	0.019	19.4	577
	1	*26.983*	*0.019*		
30-juil	2	28.1	0.018	19.35	637
	2	28	0.018	19.25	645
	2	28.1	0.018	19.25	645
	2	*28.067*	*0.018*		
31-juil	3	28.1	0.018	18.95	667
	3	28	0.018	18.6	692
	3	28.1	0.018	19.1	656
	3	*28.067*	*0.018*		
01-août	4	28.05	0.018	18.55	696
	4	28.1	0.018	19.4	634
	4			18.6	693
	4	*28.075*	*0.018*		
03-août	6	28.05	0.018	18.65	689
	6	28.1	0.018	18.65	689
	6			18.75	682
	6	*28.075*	*0.018*		
05-août	8	28.05	0.018	17.6	766
	8	28.1	0.018	18.5	700
	8			18.6	693
	8	*28.075*	*0.018*		
06-août	9	28.25	0.018	17.75	760
	9	28.25	0.018	17.7	764
	9	28.1	0.018	18.25	724
	9	*28.200*	*0.018*		
07-août	10	28.25	0.018	17.8	757
	10	28.25	0.018	18.3	720
	10	28.1	0.018	17.45	782
	10	*28.200*	*0.018*		
08-août	11	29	0.018	18.4	750
	11	29	0.018	18.75	725
	11			20.7	587
	11	*29.000*	*0.018*		
11-août	14	29	0.018	17	849
	14	29	0.018	16.6	877
	14			17.5	814
	14	*29.000*	*0.018*		

Tableau A3.1-2 Mesures de la DCO totale

Date	Temps Jour	Vol. blanc ml	F.A.S. molarité	Vol. ml	DCO mg DCO/L
12-août	15	29	0.018	16.6	877
	15	29	0.018	18.4	750
	15			16.9	856
	15	*29.000*	*0.018*		
13-août	16	29	0.018	17.65	803
	16	29	0.018	16.5	884
	16			16.2	906
	16	*29.000*	*0.018*		
14-août	17	29	0.018	17.2	835
	17	29	0.018	16.85	860
	17			16.1	913
	17	*29.000*	*0.018*		
15-août	18	29	0.018	17.2	835
	18	29	0.018	18.9	715
	18			15.7	941
	18	*29.000*	*0.018*		
18-août	21	29.2	0.018	16.7	878
	21			15.6	956
	21			16.85	868
	21	*29.200*	*0.018*		
19-août	22	29.2	0.018	15.7	949
	22			15.95	931
	22			15.9	935
	22	*29.200*	*0.018*		
20-août	23	30	0.017	15.7	978
	23			13	1163
	23			16	958
	23	*30.000*	*0.017*		
21-août	24	30	0.017	18.2	807
	24			17.2	876
	24			16.65	913
	24	*30.000*	*0.017*		
22-août	25	25.75	0.020	13.8	950
	25	25.7	0.020	14	934
	25	25.65	0.020	13.7	958
	25	*25.700*	*0.020*		

Tableau A3.1-3 Mesures de la DCO soluble

Date	Temps	Blanc	DCO	
	Jour	Abs.	Abs.	Abs.
28-juil	0	0	0.072	178
	0	0.003	0.07	173
	0	0	0.07	173
	0			
29-juil	1	0	0.068	168
	1	0.003	0.07	173
	1	0	0.071	175
	1			
30-juil	2	0	0.069	169
	2	-0.001	0.069	169
	2	0.005	0.066	162
	2			
31-juil	3	0	0.072	177
	3	-0.001	0.07	172
	3	0.005	0.066	162
	3			
01-août	4	0	0.07	175
	4		0.069	173
	4		0.072	180
	4			
03-août	6	0	0.068	170
	6		0.068	170
	6		0.068	170
	6			
05-août	8	0	0.065	163
	8		0.063	158
	8		0.063	158
	8			
06-août	9	0	0.063	155
	9	0	0.066	163
	9	0.003	0.068	168
	9			
07-août	10	0	0.063	155
	10	0	0.065	160
	10	0.003	0.065	160
	10			
08-août	11	0	0.059	147
	11	-0.001	0.059	147
	11	0.002	0.066	164
	11			
11-août	14	0	0.053	132
	14	-0.001	0.054	134
	14	0.002	0.056	139
	14			

Tableau A3.1-3 Mesures de la DCO soluble

Date	Temps Jour	Blanc Abs.	DCO Abs.	DCO mg/L
12-août	15	0	0.055	137
	15	-0.001	0.053	132
	15	0.002	0.06	149
	15			
13-août	16	0	0.053	133
	16		0.054	135
	16		0.054	135
	16			
14-août	17	0	0.054	135
	17		0.053	133
	17		0.052	130
	17			
15-août	18	0	0.051	129
	18	-0.001	0.051	129
	18	-0.001	0.05	127
	18			
18-août	21	0	0.05	125
	21		0.051	128
	21		0.047	118
	21			
19-août	22	0	0.046	115
	22		0.049	123
	22		0.05	125
	22			
20-août	23	0	0.052	130
	23		0.051	128
	23		0.051	128
	23			
21-août	24	0	0.05	125
	24		0.049	123
	24		0.051	128
	24			
22-août	25	0	0.059	148
	25		0.056	140
	25		0.06	150
	25			

Tableau A3.1-4 Mesures du glucose

Date	Temps	Blanc	Glucose	
	Jour	Abs.	Abs.	mg/L
28-juil	0	0	0.028	3
	0	0.001	0.043	4
	0	-0.002	0.031	3
	0	*0.000*		
29-juil	1	0	0.041	4
	1	0.001	0.057	6
	1	-0.002	0.057	6
	1	*0.000*		
30-juil	2	0	0.024	2
	2	-0.001	0.026	2
	2	0.007	0.026	2
	2	*0.002*		
31-juil	3	0	0.026	3
	3	0.001	0.03	3
	3	-0.001	0.03	3
	3	*0.000*		
01-août	4	0	0.027	3
	4	0.001	0.026	3
	4	-0.001	0.027	3
	4	*0.000*		
03-août	6	0	0.007	1
	6	-0.004	0.04	4
	6	0.008	0.01	1
	6	*0.001*		
05-août	8	0	0.022	2
	8	-0.002	0.017	2
	8	0.003	0.021	2
	8	*0.000*		
06-août	9	0	0.02	2
	9	-0.002	0.021	2
	9	0.003	0.016	2
	9	*0.000*		
07-août	10	0	0.026	3
	10	-0.002	0.029	3
	10	0	0.027	3
	10	*-0.001*		
08-août	11	0	0.031	3
	11	-0.002	0.034	4
	11	0	0.028	3
	11	*-0.001*		
11-août	14	0	0.033	3
	14	0.001	0.02	2
	14	-0.003	0.02	2
	14	*-0.001*		

Tableau A3.1-4 Mesures du glucose

Date	Temps Jour	Blanc Abs.	Glycogène Abs.	Abs.
12-août	15	0	0.016	2
	15	-0.002	0.022	2
	15		0.013	1
	15	*-0.001*		
13-août	16	0	0.014	2
	16	-0.002	0.022	2
	16		0.016	2
	16	*-0.001*		
14-août	17	0	0.031	3
	17	0	0.028	3
	17	0.003	0.032	3
	17	*0.001*		
15-août	18	0	0.028	3
	18	0	0.025	2
	18	0.003	0.024	2
	18	*0.001*		
18-août	21	0	0.025	3
	21		0.037	4
	21		0.033	3
	21	*0.000*		
19-août	22	0	0.028	3
	22		0.029	3
	22		0.028	3
	22	*0.000*		
20-août	23	0	0.043	4
	23		0.043	4
	23		0.028	3
	23	*0.000*		
21-août	24	0	0.036	3
	24	0.007	0.054	5
	24	0.001		0
	24	*0.003*	*0.045*	
22-août	25	0	0.034	3
	25	0.007	0.034	3
	25	0.001	0.045	4
	25	*0.003*		

Tableau A3.1-5 Mesures du glycogène

Date	Temps	Blanc	Glycogène	
	Jour	Abs.	Abs.	Abs.
28-juil	0	0	0.158	5
	0	0.001	0.158	5
	0	-0.002	0.153	4
	0	*0.000*		
29-juil	1	0	0.074	11
	1	0.001	0.082	12
	1	-0.002	0.078	11
	1	*0.000*		
30-juil	2	0	0.091	13
	2	-0.001	0.082	11
	2	0.007	0.089	12
	2	*0.002*		
31-juil	3	0	0.101	14
	3	0.001	0.079	11
	3	-0.001	0.073	10
	3	*0.000*		
01-août	4	0	0.154	22
	4	0.001	0.135	19
	4	-0.001	0.147	21
	4	*0.000*		
03-août	6	0	0.106	15
	6	-0.004	0.096	13
	6	0.008	0.119	17
	6	*0.001*		
05-août	8	0	0.101	14
	8	-0.002	0.101	14
	8	0.003	0.084	12
	8	*0.000*		
06-août	9	0	0.099	14
	9	-0.002	0.095	13
	9	0.003	0.078	11
	9	*0.000*		
07-août	10	0	0.122	17
	10	-0.002	0.111	16
	10	0	0.095	14
	10	*-0.001*		
08-août	11	0	0.147	21
	11	-0.002	0.124	18
	11	0	0.134	19
	11	*-0.001*		
11-août	14	0	0.122	17
	14	0.001	0.142	20
	14	-0.003	0.156	22
	14	*-0.001*		

Tableau A3.1-5 Mesures du glycogène

Date	Temps Jour	Blanc Abs.	Glycogène Abs.	mg/L
12-août	15	0	0.038	
	15	-0.002	0.043	
	15		0.037	
	15	*-0.001*		
13-août	16	0	0.134	19
	16	-0.002	0.168	24
	16		0.174	25
	16	*-0.001*		
14-août	17	0	0.082	12
	17	0	0.131	19
	17	0.003	0.124	18
	17	*0.001*		
15-août	18	0	0.119	17
	18	0	0.127	18
	18	0.003	0.117	16
	18	*0.001*		
18-août	21	0	0.14	20
	21		0.142	20
	21		0.09	13
	21	*0.000*		
19-août	22	0	0.099	14
	22		0.059	8
	22		0.072	10
	22	*0.000*		
20-août	23	0	0.08	11
	23		0.067	9
	23		0.066	9
	23	*0.000*		
21-août	24	0	0.113	16
	24	0.007	0.087	12
	24	0.001	0.071	10
	24	*0.003*		
22-août	25	0	0.207	29
	25	0.007	0.184	26
	25	0.001	0.162	23
	25	*0.003*		

Tableau A3.1-6 Mesures du NH_4^+

Date	Temps Jour	mV	NH_4^+ mg N/L
28-juil	0	20.8	49
	0	20.4	50
	0	19.7	51
	0		
29-juil	1	23.5	44
	1	22.9	45
	1	23	45
	1		
30-juil	2	25.4	41
	2	25.1	41
	2	25.1	41
	2		
31-juil	3	26.9	39
	3	26.4	39
	3	26.3	40
	3		
01-août	4	28.7	36
	4	27.7	37
	4	27.6	38
	4		
03-août	6	30	34
	6	29.4	35
	6	28.9	36
	6		
05-août	8	31	33
	8	30.6	33
	8	30.5	34
	8		
06-août	9	32.3	31
	9	31.6	32
	9	30.8	33
	9		
07-août	10	32.5	31
	10	31.4	32
	10	29.8	34
	10		
08-août	11	31.4	32
	11	31.6	32
	11	31.4	32
	11		
11-août	14	34.8	28
	14	33.4	30
	14	32.8	31
	14		

Tableau A3.1-6 Mesures du NH_4^+

Date	Temps Jour	mV	NH_4^+ mg N/L
12-août	15	33.7	30
	15	32.6	31
	15	32.3	31
	15		
13-août	16	32.7	31
	16	32.2	31
	16	31.8	32
	16		
14-août	17	32.5	31
	17	32.5	31
	17	32.5	31
	17		
15-août	18	33.6	30
	18	32.9	31
	18	32.5	31
	18		
18-août	21	36.2	27
	21	36	27
	21	35.5	28
	21		
19-août	22	32.6	31
	22	32.4	31
	22	32.4	31
	22		
20-août	23	32.8	31
	23	33.5	30
	23	33.2	30
	23		
21-août	24	34.4	29
	24	33.5	30
	24	33.9	29
	24		
22-août	25	33.2	30
	25	33.3	30
	25	33.1	30
	25		

Tableau A3.1-7 Mesures de la respiration

Date	Temps Jour	rO2 endogène mg O_2/L/j	rO2 maximal mg O_2/L/j
28-juil	0	7.8	74.8
29-juil	1	63.8	267.6
30-juil	2	41.2	325.1
31-juil	3	54.0	363.2
01-août	4	34.5	0.0
03-août	6	47.1	501.5
05-août	8	48.0	406.0
06-août	9	53.3	389.4
07-août	10	62.6	381.0
08-août	11	60.4	406.4
11-août	14	47.0	420.3
12-août	15	56.4	416.6
13-août	16	52.9	480.8
14-août	17	58.0	498.4
15-août	18	53.5	558.9
18-août	21	50.1	506.0
19-août	22	63.2	494.7
20-août	23	82.0	539.2
21-août	24	85.3	491.0
22-août	25	67.0	579.8

ANNEXE 3.2 Cuvée en croissance exponentielle

Tableau A3.2-1 Mesures de la concentration d'ADN

	Temps	ADN		
		Lecture		ADN/ml
	heures	luminosité	ng/ml	ng/ml
t-1	-1	22	26	214
t-1	-1	31	36	302
t-1	-1	28	33	273
t-1	-1	31	36	302
t0	0	47	55	458
t0	0	45	53	438
t0	0	46	54	448
t0	0	48	56	467
t1	0.5	55	64	535
t1	0.5	56	65	545
t1	0.5	42	49	409
t1	0.5	46	54	448
t2	1	36	42	351
t2	1	52	61	506
t2	1	49	57	477
t2	1	40	47	389
t3	1.5	62	72	604
t3	1.5	55	64	535
t3	1.5	53	62	516
t3	1.5	59	69	574
t4	2	54	63	526
t4	2	57	67	555
t4	2	55	64	535
t4	2	56	65	545
t5	3	70	82	682
t5	3	75	88	730
t5	3	70	82	682
t5	3	76	89	740
t6	4	78	91	759
t6	4	83	97	808
t6	4	80	93	779
t6	4	77	90	750
t7	5	86	100	837
t7	5	91	106	886
t7	5	77	90	750
t7	5	80	93	779
t8	6	84	98	818
t8	6	81	95	789
t8	6	73	85	711
t8	6	77	90	750
t9	7	80	93	779
t9	7	80	93	779
t9	7	86	100	837
t9	7	77	90	750

Tableau A3.2-1 Mesures de la concentration d'ADN

	Temps	ADN		
		Lecture		ADN/ml
	heures	luminosité	ng/ml	ng/ml
t10	8	95	111	925
t10	8	95	111	925
t10	8	91	106	886
t10	8	86	100	837
t11	9	109	127	1061
t11	9	102	119	993
t11	9	22	26	
t11	9	109	127	1061
t12	10	125	146	1217
t12	10	122	143	1188
t12	10	113	132	1100
t12	10	117	137	1139
t13	11	127	148	1237
t13	11	129	151	1256
t13	11	139	162	1353
t13	11	138	161	1344
t14	12	121	141	1178
t14	12	120	140	1168
t14	12	133	155	1295
t14	12	117	137	1139
t15	13	133	155	1295
t15	13	135	158	1314
t15	13	142	166	1383
t15	13	144	168	1402
t16	14	145	169	1412
t16	14	131	153	1275
t16	14	152	178	1480
t16	14	139	162	1353
t17	15	158	185	1538
t17	15	163	190	1587
t17	15	150	175	1460
t17	15	156	182	1519
t18	16	175	204	1704
t18	16	178	208	1733
t18	16	147	172	1431
t18	16	177	207	1723
t19	17	190	222	1850
t19	17	201	235	1957
t19	17	203	237	1976
t19	17	146	171	
t20	18	203	237	1976
t20	18	210	245	2045
t20	18	213	249	2074
t20	18	205	240	1996

Tableau A3.2-1 Mesures de la concentration d'ADN

	Temps	ADN		
		Lecture		ADN/ml
	heures	luminosité	ng/ml	ng/ml
t21	23	240	280	2337
t21	23	220	257	2142
t21	23	216	252	2103
t21	23	222	259	2161
t22	26	242	283	2356
t22	26	252	294	2454
t22	26	248	290	2415
t22	26	239	279	2327
t25	30.5	260	304	2531
t25	30.5	310	362	3018
t25	30.5	311	363	3028
t25	30.5	257	300	2502
t26	43	299	349	2911
t26	43	299	349	2911
t26	43	320	374	3116
t26	43	301	352	2931
t27	50.5	277	324	2697
t27	50.5	322	376	3135
t27	50.5	289	338	2814
t27	50.5	269	314	2619
t28	69.5	313	366	3047
t28	69.5	280	327	2726
t28	69.5	313	366	3047
t28	69.5	299	349	2911

Tableau A3.2-2 Mesures de la DCO totale

	Temps	Blanc	F.A.S.	DCOtotale	
		Vol.		Vol.	DCO
	heure	ml	molarité	ml	mg/L
t-1	-1	26.5	0.019	14.45	926
t-1	-1	26.55	0.019	14.5	922
t-1	-1	26.35	0.019	14.65	
t-1	-1	*26.467*	*0.019*		
t0	0	26.5	0.019	5.7	
t0	0	26.55	0.019	6.1	1570
t0	0	26.35	0.019	6.2	1562
t0	0	*26.467*	*0.019*		
t1	0.5	26.5	0.019	6.5	1539
t1	0.5	26.55	0.019	6.6	1531
t1	0.5	26.35	0.019	6.5	1539
t1	0.5	*26.467*	*0.019*		
t2	1	26.5	0.019	6.8	1516
t2	1	26.55	0.019	6.5	
t2	1	26.35	0.019	6.7	1524
t2	1	*26.467*	*0.019*		
t3	1.5	26.5	0.019	6.4	
t3	1.5	26.55	0.019	6.8	1516
t3	1.5	26.35	0.019	6.75	1520
t3	1.5	*26.467*	*0.019*		
t4	2	26.5	0.019	6.65	1527
t4	2	26.55	0.019	6.5	
t4	2	26.35	0.019	6.65	1527
t4	2	*26.467*	*0.019*		
t5	3	26.5	0.019	6.75	1520
t5	3	26.55	0.019	6.75	1520
t5	3	26.35	0.019	6.85	1512
t5	3	*26.467*	*0.019*		
t6	4	26.5	0.019	6.9	1508
t6	4	26.55	0.019	6.7	1524
t6	4	26.35	0.019	7.1	1493
t6	4	*26.467*	*0.019*		
t7	5	26.5	0.019	6.95	1504
t7	5	26.55	0.019	6.9	1508
t7	5	26.35	0.019	7.05	1497
t7	5	*26.467*	*0.019*		
t8	6	26.5	0.019	6.7	
t8	6	26.55	0.019	7	1500
t8	6	26.35	0.019	6.9	1508
t8	6	*26.467*	*0.019*		
t9	7	26.5	0.019	6.9	1508
t9	7	26.55	0.019	7	1500
t9	7	26.35	0.019	6.9	1508
t9	7	*26.467*	*0.019*		

Tableau A3.2-2 Mesures de la DCO totale

	Temps	Blanc	F.A.S.	DCOtotale	
		Vol.		Vol.	DCO
	heure	ml	molarité	ml	mg/L
t10	8	26.5	0.019	7.25	1481
t10	8	26.55	0.019	7.15	1489
t10	8	26.35	0.019	7.1	1493
t10	8	*26.467*	*0.019*		
t11	9	26.5	0.019	7	1500
t11	9	26.55	0.019	7.15	1489
t11	9	26.35	0.019	7.15	1489
t11	9	*26.467*	*0.019*		
t12	10	26.5	0.019	7.4	1470
t12	10	26.55	0.019	7.3	1477
t12	10	26.35	0.019	7.1	1493
t12	10	*26.467*	*0.019*		
t13	11	26.5	0.019	7.3	1477
t13	11	26.55	0.019	7.4	1470
t13	11	26.35	0.019	7.4	1470
t13	11	*26.467*	*0.019*		
t14	12	26.5	0.019	7.65	1450
t14	12	26.55	0.019	7.8	1439
t14	12	26.35	0.019	6.85	1512
t14	12	*26.467*	*0.019*		
t15	13	26.5	0.019	8.05	1420
t15	13	26.55	0.019	7.65	1450
t15	13	26.35	0.019	7.85	1435
t15	13	*26.467*	*0.019*		
t16	14	26.5	0.020	9.2	1381
t16	14	26.55	0.020	8.45	1441
t16	14	26.35	0.020	8.25	1457
t16	14	*26.467*	*0.020*		
t17	15	26.5	0.020	8.65	1425
t17	15	26.55	0.020	9	1397
t17	15	26.35	0.020	8.9	1405
t17	15	*26.467*	*0.020*		
t18	16	26.5	0.020	9.4	1365
t18	16	26.55	0.020	9.3	1373
t18	16	26.35	0.020	9.05	1393
t18	16	*26.467*	*0.020*		
t19	17	26.5	0.020	9.45	1361
t19	17	26.55	0.020	9.2	1381
t19	17	26.35	0.020	9	1397
t19	17	*26.467*	*0.020*		

Tableau A3.2-2 Mesures de la DCO totale

	Temps	Blanc	F.A.S.	DCOtotale	
		Vol.		Vol.	DCO
	heure	ml	molarité	ml	mg/L
t20	18	26.5	0.020	9.5	1357
t20	18	26.55	0.020	9.5	1357
t20	18	26.35	0.020	9.1	1389
t20	18	*26.467*	*0.020*		
t21	23	26.5	0.020	9.5	1357
t21	23	26.55	0.020	9.3	1373
t21	23	26.35	0.020	9.5	1357
t21	23	*26.467*	*0.020*		
t22	26	26.5	0.020	9.75	1337
t22	26	26.55	0.020	9.65	1345
t22	26	26.35	0.020	9.8	1333
t22	26	*26.467*	*0.020*		
t25	30.5	26.1	0.020	11.5	1139
t25	30.5	25.95	0.020	10.65	1205
t25	30.5	26.05	0.020	10.65	1205
t25	30.5	*26.033*	*0.020*		
t26	43	26.1	0.020	9.1	1327
t26	43	25.95	0.020	9.25	1315
t26	43	26.05	0.020	8.75	1354
t26	43	*26.033*	*0.020*		
t27	50.5	26.1	0.020	9.3	1311
t27	50.5	25.95	0.020	9.65	1284
t27	50.5	26.05	0.020	9.55	1292
t27	50.5	*26.033*	*0.020*		
t28	69.5	26.1	0.020	10	1256
t28	69.5	25.95	0.020	9.7	1280
t28	69.5	26.05	0.020	10	1256
t28	69.5	*26.033*	*0.020*		

Tableau A3.2-3 Mesures de la DCO soluble

	Temps	Blanc	F.A.S.	DCOsoluble	
		Vol.		Vol.	DCO
	heure	ml	molarité	ml	mg/L
t-1	-1	26.5	0.020	16.1	829
t-1	-1	26.55	0.020	16.1	829
t-1	-1	26.35	0.020	16.3	813
t-1	-1	*26.467*	*0.020*		
t0	0	26.5	0.020	8	1477
t0	0	26.55	0.020	7.95	1481
t0	0	26.35	0.020	8	1477
t0	0	*26.467*	*0.020*		
t1	0.5	26.5	0.020	9.2	1381
t1	0.5	26.55	0.020	9.15	1385
t1	0.5	26.35	0.020	9	1397
t1	0.5	*26.467*	*0.020*		
t2	1	26.5	0.020	9.4	1365
t2	1	26.55	0.020	9.05	1393
t2	1	26.35	0.020	9.2	1381
t2	1	*26.467*	*0.020*		
t3	1.5	26.5	0.020	9.7	1341
t3	1.5	26.55	0.020	9.5	1357
t3	1.5	26.35	0.020	9.8	1333
t3	1.5	*26.467*	*0.020*		
t4	2	26.5	0.020	9.45	1361
t4	2	26.55	0.020	9.5	1357
t4	2	26.35	0.020	9.45	1361
t4	2	*26.467*	*0.020*		
t5	3	26.5	0.020	9.85	1329
t5	3	26.55	0.020	9.8	1333
t5	3	26.35	0.020	9.9	1325
t5	3	*26.467*	*0.020*		
t6	4	26.5	0.020	10.1	1309
t6	4	26.55	0.020	10.3	1293
t6	4	26.35	0.020	10.15	1305
t6	4	*26.467*	*0.020*		
t7	5	26.5	0.020	10.5	1277
t7	5	26.55	0.020	10.35	1289
t7	5	26.35	0.020	10.35	1289
t7	5	*26.467*	*0.020*		
t8	6	26.5	0.020	10.8	1253
t8	6	26.55	0.020	11	1237
t8	6	26.35	0.020	10.8	1253
t8	6	*26.467*	*0.020*		
t9	7	26.5	0.020	11.15	1225
t9	7	26.55	0.020	11.2	1221
t9	7	26.35	0.020	11.25	1217
t9	7	*26.467*	*0.020*		

Tableau A3.2-3 Mesures de la DCO soluble

	Temps	Blanc	F.A.S.	DCOsoluble	
		Vol.		Vol.	DCO
	heure	ml	molarité	ml	mg/L
t10	8	26.5	0.020	11.65	1185
t10	8	26.55	0.020	11.7	1181
t10	8	26.35	0.020	11.6	1189
t10	8	*26.467*	*0.020*		
t11	9	26.5	0.020	12.3	1133
t11	9	26.55	0.020	12.15	1145
t11	9	26.35	0.020	11.85	1169
t11	9	*26.467*	*0.020*		
t12	10	26.5	0.020	12.35	1129
t12	10	26.55	0.020	12.35	1129
t12	10	26.35	0.020	12.45	1121
t12	10	*26.467*	*0.020*		
t13	11	26.5	0.020	12.65	1105
t13	11	26.55	0.020	12.7	1101
t13	11	26.35	0.020	12.95	1081
t13	11	*26.467*	*0.020*		
t14	12	26.5	0.020	13.2	1061
t14	12	26.55	0.020	13.5	1037
t14	12	26.35	0.020	13.55	1033
t14	12	*26.467*	*0.020*		
t15	13	26.5	0.020	13.9	1005
t15	13	26.55	0.020	13.8	1013
t15	13	26.35	0.020	13.9	1005
t15	13	*26.467*	*0.020*		
t16	14	26.5	0.020	14.5	957
t16	14	26.55	0.020	14.5	957
t16	14	26.35	0.020	14.6	949
t16	14	*26.467*	*0.020*		
t17	15	26.5	0.020	15.05	913
t17	15	26.55	0.020	14.95	921
t17	15	26.35	0.020	15.25	897
t17	15	*26.467*	*0.020*		
t18	16	26.5	0.020	15.35	889
t18	16	26.55	0.020	15.6	869
t18	16	26.35	0.020	15.4	885
t18	16	*26.467*	*0.020*		
t19	17	26.5	0.020	15.95	841
t19	17	26.55	0.020	15.85	849
t19	17	26.35	0.020	16.1	829
t19	17	*26.467*	*0.020*		
t20	18	26.5	0.020	15.9	845
t20	18	26.55	0.020	15.8	853
t20	18	26.35	0.020	15.8	853
t20	18	*26.467*	*0.020*		

Tableau A3.2-3 Mesures de la DCO soluble

	Temps	Blanc	F.A.S.	DCOsoluble	
		Vol.		Vol.	DCO
	heure	ml	molarité	ml	mg/L
t21	23	26.5	0.020	15.85	849
t21	23	26.55	0.020	15.45	881
t21	23	26.35	0.020	15.8	853
t21	23	*26.467*	*0.020*		
t22	26	26.5	0.020	15.6	869
t22	26	26.55	0.020	15.7	861
t22	26	26.35	0.020	15.75	857
t22	26	*26.467*	*0.020*		
t25	30.5	26.1	0.020	15.9	794
t25	30.5	25.95	0.020	15.8	802
t25	30.5	26.05	0.020	15.8	802
t25	30.5	*26.033*	*0.020*		
t26	43	26.1	0.020	16.1	778
t26	43	25.95	0.020	15.8	802
t26	43	26.05	0.020	16.05	782
t26	43	*26.033*	*0.020*		
t27	50.5	26.1	0.020	15.5	825
t27	50.5	25.95	0.020	15.65	814
t27	50.5	26.05	0.020	15.6	818
t27	50.5	*26.033*	*0.020*		
t28	69.5	26.1	0.020	15.7	810
t28	69.5	25.95	0.020	15.6	818
t28	69.5	26.05	0.020	15.9	794
t28	69.5	*26.033*	*0.020*		

Tableau A3.2-4 Mesures du glucose

	Temps	Blanc	Glucose	
	heure	Abs.	Abs.	mg/L
t-1	-1	0	0.025	9
t-1	-1	0.002	0.016	6
t-1	-1		0.012	4
t-1	-1	*0.001*	*0.018*	
t0	0	0	1.76	668
t0	0	0.002	1.75	664
t0	0		1.759	668
t0	0	*0.001*	*1.756*	
t1	0.5	0	1.543	586
t1	0.5	0.002	1.554	590
t1	0.5		1.558	591
t1	0.5	*0.001*	*1.552*	
t2	1	0	1.482	562
t2	1	0.002	1.473	559
t2	1		1.491	566
t2	1	*0.001*	*1.482*	
t3	1.5	0	1.448	549
t3	1.5	0.002	1.454	552
t3	1.5		1.444	548
t3	1.5	*0.001*	*1.449*	
t4	2	0	1.444	548
t4	2	0.002	1.434	544
t4	2		1.443	548
t4	2	*0.001*	*1.440*	
t5	3	0	1.328	504
t5	3	0.002	1.351	513
t5	3		1.341	509
t5	3	*0.001*	*1.340*	
t6	4	0	1.287	488
t6	4	0.002	1.287	488
t6	4		1.278	485
t6	4	*0.001*	*1.284*	
t7	5	0	1.224	464
t7	5	0.002	1.235	469
t7	5		1.222	464
t7	5	*0.001*	*1.227*	
t8	6	0	1.149	436
t8	6	0.002	1.178	447
t8	6		1.168	443
t8	6	*0.001*	*1.165*	
t9	7	0	1.06	402
t9	7	0.002	1.067	405
t9	7		1.065	404
t9	7	*0.001*	*1.064*	

Tableau A3.2-4 Mesures du glucose

	Temps heure	Blanc Abs.	Glucose Abs.	mg/L
t10	8	0	0.99	376
t10	8	0.002	0.987	374
t10	8		0.996	378
t10	8	*0.001*	*0.991*	
t11	9	0	0.905	343
t11	9	0.002	0.904	343
t11	9		0.902	342
t11	9	*0.001*	*0.904*	
t12	10	0	0.772	293
t12	10	0.002	0.78	296
t12	10		0.77	292
t12	10	*0.001*	*0.774*	
t13	11	0	0.682	259
t13	11	0.002	0.694	263
t13	11		0.688	261
t13	11	*0.001*	*0.688*	
t14	12	0	0.571	216
t14	12	0.002	0.58	220
t14	12		0.577	219
t14	12	*0.001*	*0.576*	
t15	13	0	0.46	174
t15	13	0.002	0.47	178
t15	13		0.468	177
t15	13	*0.001*	*0.466*	
t16	14	0	0.335	127
t16	14	0.002	0.334	126
t16	14		0.337	128
t16	14	*0.001*	*0.335*	
t17	15	0	0.204	77
t17	15	0.002	0.206	78
t17	15		0.204	77
t17	15	*0.001*	*0.205*	
t18	16	0	0.065	24
t18	16	0.002	0.064	24
t18	16		0.065	24
t18	16	*0.001*	*0.065*	
t19	17	0	0.025	9
t19	17	0.002	0.021	8
t19	17		0.026	9
t19	17	*0.001*	*0.024*	
t20	18	0	0.028	10
t20	18	0.002	0.019	7
t20	18		0.018	6
t20	18	*0.001*	*0.022*	

Tableau A3.2-4 Mesures du glucose

	Temps heure	Blanc Abs.	Glucose Abs.	mg/L
t21	23	0	0.015	5
t21	23	0.002	0.021	8
t21	23		0.021	8
t21	23	*0.001*	*0.019*	
t22	26	0	0.018	6
t22	26	0.002	0.012	4
t22	26		0.015	5
t22	26	*0.001*	*0.015*	
t25	30.5	0	0.03	11
t25	30.5	0.002	0.026	9
t25	30.5		0.011	4
t25	30.5	*0.001*	*0.022*	
t26	43	0	0.029	11
t26	43	0.002	0.045	17
t26	43		0.02	7
t26	43	*0.001*	*0.031*	
t27	50.5	0	0.016	6
t27	50.5	0.002	0.03	11
t27	50.5		0.035	13
t27	50.5	*0.001*	*0.027*	
t28	69.5	0	0.057	21
t28	69.5	0.002	0.057	21
t28	69.5		0.037	14
t28	69.5	*0.001*	*0.050*	

Tableau A3.2-5 Mesures du glycogène

	Temps	Blanc	Glycogènes	
	heure	Abs.	Abs.	mg/L
t-1	-1	0	0.024	3.2
t-1	-1	-0.001	0.026	3.4
t-1	-1	-0.002	0.047	6.1
t-1	-1	*-0.001*		
t0	0	0	0.049	6.3
t0	0	-0.001	0.042	5.4
t0	0	-0.002	0.035	4.6
t0	0	*-0.001*	0.045	5.8
ta	0.25	0	0.171	21.8
ta	0.25	-0.001	0.172	21.9
ta	0.25	-0.002	0.179	22.8
ta	0.25	*-0.001*	0.182	23.2
t1	0.5	0	0.301	38.2
t1	0.5	-0.001	0.282	35.8
t1	0.5	-0.002	0.267	33.9
t1	0.5	*-0.001*	0.267	33.9
t2	1	0	0.316	40.1
t2	1	-0.001	0.335	42.5
t2	1	-0.002	0.326	41.4
t2	1	*-0.001*	0.322	40.9
t3	1.5	0	0.348	44.2
t3	1.5	-0.001	0.361	45.8
t3	1.5	-0.002	0.346	43.9
t3	1.5	*-0.001*	0.351	44.6
t4	2	0	0.376	47.7
t4	2	-0.001	0.376	47.7
t4	2	-0.002	0.376	47.7
t4	2	*-0.001*	0.371	47.1
t5	3	0	0.454	57.6
t5	3	-0.001	0.401	50.9
t5	3	-0.002	0.401	50.9
t5	3	*-0.001*	0.398	50.5
t6	4	0	0.437	55.4
t6	4	-0.001	0.447	56.7
t6	4	-0.002	0.446	56.6
t6	4	*-0.001*	0.436	55.3
t7	5	0	0.48	60.9
t7	5	-0.001	0.489	62.0
t7	5	-0.002	0.484	61.4
t7	5	*-0.001*	0.571	72.4
t8	6	0	0.513	65.1
t8	6	-0.001	0.529	67.1
t8	6	-0.002	0.646	81.9
t8	6	*-0.001*	0.525	66.6

Tableau A3.2-5 Mesures du glycogène

	Temps	Blanc	Glycogènes	
	heure	Abs.	Abs.	mg/L
t9	7	0	0.56	71.0
t9	7	-0.001	0.667	84.6
t9	7	-0.002	0.57	72.3
t9	7	*-0.001*	0.553	70.1
t10	8	0	0.735	93.2
t10	8	-0.001	0.738	93.5
t10	8	-0.002	0.581	73.7
t10	8	*-0.001*	0.589	74.7
t11	9	0	0.65	82.4
t11	9	-0.001	0.654	82.9
t11	9	-0.002	0.639	81.0
t11	9	*-0.001*	0.65	82.4
t12	10	0	0.712	90.3
t12	10	-0.001	0.702	89.0
t12	10	-0.002	0.704	89.2
t12	10	*-0.001*	0.712	90.3
t13	11	0	0.708	89.7
t13	11	-0.001	0.706	89.5
t13	11	-0.002	0.713	90.4
t13	11	*-0.001*	0.954	120.9
t14	12	0	0.757	95.9
t14	12	-0.001	0.77	97.6
t14	12	-0.002	0.758	96.1
t14	12	*-0.001*	0.758	96.1
t15	13	0	0.775	98.2
t15	13	-0.001	0.789	100.0
t15	13	-0.002	0.772	97.8
t15	13	*-0.001*	0.778	98.6
t16	14	0	0.787	99.7
t16	14	-0.001	0.813	103.0
t16	14	-0.002	0.782	99.1
t16	14	*-0.001*	0.804	101.9
t17	15	0	0.81	102.7
t17	15	-0.001	0.818	103.7
t17	15	-0.002	0.815	103.3
t17	15	*-0.001*	0.812	102.9
t18	16	0	0.829	105.1
t18	16	-0.001	0.844	107.0
t18	16	-0.002	0.835	105.8
t18	16	*-0.001*	0.83	105.2
t19	17	0	0.827	104.8
t19	17	-0.001	0.823	104.3
t19	17	-0.002	0.825	104.6
t19	17	*-0.001*	1.227	155.4

Tableau A3.2-5 Mesures du glycogène

	Temps	Blanc	Glycogènes	
	heure	Abs.	Abs.	mg/L
t20	18	0	1.176	149.0
t20	18	-0.001	0.733	92.9
t20	18	-0.002	1.186	150.3
t20	18	*-0.001*	0.764	96.8
t21	23	0	0.503	63.8
t21	23	-0.001	0.514	65.2
t21	23	-0.002	0.504	63.9
t21	23	*-0.001*	0.507	64.3
t22	26	0	0.435	55.2
t22	26	-0.001	0.453	57.5
t22	26	-0.002	0.449	57.0
t22	26	*-0.001*	0.453	57.5
t25	30.5	0	0.334	42.4
t25	30.5	-0.001	0.347	44.1
t25	30.5	-0.002	0.334	42.4
t25	30.5	*-0.001*	0.34	43.2
t26	43	0	0.231	29.4
t26	43	-0.001	0.251	31.9
t26	43	-0.002	0.24	30.5
t26	43	*-0.001*	0.222	28.2
t27	50.5	0	0.174	22.2
t27	50.5	-0.001	0.179	22.8
t27	50.5	-0.002	0.17	21.6
t27	50.5	*-0.001*	0.181	23.0
t28	69.5	0	0.121	15.4
t28	69.5	-0.001	0.161	20.5
t28	69.5	-0.002	0.133	17.0
t28	69.5	*-0.001*	0.131	16.7

Tableau A3.2-6 Mesures du NH_4^+

	Temps	Blanc	NH_4^+	
	heure	abs	abs	mg N/L
t-1	-1	0.000	0.782	57.0
t-1	-1		0.785	57.2
t-1	-1		0.783	57.0
t-1	-1			
t0	0	0.000	0.799	58.2
t0	0		0.801	58.3
t0	0		0.801	58.3
t0	0			
t1	0.5	0.000	0.737	53.7
t1	0.5		0.74	53.9
t1	0.5		0.737	53.7
t1	0.5			
t2	1	0.000	0.759	55.3
t2	1		0.766	55.8
t2	1		0.76	55.4
t2	1			
t3	1.5	0.000	0.736	53.6
t3	1.5		0.733	53.4
t3	1.5		0.746	54.3
t3	1.5			
t4	2	0.000	0.846	
t4	2		0.862	
t4	2		0.849	
t4	2			
t5	3	0.000	0.762	55.5
t5	3		0.766	55.8
t5	3		0.768	55.9
t5	3			
t6	4	0.000	0.736	53.6
t6	4		0.736	53.6
t6	4		0.735	53.5
t6	4			
t7	5	0.000	0.741	54.0
t7	5		0.746	54.3
t7	5		0.738	53.8
t7	5			
t8	6	0.000	0.767	55.9
t8	6		0.761	55.4
t8	6		0.768	55.9
t8	6			
t9	7	0.000	0.774	56.4
t9	7		0.779	56.7
t9	7		0.77	56.1
t9	7			

Tableau A3.2-6 Mesures du NH_4^+

	Temps	Blanc	NH_4^+	
	heure	abs	abs	mg N/L
t10	8	0.000	0.698	50.8
t10	8		0.691	50.3
t10	8		0.692	50.4
t10	8			
t11	9	0.000	0.733	53.4
t11	9		0.725	52.8
t11	9		0.736	53.6
t11	9			
t12	10	0.000	0.67	48.8
t12	10		0.665	48.4
t12	10		0.668	48.7
t12	10			
t13	11	0.000	0.69	50.3
t13	11		0.694	50.6
t13	11		0.683	49.8
t13	11			
t14	12	0.000	0.66	48.1
t14	12		0.657	47.9
t14	12		0.654	47.6
t14	12			
t15	13	0.000	0.636	46.3
t15	13		0.636	46.3
t15	13		0.628	45.7
t15	13			
t16	14	0.000	0.6	43.7
t16	14		0.585	42.6
t16	14		0.593	43.2
t16	14			
t17	15	0.000	0.577	42.0
t17	15		0.576	42.0
t17	15		0.58	42.2
t17	15			
t18	16	0.000	0.546	39.8
t18	16		0.533	38.8
t18	16		0.541	39.4
t18	16			
t19	17	0.000	0.515	37.5
t19	17		0.512	37.3
t19	17		0.521	38.0
t19	17			
t20	18	0.000	0.502	36.6
t20	18		0.509	37.1
t20	18		0.505	36.8
t20	18			

Tableau A3.2-6 Mesures du NH_4^+

	Temps heure	Blanc abs	NH_4^+ abs	NH_4^+ mg N/L
t21	23	0.000	0.458	33.4
t21	23		0.465	33.9
t21	23		0.466	33.9
t21	23			
t22	26	0.000	0.44	32.1
t22	26		0.44	32.1
t22	26		0.443	32.3
t22	26			
t25	30.5	0.000	0.45	32.8
t25	30.5		0.452	32.9
t25	30.5		0.449	32.7
t25	30.5			
t26	43	0.000	0.382	27.8
t26	43		0.388	28.3
t26	43		0.389	28.3
t26	43			
t27	50.5	0.000	0.392	28.6
t27	50.5		0.396	28.8
t27	50.5		0.399	29.1
t27	50.5			
t28	69.5	0.000	0.359	26.2
t28	69.5		0.359	26.2
t28	69.5		0.359	26.2
t28	69.5			

Tableau A3.2-6 Mesures de la concentration d'acétate

	Temps	Acétate	
	heure	mg/L	mg/L
t1	0.5	0.087	1.450
t2	1	0.178	2.967
t3	1.5	0.012	0.200
t4	2	0.024	0.400
t5	3	0.055	0.917
t6	4	0.045	0.750
t7	5	0.060	1.000
t8	6	0.192	3.200
t9	7	0.143	2.383
t10	8	0.201	3.350
t11	9	0.260	4.333
t12	10	0.135	2.250
t13	11	0.221	3.683
t14	12	0.312	5.200
t15	13	0.076	1.267
t16	14	0.298	4.967
t17	15	0.301	5.017
t18	16	0.207	3.450
t19	17	0.309	5.150
t20	18	0.240	4.000
t21	23	0.188	3.133
t22	26	0.231	3.850
t25	30.5	0.365	6.083
t26	43	0.258	4.300
t27	50.5	0.409	6.817
t28	69.5	0.359	5.983

Tableau A3.2-7 Compte de la micro-faune

	Temps heure	Flagellé	Cilié libre	Cilié fixe	Rotifer	Sarcodine	total	Micro faune org./L
t-1	-1		1	5		21	27	9.0.E+05
t25	30.5			9		6	15	5.0.E+05
t27	50.5		1	5		27	33	1.1.E+06

Tableau A3.2-8 Données de respirométrie

DASYLab - V 5.50.00
WORKSHEET : Respiro
Recording Date : 05-02-13, 14:12:17
Block Length : 1
Delta : 2 sec.
Number of Channels : 1
Elapsed Time[hh:mm:ss]

Temps	Oxygène dissous	rO2
hh :mm :ss	mg/L	mg/L/h
00:05:00	9.17	0.000
00:08:30	9.17	0.027
00:12:00	9.2	0.130
00:15:30	9.23	0.000
00:19:00	9.26	0.392
00:22:30	9.26	0.709
00:26:00	9.23	1.092
00:29:30	9.19	0.913
00:33:00	9.17	0.049
00:36:30	9.19	0.607
00:40:00	9.2	0.017
00:43:30	8.51	13.687
00:47:00	8	12.648
00:50:30	7.71	12.297
00:54:00	7.52	11.330
00:57:30	7.44	10.331
01:01:00	7.44	9.102
01:04:30	7.5	7.984
01:08:00	7.64	7.053
01:11:30	7.75	6.281
01:15:00	7.88	6.144
01:18:30	7.94	6.415
01:22:00	7.97	6.178
01:25:30	7.99	5.888
01:29:00	8.01	5.634
01:32:30	8.07	5.201
01:36:00	8.13	5.064
01:39:30	8.19	4.941
01:43:00	8.24	5.021
01:46:30	8.25	5.346
01:50:00	8.23	5.434
01:53:30	8.23	5.064
01:57:00	8.24	4.913
02:00:30	8.26	4.579
02:04:00	8.31	4.501

Tableau A3.2-8 Données de respirométrie

Temps	Oxygène dissous	rO2
hh :mm :ss	mg/L	mg/L/h
02:07:30	8.37	4.565
02:11:00	8.39	4.880
02:14:30	8.36	5.356
02:18:00	8.31	5.249
02:21:30	8.29	4.900
02:25:00	8.3	4.721
02:28:30	8.32	4.701
02:32:00	8.36	4.484
02:35:30	8.42	4.631
02:39:00	8.45	5.023
02:42:30	8.41	5.373
02:46:00	8.38	5.301
02:49:30	8.35	5.016
02:53:00	8.35	4.921
02:56:30	8.36	4.734
03:00:00	8.39	4.414
03:03:30	8.45	4.689
03:07:00	8.45	5.164
03:10:30	8.4	5.330
03:14:00	8.35	5.307
03:17:30	8.32	5.102
03:21:00	8.32	4.811
03:24:30	8.33	4.684
03:28:00	8.37	4.456
03:31:30	8.44	4.692
03:35:00	8.45	5.073
03:38:30	8.41	5.428
03:42:00	8.35	5.285
03:45:30	8.32	5.054
03:49:00	8.32	4.745
03:52:30	8.35	4.733
03:56:00	8.39	4.580
03:59:30	8.42	4.973
04:03:00	8.41	5.332
04:06:30	8.37	5.386
04:10:00	8.33	5.308
04:13:30	8.32	4.928
04:17:00	8.32	4.843
04:20:30	8.35	4.757
04:24:00	8.41	4.775
04:27:30	8.42	5.084
04:31:00	8.39	5.462
04:34:30	8.35	5.422
04:38:00	8.32	5.111
04:41:30	8.3	4.903

Tableau A3.2-8 Données de respirométrie

Temps	Oxygène dissous	rO2
hh :mm :ss	mg/L	mg/L/h
04:45:00	8.32	4.845
04:48:30	8.35	4.682
04:52:00	8.41	4.664
04:55:30	8.42	5.214
04:59:00	8.39	5.502
05:02:30	8.33	5.208
05:06:00	8.3	5.089
05:09:30	8.29	4.830
05:13:00	8.31	4.617
05:16:30	8.35	4.711
05:20:00	8.38	4.778
05:23:30	8.37	5.261
05:27:00	7.52	5.261
05:30:30	8.24	5.608
05:34:00	8.22	5.464
05:37:30	8.23	5.233
05:41:00	8.24	5.042
05:44:30	8.29	4.989
05:48:00	8.32	5.048
05:51:30	8.32	5.560
05:55:00	8.29	5.846
05:58:30	8.24	5.606
06:02:00	8.23	5.361
06:05:30	8.24	4.958
06:09:00	8.29	4.921
06:12:30	8.35	5.178
06:16:00	8.37	5.552
06:19:30	8.35	5.921
06:23:00	8.32	5.987
06:26:30	8.29	5.601
06:30:00	8.27	5.396
06:33:30	8.29	5.162
06:37:00	8.3	5.004
06:40:30	8.33	5.253
06:44:00	8.32	5.684
06:47:30	8.29	5.932
06:51:00	8.24	5.890
06:54:30	8.21	5.790
06:58:00	8.21	5.520
07:01:30	8.22	5.280
07:05:00	8.26	5.080
07:08:30	8.29	5.428
07:12:00	8.29	5.782
07:15:30	8.24	6.037
07:19:00	8.2	5.968

Tableau A3.2-8 Données de respirométrie

Temps	Oxygène dissous	rO2
hh :mm :ss	mg/L	mg/L/h
07:22:30	8.19	5.953
07:26:00	8.2	5.602
07:29:30	8.24	5.242
07:33:00	8.27	5.205
07:36:30	8.27	5.489
07:40:00	8.27	6.145
07:43:30	8.21	6.248
07:47:00	8.16	6.212
07:50:30	8.16	6.039
07:54:00	8.16	5.645
07:57:30	8.19	5.590
08:01:00	8.23	5.627
08:04:30	8.23	5.907
08:08:00	8.19	6.413
08:11:30	8.13	6.384
08:15:00	8.1	5.939
08:18:30	8.1	5.457
08:22:00	8.12	5.540
08:25:30	8.13	5.540
08:29:00	7.98	5.916
08:32:30	7.91	6.439
08:36:00	7.05	6.439
08:39:30	7.55	6.613
08:43:00	7.44	6.613
08:46:30	7.31	6.613
08:50:00	6.38	5.603
08:53:30	7.4	5.603
08:57:00	7.38	5.916
09:00:30	6.43	5.916
09:04:00	7.14	7.191
09:07:30	6.91	6.998
09:11:00	6.75	6.808
09:14:30	6.62	6.546
09:18:00	6.49	6.474
09:21:30	6.41	6.284
09:25:00	6.34	6.562
09:28:30	6.26	6.965
09:32:00	6.13	7.138
09:35:30	6.01	7.063
09:39:00	5.91	6.823
09:42:30	5.83	6.737
09:46:00	5.78	6.693
09:49:30	5.75	6.701
09:53:00	5.72	6.850
09:56:30	5.67	7.159

Tableau A3.2-8 Données de respirométrie

Temps	Oxygène dissous	rO2
hh :mm :ss	mg/L	mg/L/h
10:00:00	5.6	7.266
10:03:30	5.54	7.050
10:07:00	5.52	6.932
10:10:30	5.6	6.733
10:14:00	5.96	6.688
10:17:30	6.23	6.699
10:21:00	6.42	7.036
10:24:30	6.52	7.223
10:28:00	6.59	7.158
10:31:30	6.65	7.247
10:35:00	6.7	7.180
10:38:30	6.77	6.945
10:42:00	6.85	6.896
10:45:30	6.89	7.084
10:49:00	6.92	7.415
10:52:30	6.88	7.658
10:56:00	6.86	7.639
10:59:30	6.83	7.541
11:03:00	6.82	7.358
11:06:30	6.73	7.171
11:10:00	6.52	7.177
11:13:30	6.33	7.205
11:17:00	6.15	7.737
11:20:30	5.96	7.909
11:24:00	5.77	7.926
11:27:30	5.6	7.764
11:31:00	5.41	7.678
11:34:30	5.28	7.498
11:38:00	5.16	7.258
11:41:30	5.07	7.380
11:45:00	4.98	7.728
11:48:30	4.87	7.929
11:52:00	4.78	7.869
11:55:30	4.88	7.800
11:59:00	5.19	7.662
12:02:30	5.57	7.736
12:06:00	5.87	7.555
12:09:30	6.12	7.957
12:13:00	6.29	8.198
12:16:30	6.42	8.302
12:20:00	6.52	8.278
12:23:30	6.62	8.065
12:27:00	6.7	8.115
12:30:30	6.8	7.935
12:34:00	6.88	7.772

Tableau A3.2-8 Données de respirométrie

Temps	Oxygène dissous	rO2
hh :mm :ss	mg/L	mg/L/h
12:37:30	6.93	8.113
12:41:00	6.93	8.593
12:44:30	6.88	8.698
12:48:00	6.85	8.600
12:51:30	6.84	8.437
12:55:00	6.86	8.302
12:58:30	6.89	8.202
13:02:00	6.9	8.232
13:05:30	6.89	8.507
13:09:00	6.85	8.883
13:12:30	6.81	8.971
13:16:00	6.77	8.772
13:19:30	6.74	8.759
13:23:00	6.73	8.440
13:26:30	6.76	8.409
13:30:00	6.78	8.411
13:33:30	6.78	8.774
13:37:00	6.74	9.256
13:40:30	6.7	9.264
13:44:00	6.66	9.116
13:47:30	6.67	8.883
13:51:00	6.7	8.625
13:54:30	6.72	8.714
13:58:00	6.72	8.836
14:01:30	6.68	9.249
14:05:00	6.62	9.465
14:08:30	6.56	9.497
14:12:00	6.54	9.502
14:15:30	6.52	9.441
14:19:00	6.52	9.150
14:22:30	6.52	9.012
14:26:00	6.53	9.070
14:29:30	6.52	9.501
14:33:00	6.46	9.838
14:36:30	6.42	9.891
14:40:00	6.36	9.886
14:43:30	6.33	9.604
14:47:00	6.33	9.442
14:50:30	6.36	9.329
14:54:00	6.39	9.631
14:57:30	6.39	10.080
15:01:00	6.36	10.213
15:04:30	6.32	10.318
15:08:00	6.29	10.289
15:11:30	6.26	10.096

Tableau A3.2-8 Données de respirométrie

Temps	Oxygène dissous	rO2
hh :mm :ss	mg/L	mg/L/h
15:15:00	6.26	9.918
15:18:30	6.27	9.918
15:22:00	6.3	10.091
15:25:30	6.27	10.470
15:29:00	6.2	10.818
15:32:30	6.15	10.983
15:36:00	6.1	10.608
15:39:30	6.09	10.639
15:43:00	6.06	10.436
15:46:30	6.04	10.523
15:50:00	6.03	10.511
15:53:30	5.99	11.037
15:57:00	5.93	11.198
16:00:30	5.89	11.092
16:04:00	5.88	11.035
16:07:30	5.89	10.991
16:11:00	5.92	10.657
16:14:30	5.94	10.530
16:18:00	5.95	10.940
16:21:30	5.91	11.436
16:25:00	5.88	11.552
16:28:30	5.84	11.542
16:32:00	5.82	11.468
16:35:30	5.83	11.204
16:39:00	5.85	11.080
16:42:30	5.87	11.034
16:46:00	5.92	11.056
16:49:30	5.92	11.488
16:53:00	5.86	11.474
16:56:30	5.84	11.412
17:00:00	5.84	10.890
17:03:30	5.93	9.806
17:07:00	6.09	8.033
17:10:30	6.31	5.981
17:14:00	6.55	5.753
17:17:30	6.73	6.055
17:21:00	6.87	5.982
17:24:30	7	5.476
17:28:00	7.14	5.110
17:31:30	7.27	4.852
17:35:00	7.4	4.436
17:38:30	7.52	4.396
17:42:00	7.62	4.641
17:45:30	7.64	4.678
17:49:00	7.67	4.664

Tableau A3.2-8 Données de respirométrie

Temps	Oxygène dissous	rO2
hh :mm :ss	mg/L	mg/L/h
17:52:30	7.68	4.362
17:56:00	7.72	4.144
17:59:30	7.77	3.734
18:03:00	7.84	3.610
18:06:30	7.91	3.598
18:10:00	7.94	3.959
18:13:30	7.96	4.119
18:17:00	7.93	4.052
18:20:30	7.93	3.968
18:24:00	7.94	3.737
18:27:30	7.97	3.672
18:31:00	8.01	3.536
18:34:30	8.06	3.515
18:38:00	8.09	3.988
18:41:30	8.07	4.021
18:45:00	8.04	3.936
18:48:30	8.02	3.937
18:52:00	8.03	3.712
18:55:30	8.06	3.464
18:59:00	8.1	3.350
19:02:30	8.14	3.550
19:06:00	8.16	3.836
19:09:30	8.13	4.001
19:13:00	8.09	3.915
19:16:30	8.07	3.663
19:20:00	8.07	3.495
19:23:30	8.09	3.383
19:27:00	8.12	3.329
19:30:30	8.14	3.540
19:34:00	8.13	3.625
19:37:30	8.1	3.967
19:41:00	8.07	3.741
19:44:30	8.08	3.696
19:48:00	8.07	3.446
19:51:30	8.11	3.103
19:55:00	8.14	3.156
19:58:30	8.16	3.529
20:02:00	8.16	3.559
20:05:30	8.13	3.540

ANNEXE 3.3 Cuvée avec pulses de substrat

Tableau A3.3-1 Mesures de la concentration d'ADN

	Temps	Lecture		ADN
	heures	luminosité	ng/ml	ng/ml
t-1	1	55	64	535
t-1	1	60	70	584
t-1	1	55	64	535
t-1	1			
t0	1.52	54	63	526
t0	1.52	57	67	555
t0	1.52	60	70	584
t0	1.52			
t1	1.64	60	70	584
t1	1.64	56	65	545
t1	1.64	63	74	613
t1	1.64			
t2	1.85	54	63	526
t2	1.85	63	74	613
t2	1.85	68	79	662
t2	1.85			
t3	1.99	62	72	604
t3	1.99	68	79	662
t3	1.99	65	76	633
t3	1.99			
t4	2.145	70	82	682
t4	2.145	60	70	584
t4	2.145	61	71	594
t4	2.145			
t5	2.405	71	83	691
t5	2.405	61	71	594
t5	2.405	65	76	633
t5	2.405			
t6	2.66	68	79	662
t6	2.66	66	77	643
t6	2.66	64	75	623
t6	2.66			
t7	2.92	67	78	652
t7	2.92	60	70	584
t7	2.92	58	68	565
t7	2.92			
t8	3.925	70	82	682
t8	3.925	70	82	682
t8	3.925	70	82	682
t8	3.925			
t9	4.2	96	112	935
t9	4.2	86	100	837
t9	4.2	81	95	789
t9	4.2			

Tableau A3.3-1 Mesures de la concentration d'ADN

	Temps	Lecture		ADN
	heures	luminosité	ng/ml	ng/ml
t10	4.6	111	130	
t10	4.6	82	96	798
t10	4.6	88	103	857
t10	4.6			
t11	4.865	85	99	828
t11	4.865	83	97	808
t11	4.865	88	103	857
t11	4.865			
t12	5	75	88	730
t12	5	94	110	915
t12	5	88	103	857
t12	5			
t13	5.259			
t13	5.259	74	86	720
t13	5.259	81	95	789
t13	5.259			
t14	5.607	95	111	
t14	5.607	56	65	545
t14	5.607	85	99	828
t14	5.607			
t15	5.99	110	129	1071
t15	5.99	105	123	1022
t15	5.99	115	134	1120
t15	5.99			
t16	6.207	57	67	555
t16	6.207	66	77	643
t16	6.207	54	63	526
t16	6.207			
t17	6.455	50	58	487
t17	6.455	50	58	487
t17	6.455	46	54	448
t17	6.455			
t18	6.756	48	56	467
t18	6.756	46	54	448
t18	6.756	56	65	545
t18	6.756			
t19	7.108	50	58	487
t19	7.108	53	62	516
t19	7.108	49	57	477
t19	7.108			
t20	7.81	53	62	516
t20	7.81	70	82	682
t20	7.81	64	75	623
t20	7.81			

Tableau A3.3-1 Mesures de la concentration d'ADN

	Temps	Lecture		ADN
	heures	luminosité	ng/ml	ng/ml
t21	8.51	63	74	613
t21	8.51	54	63	526
t21	8.51	53	62	516
t21	8.51			
t22	9.457	73	85	711
t22	9.457	74	86	720
t22	9.457	64	75	623
t22	9.457			
t23	11	76	89	740
t23	11	76	89	740
t23	11	74	86	720
t23	11			
t24	24.37	60	70	584
t24	24.37	70	82	682
t24	24.37	62	72	604
t24	24.37			

Tableau A3.3-2 Mesures de la DCO totale

	Temps	Blanc	F.A.S.	DCOtotale	
		Vol.		Vol.	DCO
	heures	ml	molarité	ml	mg/L
t-1	1	26.6	0.019	20.1	495
t-1	1	26.4	0.019	20	502
t-1	1	26.6	0.019	20.1	495
t-1	1	*26.533*	*0.019*		
t0	1.52	26.6	0.019	19.1	572
t0	1.52	26.4	0.019	19	579
t0	1.52	26.6	0.019	19.05	575
t0	1.52	*26.533*	*0.019*		
t1	1.64	26.6	0.019	19.15	568
t1	1.64	26.4	0.019	19	579
t1	1.64	26.6	0.019	19	579
t1	1.64	*26.533*	*0.019*		
t2	1.85	26.6	0.019	19.2	564
t2	1.85	26.4	0.019	19.3	556
t2	1.85	26.6	0.019	19.2	564
t2	1.85	*26.533*	*0.019*		
t3	1.99	26.6	0.019	19.25	560
t3	1.99	26.4	0.019	19.15	568
t3	1.99	26.6	0.019	19.35	552
t3	1.99	*26.533*	*0.019*		
t4	2.145	26.6	0.019	19.25	560
t4	2.145	26.4	0.019	19.25	560
t4	2.145	26.6	0.019	19.25	560
t4	2.145	*26.533*	*0.019*		
t5	2.405	26.6	0.019	19.3	556
t5	2.405	26.4	0.019	19.3	556
t5	2.405	26.6	0.019	19.1	572
t5	2.405	*26.533*	*0.019*		
t6	2.66	26.6	0.019	19.35	552
t6	2.66	26.4	0.019	19.2	564
t6	2.66	26.6	0.019	19.3	556
t6	2.66	*26.533*	*0.019*		
t7	2.92	26.6	0.019	19.25	560
t7	2.92	26.4	0.019	19.5	541
t7	2.92	26.6	0.019	19.5	541
t7	2.92	*26.533*	*0.019*		
t8	3.925	26.6	0.019	19.3	556
t8	3.925	26.4	0.019	19.3	556
t8	3.925	26.6	0.019	19.55	537
t8	3.925	*26.533*	*0.019*		
t9	4.2	26.6	0.019	17.95	660
t9	4.2	26.4	0.019	18.1	648
t9	4.2	26.6	0.019	18	656
t9	4.2	*26.533*	*0.019*		

Tableau A3.3-2 Mesures de la DCO totale

	Temps	Blanc	F.A.S.	DCOtotale	
		Vol.		Vol.	DCO
	heures	ml	molarité	ml	mg/L
t10	4.6	26.6	0.019	18.25	637
t10	4.6	26.4	0.019	18.05	652
t10	4.6	26.6	0.019	18.3	633
t10	4.6	*26.533*	*0.019*		
t11	4.865	26.6	0.019	18.35	629
t11	4.865	26.4	0.019	18.2	641
t11	4.865	26.6	0.019	18.1	648
t11	4.865	*26.533*	*0.019*		
t12	5	26.6	0.019	18.3	633
t12	5	26.4	0.019	18.3	633
t12	5	26.6	0.019	18.25	637
t12	5	*26.533*	*0.019*		
t13	5.259	26.6	0.019	15.95	814
t13	5.259	26.4	0.019	16	810
t13	5.259	26.6	0.019	15.85	821
t13	5.259	*26.533*	*0.019*		
t14	5.607	26.6	0.019	16.3	787
t14	5.607	26.4	0.019	16.3	787
t14	5.607	26.6	0.019	16.1	802
t14	5.607	*26.533*	*0.019*		
t15	5.99	26.6	0.019	16.3	787
t15	5.99	26.4	0.019	16.3	787
t15	5.99	26.6	0.019	16.3	787
t15	5.99	*26.533*	*0.019*		
t16	6.207	26.6	0.019	16.5	771
t16	6.207	26.4	0.019	16.4	779
t16	6.207	26.6	0.019	16.4	779
t16	6.207	*26.533*	*0.019*		
t17	6.455	26.6	0.0198	16.7	779
t17	6.455	26.4	0.0198	16.8	771
t17	6.455	26.6	0.0198	16.5	795
t17	6.455	*26.533*	*0.0198*		
t18	6.756	26.6	0.0198	16.75	775
t18	6.756	26.4	0.0198	16.4	803
t18	6.756	26.6	0.0198	16.9	763
t18	6.756	*26.533*	*0.0198*		
t19	7.108	26.6	0.0198	17	755
t19	7.108	26.4	0.0198	16.7	779
t19	7.108	26.6	0.0198	16.5	795
t19	7.108	*26.533*	*0.0198*		
t20	7.81	26.6	0.0198	16.8	771
t20	7.81	26.4	0.0198	16.65	783
t20	7.81	26.6	0.0198	16.45	799
t20	7.81	*26.533*	*0.0198*		

Tableau A3.3-2 Mesures de la DCO totale

	Temps	Blanc	F.A.S.	DCOtotale	
		Vol.		Vol.	DCO
	heures	ml	molarité	ml	mg/L
t21	8.51	26.6	0.0198	16.9	763
t21	8.51	26.4	0.0198	16.7	779
t21	8.51	26.6	0.0198	16.7	779
t21	8.51	*26.533*	*0.0198*		
t22	9.457	26.6	0.0198	16.7	779
t22	9.457	26.4	0.0198	16.85	767
t22	9.457	26.6	0.0198	16.65	783
t22	9.457	*26.533*	*0.0198*		
t23	11	26.6	0.0198	16.7	779
t23	11	26.4	0.0198	16.7	779
t23	11	26.6	0.0198	16.7	779
t23	11	*26.533*	*0.0198*		
t24	24.37	26.6	0.0198	16.6	787
t24	24.37	26.4	0.0198	18.65	
t24	24.37	26.6	0.0198	18.95	
t24	24.37	*26.533*	*0.0198*		

Tableau A3.3-3 Mesures de la DCO filtrée

	Temps	Blanc	F.A.S.	DCOfiltrée	
		Vol.		Vol.	DCO
	heures	ml	molarité	ml	mg/L
t-1	1	27.2	0.0194	25.3	149
t-1	1	27.2	0.0194	25.25	153
t-1	1	27.25	0.0194	25.2	156
t-1	1	*27.217*	*0.0194*		
t0	1.52	27.2	0.0194	24.2	234
t0	1.52	27.2	0.0194	24	250
t0	1.52	27.25	0.0194	24.2	234
t0	1.52	*27.217*	*0.0194*		
t1	1.64	27.2	0.0194	24.35	222
t1	1.64	27.2	0.0194	24.3	226
t1	1.64	27.25	0.0194	24.4	219
t1	1.64	*27.217*	*0.0194*		
t2	1.85	27.2	0.0194	24.75	191
t2	1.85	27.2	0.0194	24.75	191
t2	1.85	27.25	0.0194	24.8	188
t2	1.85	*27.217*	*0.0194*		
t3	1.99	27.2	0.0194	25.1	164
t3	1.99	27.2	0.0194	25	172
t3	1.99	27.25	0.0194	25.1	164
t3	1.99	*27.217*	*0.0194*		
t4	2.145	27.2	0.0194	25	172
t4	2.145	27.2	0.0194	25	172
t4	2.145	27.25	0.0194	24.95	176
t4	2.145	*27.217*	*0.0194*		
t5	2.405	27.2	0.0194	25.1	164
t5	2.405	27.2	0.0194	25.25	153
t5	2.405	27.25	0.0194	25.05	168
t5	2.405	*27.217*	*0.0194*		
t6	2.66	27.2	0.0194	25.15	160
t6	2.66	27.2	0.0194	25.15	160
t6	2.66	27.25	0.0194	25.1	164
t6	2.66	*27.217*	*0.0194*		
t7	2.92	27.2	0.0194	25.3	149
t7	2.92	27.2	0.0194	25.25	153
t7	2.92	27.25	0.0194	25.4	141
t7	2.92	*27.217*	*0.0194*		
t8	3.925	27.2	0.0194	25.2	156
t8	3.925	27.2	0.0194	25.3	149
t8	3.925	27.25	0.0194	25.25	153
t8	3.925	*27.217*	*0.0194*		
t9	4.2	27.2	0.0194	23.7	273
t9	4.2	27.2	0.0194	23.8	265
t9	4.2	27.25	0.0194	23.75	269
t9	4.2	*27.217*	*0.0194*		

Tableau A3.3-3 Mesures de la DCO filtrée

	Temps	Blanc	F.A.S.	DCOfiltrée	
		Vol.		Vol.	DCO
	heures	ml	molarité	ml	mg/L
t10	4.6	27.2	0.0194	24.7	195
t10	4.6	27.2	0.0194	24.55	207
t10	4.6	27.25	0.0194	24.75	191
t10	4.6	*27.217*	*0.0194*		
t11	4.865	27.2	0.0194	24.95	176
t11	4.865	27.2	0.0194	25	172
t11	4.865	27.25	0.0194	24.95	176
t11	4.865	*27.217*	*0.0194*		
t12	5	27.2	0.0194	25	172
t12	5	27.2	0.0194	25.1	164
t12	5	27.25	0.0194	25	172
t12	5	*27.217*	*0.0194*		
t13	5.259	27.2	0.0194	22.7	350
t13	5.259	27.2	0.0194	22.7	350
t13	5.259	27.25	0.0194	22.65	354
t13	5.259	*27.217*	*0.0194*		
t14	5.607	27.2	0.0194	23.4	296
t14	5.607	27.2	0.0194	23.5	288
t14	5.607	27.25	0.0194		
t14	5.607	*27.217*	*0.0194*		
t15	5.99	27.2	0.0194	24.05	246
t15	5.99	27.2	0.0194	24.2	234
t15	5.99	27.25	0.0194	24.05	246
t15	5.99	*27.217*	*0.0194*		
t16	6.207	27.2	0.0194	19.95	200
t16	6.207	27.2	0.0194	19.85	195
t16	6.207	27.25	0.0194	19.9	200
t16	6.207	*27.217*	*0.0194*		
t17	6.455	27.2	0.0194	24.65	199
t17	6.455	27.2	0.0194	24.7	195
t17	6.455	27.25	0.0194	24.5	211
t17	6.455	*27.217*	*0.0194*		
t18	6.756	27.2	0.0194	24.8	188
t18	6.756	27.2	0.0194	24.8	188
t18	6.756	27.25	0.0194	24.8	188
t18	6.756	*27.217*	*0.0194*		
t19	7.108	27.2	0.0194	25.1	164
t19	7.108	27.2	0.0194	24.9	180
t19	7.108	27.25	0.0194	24.95	176
t19	7.108	*27.217*	*0.0194*		
t20	7.81	27.2	0.0194	25.15	160
t20	7.81	27.2	0.0194	25.1	164
t20	7.81	27.25	0.0194	25.15	160
t20	7.81	*27.217*	*0.0194*		

Tableau A3.3-3 Mesures de la DCO filtrée

	Temps	Blanc	F.A.S.	DCOfiltrée	
	heures	Vol. ml	molarité	Vol. ml	DCO mg/L
t21	8.51	27.2	0.0194	25.2	156
t21	8.51	27.2	0.0194	25.2	156
t21	8.51	27.25	0.0194	25.1	164
t21	8.51	*27.217*	*0.0194*		
t22	9.457	27.2	0.0194	25.2	156
t22	9.457	27.2	0.0194	25.2	156
t22	9.457	27.25	0.0194	25.2	156
t22	9.457	*27.217*	*0.0194*		
t23	11	27.2	0.0194	25.15	160
t23	11	27.2	0.0194	25.1	164
t23	11	27.25	0.0194	25.1	164
t23	11	*27.217*	*0.0194*		
t24	24.37	27.2	0.0194	25	172
t24	24.37	27.2	0.0194	25.1	164
t24	24.37	27.25	0.0194	25.05	168
t24	24.37	*27.217*	*0.0194*		

Tableau A3.3-4 Mesures du glucose

	Temps	Blanc	Glucose	
	heures	Abs.	Abs.	mg/L
t-1	1	0	0.018	2
t-1	1	-0.002	0.024	3
t-1	1	0.013	0.032	4
t-1	1	*0.004*	*0.025*	
t0	1.52	0	0.858	108
t0	1.52	-0.002	0.859	108
t0	1.52	0.013	0.859	108
t0	1.52	*0.004*	*0.859*	
t1	1.64	0	0.5567	70
t1	1.64	-0.002	0.553	70
t1	1.64	0.013	0.554	70
t1	1.64	*0.004*	*0.555*	
t2	1.85	0	0.214	27
t2	1.85	-0.002	0.211	26
t2	1.85	0.013	0.209	26
t2	1.85	*0.004*	*0.211*	
t3	1.99	0	0.12	15
t3	1.99	-0.002	0.033	4
t3	1.99	0.013	0.031	3
t3	1.99	*0.004*	*0.061*	
t4	2.145	0	0.048	6
t4	2.145	-0.002	0.062	7
t4	2.145	0.013	0.044	5
t4	2.145	*0.004*	*0.051*	
t5	2.405	0	0.05	6
t5	2.405	-0.002	0.04	5
t5	2.405	0.013	0.026	3
t5	2.405	*0.004*	*0.039*	
t6	2.66	0	0.251	31
t6	2.66	-0.002	0.127	16
t6	2.66	0.013	0.063	8
t6	2.66	*0.004*	*0.147*	
t7	2.92	0	0.079	10
t7	2.92	-0.002	0.031	3
t7	2.92	0.013	0.059	7
t7	2.92	*0.004*	*0.056*	
t8	3.925	0	0.015	1
t8	3.925	-0.002	0.029	3
t8	3.925	0.013	0.058	7
t8	3.925	*0.004*	*0.034*	
t9	4.2	0	0.918	116
t9	4.2	-0.002	0.906	114
t9	4.2	0.013	0.915	115
t9	4.2	*0.004*	*0.913*	

Tableau A3.3-4 Mesures du glucose

	Temps	Blanc	Glucose	
	heures	Abs.	Abs.	mg/L
t10	4.6	0	0.322	40
t10	4.6	-0.002	0.322	40
t10	4.6	0.013	0.334	42
t10	4.6	*0.004*	*0.326*	
t11	4.865	0	0.03	3
t11	4.865	-0.002	0.019	2
t11	4.865	0.013	0.022	2
t11	4.865	*0.004*	*0.024*	
t12	5	0	0.051	6
t12	5	-0.002	0.03	3
t12	5	0.013	0.052	6
t12	5	*0.004*	*0.044*	
t13	5.259	0	1.639	207
t13	5.259	-0.002	1.648	208
t13	5.259	0.013	1.64	207
t13	5.259	*0.004*	*1.642*	
t14	5.607	0	1.026	129
t14	5.607	-0.002	1.036	131
t14	5.607	0.013	1.014	128
t14	5.607	*0.004*	*1.025*	
t15	5.99	0	0.456	57
t15	5.99	-0.002	0.465	58
t15	5.99	0.013	0.462	58
t15	5.99	*0.004*	*0.461*	
t16	6.207	0	0.101	12
t16	6.207	-0.002	0.113	14
t16	6.207	0.013	0.107	13
t16	6.207	*0.004*	*0.107*	
t17	6.455	0	0.019	2
t17	6.455	-0.002	0.032	4
t17	6.455	0.013	0.017	2
t17	6.455	*0.004*	*0.023*	
t18	6.756	0	0.031	3
t18	6.756	-0.002	0.06	7
t18	6.756	0.013	0.02	2
t18	6.756	*0.004*	*0.037*	
t19	7.108	0	0.027	3
t19	7.108	-0.002	0.04	5
t19	7.108	0.013	0.022	2
t19	7.108	*0.004*	*0.030*	
t20	7.81	0	0.017	2
t20	7.81	-0.002	0.022	2
t20	7.81	0.013	0.025	3
t20	7.81	*0.004*	*0.021*	

Tableau A3.3-4 Mesures du glucose

	Temps	Blanc	Glucose	
	heures	Abs.	Abs.	mg/L
t21	8.51	0	0.027	3
t21	8.51	-0.002	0.021	2
t21	8.51	0.013	0.039	4
t21	8.51	*0.004*	*0.029*	
t22	9.457	0	0.02	2
t22	9.457	-0.002	0.016	2
t22	9.457	0.013	0.03	3
t22	9.457	*0.004*	*0.022*	
t23	11	0	0.027	3
t23	11	-0.002	0.016	2
t23	11	0.013	0.02	2
t23	11	*0.004*	*0.021*	
t24	24.37	0	0.034	4
t24	24.37	-0.002	0.021	2
t24	24.37	0.013	0.024	3
t24	24.37	*0.004*	*0.026*	

	Temps	Blanc	Glycogène	
	heure	Abs.	Abs.	mg/L
t-1	1	0	0.446	56.6
t-1	1	0	0.438	55.4
t-1	1	-0.003	0.444	56.2
t-1	1	*-0.001*		
t0	1.52	0	0.446	56.0
t0	1.52	0.002	0.452	57.2
t0	1.52	0.008	0.448	56.7
t0	1.52	*0.003*		
t1	1.64	0	0.538	68.2
t1	1.64	0	0.548	69.4
t1	1.64	-0.003	0.555	70.3
t1	1.64	*-0.001*		
t2	1.85	0	0.681	86.3
t2	1.85	0	0.692	87.6
t2	1.85	-0.003	0.692	87.6
t2	1.85	*-0.001*		
t3	1.99	0	0.774	98.1
t3	1.99	0	0.78	98.7
t3	1.99	-0.003	0.788	99.7
t3	1.99	*-0.001*		
t4	2.145	0	0.776	98.4
t4	2.145	0	0.774	98.0
t4	2.145	-0.003	0.776	98.2
t4	2.145	*-0.001*		
t5	2.405	0	0.773	98.0
t5	2.405	0	0.773	97.8
t5	2.405	-0.003	0.778	98.5
t5	2.405	*-0.001*		
t6	2.66	0	0.747	94.7
t6	2.66	0	0.744	94.2
t6	2.66	-0.003	0.755	95.6
t6	2.66	*-0.001*		
t7	2.92	0	0.761	96.5
t7	2.92	0	0.757	95.8
t7	2.92	-0.003	0.781	98.9
t7	2.92	*-0.001*		
t8	3.925	0	0.738	93.5
t8	3.925	0	0.734	92.9
t8	3.925	-0.003	0.714	90.4
t8	3.925	*-0.001*		
t9	4.2	0	0.712	90.3
t9	4.2	0	0.718	90.9
t9	4.2	-0.003	0.72	91.1
t9	4.2	*-0.001*		

	Temps	Blanc	Glycogène	
	heure	Abs.	Abs.	mg/L
t10	4.6	0	0.989	125.3
t10	4.6	0	0.978	123.8
t10	4.6	-0.003	0.981	124.2
t10	4.6	*-0.001*		
t11	4.865	0	1.111	140.8
t11	4.865	0	1.118	141.5
t11	4.865	-0.003	1.113	140.9
t11	4.865	*-0.001*		
t12	5	0	1.092	138.4
t12	5	0	1.104	139.7
t12	5	-0.003	1.11	140.5
t12	5	*-0.001*		
t13	5.259	0	1.075	136.2
t13	5.259	0	1.089	137.8
t13	5.259	-0.003	1.078	136.5
t13	5.259	*-0.001*		
t14	5.607	0	1.29	163.4
t14	5.607	0	1.301	164.7
t14	5.607	-0.003	1.261	159.6
t14	5.607	*-0.001*		
t15	5.99	0	1.491	188.9
t15	5.99	0	1.482	187.6
t15	5.99	-0.003	1.486	188.1
t15	5.99	*-0.001*		
t16	6.207	0	1.598	202.4
t16	6.207	0	1.605	203.2
t16	6.207	-0.003	1.63	206.3
t16	6.207	*-0.001*		
t17	6.455	0	1.613	204.3
t17	6.455	0	1.6	202.5
t17	6.455	-0.003	1.65	208.9
t17	6.455	*-0.001*		
t18	6.756	0	1.631	206.6
t18	6.756	0	1.634	206.8
t18	6.756	-0.003	1.645	208.2
t18	6.756	*-0.001*		
t19	7.108	0	1.57	198.9
t19	7.108	0	1.583	200.4
t19	7.108	-0.003	1.581	200.1
t19	7.108	*-0.001*		
t20	7.81	0	1.511	191.4
t20	7.81	0	1.543	195.3
t20	7.81	-0.003	1.585	200.6
t20	7.81	*-0.001*		

	Temps	Blanc	Glycogène	
	heure	Abs.	Abs.	mg/L
t21	8.51	0	1.509	191.1
t21	8.51	0	1.475	186.7
t21	8.51	-0.003	1.497	189.5
t21	8.51	*-0.001*		
t22	9.457	0	1.473	186.6
t22	9.457	0	1.477	187.0
t22	9.457	-0.003	1.449	183.4
t22	9.457	*-0.001*		
t23	11	0	1.441	182.5
t23	11	0	1.336	169.1
t23	11	-0.003	1.32	167.1
t23	11	*-0.001*		
t24	24.37	0	0.807	102.3
t24	24.37	0	0.823	104.2
t24	24.37	-0.003	0.805	101.9
t24	24.37	*-0.001*		

	Temps heures	Blanc abs	NH_4^+ abs	mg N/L
t-1	1	0.000	0.614	44.7
t-1	1		0.62	45.2
t-1	1		0.62	45.2
t-1	1			
t0	1.52	0.000	0.6	43.7
t0	1.52		0.608	44.3
t0	1.52		0.597	43.5
t0	1.52			
t1	1.64	0.000	0.587	42.8
t1	1.64		0.584	42.5
t1	1.64		0.587	42.8
t1	1.64			
t2	1.85	0.000	0.558	40.6
t2	1.85		0.559	40.7
t2	1.85		0.558	40.6
t2	1.85			
t3	1.99	0.000	0.583	42.5
t3	1.99		0.584	42.5
t3	1.99		0.584	42.5
t3	1.99			
t4	2.145	0.000	0.598	43.6
t4	2.145		0.604	44.0
t4	2.145		0.6	43.7
t4	2.145			
t5	2.405	0.000	0.573	41.7
t5	2.405		0.572	41.7
t5	2.405		0.571	41.6
t5	2.405			
t6	2.66	0.000	0.574	41.8
t6	2.66		0.575	41.9
t6	2.66		0.577	42.0
t6	2.66			
t7	2.92	0.000	0.593	43.2
t7	2.92		0.585	42.6
t7	2.92		0.595	43.3
t7	2.92			
t8	3.925	0.000	0.556	40.5
t8	3.925		0.556	40.5
t8	3.925		0.552	40.2
t8	3.925			
t9	4.2	0.000	0.558	40.6
t9	4.2		0.55	40.1
t9	4.2		0.549	40.0
t9	4.2			

	Temps heures	Blanc abs	NH_4^+ abs	mg N/L
t10	4.6	0.000	0.554	40.4
t10	4.6		0.561	40.9
t10	4.6		0.562	40.9
t10	4.6			
t11	4.865	0.000	0.561	40.9
t11	4.865		0.572	41.7
t11	4.865		0.567	41.3
t11	4.865			
t12	5	0.000	0.55	40.1
t12	5		0.548	39.9
t12	5		0.55	40.1
t12	5			
t13	5.259	0.000	0.561	40.9
t13	5.259		0.559	40.7
t13	5.259		0.554	40.4
t13	5.259			
t14	5.607	0.000	0.556	40.5
t14	5.607		0.556	40.5
t14	5.607		0.553	40.3
t14	5.607			
t15	5.99	0.000	0.529	38.5
t15	5.99		0.53	38.6
t15	5.99		0.528	38.5
t15	5.99			
t16	6.207	0.000	0.525	38.2
t16	6.207		0.528	38.5
t16	6.207		0.528	38.5
t16	6.207			
t17	6.455	0.000	0.523	38.1
t17	6.455		0.528	38.5
t17	6.455		0.524	38.2
t17	6.455			
t18	6.756	0.000	0.522	38.0
t18	6.756		0.527	38.4
t18	6.756		0.522	38.0
t18	6.756			
t19	7.108	0.000	0.526	38.3
t19	7.108		0.532	38.8
t19	7.108		0.535	39.0
t19	7.108			
t20	7.81	0.000	0.526	38.3
t20	7.81		0.522	38.0
t20	7.81		0.524	38.2
t20	7.81			

	Temps heures	Blanc abs	NH_4^+ abs	mg N/L
t21	8.51	0.000	0.516	37.6
t21	8.51		0.52	37.9
t21	8.51		0.518	37.7
t21	8.51			
t22	9.457	0.000	0.512	37.3
t22	9.457		0.513	37.4
t22	9.457		0.516	37.6
t22	9.457			
t23	11	0.000	0.498	36.3
t23	11		0.5	36.4
t23	11		0.498	36.3
t23	11			
t24	24.37	0.000	0.432	31.5
t24	24.37		0.432	31.5
t24	24.37		0.426	31.0
t24	24.37			

Tableau A3.3-7 Compte de la micro-faune

	Temps	Flagellé	Cilié libre	Cilié fixe	Rotifer	Sarcodine	total	Micro faune
	heure	org.	org.	org.	org.	org.	org.	org./L
t-1	1		1	5		21	27	9.0.E+05
t27	50.5		1	5		27	33	1.1.E+06

Tableau A3.3-8 Données de respirométrie

Temps heures	rO2 mg/L/h	Temps heures	rO2 mg/L/h	Temps heures	rO2 mg/L/h
0.069479	1.16251	2.54441	4.44998	5.01197	7.05434
0.124554	1.48087	2.59867	4.22405	5.06691	6.72285
0.180165	1.55679	2.6529	4.23253	5.17748	6.20994
0.235799	1.7251	2.70718	4.239	5.23247	6.13447
0.29071	1.57026	2.76142	3.9135	5.28669	27.9263
0.345705	1.70206	2.81637	3.20341	5.3418	26.9089
0.400636	1.644	2.87198	3.04857	5.39747	26.1191
0.454962	1.54464	2.92762	2.84674	5.45244	25.7406
0.509184	1.48697	2.98256	2.91474	5.50665	25.4131
0.564124	1.65903	3.0375	2.88958	5.56161	25.3619
0.619739	1.74021	3.09245	2.80701	5.61663	25.2791
0.67468	1.54481	3.14738	2.75551	5.67088	25.4028
0.729608	1.67364	3.20303	2.90158	5.72512	25.2541
0.784528	1.7127	3.258	2.56381	5.77941	25.4134
0.838864	1.56628	3.31221	2.64578	5.83365	25.0506
0.893809	1.6391	3.36645	2.72762	5.88859	25.1227
0.949572	3.05772	3.4214	2.72271	5.94424	25.1298
1.00449	1.65293	3.47642	2.50417	5.99919	24.9073
1.05959	1.58255	3.53065	2.64243	6.05413	24.8702
1.11452	1.60512	3.58498	2.57237	6.10975	24.5632
1.16884	1.71825	3.63994	2.52999	6.1647	24.1109
1.22379	1.73067	3.69502	2.66808	6.21894	23.2961
1.27884	1.4375	3.74926	2.71962	6.2733	23.0381
1.3331	1.39388	3.80421	2.6832	6.32755	11.9525
1.38732	1.50985	3.85916	2.68935	6.38248	9.10392
1.44234	1.68983	3.9141	2.65414	6.43827	9.09718
1.49727	1.42562	3.96908	2.60897	6.49402	8.44925
1.55165	26.9491	4.02399	2.76081	6.54895	8.47698
1.60658	26.2292	4.07961	2.44897	6.60335	8.34978
1.66237	25.037	4.13454	2.6813	6.65759	8.16816
1.71729	25.1398	4.18885	2.65198	6.71255	7.95511
1.77234	24.8124	4.24379	27.4325	6.76757	8.04556
1.82796	24.4273	4.29886	26.4809	6.82256	8.0174
1.88289	24.5341	4.35311	25.9615	6.87824	7.89368
1.9379	24.2041	4.40735	25.6292	6.93401	7.8556
1.99355	17.1759	4.46167	25.5747	6.98893	7.72934
2.04916	6.81207	4.51661	25.6692	7.04403	7.44098
2.10491	5.7471	4.57165	25.5097	7.09897	7.37751
2.15999	5.30245	4.62659	25.2545	7.15334	7.20181
2.21423	5.41146	4.68232	25.5874	7.20829	6.97339
2.26916	5.12751	4.73795	25.3766	7.26399	6.7964
2.32441	4.94146	4.79357	24.7001	7.31893	6.60198
2.37934	4.89541	4.84852	9.03177	7.374	6.33724
2.43441	4.6956	4.90277	7.75309	7.42894	6.04747
2.48939	4.56104	4.95701	7.65317	7.484	5.97808

Tableau A3.3-8 Données de respirométrie

Temps heures	rO2 mg/L/h	Temps heures	rO2 mg/L/h	Temps heures	rO2 mg/L/h
7.53893	5.80038	10.1207	3.02573	12.644	3.67524
7.59399	5.92712	10.1757	3.26605	12.699	3.65596
7.64893	5.54049	10.2313	3.37427	12.7546	3.64545
7.7583	5.35371	10.2862	1.93804	12.8096	3.67575
7.81332	5.30446	10.3405	3.55518	12.8639	3.72101
7.86827	5.25601	10.3948	3.85088	12.9181	3.57116
7.92328	5.24713	10.4497	3.23114	12.9724	3.68113
7.97754	5.08282	10.5047	3.58726	13.0273	3.65684
8.03182	4.86138	10.5589	3.4411	13.0823	3.79007
8.08607	5.00826	10.6133	3.59168	13.1367	3.79522
8.14102	4.62051	10.6676	3.6772	13.1916	3.74663
8.19607	4.57205	10.7218	3.71656	13.2473	3.55497
8.25032	4.55076	10.7761	3.68302	13.3029	3.88757
8.30465	4.27185	10.8303	3.06288	13.3585	3.66175
8.35959	4.26122	10.8846	3.4426	13.4142	3.65335
8.41453	4.35582	10.9388	3.34818	13.4691	3.62678
8.46886	4.09994	10.9931	3.39472	13.5234	3.58764
8.52381	3.94881	11.048	3.37823	13.5783	3.64228
8.57884	4.16056	11.1038	3.45395	13.634	3.66543
8.63313	3.83472	11.1596	3.41413	13.6889	3.68434
8.68806	3.80873	11.2152	3.30831	13.7432	3.77892
8.74381	3.95501	11.2702	3.27689	13.7981	3.75317
8.79884	3.84811	11.3244	3.65673	13.8538	3.5378
8.8538	3.94778	11.3787	3.52548	13.9089	3.65595
8.90892	3.97947	11.4329	3.27567	13.9638	3.53369
8.964	3.8033	11.4879	3.44904	14.0196	3.88799
9.01964	3.65123	11.5428	3.3865	14.0752	3.76349
9.07527	3.8767	11.5972	3.25205	14.1302	3.79232
9.13088	3.5142	11.6522	3.37661	14.1844	3.53502
9.18651	3.82387	11.7079	3.56768	14.2387	3.58989
9.24145	3.80382	11.7628	3.55163	14.2929	3.67986
9.2964	3.50739	11.8172	3.80605	14.3472	3.68868
9.35203	3.62122	11.8722	3.80104	14.4021	3.61666
9.40767	3.95548	11.9272	3.68349	14.4579	3.80206
9.46259	3.68755	11.9822	3.59995	14.5128	3.82211
9.51687	3.78691	12.0379	3.79804	14.5677	3.71108
9.5711	3.7916	12.0935	3.55392	14.6228	3.80581
9.62536	3.65304	12.1485	3.65272	14.677	3.80204
9.6796	3.54621	12.2027	3.50957	14.732	3.6121
9.73458	3.66728	12.2577	3.69914	14.7876	3.81033
9.7902	3.38498	12.3128	3.79511	14.8425	3.61677
9.84586	3.38182	12.3677	3.65652	14.8975	3.80764
9.90089	3.41758	12.4235	3.57342	14.9531	3.82268
9.95513	3.1323	12.4784	3.65637	15.008	3.64807
10.0101	3.06475	12.5334	3.4521	15.0623	3.42565
10.0657	3.42861	12.5891	3.64539	15.1173	3.57493

Tableau A3.3-8 Données de respirométrie

Temps heures	rO2 mg/L/h	Temps heures	rO2 mg/L/h
15.173	3.63453	17.6991	3.65399
15.2286	3.69526	17.7541	3.77051
15.2842	3.7864	17.8097	3.763
15.3392	3.61532	17.8653	3.54661
15.3934	3.645	17.921	3.81678
15.4485	3.80833	17.9766	3.90616
15.5034	3.59009	18.0323	3.77165
15.5577	3.79323	18.0872	3.91465
15.6126	3.741	18.1415	3.635
15.6683	3.65741	18.1958	3.61163
15.724	3.80898	18.25	3.82565
15.7796	3.6318	18.3049	3.78488
15.8346	3.6412	18.36	3.53177
15.8896	3.50688	18.4149	3.78682
15.9445	3.90668	18.47	3.68616
15.9989	3.61268	18.5249	3.64292
16.0531	3.54051	18.58	3.80594
16.108	3.63249	18.6342	3.67548
16.1632	3.68299	18.6885	3.77598
16.2174	3.55854	18.7434	3.89566
16.2716	3.77893	18.7984	3.58553
16.3266	3.82794	18.8527	3.82166
16.3823	3.65568	18.9077	3.83965
16.438	3.63302	18.9633	3.76715
16.4929	3.91601	19.019	3.7794
16.5472	3.57164	19.0739	4.07139
16.6014	3.51669	19.129	3.75217
16.6564	3.77769	19.1847	3.84125
16.7113	3.53837	19.2403	3.95245
16.7663	3.70712	19.296	3.69884
16.8219	3.67005	19.3511	3.82833
16.8775	3.64453	19.406	3.81651
16.9332	3.99603	19.4618	3.72715
16.9881	3.79844	19.5174	3.77192
17.0424	3.66389	19.5724	3.61271
17.0966	3.83367	19.6273	3.58326
17.1516	3.83289	19.683	3.65109
17.2066	3.62134	19.7386	3.74637
17.2616	3.80011	19.7942	3.70089
17.3166	3.77559	19.8492	3.50589
17.3715	3.5618	19.9034	3.75581
17.4265	3.62437	19.9584	3.70016
17.4807	3.72253	20.0141	3.77436
17.535	3.53291		
17.5892	3.65286		
17.6442	3.5062		

ANNEXE A3.4 Essai de respirométrie du 20-12-2004

Tableau A3.4-1 Données de respirométrie

DASYLab - V 5.50.00
WORKSHEET : Respiro
Recording Date : 04-12-21, 10:05:38
Block Length : 1
Delta : 1 sec.

Temps hh :mm :ss	rO2 mg/L/h	Temps hh :mm :ss	rO2 mg/L/h	Temps hh :mm :ss	rO2 mg/L/h
00:04:59	0.864	02:21:29	7.049	04:37:59	5.661
00:08:29	0.783	02:24:59	6.906	04:41:29	5.667
00:11:59	0.536	02:28:29	7.168	04:44:59	6.085
00:15:29	0.975	02:31:59	7.340	04:48:29	6.144
00:18:59	1.069	02:35:29	7.319	04:51:59	5.942
00:22:29	1.049	02:38:59	7.288	04:55:29	5.912
00:25:59	1.120	02:42:29	7.100	04:58:59	5.662
00:29:29	0.844	02:45:59	6.875	05:02:29	5.564
00:32:59	0.954	02:49:29	6.675	05:05:59	5.583
00:36:29	1.083	02:52:59	6.738	05:09:29	5.699
00:39:59	11.428	02:56:29	6.898	05:12:59	5.919
00:43:29	11.472	02:59:59	7.086	05:16:29	6.029
00:46:59	11.273	03:03:29	7.133	05:19:59	5.973
00:50:29	10.962	03:06:59	6.943	05:23:29	6.027
00:53:59	10.378	03:10:29	6.690	05:26:59	5.653
00:57:29	9.560	03:13:59	6.405	05:30:29	5.646
01:00:59	8.755	03:17:29	6.394	05:33:59	5.441
01:04:29	8.361	03:20:59	6.425	05:37:29	5.824
01:07:59	8.514	03:24:29	6.672	05:40:59	5.938
01:11:29	8.823	03:27:59	6.778	05:44:29	5.823
01:14:59	8.745	03:31:29	6.800	05:47:59	5.800
01:18:29	8.487	03:34:59	6.260	05:51:29	5.846
01:21:59	8.226	03:38:29	6.244	05:54:59	5.565
01:25:29	7.864	03:41:59	6.147	05:58:29	5.346
01:28:59	7.728	03:45:29	6.105	06:01:59	5.337
01:32:29	7.850	03:48:59	6.094	06:05:29	5.846
01:35:59	8.176	03:52:29	6.406	06:08:59	6.071
01:39:29	8.219	03:55:59	6.602	06:12:29	6.084
01:42:59	8.299	03:59:29	6.371	06:15:59	5.713
01:46:29	7.968	04:02:59	6.174	06:19:29	5.654
01:49:59	7.716	04:06:29	6.023	06:22:59	5.582
01:53:29	7.443	04:09:59	5.872	06:26:29	5.504
01:56:59	7.293	04:13:29	5.886	06:29:59	5.347
02:00:29	7.482	04:16:59	6.009	06:33:29	5.742
02:03:59	7.720	04:20:29	6.375	06:36:59	5.849
02:07:29	7.677	04:23:59	6.372	06:40:29	5.839
02:10:59	7.579	04:27:29	6.225	06:43:59	5.650
02:14:29	7.350	04:30:59	5.950	06:47:29	5.626
02:17:59	7.265	04:34:29	5.828	06:50:59	5.483

Tableau A3.4-1 Données de respirométrie

Temps hh :mm :ss	rO2 mg/L/h	Temps hh :mm :ss	rO2 mg/L/h
06:54:29	5.453	09:31:59	5.391
06:57:59	5.671	09:35:29	5.366
07:01:29	5.937	09:38:59	5.371
07:04:59	5.903	09:42:29	5.552
07:08:29	6.020	09:45:59	5.775
07:11:59	5.965	09:49:29	6.082
07:15:29	5.624	09:52:59	5.796
07:18:59	5.540	09:56:29	5.707
07:22:29	5.510	09:59:59	5.666
07:25:59	5.426	10:03:29	5.535
07:29:29	5.733	10:06:59	5.572
07:32:59	5.866	10:10:29	5.545
07:36:29	5.911	10:13:59	5.900
07:39:59	5.789	10:17:29	5.950
07:43:29	5.659	10:20:59	5.864
07:46:59	5.511	10:24:29	5.830
07:50:29	5.551	10:27:59	5.781
07:53:59	5.641	10:31:29	5.434
07:57:29	5.798	10:34:59	5.655
08:00:59	5.922	10:38:29	5.728
08:04:29	5.815	10:41:59	6.003
08:07:59	5.832	10:45:29	6.087
08:11:29	5.506	10:48:59	6.053
08:14:59	5.550	10:52:29	6.097
08:18:29	5.387	10:55:59	5.806
08:21:59	5.587	10:59:29	5.690
08:25:29	5.837	11:02:59	5.739
08:28:59	5.841	11:06:29	5.939
08:32:29	5.750	11:09:59	6.435
08:35:59	5.539	11:13:29	6.336
08:39:29	5.588	11:16:59	5.913
08:42:59	5.463	11:20:29	6.129
08:46:29	5.413	11:23:59	5.973
08:49:59	5.859	11:27:29	5.696
08:53:29	5.895	11:30:59	5.858
08:56:59	5.983	11:34:29	6.161
09:00:29	5.928	11:37:59	6.155
09:03:59	5.553	11:41:29	6.388
09:07:29	5.372	11:44:59	6.354
09:10:59	5.254	11:48:29	6.431
09:14:29	5.317	11:51:59	6.188
09:17:59	5.671	11:55:29	6.026
09:21:29	5.848		
09:24:59	5.839		
09:28:29	5.626		

ANNEXE A3.5 Essai de respirométrie du 08-01-2005

Tableau A3.5-1 Données de respirométrie

DASYLab - V 5.50.00
WORKSHEET : Respiro
Recording Date : 05-01-08. 12:26:06
Block Length : 1
Delta : 1 sec.
Number of Channels : 1

Temps hh :mm :ss	rO2 mg/L/h	Temps hh :mm :ss	rO2 mg/L/h	Temps hh :mm :ss	rO2 mg/L/h
0:04:59	0.42188487	2:17:59	3.0980344	4:30:59	2.84594595
0:08:29	0.55945946	2:21:29	3.21586522	4:34:29	2.85763426
0:11:59	0.64854335	2:24:59	2.7529133	4:37:59	2.50730081
0:15:29	0.65754651	2:28:29	2.74422604	4:41:29	2.36451386
0:18:59	0.72925588	2:31:59	3.21712882	4:44:59	2.37446473
0:22:29	0.62390312	2:35:29	3.14573534	4:48:29	2.43606529
0:25:59	0.47211302	2:38:59	2.39199719	4:51:59	2.27258687
0:29:29	0.15321165	2:42:29	2.97909793	4:55:29	2.68657424
0:32:59	1.11465426	2:45:59	2.92255177	4:58:59	3.06518077
0:36:29	0.94469989	2:49:29	2.77850123	5:02:29	2.75275535
0:39:59	1.11196911	2:52:59	2.85068445	5:05:59	2.65561601
0:43:29	1.09854335	2:56:29	2.93439803	5:09:29	2.43969814
0:46:59	0.58994384	2:59:59	2.95082485	5:12:59	2.31776062
0:50:29	1.03488943	3:03:29	3.18380133	5:16:29	2.24052299
0:53:59	0.81976132	3:06:59	3.25945946	5:19:59	2.44380485
0:57:29	1.05573886	3:10:29	2.76286416	5:23:29	2.27669358
1:00:59	0.53087048	3:13:59	2.59843805	5:26:59	2.89791155
1:04:29	1.052106	3:17:29	2.64882415	5:30:29	2.82051597
1:07:59	0.87851878	3:20:59	2.61691822	5:33:59	2.57964198
1:11:29	1.05068445	3:24:29	2.84326079	5:37:29	2.56842752
1:14:59	0.62627238	3:27:59	2.60996841	5:40:59	2.3507722
1:18:29	0.66386451	3:31:29	3.03627589	5:44:29	2.35535275
1:21:59	0.79512109	3:34:59	2.98178308	5:47:59	2.35566866
1:25:29	0.61284661	3:38:29	2.9018603	5:51:29	2.49387504
1:28:59	0.79717445	3:41:59	2.93755704	5:54:59	2.77044577
1:32:29	1.09159354	3:45:29	2.57758863	5:58:29	3.07971218
1:35:59	1.0527378	3:48:59	2.79713935	6:01:59	2.6477185
1:39:29	6.70798526	3:52:29	2.6505616	6:05:29	2.5535802
1:42:59	6.26003861	3:55:59	2.38346788	6:08:59	2.26642681
1:46:29	5.6009126	3:59:29	2.88669709	6:12:29	2.27369252
1:49:59	4.96468936	4:02:59	3.18711829	6:15:59	2.3942085
1:53:29	4.5532292	4:06:29	2.86332046	6:19:29	2.61344331
1:56:59	4.07037557	4:09:59	2.43353808	6:22:59	2.67488592
2:00:29	4.22943138	4:13:29	2.67283257	6:26:29	2.85321165
2:03:59	4.23906634	4:16:59	2.52972973	6:29:59	2.71626887
2:07:29	4.02472797	4:20:29	2.47286767	6:33:29	2.500351
2:10:59	3.81244296	4:23:59	2.6033345	6:36:59	2.4024219
2:14:29	3.47616708	4:27:29	2.77234117	6:40:29	2.47839593

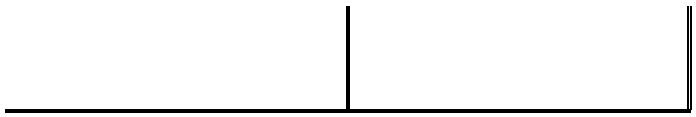

Tableau A3.5-1 Données de respirométrie

Temps hh :mm :ss	rO2 mg/L/h	Temps hh :mm :ss	rO2 mg/L/h	Temps hh :mm :ss	rO2 mg/L/h
6:43:59	2.44822745	9:21:29	2.87706213	11:58:59	2.70173745
6:47:29	2.35724816	9:24:59	2.6984205	12:02:29	2.91970867
6:50:59	2.69052299	9:28:29	2.54362935	12:05:59	3.20465076
6:54:29	2.75591436	9:31:59	2.38978589	12:09:29	3.0939277
6:57:59	2.67804493	9:35:29	2.3025974	12:12:59	3.08397684
7:01:29	2.62607932	9:38:59	2.51188136	12:16:29	2.92808002
7:04:59	2.47665848	9:42:29	2.80930151	12:19:59	2.69478764
7:08:29	2.28301158	9:45:59	2.94545455	12:23:29	2.66572481
7:11:59	2.4065286	9:49:29	2.76681292	12:26:59	2.73348543
7:15:29	2.32218322	9:52:59	2.72037557	12:30:29	2.8039312
7:18:59	2.47270972	9:56:29	2.57285013	12:33:59	2.97372763
7:22:29	2.77471043	9:59:59	2.49087399	12:37:29	3.19233065
7:25:59	2.76396981	10:03:29	2.40668656	12:40:59	3.16674272
7:29:29	2.55831871	10:06:59	2.70442261	12:44:29	3.19738505
7:32:59	2.39436644	10:10:29	2.77313092	12:47:59	3.13878554
7:36:29	2.36593542	10:13:59	2.97183222	12:51:29	2.9988417
7:39:59	2.21872587	10:17:29	2.85415936	12:54:59	2.9034398
7:43:29	2.27021762	10:20:59	2.55500175	12:58:29	2.93487188
7:46:59	2.58627589	10:24:29	2.58753948	13:01:59	3.27825553
7:50:29	2.70584415	10:27:59	2.67014742	13:05:29	3.27762372
7:53:59	2.71405756	10:31:29	2.44949105	13:08:59	3.33006318
7:57:29	2.67535978	10:34:59	2.53952264	13:12:29	3.22834327
8:00:59	2.46497016	10:38:29	2.8971218	13:15:59	2.99742015
8:04:29	2.43653913	10:41:59	2.81498772	13:19:29	3.11793612
8:07:59	2.23341523	10:45:29	2.90707266	13:22:59	2.95019305
8:11:29	2.34935065	10:48:59	2.83220428	13:26:29	3.17937873
8:14:59	2.58406458	10:52:29	2.65419446	13:29:59	3.56588276
8:18:29	2.7503861	10:55:59	2.73427518	13:33:29	3.57330642
8:21:59	2.80819586	10:59:29	2.48329238	13:36:59	3.41077572
8:25:29	2.60554581	11:02:59	2.57521937	13:40:29	3.39419095
8:28:59	2.38252018	11:06:29	2.85968761	13:43:59	3.34443665
8:32:29	2.28206388	11:09:59	2.91733942	13:47:29	3.37428923
8:35:59	2.297543	11:13:29	2.93629343	13:50:59	3.16010881
8:39:29	2.32771148	11:16:59	2.8470516	13:54:29	3.27572832
8:42:59	2.49197964	11:20:29	2.87769393	13:57:59	3.49290979
8:46:29	2.71595297	11:23:59	2.61028431	14:01:29	3.67818533
8:49:59	2.67188487	11:27:29	2.47681643	14:04:59	3.7590558
8:53:29	2.65687961	11:30:59	2.72495613	14:08:29	3.54155844
8:56:59	2.48487189	11:34:29	2.86742717	14:11:59	3.32958933
9:00:29	2.47034047	11:37:59	3.02221833	14:15:29	3.33164268
9:03:59	2.53683749	11:41:29	3.08650404	14:18:59	3.28567918
9:07:29	2.51851527	11:44:59	2.85842401	14:22:29	3.37981747
9:10:59	2.51203931	11:48:29	2.98841698	14:25:59	3.55545806
9:14:29	2.80503686	11:51:59	2.88827659	14:29:29	3.80470341
9:17:59	2.7963496	11:55:29	2.75859951	14:32:59	3.69650755

Tableau A3.5-1 Données de respirométrie

Temps hh :mm :ss	rO2 mg/L/h	Temps hh :mm :ss	rO2 mg/L/h	Temps hh :mm :ss	rO2 mg/L/h
14:36:29	3.7540014	17:13:59	5.1128466	19:51:29	8.57211304
14:39:59	3.75352756	17:17:29	5.27806246	19:54:59	8.56484732
14:43:29	3.58009829	17:20:59	5.53046682	19:58:29	8.5253598
14:46:59	3.51739207	17:24:29	5.59901719	20:01:59	8.40105302
14:50:29	3.48880309	17:27:59	5.42163916	20:05:29	8.69199716
14:53:59	3.74594595	17:31:29	5.44801685	20:08:59	9.04959635
14:57:29	3.98334503	17:34:59	5.3886276	20:12:29	9.40877499
15:00:59	3.97544753	17:38:29	5.11742717	20:15:59	9.73115128
15:04:29	3.87214812	17:41:59	5.29843805	20:19:29	9.74868373
15:07:59	3.85035101	17:45:29	5.599649	20:22:59	9.48632851
15:11:29	3.68181819	17:48:59	5.77908037	20:26:29	9.65186029
15:14:59	3.50854686	17:52:29	5.91065284	20:29:59	9.61884872
15:18:29	3.65496665	17:55:59	5.84889435	20:33:29	9.78122151
15:21:59	3.80691472	17:59:29	5.93671462	20:36:59	10.1424535
15:25:29	4.22342927	18:02:59	5.76091611	20:40:29	10.4585117
15:28:59	4.11017901	18:06:29	5.68462617	20:43:59	10.6684275
15:32:29	4.24791155	18:09:59	5.88790804	20:47:29	10.831748
15:35:59	4.0981748	18:13:29	6.23934715	20:50:59	10.8309583
15:39:29	3.83139698	18:16:59	6.51528607	20:54:29	10.7246578
15:42:59	3.8614075	18:20:29	6.58525799	20:57:59	10.6332046
15:46:29	3.93248508	18:23:59	6.35291329	21:01:29	10.9688487
15:49:59	4.13655668	18:27:29	6.36128465	21:04:59	11.4648122
15:53:29	4.44171639	18:30:59	6.30616006	21:08:29	11.8623728
15:56:59	4.55259741	18:34:29	6.36191646	21:11:59	12.0444893
16:00:29	4.49147068	18:37:59	6.29573537	21:15:29	12.1016673
16:03:59	4.29182169	18:41:29	6.6888733	21:18:59	12.0910846
16:07:29	4.28803089	18:44:59	6.86088103	21:22:29	11.944191
16:10:59	4.18046682	18:48:29	7.13587223	21:25:59	12.013689
16:14:29	4.22374519	18:51:59	7.19068094	21:29:29	12.305265
16:17:59	4.24696385	18:55:29	7.1644612	21:32:59	12.9895051
16:21:29	4.72349948	18:58:59	7.08137943	21:36:29	13.4151808
16:24:59	4.83090558	19:02:29	7.10886276	21:39:59	13.6328361
16:28:29	4.81005616	19:05:59	6.91884873	21:43:29	13.6764303
16:31:59	4.77104248	19:09:29	7.35257987	21:46:59	13.6111969
16:35:29	4.57091962	19:12:59	7.6154089	21:50:29	13.4925763
16:38:59	4.47441208	19:16:29	7.93241489	21:53:59	13.6818007
16:42:29	4.50110565	19:19:59	7.99780626	21:57:29	14.1695507
16:45:59	4.66253071	19:23:29	7.87255178	22:00:59	14.8294665
16:49:29	4.98427519	19:26:59	7.7904177	22:04:29	15.1142506
16:52:59	5.08789049	19:30:29	7.65284311	22:07:59	15.3279572
16:56:29	5.16923482	19:33:59	7.69454196	22:11:29	15.3161109
16:59:59	5.12011233	19:37:29	7.86196913	22:14:59	15.0692348
17:03:29	5.02944893	19:40:59	8.39726219	22:18:29	14.8575816
17:06:59	4.82711478	19:44:29	8.69768338	22:21:59	14.9927869
17:10:29	4.90198315	19:47:59	8.78360829	22:25:29	15.5873113

Tableau A3.5-1 Données de respirométrie

Temps hh :mm :ss	rO2 mg/L/h
22:28:59	16.2533871
22:32:29	16.6860125
22:35:59	16.8256406
22:39:29	16.8945069
22:42:59	16.7335556
22:46:29	16.6161987
22:49:59	17.0440856
22:53:29	17.6509301
22:56:59	18.1378905
23:00:29	18.3530187
23:03:59	18.4321517
23:07:29	18.3400667
23:10:59	18.263303
23:14:29	18.4037206
23:17:59	18.6611794
23:21:29	19.1606177
23:24:59	18.2618814
23:28:29	7.33204634
23:31:59	3.97876449
23:35:29	0.59120744
23:38:59	0.1001404
23:42:29	-0.02527203
23:45:59	-3.5409E-11
23:49:29	0.00742366
23:52:59	0.07818533
23:56:29	0.04501579
23:59:59	0.06886627
0:03:29	0.01721657
0:06:59	0.01721657
0:10:29	0.18085293
0:13:59	-0.04864865
0:17:29	-4.1E-11
0:20:59	-0.10787996
0:24:29	0.06081081
0:27:59	0.00679186
0:31:29	3.3545E-11
0:34:59	-0.04548965
0:38:29	-0.00916111
0:41:59	0.02558793
0:45:29	-0.07960688

ANNEXE A3.6 Essai de respirométrie du 11-01-2005

Tableau A3.6-1 Données de respirométrie

DASYLab - V 5.50.00
WORKSHEET : Respiro
Recording Date : 05-01-11, 09:24:00
Block Length : 1
Delta : 1 sec.
Number of Channels : 1

Temps hh :mm :ss	rO2 mg/L/h	Temps hh :mm :ss	rO2 mg/L/h	Temps hh :mm :ss	rO2 mg/L/h
00:57:29	0.458	03:10:29	2.355	05:23:29	2.863
01:00:59	0.544	03:13:59	2.425	05:26:59	3.496
01:04:29	0.523	03:17:29	2.721	05:30:29	3.526
01:07:59	0.556	03:20:59	2.733	05:33:59	2.603
01:11:29	0.288	03:24:29	2.826	05:37:29	3.209
01:14:59	0.416	03:27:59	2.588	05:40:59	3.228
01:18:29	0.127	03:31:29	2.630	05:44:29	3.200
01:21:59	0.161	03:34:59	2.462	05:47:59	3.165
01:25:29	0.595	03:38:29	2.560	05:51:29	3.109
01:28:59	0.628	03:41:59	2.606	05:54:59	2.769
01:32:29	6.630	03:45:29	2.552	05:58:29	2.709
01:35:59	6.151	03:48:59	2.918	06:01:59	2.705
01:39:29	5.734	03:52:29	2.892	06:05:29	3.344
01:42:59	5.239	03:55:59	2.730	06:08:59	3.360
01:46:29	4.623	03:59:29	2.560	06:12:29	3.491
01:49:59	4.270	04:02:59	2.382	06:15:59	3.281
01:53:29	7.282	04:06:29	2.679	06:19:29	3.064
01:56:59	4.188	04:09:59	2.396	06:22:59	3.054
02:00:29	3.958	04:13:29	2.819	06:26:29	2.920
02:03:59	3.561	04:16:59	3.006	06:29:59	2.816
02:07:29	3.396	04:20:29	2.951	06:33:29	3.495
02:10:59	3.096	04:23:59	2.784	06:36:59	3.263
02:14:29	3.451	04:27:29	2.722	06:40:29	3.385
02:17:59	3.593	04:30:59	2.555	06:43:59	3.287
02:21:29	2.976	04:34:29	2.386	06:47:29	3.132
02:24:59	3.316	04:37:59	2.536	06:50:59	3.086
02:28:29	3.285	04:41:29	2.804	06:54:29	2.893
02:31:59	3.095	04:44:59	2.979	06:57:59	3.113
02:35:29	2.846	04:48:29	3.089	07:01:29	3.297
02:38:59	2.457	04:51:59	2.758	07:04:59	3.591
02:42:29	2.490	04:55:29	2.741	07:08:29	3.404
02:45:59	2.556	04:58:59	2.836	07:11:59	3.425
02:49:29	2.516	05:02:29	2.343	07:15:29	3.356
02:52:59	2.556	05:05:59	2.601	07:18:59	3.138
02:56:29	2.845	05:09:29	2.810	07:22:29	3.017
02:59:59	3.628	05:12:59	3.082	07:25:59	3.358
03:03:29	2.434	05:16:29	3.195	07:29:29	3.424
03:06:59	2.534	05:19:59	2.754	07:32:59	3.534

Tableau A3.6-1 Données de respirométrie

Temps hh :mm :ss	rO2 mg/L/h	Temps hh :mm :ss	rO2 mg/L/h	Temps hh :mm :ss	rO2 mg/L/h
07:36:29	3.606	10:13:59	4.081	12:51:29	6.498
07:39:59	3.422	10:17:29	4.478	12:54:59	6.221
07:43:29	3.361	10:20:59	4.648	12:58:29	6.103
07:46:59	3.281	10:24:29	4.491	13:01:59	6.267
07:50:29	3.230	10:27:59	4.637	13:05:29	6.305
07:53:59	3.279	10:31:29	4.374	13:08:59	6.691
07:57:29	3.600	10:34:59	4.358	13:12:29	6.950
08:00:59	3.847	10:38:29	4.279	13:15:59	6.910
08:04:29	3.710	10:41:59	4.488	13:19:29	6.792
08:07:59	3.642	10:45:29	4.533	13:22:59	6.731
08:11:29	3.483	10:48:59	4.860	13:26:29	6.657
08:14:59	3.314	10:52:29	4.893	13:29:59	6.691
08:18:29	3.333	10:55:59	4.836	13:33:29	6.732
08:21:59	3.224	10:59:29	4.869	13:36:59	7.145
08:25:29	3.685	11:02:59	4.705	13:40:29	7.499
08:28:59	3.750	11:06:29	4.619	13:43:59	7.531
08:32:29	3.905	11:09:59	4.446	13:47:29	7.482
08:35:59	3.780	11:13:29	4.908	13:50:59	7.233
08:39:29	3.622	11:16:59	5.142	13:54:29	7.272
08:42:59	3.465	11:20:29	5.200	13:57:59	7.179
08:46:29	3.330	11:23:59	5.153	14:01:29	7.471
08:49:59	3.445	11:27:29	4.973	14:04:59	7.626
08:53:29	3.609	11:30:59	4.885	14:08:29	7.977
08:56:59	3.846	11:34:29	4.802	14:11:59	8.306
09:00:29	4.009	11:37:59	4.842	14:15:29	8.198
09:03:59	3.955	11:41:29	5.114	14:18:59	8.306
09:07:29	3.694	11:44:59	5.383	14:22:29	7.993
09:10:59	3.688	11:48:29	5.475	14:25:59	7.848
09:14:29	3.379	11:51:59	5.433	14:29:29	7.897
09:17:59	3.666	11:55:29	5.418	14:32:59	8.247
09:21:29	3.926	11:58:59	5.590	14:36:29	8.640
09:24:59	4.052	12:02:29	4.972	14:39:59	8.655
09:28:29	4.311	12:05:59	5.269	14:43:29	8.578
09:31:59	4.142	12:09:29	5.479	14:46:59	8.737
09:35:29	4.013	12:12:59	5.799	14:50:29	8.647
09:38:59	3.822	12:16:29	5.943	14:53:59	8.536
09:42:29	3.845	12:19:59	6.066	14:57:29	8.586
09:45:59	3.829	12:23:29	5.749	15:00:59	8.919
09:49:29	4.160	12:26:59	5.739	15:04:29	9.334
09:52:59	4.401	12:30:29	5.491	15:07:59	9.458
09:56:29	4.334	12:33:59	5.680	15:11:29	9.683
09:59:59	4.337	12:37:29	5.830	15:14:59	9.622
10:03:29	4.184	12:40:59	6.154	15:18:29	9.237
10:06:59	4.088	12:44:29	6.347	15:21:59	9.450
10:10:29	4.079	12:47:59	6.414	15:25:29	9.529

Tableau A3.6-1 Données de respirométrie

Temps hh :mm :ss	rO2 mg/L/h	Temps hh :mm :ss	rO2 mg/L/h	Temps hh :mm :ss	rO2 mg/L/h
15:28:59	9.773	18:06:29	15.936	20:43:59	22.210
15:32:29	10.141	18:09:59	15.859	20:47:29	22.595
15:35:59	10.766	18:13:29	16.090	20:50:59	22.581
15:39:29	10.884	18:16:59	16.172	20:54:29	19.724
15:42:59	10.919	18:20:29	16.323	20:57:59	16.693
15:46:29	10.464	18:23:59	16.251	21:01:29	15.261
15:49:59	10.358	18:27:29	16.655	21:04:59	14.708
15:53:29	10.357	18:30:59	16.690	21:08:29	14.413
15:56:59	10.875	18:34:29	16.415	21:11:59	14.637
16:00:29	11.361	18:37:59	16.690	21:15:29	14.486
16:03:59	11.356	18:41:29	16.628	21:18:59	14.930
16:07:29	11.457	18:44:59	16.531	21:22:29	14.958
16:10:59	11.947	18:48:29	17.086	21:25:59	15.013
16:14:29	11.679	18:51:59	16.554	21:29:29	15.120
16:17:59	11.589	18:55:29	17.543	21:32:59	15.317
16:21:29	11.504	18:58:59	17.737	21:36:29	15.379
16:24:59	11.783	19:02:29	17.616	21:39:59	15.145
16:28:29	12.114	19:05:59	17.052	21:43:29	15.472
16:31:59	12.542	19:09:29	15.755	21:46:59	16.375
16:35:29	12.602	19:12:59	17.481	21:50:29	16.914
16:38:59	12.934	19:16:29	17.448	21:53:59	17.563
16:42:29	12.779	19:19:59	17.707	21:57:29	17.458
16:45:59	12.780	19:23:29	18.308	22:00:59	17.044
16:49:29	12.452	19:26:59	18.288	22:04:29	17.608
16:52:59	12.748	19:30:29	18.149	22:07:59	17.361
16:56:29	13.072	19:33:59	17.903	22:11:29	17.287
16:59:59	13.794	19:37:29	18.680	22:14:59	17.517
17:03:29	14.042	19:40:59	18.588	22:18:29	18.137
17:06:59	14.181	19:44:29	18.029	22:21:59	18.347
17:10:29	14.079	19:47:59	18.398	22:25:29	17.604
17:13:59	14.061	19:51:29	19.507	22:28:59	17.986
17:17:29	13.859	19:54:59	20.015	22:32:29	17.212
17:20:59	13.861	19:58:29	19.755	22:35:59	17.745
17:24:29	14.212	20:01:59	18.935	22:39:29	17.916
17:27:59	14.787	20:05:29	18.605	22:42:59	17.094
17:31:29	15.308	20:08:59	19.107	22:46:29	19.224
17:34:59	15.390	20:12:29	19.768	22:49:59	19.817
17:38:29	15.452	20:15:59	19.600	22:53:29	19.769
17:41:59	15.196	20:19:29	19.069	22:56:59	20.417
17:45:29	15.030	20:22:59	18.563	23:00:29	20.238
17:48:59	14.954	20:26:29	19.824	23:03:59	19.743
17:52:29	14.849	20:29:59	19.659	23:07:29	19.762
17:55:59	15.665	20:33:29	19.545	23:10:59	19.011
17:59:29	15.697	20:36:59	17.997	23:14:29	20.934
18:02:59	16.254	20:40:29	19.491	23:17:59	21.635

Tableau A3.6-1 Données de respirométrie

Temps hh :mm :ss	rO2 mg/L/h
23:21:29	22.237
23:24:59	22.168
23:28:29	21.649
23:31:59	20.669
23:35:29	21.289
23:38:59	21.896
23:42:29	21.235
23:45:59	22.372
23:49:29	22.747
23:52:59	21.873
23:56:29	18.887
23:59:59	12.348
00:03:29	7.401
00:06:59	6.872
00:10:29	7.202
00:13:59	7.281
00:17:29	7.342
00:20:59	7.078
00:24:29	6.946
00:27:59	6.966
00:31:29	6.401
00:34:59	6.568
00:38:29	6.710
00:41:59	6.910
00:45:29	6.872

ANNEXE A3.7 Essai de respirométrie du 08-12-2004

(Dose : 100 mg DCO/L)

Tableau A3.7-1 Mesures de la concentration d'ADN

	Temps		ADN	
		Lecture	Lecture	
	minutes	luminosité	ng/ml	ng/ml
t0	0	260	304	2374
t0	0	266	311	2429
t0	0	270	315	2466
t0	0	304	355	2776
t1	5			
t1	5			
t1	5			
t1	5			
t2	15	295	345	2757
t2	15	275	321	2570
t2	15	274	320	2561
t2	15	297	347	2776
t7	180	254	297	2473
t7	180	282	329	2746
t7	180	306	358	2979
t7	180	346	404	3369

Tableau A3.7-2 Mesures de la DCO totale

	Temps	Blanc	F.A.S.	DCOtotale	
		Vol.		Vol.	DCO
	minutes	ml	molarité	ml	mg DCO/L
t0	0	27.1		7.1	1483
t0	0	27		7.15	1479
t0	0	27		6.35	1539
t0	0	*27.033*	*0.019*		
t1	5	27.1		6.1	1557
t1	5	27		6.2	1550
t1	5	27		6.2	1550
t1	5	*27.033*	*0.019*		
t2	15	27.1		6.3	1543
t2	15	27		6.1	1557
t2	15	27		6.1	1557
t2	15	*27.033*	*0.019*		
t7	180	27.1		6.6	1520
t7	180	27		5.5	1602
t7	180	27		6.5	1528
t7	180	*27.033*	*0.019*		

Tableau A3.7-3 Mesures de la DCO soluble

	Temps	**Blanc**	**F.A.S.**	**DCOfiltrée**	
		Vol.		**Vol.**	**DCO**
	minutes	**ml**	**molarité**	**ml**	**mg DCO/L**
t0	0	27.1		18.4	642
t0	0	27		18.65	624
t0	0	27			
t0	0	*27.033*	*0.019*		
t1	5	27.1		18.8	613
t1	5	27		18.6	627
t1	5	27		18.8	613
t1	5	*27.033*	*0.019*		
t2	15	27.1		18.3	650
t2	15	27		18.35	646
t2	15	27		18.55	631
t2	15	*27.033*	*0.019*		
t7	180	27.1		18.6	627
t7	180	27		18.4	642
t7	180	27		18.4	642
t7	180	*27.033*	*0.019*		

Tableau A3.7-4 Mesures du glucose

	Temps	Blanc	Glucose	
	minutes	Abs.	Abs.	mg/L
t0	0	0	0.068	9
t0	0	0	0.065	8
t0	0		0.091	
t0	0	*0.000*	*0.075*	
t1	5	0	0.065	8
t1	5	0	0.074	9
t1	5		0.072	9
t1	5	*0.000*	*0.070*	
t2	15	0	0.067	8
t2	15	0	0.061	8
t2	15		0.069	9
t2	15	*0.000*	*0.066*	
t7	180	0	0.056	7
t7	180	0	0.059	7
t7	180		0.062	8
t7	180	*0.000*	*0.059*	

Tableau A3.7-5 Mesures du glycogène

	Temps	Blanc	Glycogène	
	minutes	Abs.	Abs.	mg/L
t0	0	0	0.361	46
t0	0	0	0.349	44
t0	0		0.341	43
t0	0	*0.000*	0.347	44
t1	5	0	0.653	83
t1	5	0	0.64	81
t1	5		0.659	83
t1	5	*0.000*	0.649	82
t2	15	0	0.709	90
t2	15	0	0.733	93
t2	15		0.715	91
t2	15	*0.000*	0.704	89
t7	180	0	0.636	81
t7	180	0	0.637	81
t7	180		0.636	81
t7	180	*0.000*	0.636	81

Tableau A3.7-6 Mesures du glycogène

	Temps	Blanc	NH_4^+	
	minutes	abs	abs	mg NH_4^+/L
t0	0	0.000	0.229	21.4
t0	0		0.232	21.7
t0	0		0.233	21.8
t0	0			
t1	5	-0.008	0.269	25.9
t1	5		0.268	25.8
t1	5		0.273	26.3
t1	5			
t2	15	-0.008	0.258	24.9
t2	15		0.261	25.2
t2	15		0.256	24.7
t2	15			
t7	180	-0.003	0.232	22.0
t7	180		0.234	22.2
t7	180		0.234	22.2
t7	180			

Tableau A3.7-7 Compte de la micro-faune

	Temps	Flagellé	Cilié libre	Cilié fixe	Rotifer	Sarcodine	total	Micro faune
	heure	org.	org.	org.	org.	org.	org.	org./L
t0	0			7		7	14	4.7.E+05
t2	15			7		7	14	4.7.E+05
t7	180			7		7	14	4.7.E+05

DASYLab - V 5.50.00
WORKSHEET : Respirofermé
Recording Date : 04-12-08, 10:30:55
Block Length : 1
Delta : 1 sec.
Number of Channels : 1
Elapsed Time[hh:mm:ss]

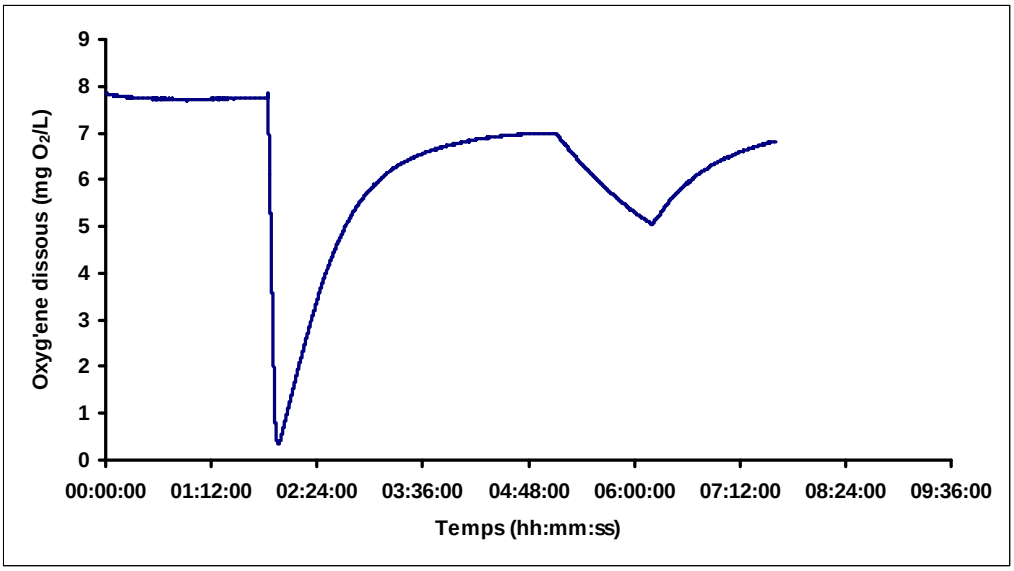

Figure A3.7-1 Mesures de la concentration en oxygène dissous dans le réacteur

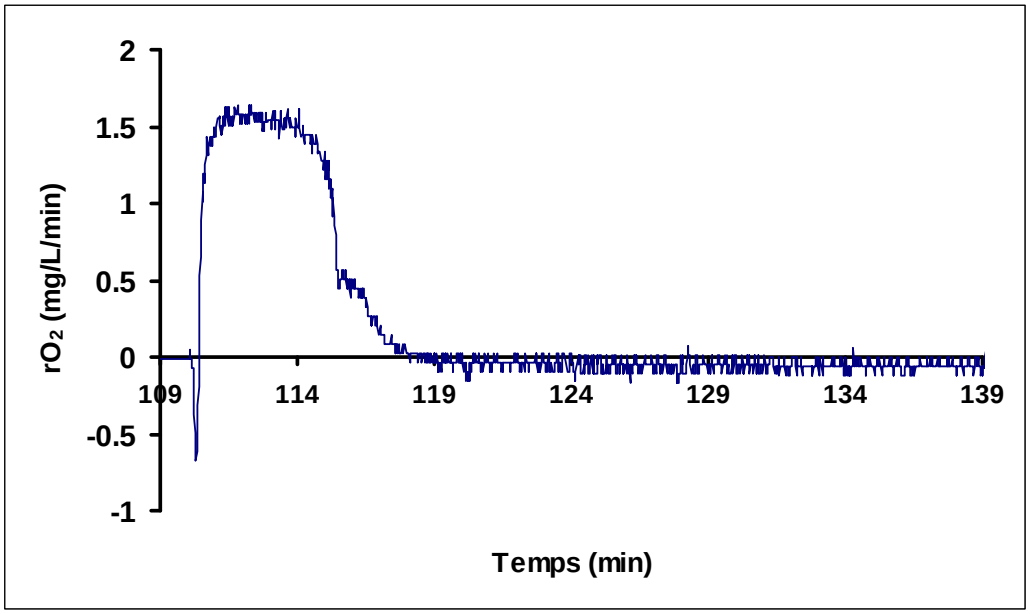

Figure A3.7-2 Taux de respiration dans le réacteur

ANNEXE A3.8 Essai de respirométrie du 29-11-2004

(Dose : 65 mg DCO/L)

Tableau A3.8-1 Mesures de la concentration d'ADN

	Temps	Lecture	ADN	
	minutes	luminosité	ng/ml	ng/ml
t0	0	310	362	2898
t0	0	308	360	2879
t0	0	260	304	2430
t0	0	275	321	2570
t5	60	376	439	3661
t5	60	342	400	3330
t5	60	349	408	3398
t5	60	356	416	3466
t7	180	340	397	3310
t7	180	363	424	3534
t7	180	320	374	3116
t7	180	335	391	3262

Tableau A3.8-2 Mesures de la DCO totale

	Temps	Blanc	F.A.S.	DCOtotale	
		Vol.		Vol.	DCO
	minutes	ml	molarité	ml	mg DCO/L
t0	0	26.5		5.1	1649
t0	0	26.5		5	1657
t0	0	26.5		5.1	1649
t0	0	*26.500*	*0.019*		
t1	5	26.5		4.7	1680
t1	5	26.5		4.7	1680
t1	5	26.5		4.8	1672
t1	5	*26.500*	*0.019*		
t2	15	26.5		4.9	1665
t2	15	26.5		4.9	1665
t2	15	26.5		5	1657
t2	15	*26.500*	*0.019*		
t3	30	26.5		5.1	
t3	30	26.5		4.8	1672
t3	30	26.5		4.9	1665
t3	30	*26.500*	*0.019*		
t4	45	26.5		5	
t4	45	26.5		5.2	1642
t4	45	26.5		5.25	1638
t4	45	*26.500*	*0.019*		
t5	60	26.5		4.95	1661
t5	60	26.5		4.95	1661
t5	60	26.5		4.85	1669
t5	60	*26.500*	*0.019*		
t6	120	26.5		4.75	1676
t6	120	26.5		5.1	
t6	120	26.5		4.9	1665
t6	120	*26.500*	*0.019*		
t7	180	26.5		5.25	
t7	180	26.5		4.9	1665
t7	180	26.5		4.9	1665
t7	180	*26.500*	*0.019*		

Tableau A3.8-3 Mesures de la DCO filtrée

	Temps	Blanc	F.A.S.	DCOfiltrée	
		Vol.		Vol.	Vol.
	minutes	ml	molarité	ml	ml
t0	0	26.5		17.3	709
t0	0	26.5		17.25	713
t0	0	26.5		17.25	713
t0	0	*26.500*	*0.019*		
t1	5	26.5		17.25	713
t1	5	26.5		17.3	709
t1	5	26.5		17.3	709
t1	5	*26.500*	*0.019*		
t2	15	26.5		17.2	717
t2	15	26.5		17.3	709
t2	15	26.5		17.2	717
t2	15	*26.500*	*0.019*		
t3	30	26.5		17.2	717
t3	30	26.5		17.2	717
t3	30	26.5		17.15	721
t3	30	*26.500*	*0.019*		
t4	45	26.5		17.4	701
t4	45	26.5		17.2	717
t4	45	26.5		17.5	694
t4	45	*26.500*	*0.019*		
t5	60	26.5		17.3	709
t5	60	26.5		17.5	694
t5	60	26.5		17.3	709
t5	60	*26.500*	*0.019*		
t6	120	26.5		17.2	717
t6	120	26.5		17.3	709
t6	120	26.5		17.3	709
t6	120	*26.500*	*0.019*		
t7	180	26.5		16.7	
t7	180	26.5		17.3	709
t7	180	26.5		17.15	721
t7	180	*26.500*	*0.019*		

Tableau A3.8-4 Mesures du glucose

	Temps	Blanc	Glucose	
	minutes	Abs.	Abs.	mg/L
t0	0	0	0.073	10
t0	0	0.003	0.046	7
t0	0	-0.004	0.047	7
t0	0	*0.000*	*0.055*	
t1	5	0	0.048	7
t1	5	0.003	0.046	7
t1	5	-0.004	0.047	7
t1	5	*0.000*	*0.047*	
t2	15	0	0.047	7
t2	15	0.003	0.052	7
t2	15	-0.004	0.053	8
t2	15	*0.000*	*0.051*	
t3	30	0	0.071	10
t3	30	0.003	0.054	8
t3	30	-0.004	0.059	8
t3	30	*0.000*	*0.061*	
t4	45	0	0.057	8
t4	45	0.003	0.063	9
t4	45	-0.004	0.06	8
t4	45	*0.000*	*0.060*	
t5	60	0	0.073	10
t5	60	0.003	0.058	8
t5	60	-0.004	0.063	9
t5	60	*0.000*	*0.065*	
t6	120	0	0.058	8
t6	120	0.003	0.059	8
t6	120	-0.004	0.076	11
t6	120	*0.000*	*0.064*	
t7	180	0	0.054	8
t7	180	0.003	0.056	8
t7	180	-0.004	0.057	8
t7	180	*0.000*	*0.056*	

Tableau A3.8-5 Mesures du glycogène

	Temps	Blanc	Glycogènes	
	minutes	Abs.	Abs.	mg/L
t0	0	0	0.593	84
t0	0	0.003	0.603	85
t0	0	-0.004	0.593	83
t0	0	*0.000*	0.597	85
t1	5	0	0.834	118
t1	5	0.003	0.823	116
t1	5	-0.004	0.81	114
t1	5	*0.000*	0.803	114
t2	15	0	0.855	120
t2	15	0.003	0.864	122
t2	15	-0.004	0.838	118
t2	15	*0.000*	0.833	118
t3	30	0	0.826	116
t3	30	0.003	0.826	116
t3	30	-0.004	0.823	115
t3	30	*0.000*	0.933	132
t4	45	0	0.822	116
t4	45	0.003	0.824	116
t4	45	-0.004	0.824	116
t4	45	*0.000*	0.827	117
t5	60	0	0.89	125
t5	60	0.003	0.817	115
t5	60	-0.004	0.818	115
t5	60	*0.000*	0.805	114
t6	120	0	0.834	118
t6	120	0.003	0.783	110
t6	120	-0.004	0.771	108
t6	120	*0.000*	0.784	111
t7	180	0	0.765	108
t7	180	0.003	0.725	102
t7	180	-0.004	0.734	103
t7	180	*0.000*	0.746	105

Tableau A3.8-6 Mesures du NH_4^+

	Temps	Blanc	NH_4^+	
	minutes	abs	abs	mg NH_4^+/L
t0	0	0.000	0.274	25.7
t0	0		0.269	25.2
t0	0		0.27	25.3
t0	0			
t1	5	0.000	0.29	27.2
t1	5		0.291	27.3
t1	5		0.29	27.2
t1	5			
t2	15	0.007	0.279	25.5
t2	15		0.284	25.9
t2	15		0.286	26.1
t2	15			
t3	30	0.007	0.291	26.6
t3	30		0.285	26.0
t3	30		0.288	26.3
t3	30			
t4	45	0.011	0.283	25.5
t4	45		0.291	26.2
t4	45		0.288	25.9
t4	45			
t5	60	0.011	0.289	26.0
t5	60		0.294	26.5
t5	60		0.297	26.8
t5	60			
t6	120	0.006	0.276	25.3
t6	120		0.277	25.4
t6	120		0.283	25.9
t6	120			
t7	180	0.006	0.265	24.3
t7	180		0.267	24.4
t7	180		0.265	24.3
t7	180			

Tableau A3.8-7 Compte de la micro-faune

	Temps	Flagellé	Cilié libre	Cilié fixe	Rotifer	Sarcodine	total	Micro faune
	heure	org.	org.	org.	org.	org.	org.	org./L
t0	0			15		27	42	1.4.E+06
t2	15			15		27	42	1.4.E+06
t3	30			15		27	42	1.4.E+06
t4	45			15		27	42	1.4.E+06
t5	60			15		27	42	1.4.E+06
t6	120			15		27	42	1.4.E+06
t7	180			15		27	42	1.4.E+06

DASYLab - V 5.50.00
WORKSHEET : Respirofermé
Recording Date : 04-11-29, 13:30:45
Block Length : 1
Delta : 1 sec.
Number of Channels : 1

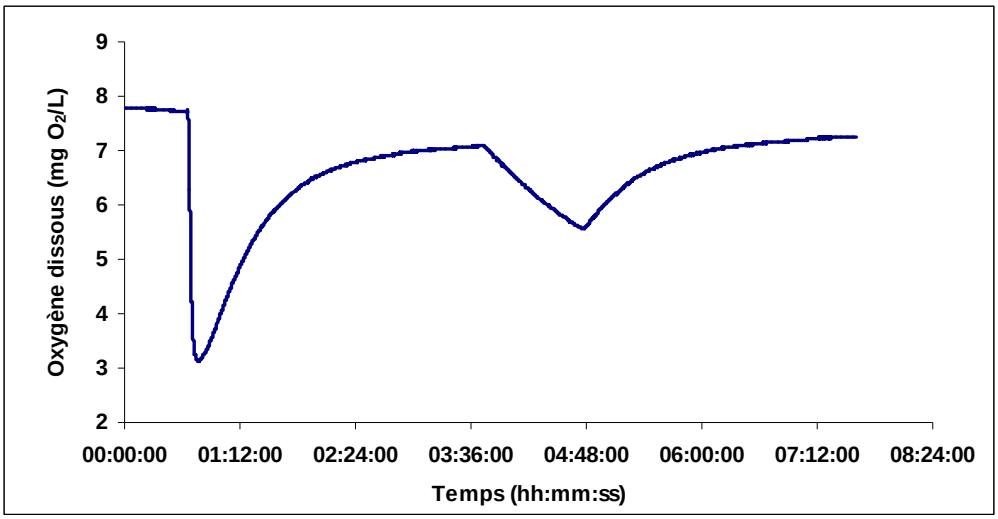

Figure A3.8-1 Mesures de la concentration en oxygène dissous dans le réacteur

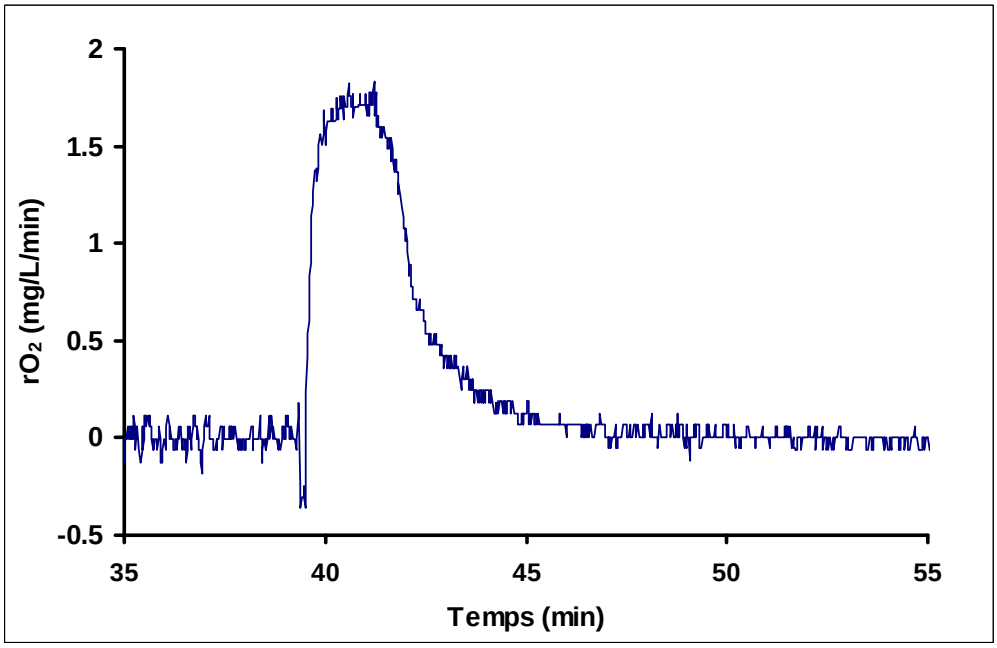

Figure A3.8-2 Taux de respiration dans le réacteur